



**Understanding flesh colour variation in Atlantic salmon:  
molecular mechanisms and genetic effect**

Dr Gianluca Amoroso - Aquaculture Scientist at Petuna

Dr Chan D.H. Nguyen - PhD graduate, University of the Sunshine Coast

Ms Thu T.M. Vo - PhD candidate, University of the Sunshine Coast

Dr Tomer Ventura - University of the Sunshine Coast

Prof Abigail Elizur - University of the Sunshine Coast

**20/10/2020**

FRDC Project No **2014-248**

### ***Please Note – Final Report Requirements – accessibility***

*Under the Disability Discrimination Act 1992, Australian Government agencies are required to ensure information and services are provided in a non-discriminatory accessible manner – the FRDC and as a result all content produced as part of our projects also need to meet these requirements.*

*The Web Content Accessibility Guidelines outlines ways to make digital content more accessible to the broadest audience – <https://guides.service.gov.au/content-guide/accessibility-inclusivity/>*

*While there are many aspects to this, a key focus for principal investigators is to ensure that PDF documents are accessible. To make a PDF accessible you must make sure structural elements such as headings are marked-up so that a screen reader can follow the logical order of the content. The FRDC will update the final report design standard to highlight these requirements. We are regularly working to improve what we deliver to end users and this is part of that.*

© Year Fisheries Research and Development Corporation.  
All rights reserved.

ISBN 978-1-925476-12-5

**Understanding flesh colour variation in Atlantic salmon:  
molecular mechanisms and genetic effect**

2014-248

2020

**Ownership of Intellectual property rights**

Unless otherwise noted, copyright (and any other intellectual property rights, if any) in this publication is owned by the Fisheries Research and Development Corporation

This publication (and any information sourced from it) should be attributed to Amoroso, G., Ventura, T. and Elizur, A., FRDC, 2020, *Understanding flesh colour variation in Atlantic salmon: molecular mechanisms and genetic effect*, University of the Sunshine Coast, October CC BY 3.0]

**Creative Commons licence**

All material in this publication is licensed under a Creative Commons Attribution 3.0 Australia Licence, save for content supplied by third parties, logos and the Commonwealth Coat of Arms.



Creative Commons Attribution 3.0 Australia Licence is a standard form licence agreement that allows you to copy, distribute, transmit and adapt this publication provided you attribute the work. A summary of the licence terms is available from <https://creativecommons.org/licenses/by/3.0/au/>. The full licence terms are available from <https://creativecommons.org/licenses/by-sa/3.0/au/legalcode>.

Inquiries regarding the licence and any use of this document should be sent to: [frdc@frdc.com.au](mailto:frdc@frdc.com.au)

**Disclaimer**

The authors do not warrant that the information in this document is free from errors or omissions. The authors do not accept any form of liability, be it contractual, tortious, or otherwise, for the contents of this document or for any consequences arising from its use or any reliance placed upon it. The information, opinions and advice contained in this document may not relate, or be relevant, to a readers particular circumstances. Opinions expressed by the authors are the individual opinions expressed by those persons and are not necessarily those of the publisher, research provider or the FRDC.

The Fisheries Research and Development Corporation plans, invests in and manages fisheries research and development throughout Australia. It is a statutory authority within the portfolio of the federal Minister for Agriculture, Fisheries and Forestry, jointly funded by the Australian Government and the fishing industry.

**Researcher Contact Details**

Name: Professor Abigail Elizur  
Address: Sippy Downs Drive,  
Sippy Downs, Qld 4556  
Phone: 07-54594813  
Fax:  
Email: [AElizur@usc.edu.au](mailto:AElizur@usc.edu.au)

**FRDC Contact Details**

Address: 25 Geils Court  
Deakin ACT 2600  
Phone: 02 6285 0400  
Fax: 02 6285 0499  
Email: [frdc@frdc.com.au](mailto:frdc@frdc.com.au)  
Web: [www.frdc.com.au](http://www.frdc.com.au)

In submitting this report, the researcher has agreed to FRDC publishing this material in its edited form.

# Table of Contents

<i>Please Note – Final Report Requirements – accessibility</i> .....	2
<b>List of Figures</b> .....	<b>8</b>
<b>List of Tables</b> .....	<b>12</b>
<b>Acknowledgments</b> .....	<b>13</b>
<b>Executive Summary</b> .....	<b>14</b>
Keywords .....	17
<b>Section 1</b> .....	<b>18</b>
<b><i>Aim 1: Identify the type of flesh colour variations and their prevalence at Petuna and assess the magnitude of their economic impact.</i></b> .....	<b>18</b>
<b>1.1 Flesh colour issue in Petuna stocks - background</b> .....	<b>18</b>
1.1.1 Economic impact of inadequate flesh colour within Petuna .....	18
1.1.2 Remarks .....	18
<b>1.2 Flesh colour in Atlantic salmon – A review</b> .....	<b>19</b>
1.2.1 Carotenoids and their importance .....	19
1.2.2 Carotenoids metabolism .....	19
1.2.3 Variation in flesh colour .....	20
1.2.4 Flesh colour assessment .....	21
<b>Section 2</b> .....	<b>24</b>
<b><i>Aim 2: Identify molecular events associated with reduced flesh colour in gut and liver. ...</i></b> <b>24</b>	
<b>2.1 Longitudinal assessment of a commercial stock affected by colour variation to first detect variation and then describe occurrence pattern and development</b> .....	<b>24</b>
2.1.1 Background .....	24
2.1.2 Materials and Methods .....	25
2.1.3 Results and Discussion .....	27
2.1.4 Final remarks .....	35
<b>2.2 Atlantic Salmon gut microbiota profile correlates with flesh pigmentation: cause or effect?</b> <b>36</b>	
2.2.1 Abstract .....	36
2.2.2 Introduction .....	36
2.2.3 Materials and methods .....	38
2.2.3.1 Study Design and Sample Collection .....	38
2.2.3.2 DNA Extraction and MiSeq Sequencing .....	39
2.2.3.3 Microbial Community Profiling .....	39
2.2.3.4 Biomarker Discovery .....	39
2.2.3.5 Predicting Function and Metagenome Contribution .....	39
2.2.4 Results .....	40
2.2.4.1 The Microbiota Shift Is Strongly Correlated with Temperature Change; However, the Taxa Relating to Flesh Colour Are Differentiated Independent of the Time Point .....	40
2.2.4.2 Differential Taxa Reveal the Features Across Metadata .....	42
2.2.4.3 Prediction of Functional Composition Based on the Bacterial Metagenome .....	45
2.2.4.4 Predicted Terpenoid Biosynthesis, Esterification, Lipid, Carotenoid, and Lipopolyprotein Metabolic Pathways Shared the Same Microbiota Taxa in the Unfavorable Colour Phenotypes .....	49
2.2.5 Discussion .....	51
2.2.6 Conclusions .....	55
<b>2.3 Identification of molecular events associated with reduced flesh colour in gut and liver by transcriptome analysis, library benchmark study and SNPs exploration</b> .....	<b>56</b>
2.3.1 Background .....	56

2.3.2 Materials and methods: transcriptome analysis.....	56
2.3.2.1 Samples selection and RNA extraction .....	56
2.3.2.3 Transcriptome analysis.....	58
2.3.3 Results and Discussion: transcriptome analysis.....	59
2.3.3.1 Low colour-None banding versus Low colour-Banded (LN_vs_LB) .....	62
2.3.3.2 High colour-None banding versus High colour-Banded (HN_vs_HB) .....	64
2.3.3.3 High colour-Banded versus Low colour-Banded (HB_vs_LB) .....	66
2.3.3.4 High colour-None banding versus Low colour-None banding (HN_vs_LN).....	68
2.3.4 Final remarks: transcriptome analysis.....	71
2.3.5 Materials and methods: library benchmark study and SNPs exploration.....	72
2.3.5.1 Library preparation and sequencing .....	72
2.3.5.2 Transcript coverage .....	72
2.3.5.3 Differential expression analysis .....	72
2.3.5.4 RT-qPCR validation .....	72
2.3.5.5 Single nucleotide-polymorphisms (SNPs) analysis .....	73
2.3.6 Results and Discussion: library benchmark study and SNPs exploration .....	74
2.3.6.1 Library preparation and RNA-sequencing.....	74
2.3.6.2 Gene body coverage .....	74
2.3.6.3 Distribution of reads on different transcript length .....	75
2.3.6.4 Differentially expressed genes .....	76
2.3.6.5 RT-qPCR validation .....	78
2.3.6.6 SNP analysis .....	80
2.3.7 Conclusions.....	83
<b>2.4 Assessing the pyloric caeca and distal gut microbiota correlation with flesh colour in Atlantic salmon (<i>Salmo salar</i> L., 1758) .....</b>	<b>84</b>
2.4.1 Abstract .....	84
2.4.2 Introduction.....	84
2.4.3 Materials and methods.....	86
2.4.3.1 Study design and sample collection .....	86
2.4.3.2 DNA extraction and MiSeq sequencing.....	87
2.4.3.3 Microbial community profiling.....	87
2.4.3.4 Functional and metabolic pathway prediction .....	88
2.4.4 Results .....	88
2.4.4.1 The distinct difference between microbiota in the distal gut and the pyloric caeca .....	88
2.4.4.2 Distal gut microbiota correlates with salmon flesh colour .....	91
2.4.4.3 The correlation of microbiota in the pyloric caeca with banding status .....	91
2.4.4.4 Predictive function annotation of taxon composition related to banding in the pyloric caeca .....	94
2.4.5 Discussion .....	95
2.4.6 Conclusions.....	99
<b>2.5 Additional investigations on molecular and metabolic aspects of flesh colour .....</b>	<b>100</b>
2.5.1 Transcriptomic analysis on muscle and pyloric caeca associated with reduced flesh colour.....	100
2.5.1.2 Materials and methods .....	100
2.5.1.2.1 Transcriptomic analysis .....	100
2.5.1.2.2 RT-qPCR validation .....	102
2.5.1.2.3 Muscle histology.....	102
2.5.1.3 Results and discussion .....	102
2.5.1.3.1 General results .....	102
2.5.1.3.2 Comparison of different phenotypes (HN vs HB) in the front dorsal (FD) region .....	106
2.5.1.3.3 Comparison of different phenotypes (HN vs HB vs pale) in the back central (BC) region .....	108
2.5.1.3.4 Qualitative microscopic image analysis of muscle from different regions and colour phenotypes .....	111
2.5.1.3.5 Summary of muscle transcriptomic analysis .....	114
2.5.1.3.6 Comparison of different phenotypes (HN vs HB vs pale) in the pyloric caeca (PC) .....	114

2.5.1.3.7 Validation of DEGs using qPCR.....	117
2.5.1.4 Conclusions .....	118
2.5.2 Investigating the correlation between the metabolism of carotenoids and flesh colour in Atlantic salmon .....	119
2.5.2.1 Materials and methods .....	120
2.5.2.1.1 Standards and chemicals.....	120
2.5.2.1.2 Tissue and blood sample collection .....	120
2.5.2.1.3 Carotenoid extraction .....	120
2.5.2.1.4 Preparing a standard solution .....	121
2.5.2.1.5 Application of LC-MS using uHPLC/QTOF-MS (SCIEX X500R) for the analysis of carotenoid metabolites.....	121
2.5.2.1.6 LC-MS system with DAD-uHPLC/QQQ-MS (6470 Agilent Technologies) for the quantification of E-Ast/Can.....	122
2.5.2.2 Results.....	122
2.5.2.2.1 Quantification of all trans-astaxanthin and trans-canthaxanthin in multiple tissues and comparison of different flesh colour phenotypes.....	122
2.5.2.2.2 Determination of astaxanthin and canthaxanthin metabolites in multiple tissues in comparison of different flesh colour phenotypes.....	127
2.5.2.3 Discussion .....	127
2.5.2.3.1 The usage of E-Ast/E-Can and total Ast/Can in farmed Atlantic salmon .....	127
2.5.2.3.2 A hypothesized carotenoid metabolic pathway in Atlantic salmon .....	128
2.5.2.4 Conclusions .....	130
<b>Section 3 .....</b>	<b>131</b>
<b><i>Aim 3: Establish if there is a correlation between genetic background and reduced flesh colour.....</i></b>	<b>131</b>
3.1 Background and trial design.....	131
3.2 Summer mortality DNA sampling and post-summer performance including colour assessment with DNA sampling .....	133
3.2.1 Aims .....	133
3.2.2 Sampling design and methods of summer mortality DNA sampling.....	133
3.2.3 Sampling design and methods of post-summer assessment.....	134
3.2.4 Genetic methods .....	135
3.2.5 Colour assessment methodology.....	135
3.2.6 Techniques to calculate flesh colour loss .....	136
3.2.7 Statistical analysis .....	137
3.2.8 Results .....	138
3.2.8.1 Assessment data .....	138
3.2.8.2 Parentage assignment .....	139
3.2.8.3 Mortality distribution .....	140
3.2.8.4 Flesh colour .....	141
3.2.8.5 Heritability and trait correlation .....	142
3.3 Harvest performance and colour assessment with DNA sampling.....	146
3.3.1 Aims and commercial outcome .....	146
3.3.2 Materials and methods.....	147
3.3.3 Results .....	148
3.3.4 Conclusions.....	153
<b>Conclusions .....</b>	<b>155</b>
<b>Implications.....</b>	<b>157</b>
<b>Recommendations.....</b>	<b>157</b>
Further development .....	157

***Extension and Adoption..... 158***  
    ***Project coverage ..... 158***  
***Project materials developed ..... 159***  
***Appendices..... 160***  
***FRDC FINAL REPORT CHECKLIST ..... 1***

## List of Figures

<b>Fig. 1.1</b> The SalmoFan™ it is used to visually assess flesh colour level in Atlantic salmon (www.dsm.com). .....	22
<b>Fig. 2.1</b> Photos taken in a light box against a SalmoFan™ showing an Atlantic salmon fillet A) displaying a good flesh colour and B) affected by banding and general paleness (individuals from sampling in May). .....	24
<b>Fig. 2.2</b> Main environmental conditions (Average temperature °C, Salinity ppt and Oxygen saturation %) measured at the site during the assessment timeframe. The red arrows indicate the sampling events and the time these were carried out. 25	
<b>Fig. 2.3</b> Atlantic salmon fillet affected by banding showing the regions assessed during visual and Minolta colour assessment: 1 front dorsal and 2 back central. ....	27
<b>Fig. 2.4</b> Prevalence of deformities, gonads and intestine status during the sampling events carried out. In May, fish collected from cage 24 were starved for harvest resulting in an either an empty gut or containing casts. ....	28
<b>Fig. 2.5</b> Percentage (%) of fish that were found with no faeces in the gut (defined non feeder) plotted against the average temperature (°C) at the site during the samplings carried out (May sampling excluded from the graph as fish were starved and data averaged for the two cages in the first two sampling events). .....	29
<b>Fig. 2.6</b> Fish growth (kg) plotted against the average temperature (°C) at the site during the samplings carried out (data averaged for the two cages in the first two sampling events). .....	30
<b>Fig. 2.7</b> Average (±SD) colour score visually assigned according to SalmoFan™ to the front dorsal and back central region of Atlantic salmon sampled from the two cages assessed (23 and 24) during the sampling events carried out so far. ....	32
<b>Fig. 2.8</b> Whisker box plots of the colour score visually assigned according to SalmoFan™ to the front dorsal (top) and back central (bottom) regions of Atlantic salmon sampled from the two cages assessed (23 and 24) during the sampling events carried out. ....	33
<b>Fig. 2.9</b> Prevalence of banding categorised by severity plotted against average colour (average of the two regions assessed) and the average colour of the two regions assessed considered separately in Atlantic salmon sampled from the two cages assessed (23 and 24) during the sampling events carried out. ....	33
<b>Fig. 2.10</b> From top to bottom, L*, a* and b* values measured with the Minolta colourimeter in the two designated regions of the fillet (front dorsal and back central) during the samplings carried out (measurements were not taken in December). .....	34
<b>Fig. 2.11</b> Study design summary. a) a graph presenting the average temperature trending (blue columns) from Dec 2016 to Nov 2017. The flesh colour fluctuation in the population part of the study along the timeline is presented as front-dorsal colour (gray box), and back-central colour (orange box). The three-sampling time-points were Mar, Jun, and Aug (red arrows). b) an example of a fillet with good colour and no or the minimal difference between the dorsal and central area (no banding), and c) a pale fillet with uneven colour between the aforementioned areas (severe/ moderate banding). ....	38
<b>Fig. 2.12</b> a) A bar-plot presenting the microbiota shift across time-points. Phylum, class, order, family, genus, and species were shortened as P, C, O, F, G, and S, respectively. b) A PCoA of weighted Unifrac distance of the microbial taxa across time points: Mar (orange) was closely clustered while the taxa in Jun (blue) and Aug (red) were scattered. ....	41
<b>Fig. 2.13</b> a) Statistic PERMANOVA of the β-diversity of both weighted and unweighted Unifrac distance metrics in three categories: time-point, fleshcolour, and banding-status. * P ≤ 0.05, ** P ≤ 0.01, *** P ≤ 0.001. b) Spearman's correlation of the taxa and the groups in three categories. ....	42
<b>Fig. 2.14</b> Significantly differentiated taxa across metadata: a) time-point and b) flesh-colour. Phylum, class, order, family, genus, and species were shortened as P, C, O, F, G, and S, respectively. ....	43
<b>Fig. 2.15</b> The balance tree generated from the hierarchical clustering of OTUs over the time-points. The OTUs abundance values were log-transformed. Differentially represented families (F) and genus (G) clusters are detailed. ....	44
<b>Fig. 2.16</b> The balance tree generated from the hierarchical clustering of OTUs over the flesh colour groups. The OTUs abundance values were log-transformed. Differentially represented families (F) and genus (G) clusters are detailed. ....	44
<b>Fig. 2.17</b> The balance tree generated from the hierarchical clustering of OTUs over the flesh colour groups for each time point a) Mar, b) Jun, and c) Aug. The OTUs abundance values were log-transformed. Differentially represented families (F) and genus (G) clusters are detailed. ....	46
<b>Fig. 2.18</b> The balance tree generated from the hierarchical clustering of OTUs over the banding-status groups. The OTUs abundance values were log-transformed. Differentially represented families (F) and genus (G) clusters are detailed. ....	47
<b>Fig. 2.19</b> The prediction of metabolic pathways across the categories Flesh-colour and banding-status. The differential metabolic pathways that were predicted for a) flesh-colour: Flesh23–24 (red), Flesh25–26 (blue), Flesh29–31 (gray); and b) banding-status: Moderate (red), severe (blue) indicated the most common pathways for each category. c) Pearson's correlation of the metabolic pathways across the groups in all categories. The abundance of the metabolic pathways was log-transformed. ....	48
<b>Fig. 2.20</b> Differential KEGG pathways and Pearson's correlation of a), b) terpenoid biosynthesis, c), d) carotenoids, e), f) lipid, g), h) esterification, and i), j) lipopolyproteins metabolic pathways in response to flesh colour. Phylum, class, order, family, genus, and species were shortened as P, C, O, F, G, and S, respectively. The flesh colour groups were coloured as (red) Flesh21–22, (blue) Flesh23–24, (gray) Flesh25–26, (orange) Flesh27–28, and (green) Flesh29–31. ....	50
<b>Fig. 2.21</b> Differential KEGG pathways and Pearson's correlation a), b) terpenoid biosynthesis, c), d) carotenoids, e), f) lipid, g), h) esterification, and i), j) lipopolyproteins metabolic pathways in response to banding. Phylum, class, order, family, genus, and species were shortened as P, C, O, F, G, and S, respectively. The banding groups were coloured as (blue) none banding, (red) moderate banding, and (gray) severe banding. ....	51

<b>Fig. 2.22</b> The transition of flesh colour from pale to pink-red correlated with the transition of the microbiota composition. ....	55
<b>Fig. 2.23</b> The workflow of liver and gut transcriptomic analysis.....	58
<b>Fig. 2.24</b> The number of differentially expressed genes with four comparisons.....	62
<b>Fig. 2.25</b> The exogenous lipoprotein pathway modified from <sup>138</sup> .....	65
<b>Fig. 2.26</b> The endogenous lipoprotein pathway modified from <sup>138</sup> .....	65
<b>Fig. 2.27</b> The pathway of fatty acid degradation with upregulated O-palmitoyltransferase 1, liver isoform-like (orange colour).....	68
<b>Fig. 2.28</b> The pathway of HDL metabolism modified from <sup>138</sup> .....	69
<b>Fig. 2.29</b> Gene body coverage (a) and SH2 domain-containing protein 4A-like (Sh24a) gene body coverage (b) from the QuantSeq and TrueSeq libraries. Each line in Figure 1a represents the coverage of mapped reads from every library along with transcripts from the 5' to 3' ends in the whole Atlantic salmon genome. Figure 1b shows the distribution of mapped reads from QuantSeq and TrueSeq libraries on the exons of Sh2a4 gene from 5' to 3' end.....	74
<b>Fig. 2.30</b> Read counts (A) and percentage of mapped reads (B) for transcripts of different lengths between QuantSeq and TrueSeq libraries.....	76
<b>Fig. 2.31</b> Venn diagram of DEGs from TrueSeq and QuantSeq libraries and the variation within biological replicates of the 11 DEGs in Lexogen and TrueSeq data. HN - high colour none banding, LB - low colour, banding. ....	77
<b>Fig. 2.32</b> Comparison of variations within biological replicates of 15 DEGs in different libraries and RT-qPCR validation; a) In QuantSeq library; b) In TrueSeq library; c) In RT-qPCR.....	79
<b>Fig. 2.33</b> Structure of the NOX/Duox homologs (a) <sup>191</sup> and schematic illustration of SNPs on Dual oxidase 2 and Dual oxidase maturation factor (b).....	82
<b>Fig. 2.34</b> Examples of salmon fillets including high colour index with pink–red colour over whole fillet, low colour index with pale colour over whole fillet and banding with a colour difference between the dorsal (orange oval) and central back areas (black oval).....	85
<b>Fig. 2.35</b> Schematic drawing of the salmon gastrointestinal tract with pyloric caeca: pyloric caeca, midgut and distal gut. Dashed red rectangles and scissors denote the two regions collected in this study. ....	87
<b>Fig. 2.36</b> (A) The $\alpha$ -diversity (Shannon index) and (B) $\beta$ -diversity (principal coordinate analysis (PCoA)) by the weighted UniFrac distance between the microbiota in the distal gut and the microbiota in the pyloric caeca.....	88
<b>Fig. 2.37</b> (A) A phylogenetic tree representing the microbiota of both distal gut and pyloric caeca. The bacteria classes of <i>Actinobacteria</i> , <i>Betaproteobacteria</i> , <i>Alphaproteobacteria</i> , <i>Gammaproteobacteria</i> and Bacilli are highlighted in sky-blue, yellow, light green, pink and orange, respectively. The outer rings of circles indicate the presence, as percentages, of the corresponding taxa in the distal gut (purple circles) and the pyloric caeca (blue circles). (B) The differential taxa representing the distal gut (red bars) and pyloric caeca (blue bars). Phylum, class, order, family, genus and species are shortened to P, C, O, F, G and S, respectively. ....	90
<b>Fig. 2.38</b> Pearson's correlation between the distal gut microbiota and flesh colour phenotypes. The flesh colour phenotypes are presented as Flesh21-22 to Flesh27-29. The prefix "Di" represents the "distal gut" dataset. Phylum, class, order, family, genus and species are shortened to P, C, O, F, G and S, respectively. ....	91
<b>Fig. 2.39</b> (A) Principal coordinate analysis (PCoA) of the pyloric caeca microbiota, which was distanced with the weighted UniFrac algorithm with the PERMANOVA test. The flesh colour phenotypes are presented as follows: Flesh21-22 in red, Flesh23-24 in blue, Flesh25-26 in orange and Flesh27-29 in green. (B) Pearson's correlation of the pyloric caeca microbiota and flesh colour phenotypes. The flesh colour phenotypes are presented as Flesh21-22 to Flesh27-29. (C) LEfSE analysis with ANOVA test for each differential taxon; Flesh23-24 in red and Flesh27-29 in blue. (D) Spare partial least squares regression analysis to reveal the composition of the taxa that contributed to the phenotypes: Flesh21-22 in red, Flesh23-24 in blue, Flesh25-26 in grey and Flesh27-29 in yellow. Phylum, class, order, family, genus and species are shortened to P, C, O, F, G and S, respectively.....	92
<b>Fig. 2.40</b> (A) Principal coordinate analysis (PCoA) of the pyloric caeca microbiota, which was distanced with the weighted UniFrac algorithm with the PERMANOVA test. The banding phenotypes are presented as follows: None-banding in blue, Moderate-banding in red, and Severe-banding in orange. (B) Pearson's correlation of the pyloric caeca microbiota and banding phenotypes: None-banding, Moderate-banding and Severe-banding. (C) LEfSE analysis with ANOVA test for each differential taxon; None-banding in red and Severe-banding in blue. (D) Spare partial least squares regression analysis to reveal the composition taxa that contributed to the phenotypes: None-banding in blue, Moderate-banding and Severe-banding in grey. Phylum, class, order, family, genus and species are shortened to P, C, O, F, G and S, respectively.....	93
<b>Fig. 2.41</b> Regression model analysis to identify complex associations between phenotypes - (A) flesh-colour and (B) banding status - and <i>Carnobacterium</i> (G).....	94
<b>Fig. 2.42</b> Functional annotation of the pyloric caeca taxon composition differentiated in the different banding phenotypes. (A) Redundancy RDA analysis with * $p < 0.05$ , and (B) LEfSE analysis.....	95
<b>Fig. 2.43</b> The grouping of experimental fish based on the flesh colour, and FD (front dorsal) and BC (back central) regions sampled are marked by white squares. ....	101
<b>Fig. 2.44</b> Principal component analysis (PCA) of sequencing data comparing different tissues and different groups within each tissue. a) The comparison of PC, FD and BC regions; b) The comparison of HN (high), HB (banded) and pale fish in the PC; c) The comparison of HN (high), HB (banded) and pale fish in the BC region; d) The comparison of HN (high) and HB (banded) fish in the FD region. ....	104
<b>Fig. 2.45</b> Differentially expressed genes in comparisons between different phenotypes for each tissue.....	105

<b>Fig. 2.46</b> Visualization of genes differentially expressed (DEGs) between high colour - no banding (HN) and high colour - banded (HB) fish when comparing the back central (BC) and front dorsal (FD) regions. a) Venn diagram showing the overlapping DEGs between HN and HB groups b) The number of DEGs in HN and HB groups. ....	105
<b>Fig. 2.47</b> Important highly expressed genes in the front dorsal (FD) region. An average normalized count across transcripts is shown. Data is shown as Mean $\pm$ SE. (n=5). Means with different letters indicate significant differences (P < 0.05).....	106
<b>Fig. 2.48</b> Reverse cholesterol transport from peripheral tissues to liver by high-density lipoprotein (HDL). HDL particles carry cholesterol from peripheral tissues to the liver and also embed cholesteryl esters (CEs) by interchanging them for triglycerides (TG) with TG-rich lipoproteins. Gathering of CEs transforms the particle to spherical HDL3. HDL3 transfers CE, ApoA, ApoC and ApoE to enlarge its particle size which matures into HDL2. HDL2 then disposes of CE by docking into the scavenger receptor type B class I (BI). In this way, HDL enables the maintenance of extracellular cholesterol pool. Modified from <sup>271</sup> . HDL, high-density lipoprotein; VLDL, very low-density lipoprotein; CE-Ax, cholesteryl ester-Astaxanthin; Apo AI, apolipoprotein AI; All, apolipoprotein All; CI, apolipoprotein CI; E, apolipoprotein E; LCAT, lecithin:cholesterolacyl transferase. ....	108
<b>Fig. 2.49</b> The expression of important highly expressed genes in the back central region: HN vs Pale and HB vs Pale. An average normalized count across transcripts is presented. Data is shown as Mean $\pm$ SE, (n=5). Means with different letters indicate significant differences (P < 0.05). ....	110
<b>Fig. 2.50</b> Microscopy images of muscle showing the structural variations among HN (A and B) and HB fish (C and D). Figures A and B present longitudinal sections, while Figures C and D show transverse sections. MF: myofibrils; MC: myocommata; SR: sarcoplasmic reticulum; IM: intermyofibrillar spaces. ....	112
<b>Fig. 2.51</b> Histological sections of muscle showing structural variations among HN (A and B) HB fish (C and D) and pale fish (E and F). Figures A, C and E present longitudinal sections, while Figures B, D and F show transverse sections. MF: myofibrils; MC: myocommata; SR: sarcoplasmic reticulum; IM: intermyofibrillar spaces. ....	113
<b>Fig. 2.52</b> The expression of important highly expressed genes in the pyloric caeca (PC): HN vs Pale and HB vs Pale. An average normalized count across transcripts is presented. Data is shown as Mean $\pm$ SE. (n=5). Means with different letters indicate significant differences (P < 0.05). ....	115
<b>Fig. 2.53</b> Apolipoprotein in the transport pathway of lipoprotein metabolism: the chylomicrons (modified from <sup>271</sup> ). TG-Ax, triglycerides-Astaxanthin; B48, apolipoprotein B48; AI, apolipoprotein AI; All, apolipoprotein All; AIV, apolipoprotein AIV; AV, apolipoprotein AV; CI, apolipoprotein CI; CII, apolipoprotein CII; CIII, apolipoprotein CIII; E, apolipoprotein E; All, CE, cholesteryl esters; LDL receptor, low-density lipoprotein receptor; LRP, LDL receptor-like protein. ....	116
<b>Fig. 2.54</b> Some typical DEGs in multiple tissues were validated using qPCR. In back central (BC) region: Acta2, Myo1b and Lipase; in front dorsal (FD) region: Lepr, ApoCI; in pyloric caeca: ApoAI, Aactn1l. The averages significantly different from other ones are highlighted by “*” (P < 0.05) or “***” (P < 0.01) symbol. ....	118
<b>Fig. 2.55</b> The TOF-MS fragment ions of all-trans-Astaxanthin (a) and trans-Canthaxanthin (b) standards. ....	122
<b>Fig. 2.56</b> The standard curve for quantification using LC-MS/QQQ. a) astaxanthin; b) canthaxanthin. The black dots represent the standard values (E_Ast or E-Can) while green dots stand for the internal standard (E-Apo). ....	123
<b>Fig. 2.57</b> The predicted pathway and semi-quantitative analysis of astaxanthin, canthaxanthin and their metabolites in multiple organs of Atlantic salmon. ....	126
<b>Fig. 2.58</b> Comparisons between the proportion of E-Ast/E-Can and total Ast/Can in different flesh colour phenotypes and multiple tissues. A) The proportion of E-Ast; B) The proportion of total Ast; C) The proportion of E-Can; D) The proportion of total Can. ....	128
<b>Fig. 2.59</b> The hypothesised metabolic conversation of Astaxanthin and Canthaxanthin from <sup>312</sup> . ....	129
<b>Fig. 3.1</b> Panel showing the different steps of the spawning for the genetic component trial: A) fertilisation of eggs in a bowl with the label identifying the female used (fin-clip tube ID), B) Tray incubators with the cross female-neomale identification code (the neomale code is not reported for the following trays as position of trays will never change until pooling). Each tray was divided in half by using a segregator to allow allocation of two progenies, C) Dr Amoroso placing the fertilised eggs into a tray incubator. ....	132
<b>Fig. 3.2</b> Number of samples collected (cages pooled) per week (weekly events pooled) plotted against the average weekly temperature at the site. ....	134
<b>Fig. 3.3</b> Images taken inside the lightbox with standardised light conditions during the post-summer assessment. A fillet with good colour (right) and one with reduced colour and banding (left). ....	135
<b>Fig. 3.4</b> Regions extracted from each fillet image. ....	136
<b>Fig. 3.5</b> Colour loss phenotype. ....	136
<b>Fig. 3.6</b> Illustration of the three methods of capturing the level of flesh colour loss with image analysis on the NQC (D-F). ....	138
<b>Fig. 3.7</b> Relationship between size, traits and cage with original and re-assigned cage number in brackets. ....	139
<b>Fig. 3.8</b> Relationship between length, condition factor, and deformity/maturity. ....	139
<b>Fig. 3.9</b> Proportion of mortality per family calculated as number of mortalities genotyped / (number of April colour samples + mortality) genotyped per family in each cage ranked from lowest to highest. ....	140
<b>Fig. 3.10</b> Proportion of mortality (cages pooled) per family in each period ranked from lowest to highest calculated as number of mortalities genotyped in a period (total mortality / number of April colour samples). ....	141
<b>Fig. 3.11</b> Relationship between colour <i>a</i> * intensity (panel a), proportion >25 Salmofan™ (panel b) colouration index (panel c), mean relative sum (panel d) and cage. ....	141

<b>Fig. 3.12</b> Relationship between weight and colour intensity (a), weight and proportion >25 SalmoFan™ (b), weight and colouration index (c), weight and mean relative sum of SalmoFan™ values (d), k and colour intensity (panel e), k and proportion SalmoFan™ values >25 (f), k and colouration index (g), k and mean relative sum of SalmoFan™ values (h). ....	142
<b>Fig. 3.13</b> Distribution of colour values in each family (assigned dam) reordered by the highest to the lowest colour (region E SalmoFan™). .....	144
<b>Fig. 3.14</b> Distribution of colour values in each family (assigned sire) reordered by the highest to the lowest colour (region E SalmoFan™). .....	145
<b>Fig. 3.15</b> Mean weight and colour (region E SalmoFan™), and proportion of mortality for each assigned parent, where the size of each circle is relative to the proportion of mortality associated with that family. High mortality families indicated in are denoted by an asterisk. ....	146
<b>Fig. 3.16</b> Different tasks performed during the harvest assessment. ....	147
<b>Fig. 3.17</b> Relationship between size traits and cage. ....	148
<b>Fig. 3.18</b> Relationship between length, condition factor, and deformity. ....	148
<b>Fig. 3.19</b> Distribution of individual colour values grouped by family (dam) reordered by mean family colour (mean relative sum of NQC and dorsal slice). ....	150
<b>Fig. 3.20</b> Distribution of individual colour values grouped by sire reordered by mean sire colour (mean relative sum of NQC and dorsal slice) .....	151
<b>Fig. 3.21</b> Relationship between family means of post-summer and harvest weight. ....	152
<b>Fig. 3.22</b> Relationship between family means of post-summer and harvest flesh colour. ....	152
<b>Fig. 3.23</b> Relationship between family mean flesh colour, harvest weight and proportion of mortality. High mortality families indicated are denoted by an asterisk. ....	153

## List of Tables

<b>Table 2.1</b> Average ( $\pm$ SD i.e. StdDev) of several performance indicators of Atlantic salmon from the two cages assessed (23 and 24) during the sampling events carried out between December 2016 – August 2017. Count of Population indicates the number of fish assessed at each sampling event.....	31
<b>Table 2.2</b> The group of samples for transcriptome analysis. All samples were collected on the 6/6 2017 and belonged to sampling group C. ....	57
<b>Table 2.3</b> Statistical sequencing data of 78 samples in <i>Salmo salar</i> . ....	59
<b>Table 2.4</b> The selective DEGs in the comparisons of LN_vs_LB .....	63
<b>Table 2.5</b> The selective DEGs in the comparisons of HN_vs_HB.....	64
<b>Table 2.6</b> The selective DEGs in the comparisons of HB_vs_LB.....	67
<b>Table 2.7</b> The selective DEGs in the comparisons of HN_vs_LN .....	70
<b>Table 2.8</b> Sixteen genes selected for validating with RT-qPCR .....	73
<b>Table 2.9</b> Eleven differential expressed genes that overlapped between the TrueSeq and QuantSeq libraries.....	78
<b>Table 2.10</b> Forty samples selected for transcriptomic analysis .....	102
<b>Table 2.11</b> The LC gradient conditions used for the separation of carotenoids .....	121
<b>Table 2.12</b> Quantitative analysis of the concentration of all-trans-astaxanthin and trans-canthaxanthin in multiple tissues in comparisons of different flesh colour phenotypes using LC/QQQ-MS system.....	125
<b>Table 3.1</b> Heritability (highlighted), genetic and phenotypic correlations for size and colour traits excluding the mean relative sum values. Genetic correlations are above the heritabilities and phenotypic correlations below the heritabilities. Roche = SalmoFan™.....	143
<b>Table 3.2</b> Heritability (highlighted), genetic and phenotypic correlations for size and colour traits excluding the colouration index. Genetic correlations are above the heritabilities and phenotypic correlations below the heritabilities. Roche = SalmoFan™.....	143
<b>Table 3.3</b> Trait heritability estimates (white text, blue background), genetic correlations (upper diagonal panel) and phenotypic correlation statistics (lower diagonal panel) considering all three assessments together. Phenotypic correlations calculation is possible for some traits only. ....	149

## Acknowledgments

The investigators would like to thank Petuna and all the staff involved in the project at all different levels and points in time for their immense help, patience, and support. Not many are aware of how much work and coordination are required to run a project of this size and duration within commercial reality. Your effort has eventually led to the achievement of a critical milestone at Petuna that is the establishment of a cutting-edge selective breeding program. Thanks again for making this project so successful. Also, thanks to Xelect for their invaluable work and assistance with all the genetic and colour analyses and for always providing results in a timely manner and in a format easy to understand and of high visual impact.

We would like to thank USC DVC-R&I, Prof Roland DeMarco, for his generous financial support of this project and USC and VIED for supporting the two talented PhD students, Dr Chan Nguyen and Ms Thi Minh Thu Vo who greatly contributed to our discoveries. We thank Dr Trong Tran for his expert support and training for our carotenoid analysis and Dr Tuan Nguyen for his expert bioinformatic support.

## Executive Summary

This report describes critical findings and new knowledge on flesh colour variation, from both a genetic and a molecular perspective, in Atlantic salmon in Tasmania. The investigation on flesh colour variation, due to its strong correlation with high seawater temperature, led to new important insights into thermal tolerance in Atlantic salmon and their performance in a context of climate change and global warming.

The project was carried out between June 2016 and June 2020 and was the result of a collaboration between the University of the Sunshine Coast (USC) and Petuna Aquaculture (Petuna), initiated by Dr Mark Porter and Prof Abigail Elizur. The principal investigator of the project was Prof. Abigail Elizur (USC) and she was supported by two co-investigator, Dr. Tomer Ventura (USC) and Dr. Gianluca Amoroso (Petuna). Two additional co-investigators from USC, Dr. Chan D.H. Nguyen and Ms Thu T.M. Vo, were included at a later stage in order to carry out part of the research required for the project completion and formed part of their PhD projects. The investigation of the fish took place in northern Tasmania where Petuna owns both freshwater and marine sites and all the laboratory work was undertaken at both USC Genecology Research Centre and at Xelect, a genetic services provider based in Scotland (UK).

This project was originally designed to study an issue which is impacting commercial production in Petuna. Flesh colour variation post-summer (at times extending to harvest), had been identified during 2015-16 by Petuna to affect commercial value. As this issue is not impacting Petuna only, this project was expected to generate important knowledge on the factors which contribute to reduced flesh colour in Atlantic salmon stocks and result in significant 'spill-over' of information that will assist the wider Tasmanian salmon industry.

Flesh colour in Atlantic salmon is considered a fundamental, if not the most important, quality parameter, and affects acceptance and price of the product. The dietary pigments responsible for flesh colour (i.e. astaxanthin and canthaxanthin) are expensive and represent 6-8% of the total production cost. Therefore, reduced flesh colour in the stock results in considerable economic losses. Several factors have been shown to impact flesh colour (e.g. environment, diet formulation, size, genetics) highlighting the complexity underlying the variation. As only a portion of the Petuna stock showed variable/reduced flesh colour (and as in other locations, the inclusion of pigments in feed currently used generally produces an acceptable product for the market), the project focused on the possible genetic effect on the trait. Furthermore, due to a general lack of knowledge of the molecular mechanisms responsible for flesh colour and its metabolism in general, which involves multiple organs and tissues, and given the opportunity to compare good and affected individuals, such investigations were also undertaken. Detection and understanding of the variation affecting flesh colour in Atlantic salmon are fundamental in order to improve marketability of the product.

The project had overall three aims:

1. Identify the type of flesh colour variations and their prevalence at Petuna and assess the magnitude of their economic impact.
2. Identify molecular events associated with reduced flesh colour in several tissues.

3. Establish if there is a correlation between genetic background and reduced flesh colour.

To achieve aim 1, the investigators started with drafting a literature review on flesh colour in Atlantic salmon. That was followed by an economic impact assessment. The economic impact of flesh colour variation could be accurately estimated by using internal data collected during standard commercial operations.

Aim 2 was achieved by running a longitudinal assessment during 2017 on a commercial stock affected by colour variation in order to first detect occurrence and development of the trait and then investigate the possible correlation between gut microbiota and colour variation as well as differences in gene expression in liver and gut between good and affected (i.e. displaying colour loss) individuals. This aim also included a further sampling in 2019 and analyses of another commercial stock at the same site, this time with known genetics (population used in aim 3), to focus on the timepoint where the highest variation in colour is usually observed (post-summer). The aim was to deepen the knowledge on the aforementioned aspects by conducting further gut microbiota, gene expression and metabolic analyses.

Aim 3 required a long planning, set up phase and execution due to the lack of a population with known genetics within the Petuna stock as well as the required infrastructure to create one and follow its entire production cycle. After the purchase of dedicated incubators and the necessary genetic analysis to exclude relatedness and detect different genetic lines, such a population was created in 2017 and then assessed in 2019. Initially, the plan was to grow the population in freshwater, transfer it to sea (keeping it separate from the rest of the stock in both phases) and assess it post-summer (i.e. a period when the highest variation in flesh colour is observed) for different performance traits, with a focus on flesh colour, to identify a possible genetic effect and also carry out scheduled experiments for aim 2. The tasks required by this aim, as well as the extensive planning within the company to guarantee their completion, attracted a lot of attention within the Petuna management team. Eventually, the attention grew to the point where Petuna requested a one-year extension of the project in order to include two additional assessments consisting of a summer mortality and a harvest genetic assessment. In fact, Petuna saw the opportunity to lay the foundation for a genetic improvement program focusing on improving flesh colour and overall general performance of fish exposed to high summer seawater temperatures in light of the current and future effects of climate change. While the post-summer and harvest assessments were run in the same way, by assessing individuals for size, flesh colour, and genetics, the summer mortality assessment was performed by collecting naturally occurring normal looking mortalities (i.e. water temperature likely being the cause of death) from January to March and identify their genetics. Overall, the outcome of this assessment would be providing the tools for producing more resilient fish that can have good quality and performance when exposed to high seawater temperatures.

## Results/key findings

The current FRDC project, since spanning over approximately four years, produced a considerable amount of results. Given the nature of the project which investigated several aspects concerning the biology of farmed Atlantic salmon, the list of findings appears to be quite vast and diverse. Nevertheless, we have tried to capture below the key findings by discussing them according to their relevant aim.

As part of aim 2, we had the possibility to describe comprehensively a recurrent flesh colour loss affecting fish stocked at a particular marine site. We were also able to collect samples during two different events in two different years (2017 and 2019) which were critical to broaden our knowledge of flesh pigmentation and its loss in Atlantic salmon, from different point of view such as microbiota effect, molecular mechanisms and metabolism.

From the analysis of the samples from 2017, we demonstrated a significant correlation between the microbiota and the colour of the fillet, meaning that fish affected by colour loss or having good colour have different microbiota. By using the same samples, we also detected in the gut and liver several groups of genes correlating in expression pattern to either the fish affected by colour loss or the ones having good colour.

From the analysis of the samples from 2019, we demonstrated a significant correlation of *Carnobacterium* (G) with fish having good colour and the absence of regional colour loss (i.e., banding). We also found a correlation of the salmon pyloric caeca microbiota with the banding phenomenon. Based on the differential gene expression observed in muscle and other tissues, we could link flesh colour loss to muscle structural integrity and metabolism of protein and lipid. We believe that the proteolytic process in muscle could cause carotenoid-binding proteins to become degraded, and as a consequence lead to the release of free carotenoids which are transported together with lipids as part of the lipid metabolic pathway. Finally, we shed further light on the metabolism of carotenoids and the dynamics of both Astaxanthin and Canthaxanthin.

As part of aim 3, we carried out the first thorough genetic investigation ever conducted on Petuna commercial stocks. We were able to demonstrate the presence of a genetic effect on flesh colour loss (as well as good colour) and performance in individuals assessed both post-summer after thermal stress and at harvest. A genetic effect was also found for thermal tolerance (reduced mortality) at high summer temperatures. These results taken together have led to the establishment of a selective breeding program at Petuna.

## Implications for relevant stakeholders

The results of this project have the potential to benefit the industry in different aspects.

Firstly, the benefits deriving from a genetic improvement are evident and this is well established. Nevertheless, our results have shown that it is possible to select fish with higher thermal tolerance and improve their quality (specifically flesh colour) and performance by running targeted assessments at critical stages of production. It is not uncommon nowadays to see on the media continuous mention of the urge for new strategies for the aquaculture sector to prevent the heavy impact of fast-changing environmental conditions leading to a rise in seawater temperatures.

Secondly, in light of the results of the molecular investigations on flesh colour, we can say that this project has contributed to the expansion of knowledge on topics which had been poorly explored and

which are of critical importance for the scientific community, the feed suppliers and the salmon industry in general. Having a deeper understanding of the role played by the microbiota, the molecular mechanisms behind flesh colour and its metabolism, paves the way to fully comprehend how pigments travel, are utilised, and ultimately deposited in Atlantic salmon. Hopefully, this will lead to feed formulations with improved pigmentation efficacy and efficiency and, given the cost of pigments inclusion, to save a considerable amount of money.

All in all, this trial has produced critical and, in part novel, findings on the molecular and genetic component of flesh colour loss and performance of fish exposed to high summer water temperatures. The clear and encouraging results have led to the establishment of the Petuna breeding program which has recently produced for the first time a generation of individuals with genetic gain. This represents the first step of producing fish that are more robust and thermal tolerant. This is particularly important in light of climate change and increasing seawater temperature, which will make it harder to produce Atlantic salmon, not just in Tasmania but all around the world. Although being one of the first places where the impact of climate change on Atlantic salmon aquaculture will be felt, Tasmania also represents an optimal experimental ground. In fact, here the industry can start experimenting and get ready, before other countries do, to cope with the new environmental challenges and eventually succeed in breeding “climate-proof” fish. The findings of this trial have demonstrated that this is achievable.

#### **Keywords**

**Atlantic salmon, *Salmo salar*, aquaculture, flesh colour, pigmentation, carotenoids, microbiome, transcriptome, genetics, thermal tolerance.**

*All procedures described in this report were carried out with the approval of the University of the Sunshine Coast Animal Ethics Committee (AN/E/16/12).*

## **Section 1**

### **Aim 1: Identify the type of flesh colour variations and their prevalence at Petuna and assess the magnitude of their economic impact.**

This section serves as introduction: it provides a clear and concise background and explains the needs for the project. This was originally prepared to fulfil aim 1 which required a description of the issues encountered as well as of their economic impact based on the data available at that time. Finally, to support what was discussed in the report, we included a thorough literature review on both issues.

#### **1.1 Flesh colour issue in Petuna stocks - background**

During the 2016 financial year (FY16), Petuna identified significant variation in flesh colour in individuals stocked at one of its marine sites. The site is located in northern Tasmania and is generally subjected to high summer temperatures (> 20°C) which, if lasting for a prolonged period of time, may expose Atlantic salmon to thermal stress which impairs feeding and growth and deleteriously impacts flesh colour. Investigations carried out within the company, suggested that the problem might lie in an impaired uptake (possibly due to loss of appetite when the water temperature is too high with consequent hypoxia) and/or loss of carotenoids already stored (possibly due to decrease in condition factor and utilisation of carotenoids to cope with oxidative stress) during summer, resulting in significant loss of colour (i.e. pale fillets) or fading that is generally accentuated in the dorsal and ventral parts of the fillet (also known as banding).

##### **1.1.1 Economic impact of inadequate flesh colour within Petuna**

Routine visual colour assessments carried out during FY16 on fish falling under two marketable size ranges (i.e. 2-4 kg and 4+ kg) found a portion of the individuals assessed being rejected for being pale. A flesh colour that does not meet the expectations of the market lead to dissatisfaction, loss of competitiveness, drop in the value of the product and consequent economic losses. In light of the quantity of pale fillets produced, in FY16 Petuna lost approximately 1.9 million AUD for not being able to sell at full sale price fillets with inadequate flesh colour. The loss was calculated by using internal data and due to the information being commercial in confidence the calculations cannot be disclosed.

##### **1.1.2 Remarks**

As shown in the previous paragraph, the unexpected severity of the problem with Atlantic salmon flesh colour in FY16 impacted Petuna considerably. The problem had been particularly significant in that year of production and could possibly be explained by the extreme summer temperatures recorded during summer 2015-2016. Nevertheless, the problem has been present for many years with the annual fluctuations in temperature resulting in variable impacts on flesh colour. The variation was observed in individuals belonging to the same year class and exposed to the same environmental conditions suggesting that a different genetic response to challenging conditions may be present.

Although the deleterious effect of summer temperatures had been ascertained, detailed understanding of the actual mechanisms behind the impaired uptake and/or loss of pigments and methods to ameliorate the issue are lacking. To tackle the issue, the current project adopted a multiple approaches design. The mechanisms underlying the issue were investigated through different molecular analyses targeting several organs involved in pigments metabolism as well as the microbiota of Atlantic salmon. The analyses aimed at detecting the pathway/s responsible for the problem and

paved the way to short-term interventions via nutritional adjustments. Furthermore, performance of populations belonging to different genetic families part of the Petuna broodstock were measured during a full production cycle to understand the genetic component of flesh colour. This analysis can eventually enable stock selection at every spawning event, preferentially, choosing the families that have shown to produce individuals able to cope with high summer temperatures and improve overall flesh colour as well as other traits highly correlated with it such as growth. This approach will lead to a reduction of the aforementioned economic losses and at the same time will ensure increased animal welfare in an environment subjected to high seawater temperature and most likely impacted by climate change in the years to come.

## **1.2 Flesh colour in Atlantic salmon – A review**

### **1.2.1 Carotenoids and their importance**

The distinctive pink-red colour of the flesh of Atlantic salmon and other salmonids, technically referred to as pigmentation, is considered a fundamental and likely the most important criterion of quality and freshness. Adequate flesh colour has a huge economic importance for Atlantic salmon producers as a properly pigmented fillet is more likely to be sold at a higher price<sup>1,2,11,12,3-10</sup>. Carotenoids are the organic pigments responsible for salmonids flesh colour. These pigments are synthesised *de novo* mainly by plants and protists, meaning that animals can assimilate them through the diet only<sup>1,10,11,13-15</sup>. Wild Atlantic salmon obtains carotenoids feeding on zooplankton or on preys that previously ingested carotenoids, while farmed Atlantic salmon rely on a synthetic form of carotenoids, which is included in commercial diets<sup>1,10,11,13-15</sup>. Two carotenoids in particular are found in the Atlantic salmon flesh, astaxanthin (3,3'- dihydroxy- $\beta$ ,  $\beta$ -carotene-4,4'-dione) and canthaxanthin ( $\beta$ , $\beta$ -carotene-4,4'-dione). Nevertheless, the most abundant (accounting for approximately the 95% of all carotenoids present) is astaxanthin which consequently is chemically synthesised and added to the diets<sup>1,3,5,7,10</sup>. Although early studies suggested that astaxanthin is better utilised and deposited compared to canthaxanthin<sup>1,3,10</sup>, most recently it has been shown that the assumption was not correct and canthaxanthin has comparable retention rate in the muscle and pigmentation efficacy<sup>15-17</sup>. Nowadays, mainly astaxanthin is used in commercial diets as it is considered more natural, being the most abundant carotenoid in wild Atlantic salmon<sup>17</sup>. Astaxanthin is included in the diets at a rate between 40 and 100 mg kg<sup>-1</sup> and the use of carotenoids in commercially produced diets represents 15-25% of the total feed costs, or about 6-10% of the total production cost<sup>6,10,15,17</sup>. Therefore, assessing the capacity to assimilate the pigment effectively has significant commercial implications.

### **1.2.2 Carotenoids metabolism**

Atlantic salmon absorbs carotenoids in the intestine and deposits them in the muscle tissue in their free (unesterified) form<sup>1,3,11</sup>. Carotenoids can be stored also in the skin and the ovaries of maturing individuals<sup>1,3</sup>. Deposition of carotenoids in the muscle starts usually at a weight > 400 g and although at a lower weight Atlantic salmon are still able to assimilate and metabolised carotenoids, these are deposited mostly in the skin<sup>1,10</sup>. Nevertheless, deposition in the muscle is still possible even in 100 g individuals<sup>18</sup>. The rate at which carotenoids are currently supplemented in diets is based on studies showing that a plateau in absorption is generally reached (i.e. no change in final pigmentation and flesh carotenoid content), likely due to saturation at the site of deposition, when Atlantic salmon are fed continuously a dose of 60 mg kg<sup>-1</sup><sup>3,7,10</sup>. However, it has been observed that absorption of higher doses of carotenoids is still possible at increasing size and when Atlantic salmon grow at a slower rate, implying interconnections between growth and pigmentation<sup>3,17</sup>. In regard to the amount of astaxanthin present in the flesh of Atlantic salmon, varying quantities between 3 and 11 mg kg<sup>-1</sup> have

been reported so far <sup>5,11</sup>. Generally, based on colour visual assessment, a carotenoid content exceeding 8 mg kg<sup>-1</sup> is acceptable by the market <sup>10</sup>.

The quantity of carotenoids that is used for flesh pigmentation varies in the range of 1 to 22% <sup>1,6,8,10,19</sup>. This poor utilisation is mainly explained by poor assimilation in the intestine where 30 to 70% of carotenoids are lost in the faeces <sup>19</sup>. Carotenoids have also lower digestibility compared to other major nutrients may underlie their poor absorption <sup>1,8,10,19,20</sup>. In addition, assimilated carotenoids are usually poorly retained in the muscle for unclear reasons <sup>19</sup>. To date, metabolism of carotenoids and mechanisms of retention in Atlantic salmon are still poorly understood <sup>13,14</sup> as well as the genes responsible for the whole metabolic process. However, it is thought that astaxanthin and canthaxanthin in Atlantic salmon may have different physiological pathways due to their selective deposition in different tissues <sup>1</sup>. Only recently,  $\alpha$ -actinin has been identified as the protein likely responsible for astaxanthin long-term retention in Atlantic salmon flesh <sup>13</sup>. Among the understood metabolic aspects, it is known that astaxanthin content in the flesh is positively correlated with fat content <sup>19</sup>. Fat and carotenoid metabolism are linked and uptake, transport and delivery of carotenoids is closely associated with the same processes involving fatty acids <sup>14</sup>. It has been demonstrated that astaxanthin is converted to idoxanthin and the protein responsible for its transport may be albumin, although further elucidation is required <sup>21</sup>. Both liver and bile play a role in the metabolism and excretion of carotenoids in Atlantic salmon <sup>10</sup>, as also confirmed through radiolabelling <sup>22</sup>. Nevertheless, astaxanthin metabolic processes in the liver require further investigation <sup>14</sup>. The exact role of carotenoids in salmonids is not understood. However, their positive biological function is confirmed by the fact that they promote growth in Atlantic salmon and enhance survival at early stages of development <sup>23</sup>. In addition, mobilisation of carotenoids from flesh of mature fish to ovaries and eggs again implies a key biological role during reproduction <sup>7,24</sup>. As extensively reviewed in <sup>1</sup>, the following roles of carotenoids have been proposed for salmonids, based on mammalian models: fertilisation hormone, source of pigments for chromatophores, function in respiration, protection from light, resistance to elevated temperature and ammonia and antioxidant. Nevertheless, to date all these functions remain elusive.

### **1.2.3 Variation in flesh colour**

Variation in pigmentation, carotenoid content and consequent impact on colour visualisation can be present in Atlantic salmon individuals belonging to the same year class and been exposed to the same conditions <sup>4,6,8,19</sup>. Given the economic relevance of flesh colour, it is critical to have a clear understanding of the reasons leading to variation. Pigment variation can be due to several factors such as the type of carotenoid fed, carotenoid concentration, fish size, physiological stage, environmental conditions, diseases, genetic background and time of carotenoid feeding <sup>6</sup>. Furthermore, there is a general variation in colour between the different parts of the fillet. In fact, astaxanthin deposition varies longitudinally resulting in the caudal part being 30-40% more pigmented than the anterior part <sup>19</sup>. Moreover, dorsal and midline areas are more pigmented than the belly flap (which has a high fat content) and the myotomes interconnections (“zebra-stripes”) <sup>19</sup>. The stage of development and sexual maturation both contribute to the variation as juvenile Atlantic salmon tend to accumulate carotenoids in the skin only up to 400 g and maturing salmon generally lose colour due to mobilisation of carotenoids from flesh and skin to ovaries, which allows pigmentation of the eggs <sup>1,4,7</sup>. Genetics has been shown to have an effect on flesh colour, with heritability being between medium to low and possibly impacting on carotenoids metabolism and influencing important traits linked to it, such as growth <sup>4,8,25,26</sup>. In particular, there seems to be a strong correlation between fish size, growth rate and

carotenoid absorption and deposition capacity<sup>4</sup>. Generally, fish which grow at a normal rate and in optimal rearing conditions are expected to present a better colour and higher content of pigments at increasing sizes due to an enhancement of absorption and deposition rates<sup>3,4</sup>. In support of that, some studies have shown considerable variation in flesh colour between fish from the same population and belonging to different weight classes implying again that bigger fish tend to have a better flesh colour<sup>4,19</sup>. In light of the above, weight class selection to meet different demand for colour by the market is considered to be a successful strategy<sup>19</sup>. On the other hand, high growth rate may impact on absorption and deposition of carotenoids<sup>4,17</sup>. It has been reported that fish which grow too fast have different muscle fibre arrangement compared to slower-growing fish and muscle fibre density has been linked to variation in colour visualisation in Atlantic salmon (i.e. density positively correlated with redness of SalmoFan™ score)<sup>27,28</sup>. Finally, in Atlantic salmon flesh colour can vary and be negatively affected by the effect of slaughter, processing and storage which lead to an enhanced loss or discolouration of the pigments<sup>1,19</sup>. It is therefore clear that many factors need to be considered for securing optimal pigmentation in the final product.

#### **1.2.4 Flesh colour assessment**

For the Atlantic salmon industry it is critical that flesh colour is assessed and measured by using quick and inexpensive methods<sup>5</sup>. As extensively reviewed in<sup>5,10,11</sup> there are currently three ways of assessing flesh colour in Atlantic salmon: estimate of colour appearance (performed visually by a sensory panel), measurement of reflectance (using a colourimeter or photography with image analysis) and chemical analysis for carotenoid quantification (HPLC analysis or near-infrared reflectance, NIR).

The most used method, being the quickest and most inexpensive, is to estimate colour appearance which involves making a visual comparison between the fillet and a card reporting a scale of colours<sup>10,11</sup>. This card is known as Colour Card for Salmonids™ (or SalmoFan™) and was created for Hoffmann-La Roche<sup>29</sup> (Fig. 1.1). The card displays different shades of pink-red based on asthaxantin pigmentation and each shade has an assigned score going from 20 to 34, being 20 the lightest shade (pale pink/yellow) and 34 the darkest (deep red). Although considered an efficient method, being based on sight, a visual assessment may present some drawbacks even if carried out by a trained sensory panel. In particular, humans have a limited ability to remember colours and their colour perception can be subjective and affected by the intensity of colour, light conditions, background of the assessment environment, presentation of the sample (e.g. superficial water film or excess of connective tissue), difference in distribution of the colour in the fillet and even fat content<sup>2,3,5,10,11,19</sup>. In fact, a higher content of lipids in the fillet can affect perception of colour and “dilute” the pigments<sup>5</sup>. Therefore, a very fat fillet with an actual high content of astaxanthin might not display the redness expected<sup>10</sup>. It is believed that lipids may impact on the appearance of the colour and make it more opaque<sup>17</sup>. An additional problem is that at astaxanthin concentration exceeding 8 mg kg<sup>-1</sup> the human eye becomes saturated and the assessment of the colour appearance cannot be performed correctly<sup>19</sup>. Although visual score is highly correlated to carotenoid concentration in the flesh (~0.99)<sup>5</sup>, again the visual score is less efficient at high carotenoid concentrations where visual score correlation with concentration becomes non-linear<sup>1,4,5,11</sup>. Standardisation of the assessment environment helps to improve visual estimate accuracy<sup>29</sup>. Light boxes can be used to standardise the conditions as illumination is under control and uniform (fluorescent lighting under the specified colour temperature >5000 K is recommended)<sup>26,30</sup>. Nevertheless, standardisation of the conditions may still be affected by light box model, light used and light box colour<sup>11</sup>.



**Fig. 1.1** The SalmoFan™ it is used to visually assess flesh colour level in Atlantic salmon ([www.dsm.com](http://www.dsm.com)).

Flesh colour can be assessed also by using instrumental colour reflectance measurements<sup>2,10,11</sup>. The most common instrument used for such analysis is the Minolta Chroma colourimeter produced by Minolta Camera Co. Ltd., Osaka, Japan, which allows to measure colour directly on the fillet<sup>10,11,19</sup>. The measurement relies on the L\*a\*b\* system based on the International Commission on Illumination recommendations where L\* represents lightness, a\* red-green chromaticity and b\* yellow-blue chromaticity. In salmon colour, a\* corresponds to redness and b\* to yellowness<sup>2,19,31</sup>. In addition, the values of quantitative Hue ( $H^{\circ}_{ab}$ ) and quantitative Chroma ( $C^*_{ab}$ ) can be retrieved from the L\*, a\*, b\* values<sup>10,11</sup>. All the aforementioned values can also be obtained by using simple photography and inexpensive or free softwares provided that photos are taken in standardised conditions (i.e. inside a light box with standardised illumination) and the superficial water film is blotted<sup>32,33</sup>. As described in<sup>11</sup>, the Hue ( $H^{\circ}_{ab}$ ) is the relationship between the fillet yellowness and redness [ $H^{\circ}_{ab} = \tan^{-1}b^*/a^*$ ] and an angular measurement where the red hue is denoted by the angle of 0° ( $H^{\circ}_{ab} = 0$ ), and the yellow hue is denoted by angle of 90° ( $H^{\circ}_{ab} = 90$ ). The  $C^*_{ab}$  is an expression of the saturation or intensity and clarity of the colour and is expressed as a relationship between the a\* & b\* values, calculated as  $C^*_{ab} = (a^{*2} + b^{*2})^{1/2}$ . The more intense the colour, the higher is the C\* value. It has been shown that a\*, b\* & C\* increase with increasing astaxanthin concentration in the fillet while L\* decreases<sup>2,5,30</sup>. In particular, a\* (redness) gives the best indication of increasing carotenoid level<sup>19</sup>. However, there seems to be no linear relationship between a\*, b\* & C\* value and the astaxanthin concentration as well as L\* and Hue<sup>5</sup>. In addition, a positive correlation between fat content in the fillet and a\* & b\* values has been found so that higher fat content results in higher a\* & b\* values at the same concentration of carotenoid<sup>34</sup>. Due to the different nature of the two methods of colour assessment it is challenging to compare the colour parameters obtained through visual assessment with those obtained by Minolta measurements<sup>2</sup>. Furthermore, the SalmoFan™, provided that is used in optimal light conditions and by trained personnel, seems to provide a more accurate prediction of the astaxanthin content in the fillet relative to the Minolta colourimeter when the concentration is high<sup>5,10</sup>. Nevertheless, both methods cannot precisely predict the carotenoid concentration in the fillet due to multiple factors affecting the measurements<sup>10,11</sup>. Hence consistency in the approach, so that comparisons can be drawn between batches, is critically important.

In regards to chemical analysis, carotenoids are usually extracted with acetone (or other solvents) and the concentration assessed by using a spectrophotometer<sup>11</sup>. Carotenoids can be then distinguished by using high-pressure liquid-chromatography (HPLC)<sup>11</sup>. A more recent method tested for carotenoids concentration measurement is the visual-near infrared spectrophotometry (VIS-NIR)<sup>32</sup>. This method seems to have a big potential being non-invasive, quick and suitable to be used on both live and stored fish<sup>32</sup>. Furthermore, it has been shown to predict carotenoids concentration with high accuracy (VIS prediction vs chemical analysis reference  $r^2$  85-92%) and to produce values highly correlated to the values obtained through digital photography ( $r^2$  83)<sup>32</sup>. Nevertheless, the NIR method still needs to be

refined and a calibration or standardisation with the two methods mostly employed, SalmoFan™ and Minolta colourimeter or image analysis, is recommended.

## Section 2

### Aim 2: Identify molecular events associated with reduced flesh colour in gut and liver.

This section is organised in five parts. The first describes a longitudinal assessment of a commercial stock affected by colour variation in order to first detect variation and then describe occurrence pattern and development. The second focuses on the correlation between flesh colour and microbiota in samples affected by colour variation from the longitudinal assessment. The third details the molecular mechanisms in gut and liver in samples affected by colour variation from, again, the longitudinal assessment. The fourth and the fifth, expand the aforementioned investigations on samples from a new assessment at the same site.

#### 2.1 Longitudinal assessment of a commercial stock affected by colour variation to first detect variation and then describe occurrence pattern and development

##### 2.1.1 Background

The assessment was carried out at the Petuna marine site Rowella where historically Atlantic salmon experience a severe decrease in flesh colour which becomes evident after summer. The reduction in colour can result in fish being pale or losing most of the flesh colour, rare and likely due to extreme summer events (several days with average daily water temperature  $> 20^{\circ}\text{C}$ )<sup>35</sup>, or more commonly be affected by 'banding' - an evident discolouration of the front dorsal region of the fillet as well as of the belly flap region (Fig. 2.1B). Banding is considered a serious quality issue and is targeted by product rejection. While reduced colour in the belly flap region can be tolerated, unless too severe, as that region appears already paler even in normally pigmented fish due to the presence of fat, a discolouration of the front dorsal area is not acceptable.

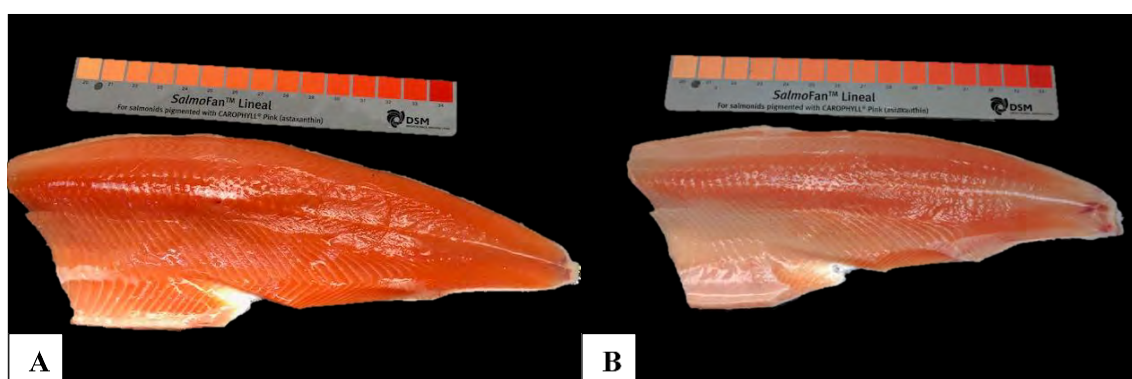


**Fig. 2.1** Photos taken in a light box against a Salmofan™ showing an Atlantic salmon fillet A) displaying a good flesh colour and B) affected by banding and general paleness (individuals from sampling in May).

Previous research has suggested that the phenomenon may be due to impaired feed uptake when the water temperature is too high with consequent hypoxia and/or loss of carotenoids (i.e. pigments) already stored, which are utilised for reasons that remain elusive<sup>35</sup>. A recent study has excluded the use and depletion of carotenoids (with banding or discolouration as direct effect) as countermeasure

to temperature-driven oxidative stress<sup>33</sup>. Furthermore, it is still not clear why discoloration occurs mostly in those specific regions although a correlation between areas with higher fat deposition and consequent faster depletion of pigments has been hypothesised. This hypothesis is likely based on the fact that fat and carotenoid metabolism are linked and uptake, transport and delivery of carotenoids is closely associated with the same processes involving fatty acids<sup>14</sup>. Furthermore, the areas affected by banding are the ones with the highest lipid content<sup>36</sup>. Nevertheless, a recent study has found that dietary fatty acid composition had no effect on astaxanthin concentration in flesh at 19°C<sup>37</sup>. The information provided by these previous investigations led the current project to assess the possible role of gut microbiome and tissues that are highly involved in carotenoids metabolism such as the muscle, liver, and the intestine. In fact, change and/or disruption in microbiome over summer may explain: 1) why fish are not willing to feed during high temperature events and/or the feed and carotenoids ingested are not properly assimilated and 2) what happens specifically in fish affected by paleness-banding relative to fish displaying good and even colour. Analysis of the gene expression of critical tissues might provide further insight into the molecular mechanisms behind the issue and may support what will be observed in the microbiome.

### 2.1.2 Materials and Methods

This assessment targeted fish transferred to Rowella on May 2016. Starting from December 2016, fish were collected from duplicate cages (number 23 and 24) belonging to the same original population (i.e. same input event). Cages were located in the same position on the farm (i.e. adjacent). During the timeframe of the assessment, both cages were fed the same commercial diet with minimal change in main ingredients over time. The environmental conditions during the assessment timeframe are shown in Fig. 2.2.

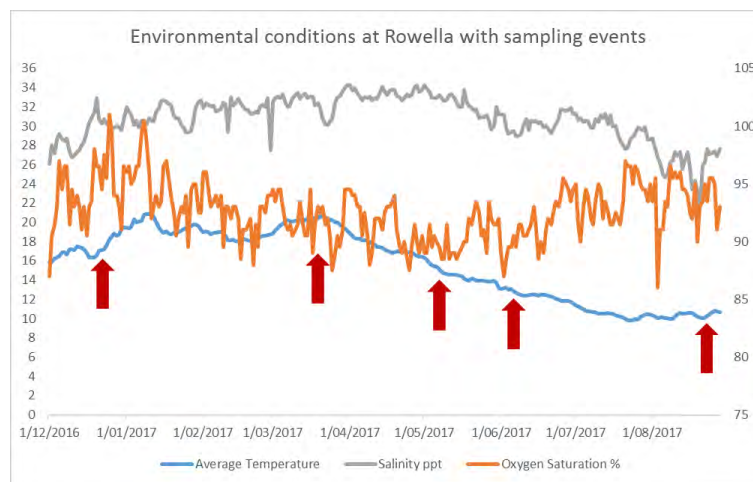


**Fig. 2.2** Main environmental conditions (Average temperature °C, Salinity ppt and Oxygen saturation %) measured at the site during the assessment timeframe. The red arrows indicate the sampling events and the time these were carried out.

Four samplings (as May and June samplings are part of the same event) were carried out based on the historical seasonal trend of flesh colour at the site (red arrows in Fig. 2.2):

- **21<sup>st</sup> of December 2016 (A)** - Control point before beginning of critical period
- **20<sup>th</sup> of March 2017 (B)**- Initial drop in flesh colour, both cages

- **8<sup>th</sup> of May 2017 and 6<sup>th</sup> of June (C)**- Lowest point in flesh colour post-summer, cage 24 and 23 respectively
- **23<sup>rd</sup> of August 2017 (pre-harvest) (D)** - Recovery after critical period, cage 23 only

On December 2016,  $n = 30$  fish were collected per cage ( $n = 60$  overall from the same population) while for the remaining time points  $n = 50$  fish were collected per cage ( $n = 100$  overall from the same population). The fish part of this assessment were all-female diploid Atlantic salmon. For cage 24, May 2017 was the last sampling time point as the cage had to be harvested while Cage 23 was sampled in June and in August (final sampling pre-harvest). At each sampling event, fish were collected before the morning meal in order to assess the feeding status based on the presence of digesta of the previous meal in the gut. Fish were crowded by using a box net and then collected with a dip-net and euthanized through a non-recoverable percussive blow to the head delivered by using an automatic stunner. Fish were then transferred into a bin containing ice slurry and immediately transported to the nearby sampling station.

At the site, for each fish weight (kg), fork length (cm), liver weight (g), gonad weight (g), presence of any deformity/anomaly and of digesta (feeding status) in the intestine were recorded. Condition factor, Specific growth rate (SGR, % body weight gain/day), Hepatosomatic (HSI) and Gonadosomatic index (GSI) were calculated as following: Condition factor = (fish weight (g)/fish length (cm)<sup>3</sup>)×100, SGR = [(Log<sub>n</sub> final fish weight (g)–Log<sub>n</sub> initial fish weight (g))/feed days]×100 HSI = (liver weight (g)/fish weight (g))×100 and GSI = (gonad weight (g)/fish weight (g))×100. For molecular analyses (i.e. microbiome and transcriptome, described in following sections), samples of distal intestine, faeces (if present and from the same area of the distal intestine sample), liver and gonads were collected from each fish and preserved in RNAlater. The samples were stored overnight at 4°C and then at -20°C (or -80°C) until analysis. Following sample collection, each fish was returned to the bin of slurry after being tagged and sent to the processing facilities for colour assessment. On the following day, each tagged fish was hand-filleted and the flesh colour of the right-side fillet was:

1. Visually assessed in a grey light box with standardised light conditions by trained factory personnel<sup>38</sup>. Each fillet was assessed in two designated regions (Fig. 2.3) and a score (20 to 34) assigned to each region according to Roche SalmoFan™ Lineal Card (Hoffman-La Roche, Basel, Switzerland). The two regions were chosen in order to detect the highest variation in colour in case of a banded fillet where the front dorsal region (1 in Fig. 2.3) is usually the most affected by discolouration while the back central region (2 in Fig. 2.3) tends to maintain colour evenness. Banding was classified by severity calculating the difference between the colour score of the back central and the front dorsal region. A difference of 0 to 1 score between regions was classified as NONE, of 2 as MODERATE and of 3 as SEVERE.
2. Instrumentally measured by using a Minolta colourimeter on the same aforementioned regions. Measurements were carried out according to the recommendations of the International Commission on Illumination<sup>31</sup>, reporting values of lightness (L\*; blackness/whiteness), redness (a\*; greenness/redness) and yellowness (b\*; blueness/yellowness). Measurements were considered either individually (per region) or as average of the two regions. Minolta measurements were not taken in December.

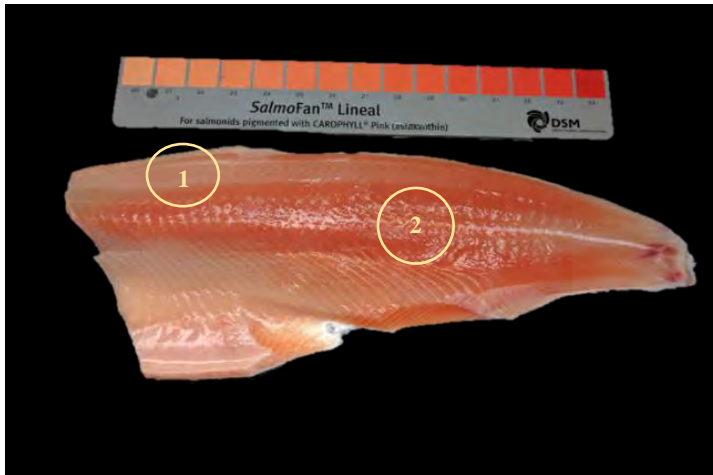


**Fig. 2.3** Atlantic salmon fillet affected by banding showing the regions assessed during visual and Minolta colour assessment: 1 front dorsal and 2 back central.

### 2.1.3 Results and Discussion

In all sampling events carried out, fish appeared to be in good health in both cages with a low level of jaw and spinal deformity, as expected for diploid populations (Fig. 2.4). A small number of fish in cage 23 were found with no gonads in both December and March and in both cages in December (Fig. 4). In March and May Cage 24 only had a small percentage of fish with white under-developed gonads while all fish had gonads in June and August (cage 23 only) (Fig. 2.4). Presence of skin lesions was low and variable over time and between cages (Fig. 2.4) and most likely ascribable to environmental conditions or external factors. With regard to presence of faeces or casts (i.e. pseudofaeces white or yellow in colour with presence of mucus) and referring to cage 23 only, which had a regular sampling regime, it is clear that the prevalence of fish not having faeces or having casts was relatively low in December, reached a peak in March and then decreased over June to disappear in August (Fig. 2.4). The situation described is even more evident looking at Fig. 2.5 where the percentage of fish having no faeces in the gut is plotted against the average temperature at the site (May sampling excluded from the graph and data averaged for the two cages in the first two sampling events). The figure shows the usual feeding pattern observed at the site over this period of the year indicating a clear deleterious effect of temperature on feeding intake. Prevalence of fish with casts in the intestine was low and variable over time (Fig. 2.4) and these were not observed in the June and August samplings. Although it has been suggested that casts in the intestine may indicate a dysfunctional digestive system<sup>39</sup>, further investigations are required to understand the meaning of their presence in the current trial. Considerations on absence of faeces and presence of casts cannot be made for the May sampling in cage 24 as fish were sampled just before harvest after a period of starvation. Nevertheless, this may explain the equal prevalence of individuals falling into the two categories (Fig. 2.4) as the high prevalence of fish with casts after starvation in May suggests that the occurrence of casts may be a natural process and possibly the stage preceding an empty intestine more than the result of a dysfunction.

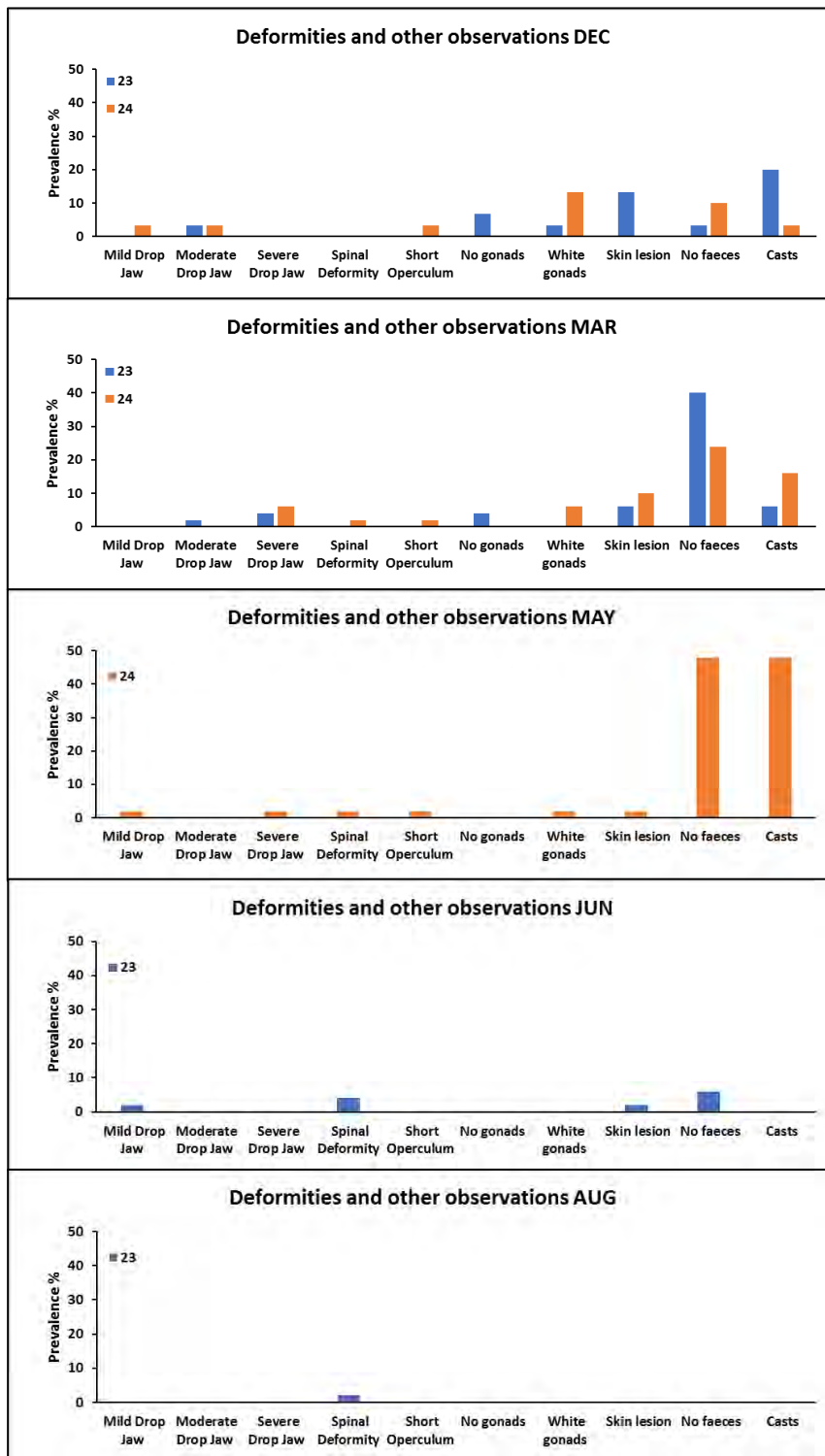


**Fig. 2.4** Prevalence of deformities, gonads and intestine status during the sampling events carried out. In May, fish collected from cage 24 were starved for harvest resulting in an either an empty gut or containing casts.

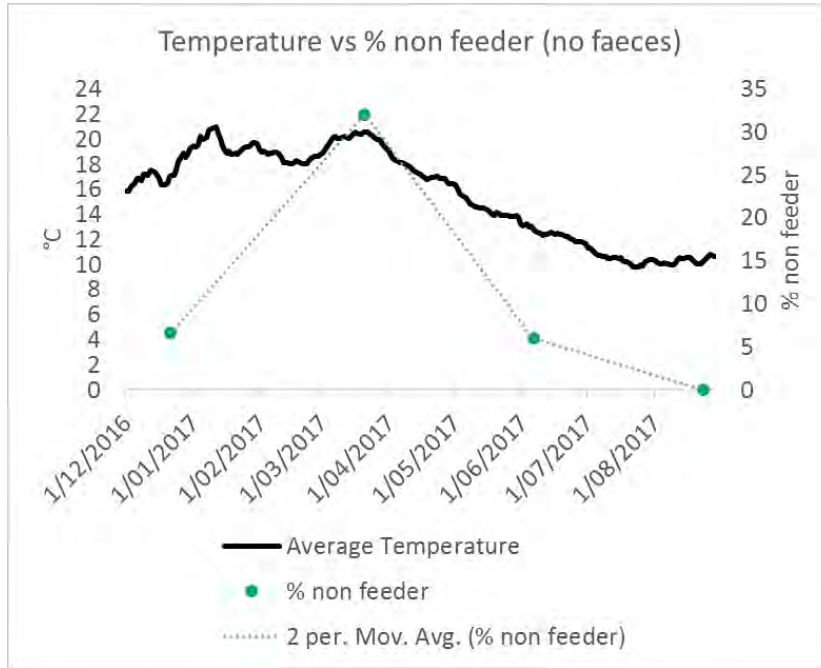


**Fig. 2.5** Percentage (%) of fish that were found with no faeces in the gut (defined non feeder) plotted against the average temperature (°C) at the site during the samplings carried out (May sampling excluded from the graph as fish were starved and data averaged for the two cages in the first two sampling events).

Considering the two cages as a pooled population where possible, fish started with an average weight of 1.34 kg in December and reached 4.53 kg by August (Table 2.1). Condition factor (CF) went from 1.38 in December to 1.77 in August (Table 2.1). It is noteworthy that weight, and as a consequence CF, increased at a slower pace between December and May compared to that observed between May and August with just 76% weight gain (specific growth rate 0.41% days<sup>-1</sup>) in the first period (138 days) and 92% (specific growth rate 0.61% days<sup>-1</sup>) in the second (107 days) (Fig. 2.6). This may be explained by the deleterious effect of summer temperatures which impacted on feeding, as previously shown. Accordingly, HSI showed an evident decrease during March and May (lowest point) and then increased and remained stable over June and August (Table 2.1). As liver functioning is closely connected to growth, the decrease observed was, again, most likely ascribable to temperature and its severe effects on fish physiology and liver health. During the entire period of the assessment (December-August), GSI did not show any significant increase (Table 2.1) staying well below what is considered the sexual maturation cut-off for Atlantic salmon (GSI 3%<sup>40</sup>) likely due to the fact that fish were exposed to artificial lighting in order to delay the onset of maturation (common practice for Atlantic salmon industry worldwide). Finally, average flesh colour seemed to decrease slightly over time, going from an average of 25.72 in December to 24.53 in June and then peaking in August to 27.81 (Table 2.1). Nevertheless, by looking at the average colour only, it is impossible to detect the magnitude of the problem experienced by fish over summer with regard of flesh colour.

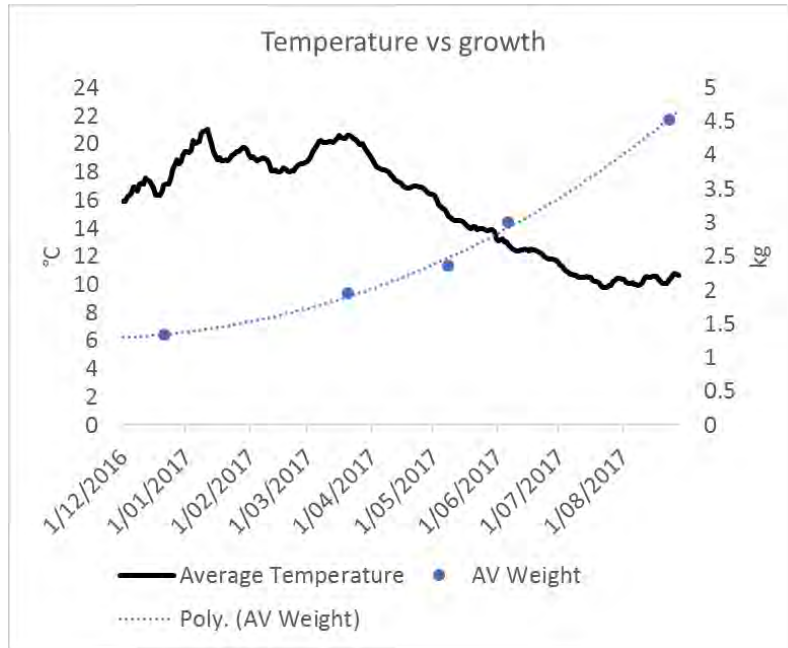


**Fig. 2.6** Fish growth (kg) plotted against the average temperature (°C) at the site during the samplings carried out (data averaged for the two cages in the first two sampling events).

**Table 2.1** Average ( $\pm$ SD i.e. StdDev) of several performance indicators of Atlantic salmon from the two cages assessed (23 and 24) during the sampling events carried out between December 2016 – August 2017. Count of Population indicates the number of fish assessed at each sampling event.

Row Labels	Average of Weight (kg)	StdDev of Weight (kg)	Average of Length (cm)	StdDev of Length (cm)	Average of Condition factor	StdDev of Condition factor	Average of HSI (%)	StdDev of HSI (%)	Average of GSI (%)	StdDev of GSI (%)	Average of Colour	StdDev of Colour	Average of Colour Front	StdDev of Colour Front	Average of Colour Back	StdDev of Colour Back	Count of Population
<b>21/12/2016</b>	<b>1.34</b>	<b>0.25</b>	<b>45.87</b>	<b>2.48</b>	<b>1.38</b>	<b>0.12</b>	<b>1.23</b>	<b>0.20</b>	<b>0.10</b>	<b>0.03</b>	<b>25.72</b>	<b>1.63</b>	<b>25.78</b>	<b>1.62</b>	<b>25.65</b>	<b>1.67</b>	<b>60</b>
23	1.23	0.21	44.63	2.22	1.37	0.11	1.27	0.20	0.10	0.02	25.90	1.46	26.00	1.46	25.80	1.49	30
24	1.46	0.24	47.10	2.09	1.39	0.13	1.20	0.19	0.09	0.03	25.53	1.78	25.57	1.76	25.50	1.83	30
<b>20/03/2017</b>	<b>1.95</b>	<b>0.35</b>	<b>51.78</b>	<b>2.36</b>	<b>1.39</b>	<b>0.14</b>	<b>1.06</b>	<b>0.16</b>	<b>0.22</b>	<b>0.48</b>	<b>25.51</b>	<b>1.81</b>	<b>24.85</b>	<b>1.99</b>	<b>26.16</b>	<b>1.73</b>	<b>100</b>
23	1.95	0.33	51.68	2.14	1.40	0.11	1.04	0.16	0.26	0.69	25.56	1.65	24.80	1.78	26.32	1.61	50
24	1.96	0.37	51.87	2.58	1.39	0.16	1.07	0.16	0.17	0.05	25.45	1.97	24.90	2.20	26.00	1.84	50
<b>8/05/2017</b>	<b>2.36</b>	<b>0.51</b>	<b>54.20</b>	<b>3.25</b>	<b>1.46</b>	<b>0.14</b>	<b>0.87</b>	<b>0.12</b>	<b>0.21</b>	<b>0.05</b>	<b>25.11</b>	<b>1.46</b>	<b>23.90</b>	<b>1.68</b>	<b>26.32</b>	<b>1.43</b>	<b>50</b>
24	2.36	0.51	54.20	3.25	1.46	0.14	0.87	0.12	0.21	0.05	25.11	1.46	23.90	1.68	26.32	1.43	50
<b>6/06/2017</b>	<b>3.01</b>	<b>0.65</b>	<b>57.28</b>	<b>3.46</b>	<b>1.58</b>	<b>0.13</b>	<b>1.15</b>	<b>0.16</b>	<b>0.24</b>	<b>0.05</b>	<b>24.53</b>	<b>1.82</b>	<b>23.86</b>	<b>2.00</b>	<b>25.20</b>	<b>1.71</b>	<b>50</b>
23	3.01	0.65	57.28	3.46	1.58	0.13	1.15	0.16	0.24	0.05	24.53	1.82	23.86	2.00	25.20	1.71	50
<b>23/08/2017</b>	<b>4.53</b>	<b>0.74</b>	<b>63.37</b>	<b>3.33</b>	<b>1.77</b>	<b>0.14</b>	<b>1.15</b>	<b>0.12</b>	<b>0.34</b>	<b>0.06</b>	<b>27.81</b>	<b>2.10</b>	<b>27.26</b>	<b>2.29</b>	<b>28.36</b>	<b>1.96</b>	<b>50</b>
23	4.53	0.74	63.37	3.33	1.77	0.14	1.15	0.12	0.34	0.06	27.81	2.10	27.26	2.29	28.36	1.96	50

In fact, considering each fillet region separately (Fig. 2.7), a dramatic and evident decrease in flesh colour was observed over time and as expected mostly in the front dorsal region (a decrease in the back central region was noticed in June just before to peak in August). Discolouration over time in the front dorsal region is even more highlighted when data are projected into a whisker plot (Fig. 2.8) which shows a decrease over May-June of the median (central horizontal line in the plot) as well as of the average (x in the plot). On the other hand, the back central region showed a longitudinal consistency of flesh colour with, again, a decrease in June only (Fig. 2.8). In both regions, flesh colour returned to satisfactory levels in August (Fig. 2.8). What said above is also clearly illustrated by the prevalence of banding and its severity which increased from December to May and then decreased over June and August (Fig. 2.8). Interestingly, the highest prevalence of banding and its severity was observed in May, when fish affected (either by moderate or severe) still displayed a good colour in particular in the central back region (Fig. 2.9). Most likely, the overall better colour resulted in a more accentuated difference between the two regions assessed. On the other hand, only a month after, the lower prevalence of banding (either moderate or severe) in June, which was the period when the biggest drop in colour was observed, was probably due to an overall severe discolouration (Fig. 2.9) that resulted in a less obvious difference between regions.

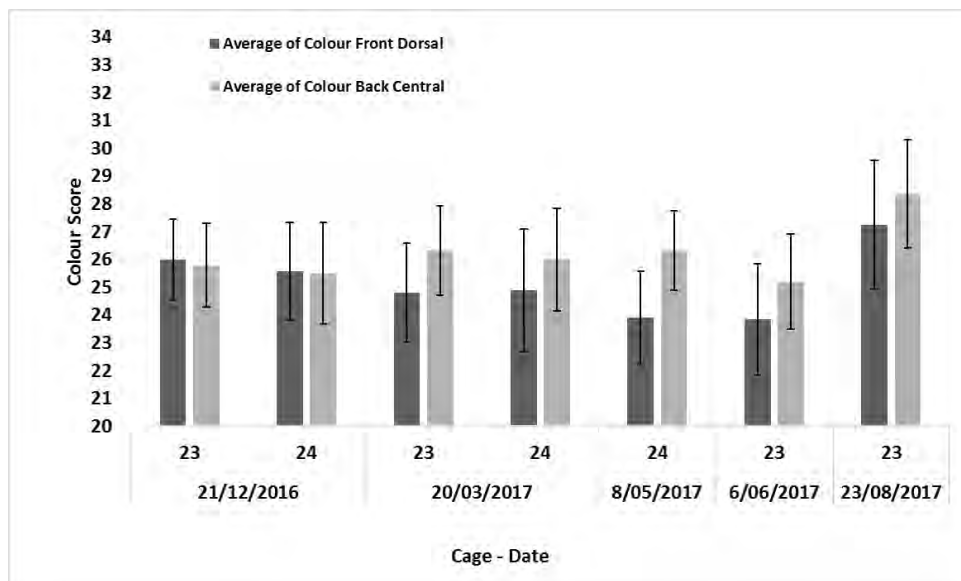


**Fig. 2.7** Average ( $\pm$ SD) colour score visually assigned according to SalmoFan™ to the front dorsal and back central region of Atlantic salmon sampled from the two cages assessed (23 and 24) during the sampling events carried out so far.

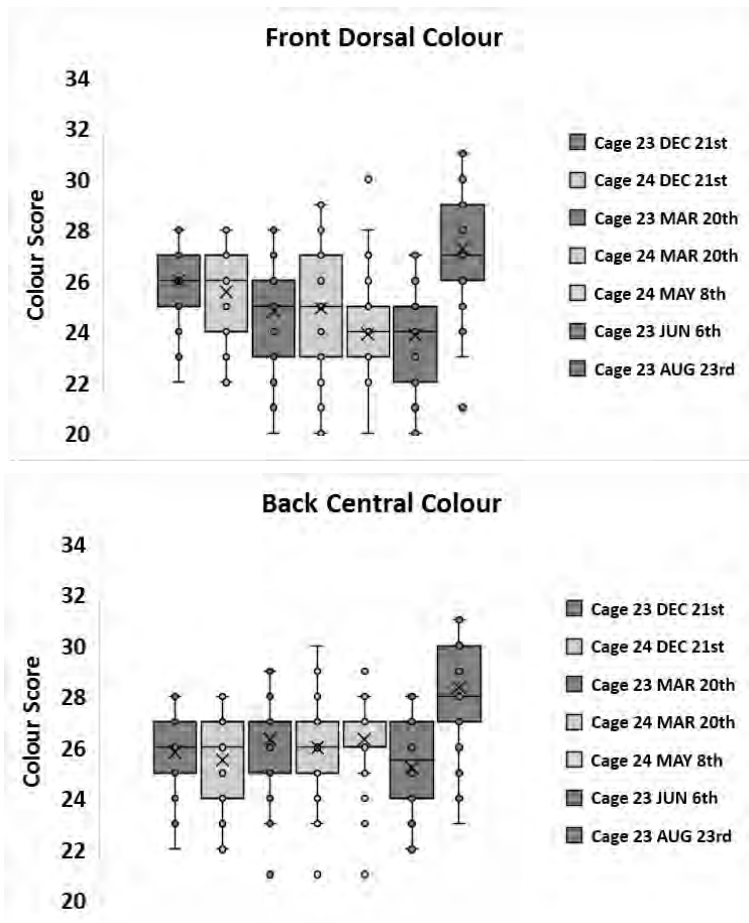


**Fig. 2.8** Whisker box plots of the colour score visually assigned according to SalmoFan™ to the front dorsal (top) and back central (bottom) regions of Atlantic salmon sampled from the two cages assessed (23 and 24) during the sampling events carried out.

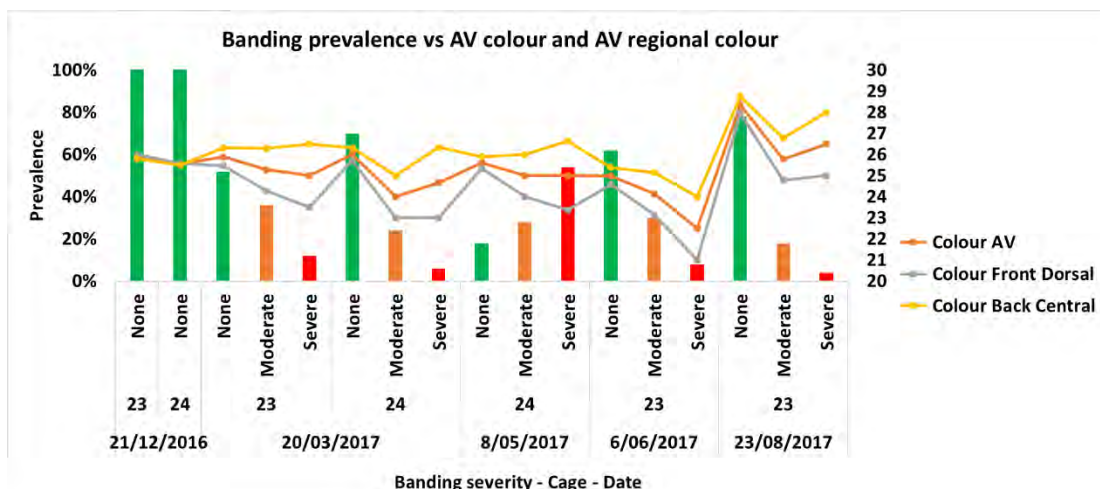


**Fig. 2.9** Prevalence of banding categorised by severity plotted against average colour (average of the two regions assessed) and the average colour of the two regions assessed considered separately in Atlantic salmon sampled from the two cages assessed (23 and 24) during the sampling events carried out.

With regard to the Minolta measurements  $L^*$ ,  $a^*$ ,  $b^*$ , these showed trends that are already clearly described in the literature<sup>5,19</sup>. Increased  $L^*$  values usually indicate more lightness (i.e. paleness) in the fillet as a result of decreased astaxanthin concentration. In the current assessment, while  $L^*$  slightly decreased in the back central region only over time confirming the observed consistency in colour, in the front dorsal region a peak was evident in May corresponding to the increased paleness in that area at that time (Fig. 2.8 vs Fig. 2.10). Nevertheless, the June sampling did not seem to match the visual scores. Increased  $a^*$  values indicate more redness (i.e. increased colour) as a result of increased astaxanthin concentration in the fillet. In the current assessment, in the front dorsal region  $a^*$  reached the lowest point in May likely for the same aforementioned reasons and, again, except for the June sampling event, it seemed to match the same trend as the visual scores (Fig. 2.8 vs Fig. 2.10). In the back central region,  $a^*$  clearly matched the trend of the visual scores although the differences between events were less obvious (Fig. 2.8 vs Fig. 2.10). Increased  $b^*$  values indicate more yellowness in the fillet. In the current assessment, in the front dorsal region  $b^*$  matched that observed for  $a^*$  but had a totally opposite trend with regard to the back central region for reasons that remain elusive (Fig. 2.8 vs Fig. 2.10). The literature reported little correlation between the Minolta measurements and the visual scores, likely due to their different methodology and sources of error, therefore care must be exercised when comparing these results<sup>26</sup>. Furthermore, the discrepancies observed in the aforementioned analyses might be due to the fact that fat content in the fillet as well as fibre muscle density, which were not measured in the current assessment, can affect both the Minolta measurements and the visual scores<sup>19,28</sup>.

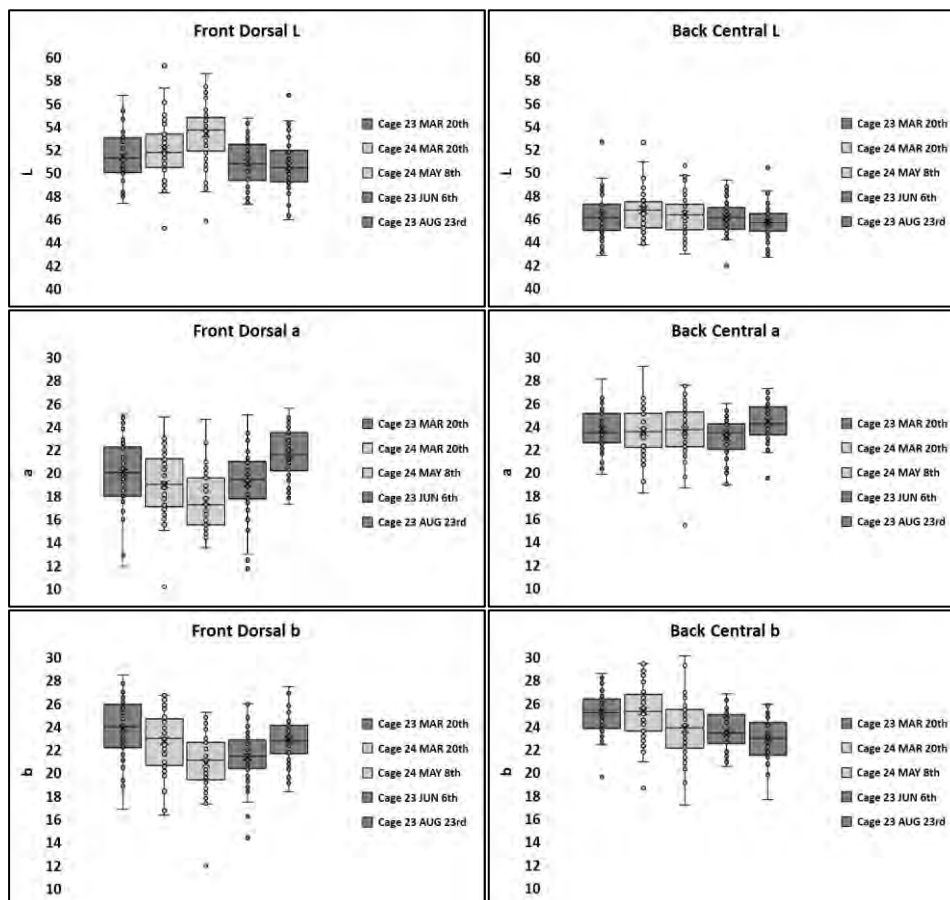


**Fig. 2.10** From top to bottom,  $L^*$ ,  $a^*$  and  $b^*$  values measured with the Minolta colourimeter in the two designated regions of the fillet (front dorsal and back central) during the samplings carried out (measurements were not taken in December).

#### **2.1.4 Final remarks**

We observed and comprehensively described a recurrent phenomenon affecting fish stocked at a particular marine site. This assessment allowed access to a considerable number of samples from different tissues, which has allowed to further understand the reasons underlying the depletion of flesh colour post-summer (following paragraphs).

It is noteworthy that the May population, which attained an average weight of 2-2.5 kg, could be harvested due to the always increasing market demand (the reason behind the loss of cage 24). This may result in harvesting a population with possibly a high prevalence of general colour loss/banding which is then subjected to intensive downgrading with consequent economic losses, stressing again how critical finding a solution to the issue is.

## 2.2 Atlantic Salmon gut microbiota profile correlates with flesh pigmentation: cause or effect?

(The entire section 2.2 has been published on the 15<sup>th</sup> of January 2020 on Marine Biotechnology <https://doi.org/10.1007/s10126-019-09939-1> and the publication is included in this report with the same text structure)

### 2.2.1 Abstract

In Tasmania (Australia), during the marine phase, it has been observed that flesh pigmentation significantly drops in summer, possibly due to high water temperatures (> 20 °C). Although this deleterious effect of summer temperatures has been ascertained, there is a lack of knowledge of the actual mechanisms behind the impaired uptake and/or loss of pigments in Atlantic salmon in a challenging environment. Since the microbial community in the fish intestine significantly changes in relation to the variations of water temperature, this study was conducted to assess how the gut microbiota profile also correlates with the flesh colour during temperature fluctuation. We sampled 68 fish at three time points covering the end of summer to winter at a marine farm in Tasmania, Australia. Flesh colour was examined in two ways: the average colour throughout and the evenness of the colour between different areas of the fillet. Using 16S rRNA sequencing of the v3–v4 region, we determined that water temperature corresponded to changes in the gut microbiome both with alpha diversity (Kruskal-Wallis tests  $P = 0.05$ ) and beta diversity indices (PERMANOVA  $P = 0.001$ ). Also, there was a significant correlation between the microbiota and the colour of the fillet (PERMANOVA  $P = 0.016$ ). There was a high abundance of *Pseudoalteromonadaceae*, Enterobacteriaceae, *Microbacteriaceae*, and *Vibrionaceae* in the pale individuals. Conversely, carotenoid-synthesizing bacteria families (*Bacillaceae*, *Mycoplasmataceae*, *Pseudomonas*, *Phyllobacteriaceae*, and *Comamonadaceae*) were found in higher abundance in individuals with darker flesh colour.

### 2.2.2 Introduction

During the marine phase, lasting 16–18 months, Atlantic salmon farmed in Tasmania (Australia) can be exposed during summer to water temperatures exceeding 20 °C, which is higher than their thermal tolerance<sup>41</sup>. During this time, fish are subjected to stress and poor feeding including starvation, and, as a result, flesh colour may gradually be depleted until Atlantic salmon reach their palest level at the end of autumn, before fully recovering by the end of winter. In some extreme cases, the uneven colour tone between the front dorsal and the back central muscles (a phenomenon commercially named “banding”) can be observed and can persist to harvest-size individuals<sup>33,35</sup>. The distinctive pink-red flesh colour of salmonids is considered a fundamental, and likely the most important, criterion of quality and freshness<sup>11</sup>. Carotenoids are the organic pigments responsible for salmonids’ flesh colour<sup>6</sup>. While wild Atlantic salmon obtain carotenoids by feeding on zooplankton or on prey that previously ingested carotenoids, farmed Atlantic salmon rely on a synthetic or natural form of carotenoids which is included in commercial diets<sup>1,11</sup>. Nowadays, Astaxanthin (Ax, a xanthophyll carotenoid found in microalgae, yeast, and crustaceans<sup>42</sup>) is used mainly in commercial diets as it is considered more natural, due to it being the most abundant carotenoid in wild Atlantic salmon<sup>17</sup>. Ax is included in diets at a rate of between 40 and 100 mg kg<sup>-1</sup>, and this inclusion represents 15–25% of the total feed costs, which is about 6–10% of the total production cost<sup>6,17</sup>. The percentage of carotenoids that are deposited in the salmon flesh varies and is in the range of 1 to 22% of that administered<sup>1,6,8,21</sup>. This poor utilization is mainly due to 30 to 70% of carotenoids being lost in the faeces, leading to poor assimilation from the intestine into the muscle<sup>21</sup>. Low digestibility of carotenoids, which is slower than other major nutrients, may also underlie their poor absorption<sup>1,6,21</sup>. Furthermore, the relationship

between flesh redness (when visually assessed) and the amount of carotenoid fed is non-linear, as the colour reaches saturation in the flesh at 12 mg kg<sup>-1</sup> <sup>19</sup>. Even with a 70% loss in the faeces, in high-carotenoid diets containing between 40 and 100 mg kg<sup>-1</sup>, up to 22mg kg<sup>-1</sup> can remain unutilized. This raises a question regarding the destiny of the unutilized digested carotenoids, whether they are lost in the faeces or employed for other purposes. This led to a hypothesis that there was a trade-off between using ingested carotenoids for either colour development (i.e., muscle deposition) or for immune defence and vitamin A synthesis <sup>43,44</sup>. Therefore, a better understanding of the mechanisms that enable gut absorption, flesh assimilation, and retention of carotenoids is of key commercial significance for salmon aquaculture farms that can experience elevated summer temperatures.

To date, the metabolism of carotenoids and its retention in Atlantic salmon, as well as the genes responsible for the whole metabolic process, are poorly understood <sup>13,14</sup>. On the other hand, the microbiota community in the intestine system of salmonids and other fish was demonstrated to be involved in the metabolism with-in the host (i.e., converting the dietary components to bioactive metabolites and immune signalling interaction) <sup>45,46</sup>. For example, protein-hydrolyzing and lactic acid bacteria *Carnobacterium divergens* was suggested as a probiotic in Atlantic salmon <sup>47,48</sup>, amylase-producing *Vibrio* spp. were isolated in the sea bass *Dicentrarchus labrax* larvae <sup>49</sup>, and amylase-producing *Aeromonas* spp., *Bacteroidaceae*, and *Clostridium* were reported in common carp *Cyprinus carpio*, channel catfish *Ictalurus punctatus*, Japanese eel *Anguilla japonica*, and tilapia *Oreochromis niloticus* <sup>50</sup>. The cellulase activity in the digestive tract of 42 fish species originated from the microbiota <sup>51</sup>. Also, protease, phytase, lipase, tannase, xylanase, and chitinase, produced by the fish endosymbiotic microbiota, emphasized the essential role of microbiota in the digestive tract; this is extensively reviewed in <sup>46</sup>. The intestine microbiotas also function by inducing the host innate immune system (reviewed in <sup>52</sup>) and stimulating the nutritional material uptake in the digestive tract (reviewed in <sup>46</sup>). Specifically, it was demonstrated that the gut microbiota was able to regulate the expression of 212 genes of zebrafish *Danio rerio* in which there were genes relating to epithelial proliferation stimulation, nutrient metabolism, and innate immune response <sup>53</sup>. Therefore, the fish gut microbiota is emerging as an essential factor in the host metabolism.

Also, carotenoids are found as the secondary metabolites synthesized and used as the protection strategy against the reactive oxygen species (ROS) in some bacteria <sup>54,55</sup>. Besides, carotenoids play a vital role in the tolerance of environmental stresses such as temperature, pH, and salinity in the living conditions of these microorganisms <sup>54</sup>. There are many forms of carotenoids produced by different microorganisms via different enzymes routes presenting as the carotenoids biosynthesis pathways evolution <sup>42</sup>. Interestingly, the carotenoid biosynthesis enzymes are quite powerful that any microorganism can provide a precursor material required for the engineered carotenoid biosynthesis pathway, and the engineered carotenoid biosynthetic genes can be expressed in many microorganisms <sup>42</sup>. More importantly, the engineered carotenoid biosynthesis pathway can alter the existing carotenoid pathway in the host <sup>42,56-58</sup>. Therefore, the relationship between the carotenoid-producing bacteria and the host salmon is worth to investigate.

The growth and nutrition quality of Atlantic salmon reared in Tasmania is believed to be associated with heat stress, oxidative stress, and the gut microbiota, leading to what is known as summer gut syndrome <sup>59</sup>. The dynamic gut microbiota community was demonstrated to correlate with the change of seasons and diet <sup>39</sup>, as well as variations between healthy and inflamed intestine <sup>60</sup> and stress by starvation versus active feeding fish <sup>61</sup>.

## 2.2.3 Materials and methods

### 2.2.3.1 Study Design and Sample Collection

Atlantic salmon individuals analysed in the current study were sampled during their second year at sea (2017) from an aquaculture lease in Tasmania (Australia) (section 2.1). Fish had been previously stocked on May 2016 and maintained in a cage containing approximately 35,000 individuals and fed a commercial diet with minimal, or no, variation over time in protein, fat, and pigment content. The sampling for each time point was chosen based on the lease's historical data showing that flesh colour deterioration starts to be manifested in March after the summer thermal stress and a period of poor feeding utilization, reaching the lowest peak in June and recovering in most of the stock in the following months (Fig. 2.11a). At each time point, distal gut samples were collected as previously described<sup>62</sup>. Briefly, the fish abdomen was incised, and the distal part of the intestine was aseptically exposed and severed. After opening the distal intestine longitudinally, a sample was collected (0.5 cm<sup>3</sup>) then washed three times in sterile 0.9% saline solution to remove non-adherent (allochthonous) bacteria and digesta. Gut samples were immediately fixed in RNAlater and stored at - 80 °C until extraction. A total of 68 female individuals from the three time points (Mar n = 28, Jun n =22, and Aug n = 18) were chosen to cover the fluctuation of the flesh colour and banding status during the change of temperature. In all the individuals analysed, GSI never exceeded 0.55 indicating that fish were not undergoing any sexual maturation. Negative samples for DNA extraction and PCR were also included. The flesh colour measurement was based on the Roche SalmoFan™ Lineal Card (Hoffman-La Roche, Basel, Switzerland), ranging from 20 to 34, in which the assumed marketable grade is 25. The total samples were also categorized by the flesh colour that was equal to 21–22 (Flesh21–22, n = 9), 23–24 (Flesh23–24, n = 18), 25–26 (Flesh25–26, n = 25), 27–28 (Flesh27–28, n = 13), and 29–31 (Flesh29–31, n = 3). The severity of banding was calculated as the colour score difference between the two areas of the fillet (dorsal and central) and categorized as none (score = 0, n = 35), (Fig. 2.11b), moderate (score = 1, n = 24), and severe (score ≥ 2, n =9) (Fig. 2.11c).

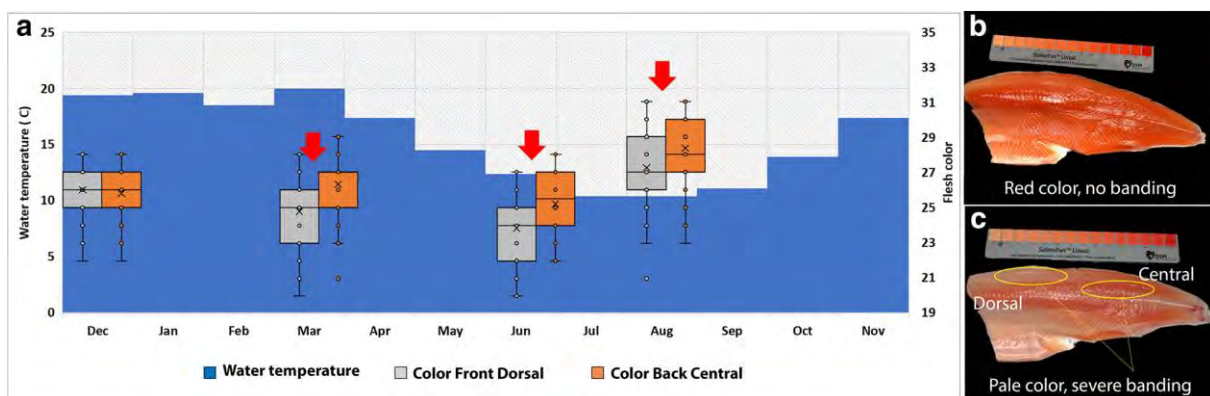


**Fig. 2.11** Study design summary. a) a graph presenting the average temperature trending (blue columns) from Dec 2016 to Nov 2017. The flesh colour fluctuation in the population part of the study along the timeline is presented as front-dorsal colour (gray box), and back-central colour (orange box). The three-sampling time-points were Mar, Jun, and Aug (red arrows). b) an example of a fillet with good colour and no or the minimal difference between the dorsal and central area (no banding), and c) a pale fillet with uneven colour between the aforementioned areas (severe/ moderate banding).

### **2.2.3.2 DNA Extraction and MiSeq Sequencing**

DNA was extracted from gut samples by using the extraction kit FastDNA Spin kit (MP Biomedicals). The DNA concentration and purity were measured by NanoDrop™ 2000 Spectrophotometer (ThermoFisher Scientific), followed by gel electrophoresis. DNA was adjusted to approximately 50 ng/μl and sent to the Australian Genome Research Facility for Illumina sequencing using MiSeq. The hypervariable region between 341 and 806 nucleotides of 16S rRNA gene was amplified with the specific primers FW-5'-CCTA YGGGRBGCASCAG and RV-5' GGACTACNNGGGTA TCTAAT, and the purified amplicons served for library preparation and sequencing (2 × 300 bp read length). The negative controls for extraction and PCR were also sequenced.

### **2.2.3.3 Microbial Community Profiling**

The 16S rRNA gene sequencing data was analyzed using Quantitative Insights into Microbial Ecology (QIIME 2 Core 2018.8) <sup>63</sup>. The raw paired-end reads were assigned to samples based on their unique barcode and were demultiplexed by Illumina scripts and transformed to fastq files. The primers and barcodes were identified and trimmed. The demultiplexed paired-end reads were merged by using QIIME 2 Core 2018.8. Quality filtering was performed using QIIME 2 Core 2018.8 with Phred score 19 to obtain high-quality sequences according to QIIME 2 quality control process <sup>64</sup>. The filtered and sorted sequences were denoised and unique sequence variants referred to as operational taxonomic units (OTUs) were generated by the Deblur workflow <sup>65</sup>. The taxonomy was assigned with VSEARCH consensus taxonomy classifier <sup>66</sup>, followed by filtering the gaps in alignments, building a phylogenetic tree with FastTree 2.1.7 <sup>67</sup> and OTU table for downstream analysis. To analyze the data, the OTU table was rarefied at 1373 reads per sample, and then the samples were grouped regarding different categories such as time point, flesh colour, and banding status. The α-diversity was computed using QIIME 2 by measuring richness and evenness via Shannon index <sup>68</sup>. The significant α-diversity difference ( $P < 0.05$ ) between groups was calculated by using a nonparametric Kruskal-Wallis test. β-diversity was clustered by weighted and unweighted UniFrac distance metrics to compare the microbial community composition between groups <sup>69</sup>; then the PCoA generated using Emperor in QIIME 2 <sup>70,71</sup>. The β-diversity's multivariate statistical analysis was carried out in QIIME 2 using the PERMANOVA test <sup>72</sup>.

### **2.2.3.4 Biomarker Discovery**

To identify significantly differential taxa of different groups (i.e., biologically relevant features), we used LEfSe <sup>73</sup> provided by Dr. Huttenhower's lab (<https://huttenhower.sph.harvard.edu/galaxy/>) with  $P < 0.05$  and the linear discriminant analysis (LDA) effect size of 3.5 to explain the difference between groups. We also used the QIIME 2 gneiss <sup>74</sup> to identify the niche taxa and to assess the change of microbiota in terms of composition influence over the change of the environmental conditions. The gradient clustering hierarchies, which define the microbiota partition, were constructed for each category: time point, flesh colour, and banding status followed by partitioning the microbiota (i.e., creating balance models) for each group. The simplicial ordinary least squares regression models were built based on the balances and were visualized by the dendrogram heatmap. Finally, the taxonomy for each balance was summarized.

### **2.2.3.5 Predicting Function and Metagenome Contribution**

The function composition of the metagenome was predicted by PICRUSt <sup>75</sup>. The predictive metagenome was grouped into categories by function. From that, the categorized pathways which statistically correlated to the phenotypes were deduced to investigate the OTU abundance and the

contribution percentage of each OTU to the specific metabolic pathway in each sample. The differentiation of the predictive functions was analyzed using LEfSe<sup>73</sup>, which integrated into a multi-functional web-server Calypso (<http://cgenome.net/wiki/index.php/Calypso>)<sup>76</sup>.

## 2.2.4 Results

This study investigated whether the Atlantic salmon gut microbiota is associated with the flesh colour due to seasonality. Sixty-eight samples collected from three different time points were assessed in the context of time points: March (Mar, n = 28), June (Jun, n = 22), August (Aug, n = 18); flesh colour: on the SalmoFan™ Lineal Card equal to 21–22 (Flesh21–22, n = 9), equal to 23–24 (Flesh23–24, n = 18), equal to 25–26 (Flesh25–26, n = 25), equal to 27–28 (Flesh27–28, n = 13), and equal to 29–31 (Flesh29–31, n = 3); banding status: none (n = 35), moderate (n = 24), severe (n = 9); and three negative control samples. After rarefying at 1373 frequency per sample (securing even depth sampling for all samples), the retained number of sequences was 91,991 (23.66%) in 67 (97.71%) samples. The sampling data, which included the information on growth, age, sex, and health status indexes, is provided in Supplemental Material S1: metadata\_file.txt (for all Supplemental Material please refer to <https://doi.org/10.1007/s10126-019-09939-1>). For consistency, all the taxonomic ranks including phylum, class, order, family, genus, and species were shortened (P, C, O, F, G, and S, respectively).

### 2.2.4.1 The Microbiota Shift Is Strongly Correlated with Temperature Change; However, the Taxa Relating to Flesh Colour Are Differentiated Independent of the Time Point

The operational taxonomic unit (OTU) abundance in each sample was clustered as the UniFrac distance<sup>69</sup> in which the metadata was sorted as three time points Mar, Jun, and Aug (Fig. 2.12a). The OTU abundance of several taxa correlated with time point in two main patterns: (i) high abundance in Mar and decline in Aug, such as *Enterobacteriaceae* (F) and *Vibrio* (G), and (ii) gradual increase from Mar to Aug, such as *Aliivibrio* (G) and *Mycoplasmataceae* (F) (Fig. 2.12a). Additionally, the taxa found in Jun were more closely related to those found in Aug and quite phylogenetically diverse, while the taxa found in Mar had a close relationship within the group (Fig. 2.12b). The  $\beta$ - diversities across the groups in the three categories were statistically analyzed in both weighted and unweighted UniFrac distance metrics. The microbiota shift over the time point was confirmed by the significantly different  $\beta$  diversity (PERMANOVA P = 0.001, Fig. 2.13a). While the banding-status showed no significant differences in the  $\beta$ -diversity, the category Flesh-colour was significantly diverse in weighted UniFrac distance metrics (PERMANOVA P = 0.016, Fig. 2.13a). Since the samples were categorized for flesh-colour regardless of the time points, the significant PERMANOVA P value indicated the differentiation of the taxa in the flesh-colour category was not affected by the time point.

The correlation of the three categories, time point, flesh colour, and banding-status, which were analyzed by the Pearson's correlation method, indicated the influence of clusters of OTUs on each phenotypic group (Fig. 2.13b). In detail, groups of Mar, Flesh23–24, and Jun shared a similar pattern of OTU abundance and correlation. This pattern indicated that these time points and phenotypes were mainly influenced by *Vibrio* (G), *Pseudoalteromonadaceae* (F), and *Enterobacteriaceae* (F), which all belong to the class *Gammaproteobacteria* (Fig. 2.13b). Another pattern was shared between non-banding, Flesh27–28, and Flesh29–31 groups, in which they were mostly enriched by *Microbacteriaceae* (F), *Bacillaceae* (F), *Mycoplasmataceae* (F), and *Pseudomonas* (G) (panel b). Interestingly, these taxa were also highly enriched in the group of Aug, and these two patterns were only different in the abundance of *Vibrio* (G) and *Pseudoalteromonadaceae* (F) (Fig. 2.13b).

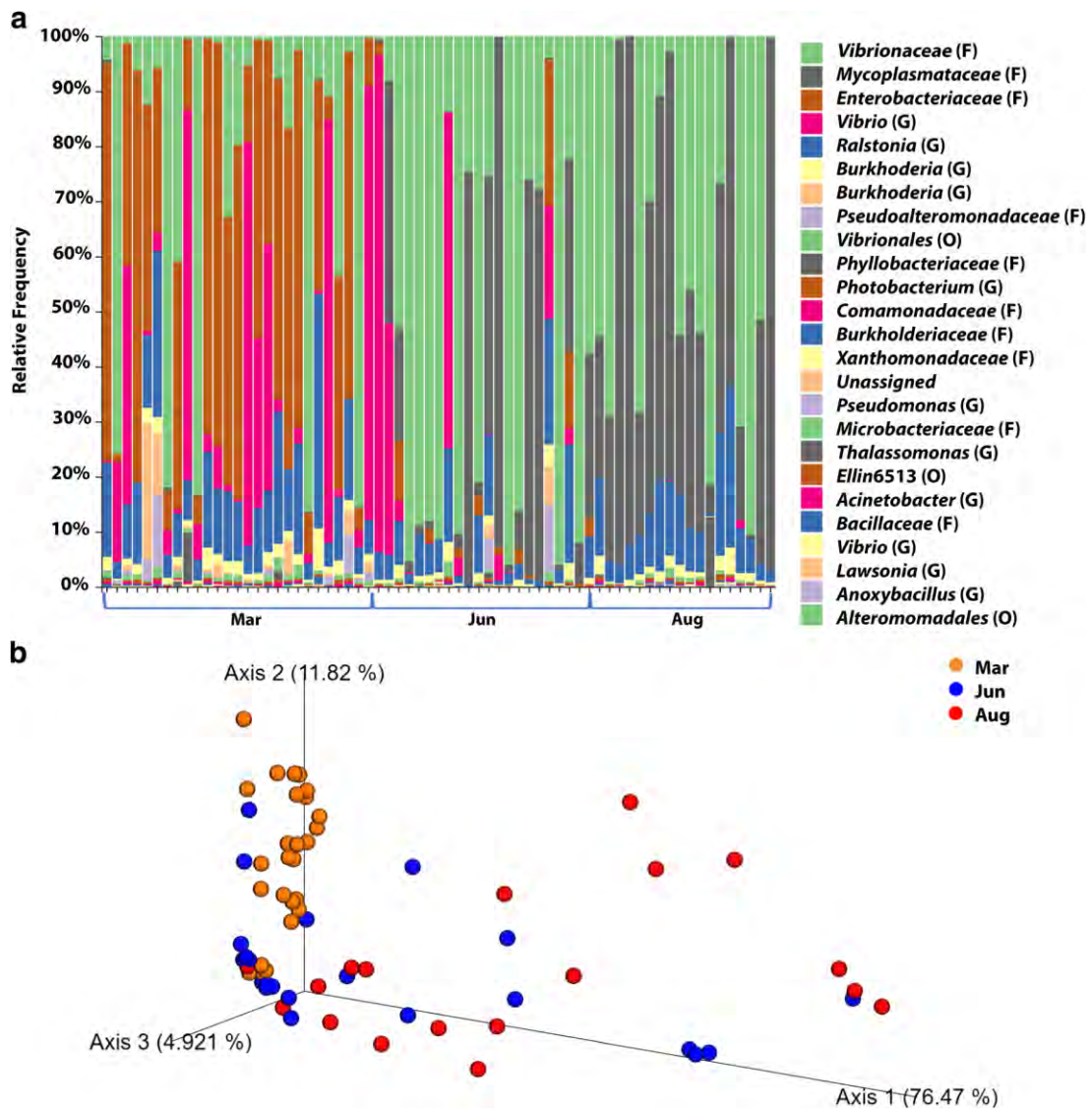


**Fig. 2.12** a) A bar-plot presenting the microbiota shift across time-points. Phylum, class, order, family, genus, and species were shortened as P, C, O, F, G, and S, respectively. b) A PCoA of weighted Unifrac distance of the microbial taxa across time points: Mar (orange) was closely clustered while the taxa in Jun (blue) and Aug (red) were scattered.

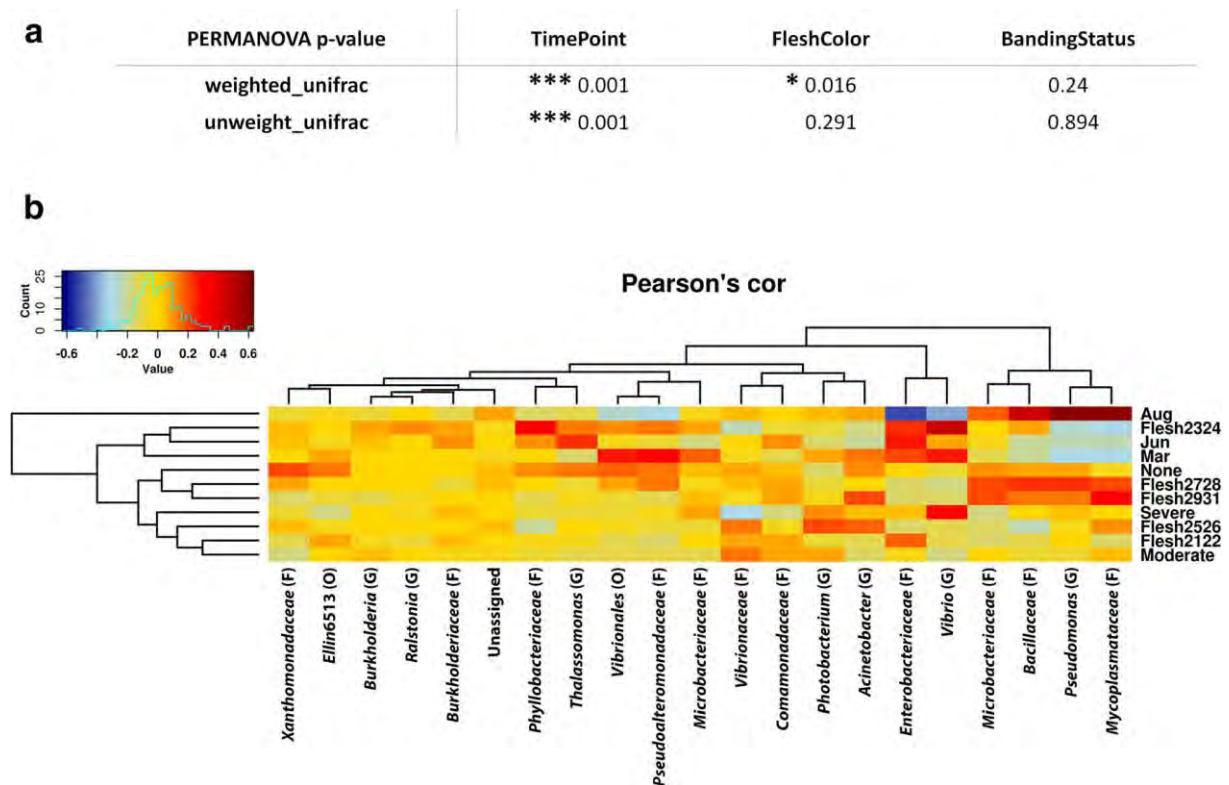


**Fig. 2.13** a) Statistic PERMANOVA of the  $\beta$ -diversity of both weighted and unweighted Unifrac distance metrics in three categories: time-point, flesh colour, and banding-status. \*  $P \leq 0.05$ , \*\*  $P \leq 0.01$ , \*\*\*  $P \leq 0.001$ . b) Spearman's correlation of the taxa and the groups in three categories.

#### 2.2.4.2 Differential Taxa Reveal the Features Across Metadata

To point out the differential taxa that were distinct for each group, LefSe was applied with  $P < 0.05$  and LDA effect size of 3.5. All the significantly differential taxa were plotted for each category including time point (Fig. 2.14a) and flesh colour (Fig. 2.14b). There were no OTUs significantly differentially present in the banding status. In the time-point category, Aug had the most diversely differential taxa while Mar had the least diversely differential taxa (Fig. 2.14a), in keeping with Jun (recovery phase) being the bridge between Mar (thermal stress phase) and Aug (optimal phase) and with diversity increasing with the correlation to the shift in temperature. The differential taxa of Aug include *Mycoplasmataceae* (F), *Bacillaceae* (F), and *Pseudomonas* (G) belonging to classes of *Mollicutes*, *Bacilli*, and *Gammaproteobacteria*, whereas the differential taxa in Mar include only OTUs belonging to the class of *Gammaproteobacteria*. The flesh colour category, which includes the samples from different levels of flesh pigmentation regardless of the time point, revealed the representing taxa associated with the best flesh colour group (Flesh29–31): *Mycoplasmataceae* (F) (belonging to *Mollicutes* (C)), *Bacillaceae* (F) (belonging to *Bacilli* (C)), and *Pseudomonas* (G) (belonging to *Gammaproteobacteria* (C)) (Fig. 2.14b). The representative for Flesh23–24 was *Vibrio* (G) (belonging to *Gammaproteobacteria* (C)) (Fig. 2.14b). There were no representatives for the other phenotypes in flesh colour.

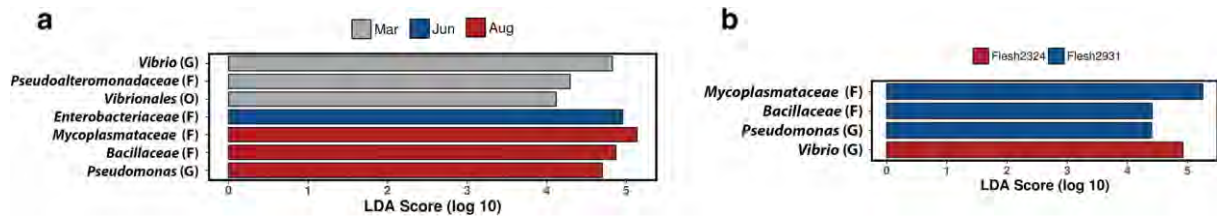


**Fig. 2.14** Significantly differentiated taxa across metadata: a) time-point and b) flesh-colour. Phylum, class, order, family, genus, and species were shortened as P, C, O, F, G, and S, respectively

The balance trees<sup>74</sup>, which included ten statistically significantly different clades of microbiota relating to each phenotype in each category (time point, flesh colour, and banding status), were built to determine the niche taxonomy that may be correlated to the phenotype. The regression model built from time point category could explain up to 22.8% of the community variance ( $R^2 = 0.228$ , Supplemental Material S3A). This regression model also showed that there was a shift of microbiota from Mar to Jun and Aug:  $R^2$  differences showed the microbiota community of Jun and Aug were 11.7% and 18.4%, respectively, differing from the microbiota community in Mar (Supplemental Material S3A). The change of the microbiota community is presented in the heatmap-of-balances tree generated from the hierarchical clustering of OTUs (Fig. 2.15). The full regression model, heatmap, and the taxa in each balance can be found in the Supplemental Material S3A. In the heatmap, the major microbiota communities in Mar were *Vibrionaceae* (F), *Pseudoalteromonadaceae* (F), *Burkholderia* (G), *Enterobacteriaceae* (F), *Ralstonia* (G), and *Microbacteriaceae* (F) (Fig. 2.15). In contrast, the major microbiota in Aug was *Vibrionaceae* (F), *Bacillaceae* (F), *Phyllobacteriaceae* (F), *Comamonadaceae* (F), *Burkholderia* (G), *Ralstonia* (G), and *Mycoplasmataceae* (F) (Fig. 2.15). Hence, there was a clear shift in the composition of the microbiota in the community from Mar to Aug. The regression model of the flesh colour showed that it could explain 9.4% of the microbiota community variance ( $R^2 = 0.094$ , Supplemental Material S3B). The balances heatmap also presented the gradual movement of the microbiota community from the group of Flesh21–22 to Flesh29–31 (Fig. 2.16), in which groups of Flesh25–26 and Flesh27–28 could explain the microbiota community variance of up to 8.14% and 8.15%, respectively (Supplemental Material S3B). In the heatmap, the differentiated taxa in Flesh27–28 and Flesh29–31 were *Phyllobacteriaceae* (F), *Mycoplasmataceae* (F), and *Bacillaceae* (F) (Fig. 2.16). In contrast, the representatives for Flesh21–22 and Flesh23–24 were *Vibrionaceae* (F), *Pseudoalteromonadaceae* (F), *Enterobacteriaceae* (F), *Microbacteriaceae* (F), and *Ralstonia* (G) (Fig. 2.16). The taxa in Flesh25–26 were the consensus between the two groups above, which included *Burkholderia* (G), *Vibrionaceae* (F), *Microbacteriaceae* (F), and *Ralstonia* (G) (Fig. 2.16). The full regression model, heatmap, and the taxa in each balance can be found in the Supplemental Material S3B.

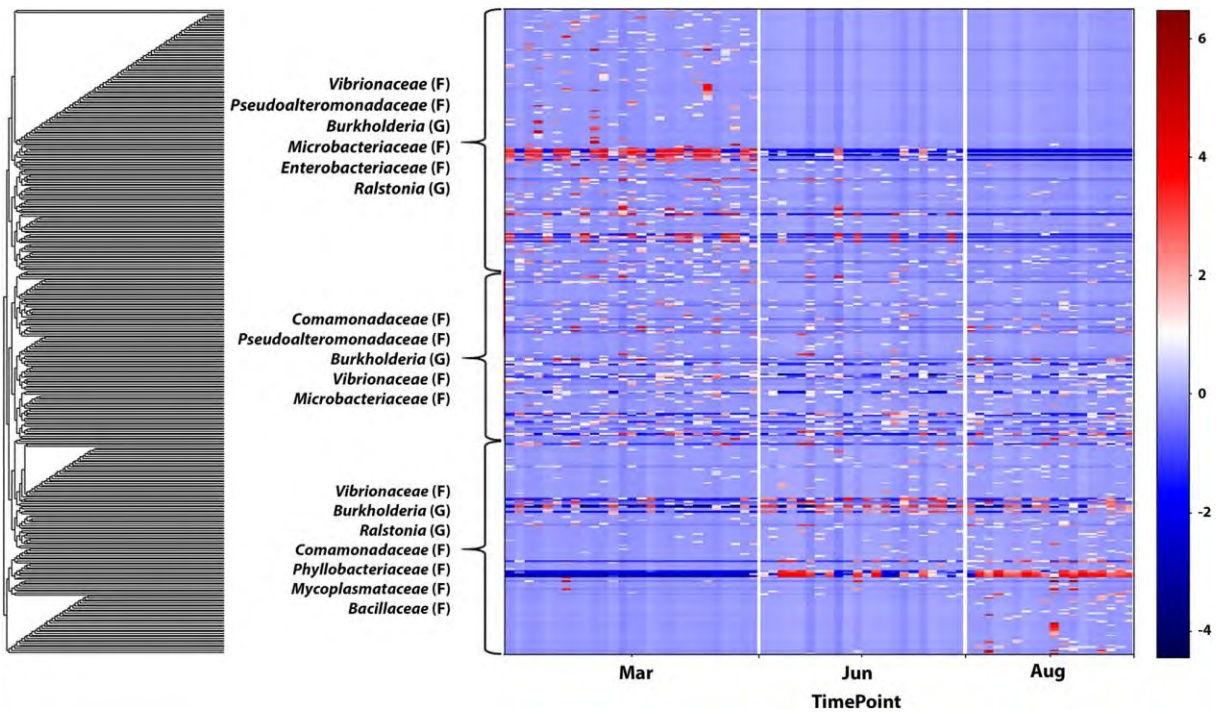


**Fig. 2.15** The balance tree generated from the hierarchical clustering of OTUs over the time-points. The OTUs abundance values were log-transformed. Differentially represented families (F) and genus (G) clusters are detailed.

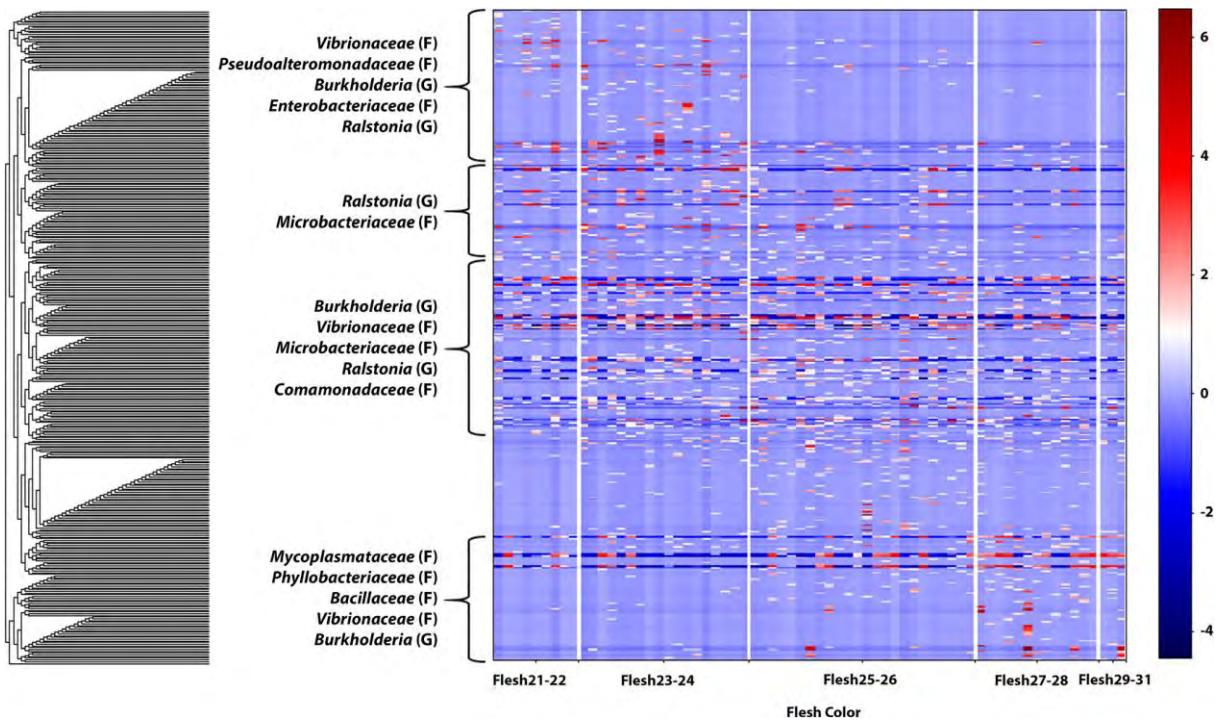


**Fig. 2.16** The balance tree generated from the hierarchical clustering of OTUs over the flesh colour groups. The OTUs abundance values were log-transformed. Differentially represented families (F) and genus (G) clusters are detailed.

To further examine whether the microbiota's transition in the flesh colour is dependent to the time point's, the samples were assessed for the flesh colour's regression model according to the time-point when they were collected (Mar, Jun, Aug in Fig. 2.17a–c, respectively). The effect of flesh colour appears to be independent of the month based on qualitative pattern similarity to the overall flesh

colour analysis. Due to the nature of sample distribution, there were no Flesh29–31 collected in Mar and Jun, and there was no Flesh21–22 in Aug (Fig. 2.17). The regression model of the flesh colour for each time point could explain 10.8% ( $R^2 = 0.1082$ ), 12.5% ( $R^2 = 0.125$ ), and 12.9% ( $R^2 = 0.1287$ ) of the microbiota variance in Mar, Jun, and Aug, respectively (Supplemental Material S3C). The balance heatmaps of flesh colour for each time point (Fig. 2.17) have the same transition pattern with the heatmap of all flesh colour samples across all time points (Fig. 2.16). This indicates that the change of microbiota associated with the flesh-colour is regardless of the time-point (i.e., the change of water temperature). The full regression model and related taxa for each balance can be found in the Supplemental Material S3C.

Unlike other categories, the banding status' regression model explained merely 4% of the microbiota community ( $R^2 = 0.04$ , Supplemental Material S3D), and the balance heatmap was not clear between the phenotypes. The microbiota communities that are hypothesized to influence the severe-banding group are *Pseudoalteromonadaceae* (F), *Vibrionaceae* (F), *Microbacteriaceae* (F), and *Enterobacteriaceae* (F) (Fig. 2.18). Also, the taxa that might influence the none banding group were identified as *Vibrionaceae* (F), *Pseudoalteromonadaceae* (F), *Burkholderia* (G), *Enterobacteriaceae* (F), and *Phyllobacteriaceae* (F) (Fig. 2.18). The full regression model, heatmap, and the taxa in each balance can be found in the Supplemental Material S3D.

#### **2.2.4.3 Prediction of Functional Composition Based on the Bacterial Metagenome**

We used PICRUSt to predict the functional composition of the metagenome as well as the gene families in a relationship with the host. There were 6909 KEGG Orthologous groups (KOs) predicted and categorized into 328 KEGG pathways. These were analyzed according to categories to identify the shared and differential pathways. The predictive functional compositions were strongly affected by the time point since the  $\beta$ -diversity was significantly different (Adonis  $P = 0.0003$ ), whereas the flesh colour and banding status were not (Adonis  $P = 0.061$  and  $P = 0.307$ , respectively). In terms of functional differentiation in the flesh colour, the predicted pathways enriched in the low colour index Flesh23–24 group included fatty acid and lipid biosynthesis, building peptidoglycan membrane, bacterial proteins mobility, and transporting proteins (Fig. 2.19a). The predicted pathways enriched in the high colour index Flesh29–31 group included synthesizing aminoacids and energy generating (Fig. 2.19a). In the banding status category, the predicted pathways enriched in the moderate banding group included sugar degradation, required for growth or energy production and amino acid biosynthesis (Fig. 2.19b). The predicted pathways enriched in the severe banding group included fatty acid and lipid biosynthesis, energy creating pathways, and amino acid biosynthesis in which lipid is co-transported from the gut together with the carotenoid<sup>77</sup>. In Pearson's correlation across groups in three categories, generally, there were two patterns. The microbiotas in the phenotypes of Flesh27–28 and Flesh29–31 had the same dominance pattern as the microbiotas in Jun, the time when the fish start to recover from the heat stress in summer. This pattern reached the ultimate level in Aug, in which the carotenoid biosynthesis and ubiquinone and other terpenoid-quinone biosynthesis were enriched (Fig. 2.19c). Conversely, the group of Flesh23–24, Flesh25–26, and especially, Mar, shared the same pattern that had the terpenoid backbone biosynthesis and was in the reverse direction to the above (Fig. 2.19c).

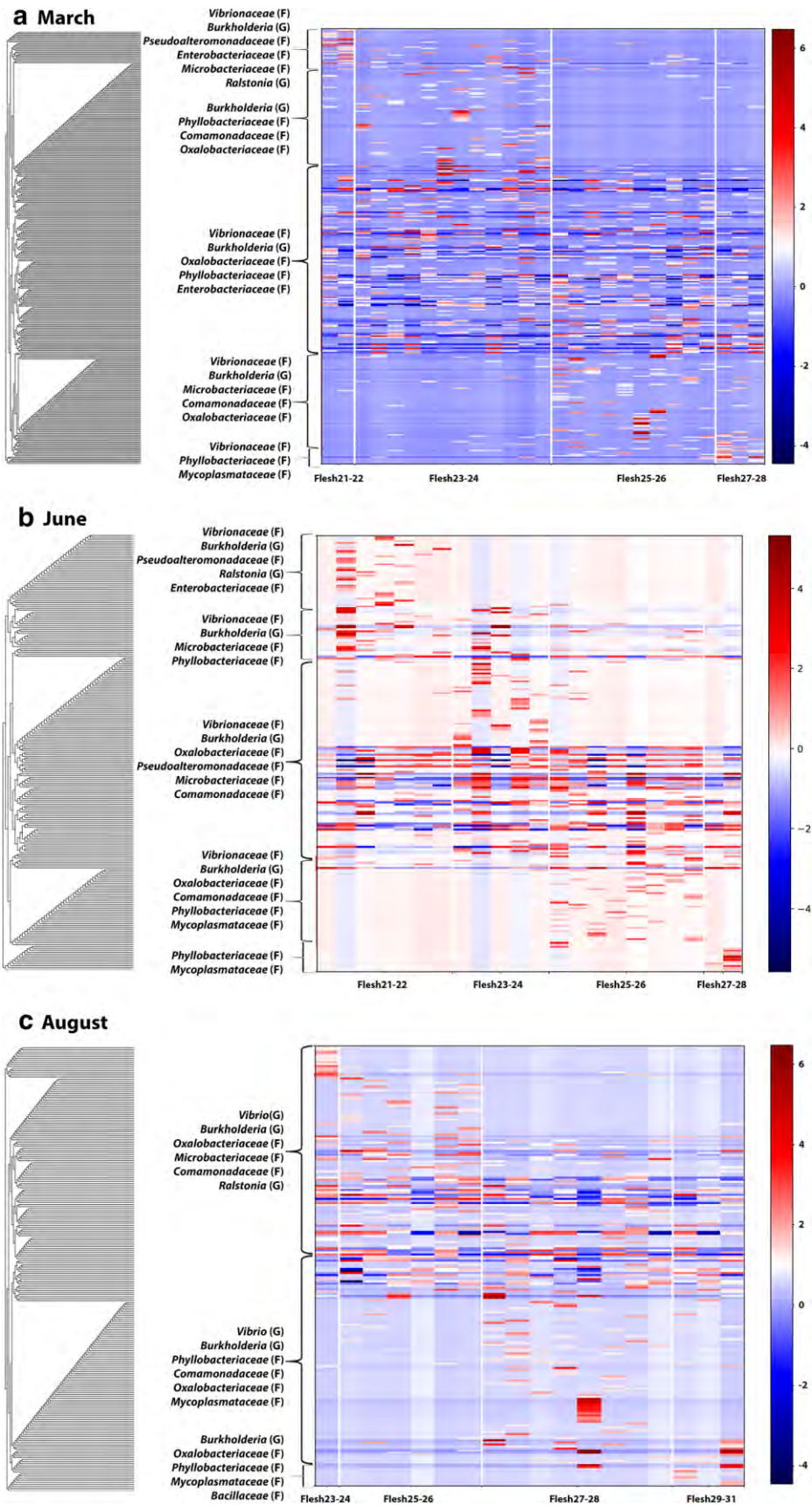


**Fig. 2.17** The balance tree generated from the hierarchical clustering of OTUs over the flesh colour groups for each time point a) Mar, b) Jun, and c) Aug. The OTUs abundance values were log-transformed. Differentially represented families (F) and genus (G) clusters are detailed.

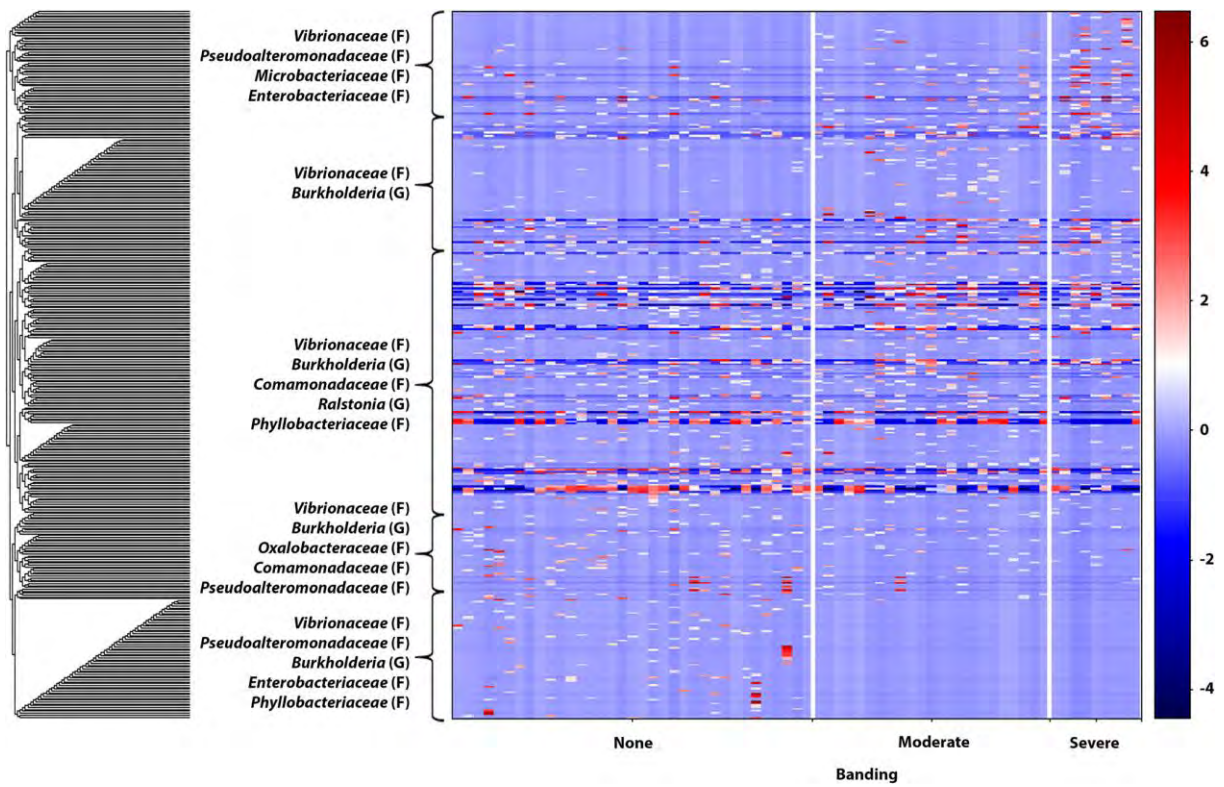


**Fig. 2.18** The balance tree generated from the hierarchical clustering of OTUs over the banding-status groups. The OTUs abundance values were log-transformed. Differentially represented families (F) and genus (G) clusters are detailed.

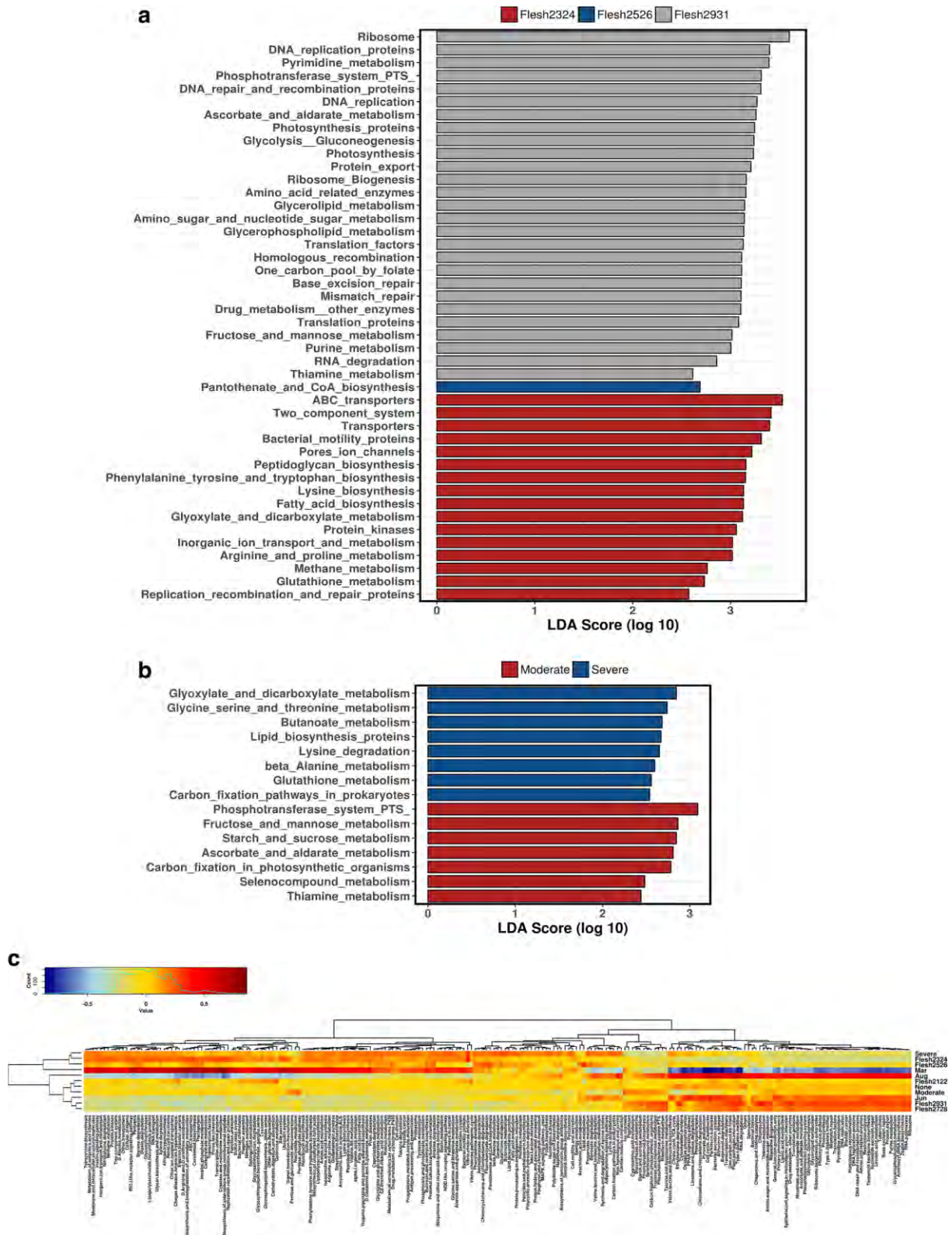


**Fig. 2.19** The prediction of metabolic pathways across the categories Flesh-colour and banding-status. The differential metabolic pathways that were predicted for a) flesh-colour: Flesh23–24 (red), Flesh25–26 (blue), Flesh29–31 (gray); and b) banding-status: Moderate (red), severe (blue) indicated the most common pathways for each category. c) Pearson's correlation of the metabolic pathways across the groups in all categories. The abundance of the metabolic pathways was log-transformed.

#### **2.2.4.4 Predicted Terpenoid Biosynthesis, Esterification, Lipid, Carotenoid, and Lipopolyprotein Metabolic Pathways Shared the Same Microbiota Taxa in the Unfavorable Colour Phenotypes**

We have confirmed that the microbiota are changing over the time points, and this indicates the dominant taxa at each time point. To further analyze which taxa could affect (or be affected by) the flesh colour and banding status, five relevant metabolic pathways were chosen: carotenoids, terpenoid, lipid, esterification, and lipopolyprotein metabolic pathways. For each pathway, the outcome presented the OTUs abundances in each sample. The predicted metabolic pathways in this study had their own typical taxa representative for good colour phenotype in the flesh (Fig. 2.20) and the banding status (Fig. 2.21). For example, for the phenotype Flesh29–31, there were *Bacillaceae* (F) in the terpenoid pathway (Fig. 2.20a); *Burkholderiaceae* (F), *Comamonadaceae* (F), and *Oxalobacteraceae* (F) (all belonged to the order *Burkholderiales*) in the carotenoids pathway (Fig. 2.20c); and *Mycoplasmataceae* (F) and *Geobacillus* (G) in the lipopolyprotein pathway (Fig. 2.20i). For the non-banding phenotype, there were *Vibrionaceae* (F) and *Mycobacterium* (G) in the terpenoid pathway (Fig. 2.21a); *Xanthomonadaceae* (F) in the carotenoid pathway (Fig. 2.21c); *Vibrionaceae* (F), *Mycoplasmataceae* (F), *Rhizobiales* (O), and *Burkholderia bryophila* in the lipid and esterification pathway (Fig. 2.20e, g); and *Vibrionaceae* (F), *Mycoplasmataceae* (F), *Burkholderia bryophila*, and *Bradyrhizobiaceae* (F) in the lipopolyprotein pathway (Fig. 2.21i). Interestingly, all these pathways had the same typical taxa in the least favorable colour phenotype and severe banding, which was clearly demonstrated by the Pearson's correlation heatmaps in Fig. 2.20 and 2.21: *Enterobacteriaceae* (F), *Vibrio* (G), *Aliivibrio fischeri*, and *Pseudoalteromonadaceae* (F).

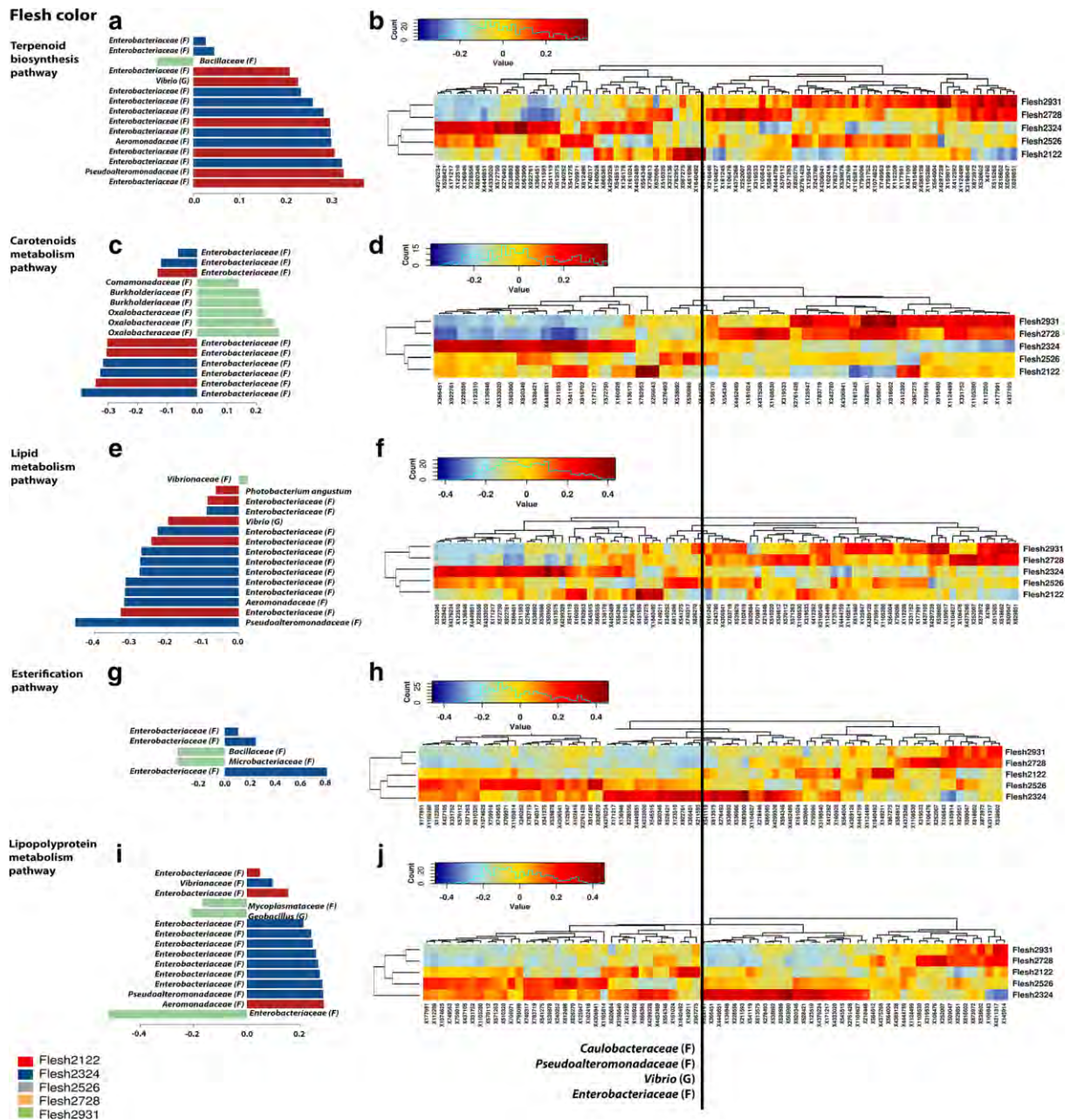


**Fig. 2.20** Differential KEGG pathways and Pearson's correlation of a), b) terpenoid biosynthesis, c), d) carotenoids, e), f) lipid, g), h) esterification, and i), j) lipopolyproteins metabolic pathways in response to flesh colour. Phylum, class, order, family, genus, and species were shortened as P, C, O, F, G, and S, respectively. The flesh colour groups were coloured as (red) Flesh21–22, (blue) Flesh23–24, (gray) Flesh25–26, (orange) Flesh27–28, and (green) Flesh29–31.



growth rate, such as salinity and oxygen saturation<sup>78–80</sup>. Especially, the combination of high temperature (> 20.1 °C) and low dissolved oxygen level (< 35% saturation) create a challenging environment that leads to poor appetite and affects metabolism and growth regulation in Atlantic salmon<sup>81,82</sup>. However, in the site where the sampling was conducted, the dissolved oxygen level is extremely well maintained that it is never lower than 85% saturation (data not shown). Therefore, the fluctuation of temperature was the focus in this study. The samples were collected in three time points, Mar, Jun, and Aug, which covered the temperature change from warmer temperatures in Mar (> 20 °C; thermal stress) to cooler in Aug (10 °C; optimal condition<sup>41</sup>). Since the samples were collected at three time points along the year which were parallel with the fish growth, there was a difference in fish size and age between sampling events (i.e., time point). To eliminate the variance factor coming from the fish size/age which might lead to the possible difference of microbiota community, the fish were selected at the similar size/age in each time point for the analysis (Supplemental Material S1). In each time point, the samples were collected from individuals with variable flesh colour and banding status. The 16S rRNA gene sequencing data were analysed based on three metadata (i.e., three categories of samples): time point, flesh colour, and banding status. Most of the taxa are provided at family (F) and genus (G) (levels 5 and 6, respectively) which are next to the lowest level (level 7: species). There are only four taxa mentioned at level 4 (order) (in Figs. 2.11a, 2.12, 2.13a, 2.19a (*Vibrionales*, *Ellin6513*, *Alteromonadales*, *Rhizobiales*). In QIIME analysis, there were some taxa revealed at species level, but not for the majority. Therefore, we chose family and genus levels to present the taxonomy. When examining the salmon gut microbiota, we observed that it was highly impacted by the timing of the sampling (i.e., the change of temperature over time). The fluctuation of temperature was already demonstrated to affect the Atlantic salmon gut microbiota in Tasmania, in a different location from the current study, with differential bacterial diversity during summer being dominated by *Vibrio* spp. and accompanied by a dramatic decrease in lactic acid bacteria<sup>59</sup>. We have confirmed the clear transitions of the microbiota population over the time points, from the dominance of *Enterobacteriaceae* (F), *Pseudoalteromonadaceae* (F), and *Vibrionaceae* (F) in Mar to the dominance of *Bacillaceae* (F), *Mycoplasmataceae* (F), *Phyllobacteriaceae* (F), and *Burkholderia* (G) in Aug, consistent with previous studies<sup>39,59,83</sup>. Zarkasi et al. characterized the gastrointestinal tract and fecal microbiota across a 13-month period and confirmed the influence of time (temperature) and diets on the change of the gastrointestinal microbiota. They also confirmed the dominance of *Vibrionaceae* (F) in midsummer, demonstrating the similar trending of *Enterobacteriaceae* (F) in Mar and *Mycoplasmataceae* (F) in Aug<sup>39,83</sup>. The dominant taxa in Mar (Fig. 2.14a) all belonged to two classes, *Alphaproteobacteria* (C) and *Gammaproteobacteria* (C), which include a wide range of aerobic bacteria having diverse catabolism pathways<sup>39</sup> and potentially affecting the host physiology and immune system<sup>84</sup>. The dominance of *Mycoplasmataceae* (F) in Aug and in the high flesh-colour index group of Flesh29–31 (Fig. 2.14b) is interesting since it has not been considered previously in the context of flesh colour but sporadically presented in the host gastrointestinal tract as an influencer of the microbiota community<sup>83,85</sup>. The Aug samples were also enriched and diverse with a wide range of taxa belonging to *Tenericutes* (P), *Actinobacteria* (P), *Alphaproteobacteria* (C), *Gammaproteobacteria* (C), *Firmicutes* (P), especially *Mycoplasmataceae* (F), and *Bacillaceae* (F) (Fig. 2.14a). These clear transitions of the gut microbiotas over the time points may not be affected by the microbiotas either in the water or in the diet. In the previous studies, the dominant microbiotas found in the salmon gut were significantly different with the dominant microbiotas found in surrounding water<sup>86,87</sup> and diet<sup>86,88,89</sup>. There is evidence that regardless of the dynamic change, the gut microbiotas community must maintain the strong core members to adapt to the gut environment<sup>90–92</sup>. Furthermore, environmental

microbes tend to decline after the core microbes have colonized the gut <sup>39</sup>. This confirms the distinction of the inside- and outside-host microbiotas.

Regardless of the time point, distinct microbiota profiles were associated with the flesh colour and were independent of the temperature change. The  $\beta$ -diversity of the flesh colour groups were significantly different at PERMANOVA  $P = 0.016$  in weighted UniFrac distance metrics (Fig. 2.13b). The regression model of all samples could explain up to 9.4% of the microbiota variance (Fig. 2.16, Supplemental Material S3B). Furthermore, the regression model was also built for flesh colour samples according to the collecting time point, and they were all the same (Fig. 2.17) and could explain up to 10.8%, 12.5%, and 12.9% of the microbiota variance for the flesh colour in Mar, Jun, and Aug, respectively (Supplemental Material S3C). Therefore, the microbiota associated with different levels of flesh colour is predicted to have an impact on the colour formation in the flesh. There was a shift of microbiota communities from the phenotype of pale flesh to pink-red flesh. Flesh21–22 was enriched with *Vibrionaceae* (F), *Pseudoalteromonadaceae* (F), *Enterobacteriaceae* (F), and *Ralstonia* (G) (Figs. 2.16 and 2.17). Flesh 23–24 and Flesh25–26 were enriched with *Vibrionaceae* (F), *Pseudoalteromonadaceae* (F), *Enterobacteriaceae* (F), *Ralstonia* (G), *Microbacteriaceae* (F), *Burkholderia* (G), and *Comamonadaceae* (F) (Fig. 2.16 and 2.17). *Vibrionaceae* (F), *Pseudoalteromonadaceae* (F), and *Enterobacteriaceae* (F) are quite common in the salmon intestinal tract <sup>83,90</sup>, and *Microbacteriaceae* (F) was exclusively found in healthy salmon eggs <sup>93</sup>. *Burkholderia* (G), *Ralstonia* (G), and *Comamonadaceae* (F) are found as the common bacteria in the digesta compartments along the salmon intestine <sup>62</sup>. In addition, *Comamonadaceae* (F)'s abundance significantly changed between genetically distinct salmon populations <sup>94</sup>. The group of high colour index Flesh29–31 was differentiated with *Mycoplasmataceae* (F), *Bacillaceae* (F), *Pseudomonas* (G), and *Phyllobacteriaceae* (F) (Figs. 2.14b, 2.16, and 2.17). *Pseudomonas* (G) is able to generate red carotenoid pigment spirilloxanthin <sup>95</sup>. *Bacillaceae* (F) is considered a beneficial taxon and is dominant in healthy fish as they can produce antibiotics, vitamins, and digestive enzymes <sup>96</sup>. *Mycoplasmataceae* (F) can produce carotenoids <sup>97</sup>. *Phyllobacteriaceae* (F) was dominant in salmon reared in low salinity <sup>98</sup>, in hatchlings of salmon <sup>99</sup>, and in the skin of infected salmon challenged with *L. salmonis* copepods <sup>100</sup>. To our knowledge, these microbiotas have not been linked with any phenotype yet. Since the  $\beta$ -diversity of the flesh colour phenotypes was significantly different, it is possible that the taxa *Mycoplasmataceae* (F), *Bacillaceae* (F), *Pseudomonas* (G), and *Phyllobacteriaceae* (F) contribute to the carotenoid metabolism in Atlantic salmon.

Functional composition analysis of the OTUs predicted 6909 KEGG Orthologous groups (KOs), categorized into 328 KEGG pathways. The functional composition was strongly influenced by the time point. Due to the broad impact temperature has on the microbiota, both the OTU abundance, predictive functions, and their relative metagenome were expected to be significantly affected. Besides the carotenoids and terpenoid metabolism, we selected a further three relevant metabolic pathways that are predicted to be involved in the carotenoids metabolism and deposition: lipid <sup>77</sup>, esterification <sup>101,102</sup> and lipopolyprotein metabolism <sup>21,103–105</sup>. In the unfavorable colour phenotypes, all five metabolic pathways discussed in this study (Figs. 2.20 and 2.21) shared similar taxa that were *Aeromonadaceae* (F), *Pseudoalteromonadaceae* (F), *Vibrio* (F), and *Enterobacteriaceae* (F) in groups of Flesh21–22 and Flesh23–24 (Fig. 2.20); *Enterobacteriaceae* (F), *Vibrio* (G), *Pseudomonadaceae* (F), *Mesorhizobium* (G), Ellin6513 (O), *Ralstonia* (G), *Burkholderia* (G), and *Caulobacter* (G) in the group of severe banding (Fig. 2.21). In previous studies, the dominating taxa occupying the fish intestine include *Vibrio* (G) for chitin-decomposing function <sup>106</sup>; *Bacteroidaceae* (F), *Clostridium* (G), *Acinetobacter* (G), *Enterobacteriaceae* (F), *Bacillus* (G), and *Pseudomonas* (G) for hydrocarbon-degradation <sup>50</sup>; and *Actinobacteria* (P), *Bacteroidetes* (P), *Firmicutes* (P), and *Proteobacteria* (P) for triggering immunity <sup>107</sup>.

The relationship of the gut microbiota and the host is categorized into two main groups: symbiosis (i.e., the microbiota participates in the normal metabolism and immune induction) and dysbiosis (i.e., the interaction between the gut and the microbiota is significantly affected by environmental stresses, infection, and diseases) (reviewed in <sup>108</sup>). In the symbiosis, there is a state called “altered symbiosis,” in which the microbiota change due to the change of the biological state of the host, or the environmental stresses; however, this change of microbiota does not affect the host health. The altered symbiosis can happen in the short or long term and is considered normal (reviewed in <sup>108</sup>). The fish in this study were all healthy; therefore, the interaction between the microbiota and the pale-colour individuals may fall into the state of “altered symbiosis.” Interestingly, the gut microbiota have been demonstrated to change/regulate the fish’s gene expression pattern <sup>109–111</sup>. Therefore, the similarity in the microbiota composition in the low colour index and severe banding individuals suggests that these microorganisms may play a role in colour-related gene expression. Many bacteria species are able to produce carotenoids or terpenoids, a diverse group of organic compounds, via either the mevalonate pathway or the MEP pathway (reviewed in <sup>112</sup>) for different purposes, for example, pigmentation (carotenoids), electron carriers (ubiquinone), and membrane component (phytosterols) (reviewed in <sup>113</sup>). Specifically, terpenoids are generated by prokaryotes in the natural environment or in the host in which part of these metabolites is transferred to the host <sup>114</sup>. In the group of Flesh27–28, Flesh29–31, and none-banding phenotypes, there are diverse microbiota that could contribute to each metabolic pathway (Figs. 2.20 and 2.21). For example, *Bacillaceae* (F), *Mycobacterium* (G), and *Vibrionaceae* (F), which all have the Terpenoid biosynthesis pathway, were found in the groups of Flesh29–31 and none-banding; similarly, *Mycoplasmataceae* (F), *Bacillaceae* (F), and *Bradyrhizobiaceae* (F), which all have the Lipopolyprotein pathway, were found in the groups of Flesh29–31 and none-banding (Figs. 2.20 and 2.21). Predicted carotenoid synthesis ability was found throughout the genus *Mycobacterium* (G) <sup>115</sup>. *Bradyrhizobiaceae* (F), which is found as the natural endosymbiont in plants roots <sup>116,117</sup>, is able to produce a wide range of bacteriochlorophylla and canthaxanthin <sup>118</sup>. In these good phenotype groups, *Mycoplasmataceae* (F), which can produce carotenoids <sup>97</sup>, is also abundant (Figs. 2.20 and 2.21). *Mycoplasmataceae* (F) includes two major genera: one requires sterols for growth and the other one does not and can synthesize non-saponifiable lipids (i.e., including terpenoids) <sup>119</sup>. However, when the non-sterols requiring *Mycoplasmataceae* (F) were supplied with cholesterol as a sterol, they utilized it in the same manner as the sterol-requiring organism <sup>120</sup>, suggesting that the non-sterols requiring *Mycoplasmataceae* (F) also possess the sterols-utilizing mechanism. In another circumstance, demonstrated that the sterols required for the growth of *Mycoplasma hominis* could be substituted by the hydroxylated carotenoid C40, but not the carotenoid precursors <sup>121</sup>. The authors, therefore, hypothesized that the sterols-requiring organism was lacking some of the enzymes in the biosynthetic pathway needed to produce carotenoids <sup>121</sup>. However, the carotenoid synthesis ability was later discovered in *M. pneumoniae*, a sterol-requiring species <sup>122</sup> which hosts the MEP-like pathway for carotenoid synthesis <sup>97</sup>. Therefore, it is likely that regardless of which genera of *Mycoplasmataceae* (F) (the sterols- or non-sterol-requiring) were present, the carotenoid synthesis mechanism is there to ensure their growth in the sterol deficient situation, and hence they can support colour formation in the fish. In addition, it is possible that the taxa *Bradyrhizobiaceae* (F), *Brevundimonas diminuta*, *Mycoplasmataceae* (F), *Pseudomonas* (G), and *Mycobacterium* (G), which appeared in the group of high colour index individuals, contribute to the carotenoid production which is utilized by the salmon. Further investigation is needed to confirm this hypothesis. We recommend further study of the communication of these microbiota and the salmon as the gnotobiotic model, which introduces the known microbiota to germ-free fish, as has been extensively studied in the zebrafish <sup>123</sup>.

## 2.2.6 Conclusions

In summary, we confirmed the significant influence of water temperature on the gut microbiota of the Atlantic salmon. We also demonstrated that the transition of the microbiota community is correlated with the shift of flesh colour (Fig. 2.22). Furthermore, our results predict the relationship between groups of microbiotas with either pale- or well-coloured fish. Further investigations of the interaction between these microbiotas and gene expression patterns relevant to flesh colour are recommended.

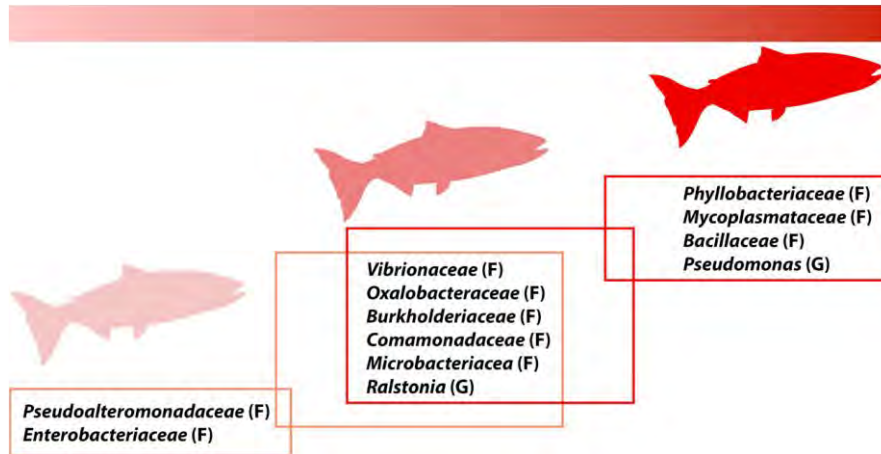


Fig. 2.22 The transition of flesh colour from pale to pink-red correlated with the transition of the microbiota composition.

## **2.3 Identification of molecular events associated with reduced flesh colour in gut and liver by transcriptome analysis, library benchmark study and SNPs exploration**

### **2.3.1 Background**

Flesh colour in Atlantic salmon is given by the deposition of ingested carotenoids from the food. In Tasmania, high summer temperatures (relative to the Atlantic salmon native geographical distribution), can result in chronic thermal stress which leads to lack of food consumption. Consequently, variation in carotenoid absorption in the digestive system, carotenoid catabolism in the liver and differential retention in the muscle are evident. Key genes that affect the absorption, delivery and metabolism of carotenoids in these organs were identified in previous studies. In our study, transcriptomic analyses have been conducted on the liver and the hindgut to better understand the molecular mechanisms associated with flesh colour. After completing the liver and gut transcriptome analysis (based on sampling conducted in 2017, section 2.2), a benchmark study was carried out on the hindgut, comparing two sequencing methodologies to assess if the low coverage transcriptomic analysis (which costs less and enables more samples to be sequenced) provided sufficient data for understanding the molecular basis of colour variations.

In addition, following the results of the benchmark study single nucleotide-polymorphisms (SNPs) analysis was performed to find reliable interesting SNPs that might be gene markers for the pale-banded fish.

### **2.3.2 Materials and methods: transcriptome analysis**

#### **2.3.2.1 Samples selection and RNA extraction**

From the aforementioned sampling event, samples of liver and gut were collected from each fish then immediately preserved in RNAlater (stored overnight at 4 °C and then at – 80 °C until analysis). For RNA extraction, 39 individuals were selected from the time point C samples, focusing on those which had various weight, flesh colour and banding status (n1 = 39 liver samples, n2 = 39 gut samples) (Table 2.2).

Total RNA was extracted from liver and gut using RNeasy mini Kit (Qiagen, Cat no./ID: 74104), treated with DNase I (RNase-free) (Biolabs, Cat no. M0303S) for gDNA removal, according to the manufacturer's manual. The quantity, quality and integrity of extracted RNA were identified using NanoDrop 2000 spectrophotometer (ThermoFisher Scientific, USA) and Agilent 2100 Bioanalyzer (Agilent Technologies, Inc., USA). RNA samples used in library preparation were chosen based on the following criteria: A260/280 ratio within 2.0-2.2, A260/A230 ratios > 1.8 and RIN (RNA Integrity Number) values > 9.

**Table 2.2** The group of samples for transcriptome analysis<sup>1</sup>. All samples were collected on the 6/6 2017 and belonged to sampling group C.

Weight (kg)	Rounded colour	Banding	Liver sample	Gut sample
2.075	21	Moderate	C0317	C0320
2.215	21	None	C0209	C0212
1.77	21	Severe	C0261	C0264
2.77	22	Moderate	C0221	C0224
1.76	22	Moderate	C0245	C0248
2.56	22	Moderate	C0389	C0392
2.64	22	Moderate	C0393	C0396
2.91	22	None	C0269	C0272
3.335	22	None	C0285	C0288
2.895	22	None	C0381	C0384
2.655	22	None	C0397	C0400
2.6	22	Severe	C0217	C0220
3.66	22	Severe	C0253	C0256
2.625	24	Moderate	C0273	C0276
2.8	24	None	C0325	C0328
3.45	24	None	C0357	C0360
2.855	24	None	C0369	C0372
3.8	24	None	C0385	C0388
2.975	25	Moderate	C0265	C0268
3.145	25	Moderate	C0301	C0304
2.205	25	Moderate	C0377	C0380
3.245	25	None	C0201	C0204
3	25	None	C0205	C0208
2.75	25	None	C0229	C0232
2.905	26	Moderate	C0289	C0292
3.845	26	Moderate	C0305	C0308
3.815	26	Moderate	C0345	C0348
3.13	26	Moderate	C0353	C0356
2.91	26	None	C0213	C0216
3.235	26	None	C0237	C0240
3.32	26	None	C0293	C0296
3.935	26	None	C0297	C0300
3.08	26	None	C0349	C0352
2.61	26	None	C0373	C0376
4.655	27	Moderate	C0341	C0344
2.99	27	None	C0233	C0236
3.425	27	None	C0309	C0312
3.77	27	None	C0333	C0336
4.115	27	None	C0361	C0364

	High colour	Low colour
Rounded colour	≥ 25	≤ 24

	No banding	Banding
Banding	None	Moderate, Severe

<sup>1</sup> Grouping samples

### 2.3.2.2 Libraries preparation and sequencing

cDNA synthesis and library preparation were performed using QuantSeq 3' mRNA-Seq Library Kit for Illumina (FWD) (Lexogen, Cat no./ID: 015.96), Purification Module with Magnetic Beads (Lexogen, Cat no./ID: 022.96) and PCR Add-on Kit for Illumina (Lexogen, Cat no./ID: 020.96), according to the manufacturer's instructions. Library quantity was measured using Quantus Fluorometer (Promega Corporation). Sequencing were done employing a 100 bp single-end reads Illumina HiSeq 2500 at the Australian Genome Research Facility (AGRF).

### 2.3.2.3 Transcriptome analysis

The workflow of transcriptomic analysis was summarized and illustrated in Fig. 2.23. The quality of raw reads was examined using FastQC v.0.11.6<sup>124</sup>. Sequencing adapter poly-A tail, and low quality reads were trimmed using the BBDuk module in BBDuk v.38.22 (–<https://sourceforge.net/projects/bbmap/>) with the following parameter “ref=polyA.fa.gz,truseq.fa.gz ftl=8 k=13 ktrim=r useshortkmers=t mink=5 qtrim=r trimq=10 minlength=20”. Trimmed reads were aligned to the *S. salar* genome (Atlantic Salmon Genome - ICSASG\_v2, [https://www.ncbi.nlm.nih.gov/assembly/GCF\\_000233375.1/#/def](https://www.ncbi.nlm.nih.gov/assembly/GCF_000233375.1/#/def)) using HISAT2 v.2.1.0 with the default parameters<sup>125</sup>. Read counting was determined using HTSeq v.0.9.1<sup>126</sup>. For each comparison, genes with less than 10 reads across all samples were discarded. Differentially-expressed gene (DEG) analysis was conducted by DESeq2 in R (version 3.4.1)<sup>127</sup>. A gene was considered as DEG between two conditions when the following applied:  $|\log_2(\text{fold change})| > 1$ , p-adjusted value  $< 0.05$ . All DEGs were annotated using Blast2GO v.5.2.1<sup>128</sup> to assign gene ontology (GO) terms and Kyoto Encyclopedia of Genes and Genomes (KEGG) pathways. For each tissue, four pairs of comparison were defined to investigate the DEG based on two main criteria: colour score and banding factors. For the colour score factor, the difference between none and banding condition was assessed at low (LN\_vs\_LB) or high score level (HN\_vs\_HB). Similarly, the variance between low and high score level was tested at none (HN\_vs\_LN) or banding (HB\_vs\_LB) for the banding factor.

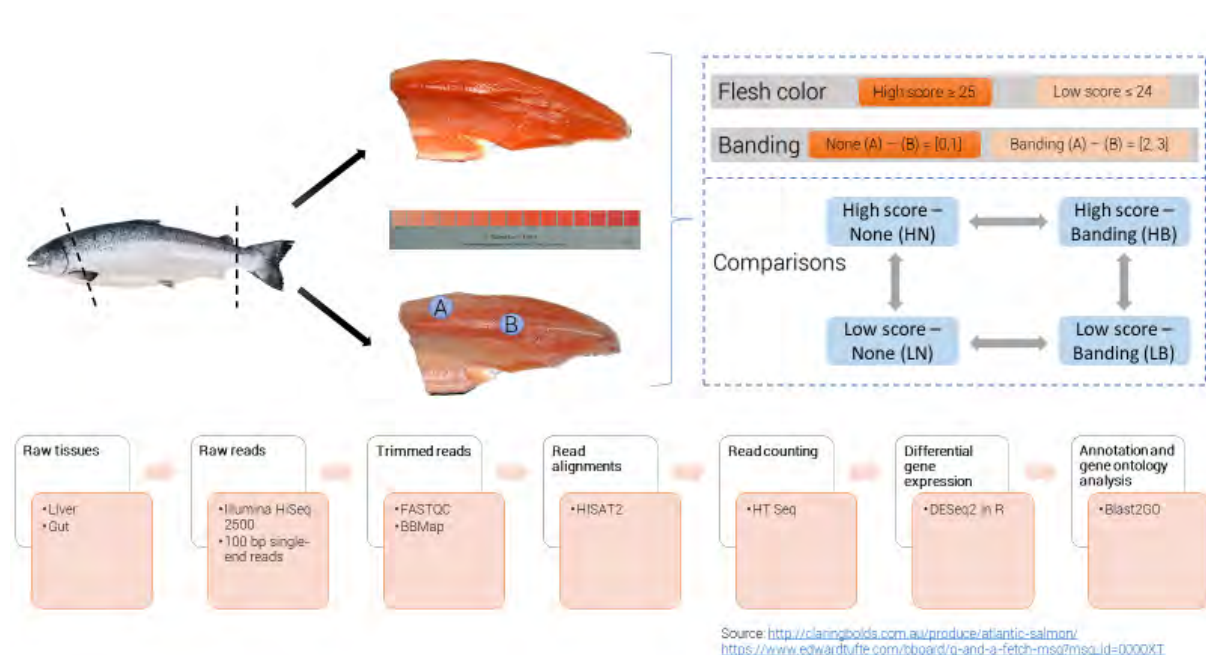


Fig. 2.23 The workflow of liver and gut transcriptomic analysis

### 2.3.3 Results and Discussion: transcriptome analysis

All 78 libraries were loaded on one lane of a flow-cell of Illumina HiSeq 2500 for RNA sequencing. In summary, these 78 libraries created 235,604,427 single-end reads. Each library generated between >700 thousand and higher than 23 million reads. On average, approximately 3.02 million reads of each library were kept following trimming adapter and quality filtering. The number of reads mapped onto the *S. salar* reference genome ranged between 79.76 to 89.12%. The result of sequencing, trimming and mapping was recorded in Table 2.3. From 78 libraries, 32 samples (2 tissues x 2 score levels x 2 banding levels x 4 specimens) were chosen to further analysis following the two criteria: score and banding. There are four groups including high none, low none, high banding and low banding, in which each group has 4 specimens.

**Table 2.3** Statistical sequencing data of 78 samples in *Salmo salar*.<sup>2</sup>

Sample ID	Raw reads	Data Yield (Gb)	Trimmed reads	Mapping rate (%)
<b>C204</b>	<b>1,604,246</b>	<b>0.16</b>	<b>1,541,246</b>	<b>84.32</b>
C208	2,745,323	0.28	2,620,810	86.08
C212	2,612,732	0.26	2,511,889	85.81
<b>C216</b>	<b>1,405,729</b>	<b>0.14</b>	<b>1,333,958</b>	<b>84.39</b>
<b>C220</b>	<b>2,667,961</b>	<b>0.27</b>	<b>2,541,652</b>	<b>85.11</b>
<b>C224</b>	<b>2,643,696</b>	<b>0.27</b>	<b>2,565,487</b>	<b>86.44</b>
C232	3,628,158	0.37	3,513,140	86.51
C236	4,965,013	0.5	4,736,595	86.99
C240	1,176,966	0.12	1,141,813	86.98
C248	762,180	0.08	737,022	87.67
<b>C256</b>	<b>2,375,238</b>	<b>0.24</b>	<b>2,307,620</b>	<b>86.49</b>
C264	2,021,558	0.2	1,951,801	86.58
C268	1,598,893	0.16	1,531,151	88.01
C272	1,583,360	0.16	1,529,655	86.93
C276	5,414,238	0.55	5,139,178	86.64
C288	5,494,669	0.55	5,287,025	86.5
<b>C292</b>	<b>2,501,552</b>	<b>0.25</b>	<b>2,416,188</b>	<b>86.44</b>
C296	1,124,564	0.11	1,064,995	82.9
C300	3,088,592	0.31	2,948,052	87.18
<b>C304</b>	<b>2,793,147</b>	<b>0.28</b>	<b>2,648,122</b>	<b>85.95</b>
C308	2,026,880	0.2	1,896,585	82.53
C312	2,560,419	0.26	2,443,517	86.07
C320	1,210,075	0.12	1,160,193	84.98
<b>C328</b>	<b>1,188,456</b>	<b>0.12</b>	<b>1,153,789</b>	<b>86.17</b>
<b>C336</b>	<b>2,242,804</b>	<b>0.23</b>	<b>2,172,191</b>	<b>82.14</b>
C344	2,276,849	0.23	2,192,523	85.79

<sup>2</sup> The samples highlighted in “green color” are chosen for differentially-expressed gene analysis. C292, C348, C356, C304 and C289, C301, C265, C353 represent four replicates for high banding group of gut and liver tissue; C220, C224, C256, C396 and C253, C217, C273, C393 represent four replicates for low banding group of gut and liver tissue; C376, C204, C336, C216 and C349, C293, C309, C373 represent four replicates for high none group of gut and liver tissue; C384, C328, C372, C388 and C369, C325, C381, C209 represent four replicates for low none group of gut and liver tissue.

<b>C348</b>	<b>2,946,653</b>	<b>0.3</b>	<b>2,756,189</b>	<b>82.71</b>
C352	1,717,307	0.17	1,665,009	85.47
<b>C356</b>	<b>1,465,264</b>	<b>0.15</b>	<b>1,392,054</b>	<b>84.85</b>
C360	1,971,371	0.2	1,893,830	86.17
C364	6,521,418	0.66	6,140,806	84.48
<b>C372</b>	<b>3,388,711</b>	<b>0.34</b>	<b>3,238,715</b>	<b>83.72</b>
<b>C376</b>	<b>1,248,981</b>	<b>0.13</b>	<b>1,198,387</b>	<b>79.76</b>
C380	1,034,125	0.1	1,005,599	87.31
<b>C384</b>	<b>2,631,602</b>	<b>0.27</b>	<b>2,506,739</b>	<b>86.74</b>
<b>C388</b>	<b>12,751,399</b>	<b>1.29</b>	<b>11,986,796</b>	<b>86.1</b>
C392	1,631,850	0.16	1,595,091	84.65
<b>C396</b>	<b>2,147,771</b>	<b>0.22</b>	<b>2,071,964</b>	<b>87.34</b>
C400	7,172,623	0.72	6,766,820	87.21
C201	1,981,254	0.2	1,845,931	87.46
C205	2,771,012	0.28	2,670,802	87.83
<b>C209</b>	<b>5,406,458</b>	<b>0.55</b>	<b>5,056,480</b>	<b>88.77</b>
C213	1,575,627	0.16	1,526,805	87.8
<b>C217</b>	<b>7,514,179</b>	<b>0</b>	<b>7,305,711</b>	<b>87.87</b>
C221	3,669,579	0.76	3,440,845	87.69
C229	1,977,787	0.2	1,910,460	86.64
C233	2,710,930	0.27	2,574,973	88.6
C237	3,061,389	0.31	2,834,592	87.17
C245	1,545,222	0.16	1,481,893	87.71
<b>C253</b>	<b>2,181,017</b>	<b>0.22</b>	<b>2,106,208</b>	<b>86.62</b>
C261	2,436,089	0.25	2,218,543	88.62
<b>C265</b>	<b>2,168,357</b>	<b>0.22</b>	<b>2,113,865</b>	<b>86.66</b>
C269	2,154,100	0.22	2,046,941	87.4
<b>C273</b>	<b>1,759,351</b>	<b>0.18</b>	<b>1,682,949</b>	<b>86.48</b>
C285	2,266,016	0.23	2,145,186	87.54
<b>C289</b>	<b>2,319,395</b>	<b>0.23</b>	<b>2,195,095</b>	<b>85.45</b>
<b>C293</b>	<b>3,445,561</b>	<b>0.35</b>	<b>3,311,025</b>	<b>86.72</b>
C297	2,301,795	0.23	2,161,196	85.4
<b>C301</b>	<b>3,733,741</b>	<b>0.38</b>	<b>3,535,749</b>	<b>87.46</b>
C305	1,993,022	0.2	1,919,506	87.19
<b>C309</b>	<b>1,674,935</b>	<b>0.17</b>	<b>1,607,775</b>	<b>86.48</b>
C317	1,282,889	0.13	1,205,126	86.43
<b>C325</b>	<b>2,669,681</b>	<b>0.27</b>	<b>2,522,641</b>	<b>87.34</b>
C333	5,177,638	0.52	4,846,512	85.75
C341	1,032,725	0.1	972,777	86.55
C345	2,145,121	0.22	2,029,502	87.77
<b>C349</b>	<b>2,676,457</b>	<b>0.27</b>	<b>2,551,487</b>	<b>87.49</b>
<b>C353</b>	<b>978,116</b>	<b>0.1</b>	<b>945,122</b>	<b>85.98</b>
C357	4,305,112	0.43	4,052,932	87.3
C361	1,984,146	0.2	1,873,555	87.78
<b>C369</b>	<b>2,325,224</b>	<b>0.23</b>	<b>2,220,895</b>	<b>86.29</b>

<b>C373</b>	<b>2,264,431</b>	<b>0.23</b>	<b>2,133,341</b>	<b>87.02</b>
C377	1,532,333	0.15	1,483,212	89.12
<b>C381</b>	<b>23,981,683</b>	<b>2.42</b>	<b>20,644,568</b>	<b>87.11</b>
C385	1,779,935	0.18	1,699,547	86.8
C389	3,545,125	0.36	3,171,731	87.48
<b>C393</b>	<b>2,063,376</b>	<b>0.21</b>	<b>1,994,754</b>	<b>86.85</b>
C397	4,871,246	0.49	4,618,058	87.72
<b>Sum</b>	<b>235,604,427</b>	<b>23.41</b>	<b>221,962,486</b>	
<b>Average</b>	<b>3,020,569.58</b>	<b>0.30</b>	<b>2,845,672.90</b>	<b>86.39</b>

We compared and determined the number of DEGs between four groups to detect colouration-related genes following the thresholds of log2 fold change and P-adjusted value set. In total, 260 DEGs were identified, of which 158 were up-regulated and 102 were down-regulated. The high none and low none (HN\_vs\_LN) comparison had the highest number of DEGs with 171 genes, meanwhile the lowest DEGs was recorded in the high banding and low banding (HB\_vs\_LB) comparison with 24 genes. For the score factor, the number of DEGs were 39 and 26 for low none and low banding (LN\_vs\_LB) and high none and high banding (HN\_vs\_HB), respectively. There were no DEGs detected for the comparison of HN and HB in the liver tissue though 26 DEGs were found in the gut. The number of DEGs of each comparison was illustrated in Fig. 2.24.

The above 260 DEGs were annotated further with Uniprot/Swissprot and KEGG database using Blast2GO. All Gene Ontology (GO) terms were categorized into three terms including Biological Processes, Molecular Functions and Cellular Components. There are 240 DEGs were assigned to Cellular Components, while Biological Process and Molecular Functions had 237 and 231 genes, respectively. To investigate the relating signal pathway, the DEGs were annotated using KEGG database. Using Blast2GO, 57 DEGs were assigned to 104 KEGG pathways. The biosynthesis of antibiotics was identified, which involved the highest number of DEGs, 7 genes more than other analyzed pathways. This pathway belonged to the comparison of high none and low none (HN\_vs\_LN).

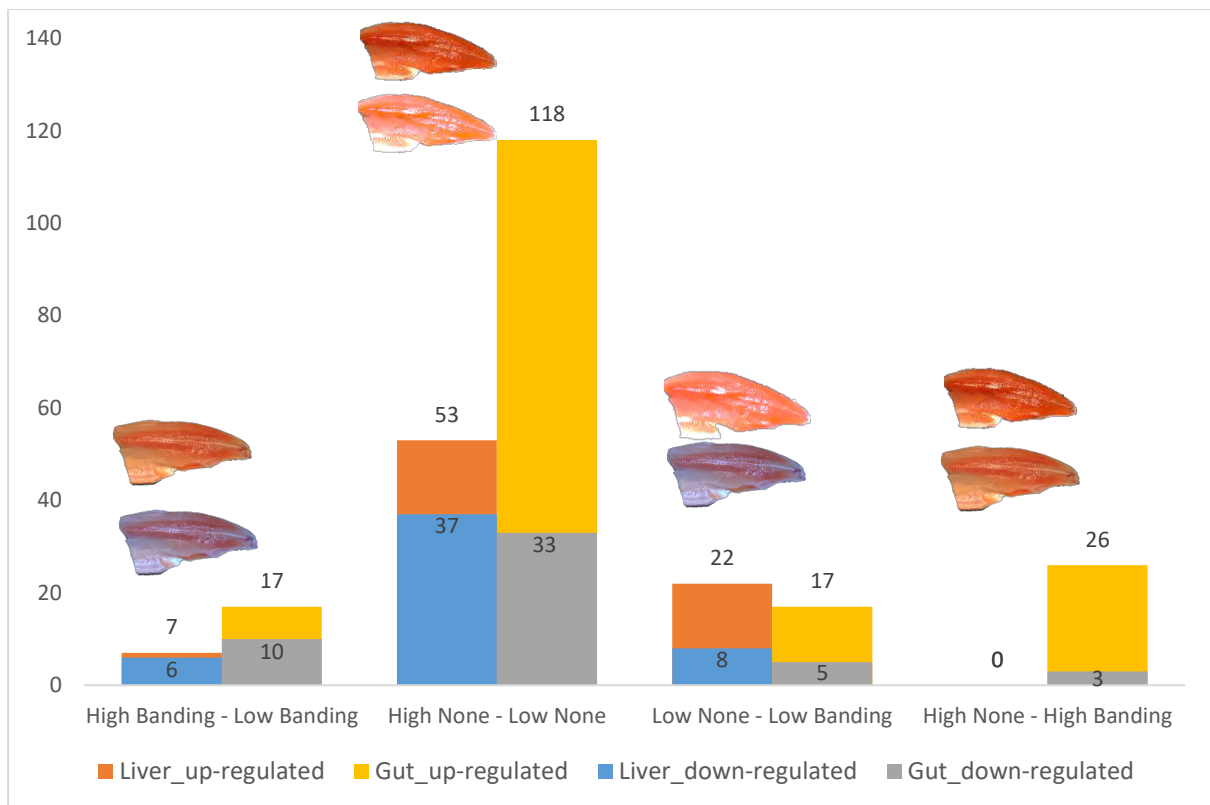


**Fig. 2.24** The number of differentially expressed genes with four comparisons

Based on previous studies on vertebrate species, from a total of 260 DEGs, 40 genes were further analyzed in four comparisons. In general, in fish with high colour score or none banding, we found that there were many up-regulated genes that are involved in lipid metabolism, fatty acid metabolism, oxidative stress and starvation. In contrast, genes upregulated in individuals with reduced flesh colour or banding, were identified to be structure proteins and genes involved in oxidative stress regulation. In the next section, we will discuss the short list of genes highlighted following each comparison.

### 2.3.3.1 Low colour-None banding versus Low colour-Banded (LN\_vs\_LB)

In total, 39 DEGs were detected in liver and gut transcriptomes between the two conditions tested, in which 26 genes expressed highly in low colour-none banding fish, while there are only 13 up-regulated genes in low colour-banded fish. In low colour-none banding fish, 9 genes including tropomyosin alpha-1 chain-like (tpm1-like), alpha smooth muscle actin (acta2), non-muscle caldesmon-like (cald1-like), transforming growth factor beta-induced 68kDa (tgfβ1), PDZ and LIM domain protein 3 (pdlim3), desmin-like (des-like) and synaptopodin-2-like (synpo2-like) were identified, all are encoding for muscle structural proteins (Table 2.4). These tpm1-like, cald1-like, acta2 and des-like genes have important roles in regulating the assembly, dynamics and stability of microfilament, F-actin, the muscle contraction, while synpo2-like is involved in actin bundling<sup>129-133</sup>. Besides, tgfβ1 is known to play a major function in myofibroblast differentiation during wound healing and fibro-contractile disease<sup>129</sup>. In a previous carotenoids-binding protein study, it was found that in the white muscle of Atlantic salmon and rainbow trout, the ratio of carotenoids : F-actin was recorded to be at its highest when compared with other proteins<sup>134</sup>. This result indicated that the carotenoid level has a strong correlation with F-actin protein in the Atlantic salmon muscle. Therefore, we propose that the muscle contraction and actin bundling correlates with the banding eventuation, and perhaps also with the carotenoid content in Atlantic salmon.

**Table 2.4** The selective DEGs in the comparisons of LN\_vs\_LB<sup>3</sup>

Tissue	Gene name	Protein name	Log2 Fold change	Function
<b>Structure protein</b>				
	tpm1-like	Tropomyosin alpha-1 chain-like	1.18	Regulating muscle contraction
	acta2	Alpha smooth muscle actin (LOC106578961)	1.46	Major component of contractile apparatus
		(LOC106589387)	1.29	
	cald1-like	Non-muscle caldesmon-like	1.36	Regulation of cell contraction and intracellular motional processes
Gut	tgfb1	Transforming growth factor, beta-induced, 68kDa	1.10	Regulating the expression of alpha-SM actin
	pdlim3	PDZ and LIM domain protein 3	1.49	Enhance the crosslinking of actin
	des-like	Desmin-like (LOC106574241)	2.16	Maintaining the structure of muscles
		(LOC106575168)	2.29	
	synpo2-like	Synaptopodin-2-like	1.35	Forming actin filament and bundling
<b>Oxidative stress, starvation, thermal acclimation and immune responses</b>				
Liver	serp1	Stress-associated endoplasmic reticulum protein 1	1.03	Responding to hypoxia and/or reoxygenation or other forms of stress
	txndc17	Thioredoxin domain-containing protein 17	1.08	Protecting the ovary and/or oocyte from oxidative stress

Furthermore, the low colour-none banding fish appeared to respond to stress conditions by overexpressing (1) stress-associated endoplasmic reticulum protein 1 (*serp1*), a protein that responded in the stress condition of cells and (2) thioredoxin domain containing protein 17 (*txndc17*), which was shown to protect the ovary or oocyte from oxidative stress<sup>135</sup> (Table 2.4). We hypothesize that in low colour-none banding fish, these DEGs protect the fish from stress conditions that impacted the structure of muscle proteins and other organs. In contrast, for the low colour-banding comparison, the down regulation of these genes suggests that the white muscle did not bundle up and contract, causing F-actin, the muscle protein in the white muscle to deconstruct and perhaps degrade. Consequently, this phenomenon may result in reduced binding of astaxanthin and its metabolites with F-actin, noticeably decreasing the low colour-banded fish. Examination of muscle fibers in banded fish from the different coloured regions can corroborate this hypothesis.

<sup>3</sup> Note: Log2 Fold change  $\geq 1$ : upregulated in the low color-none banding fish; Log2 Fold change  $\leq -1$ : upregulated in the low color-banding fish.

### 2.3.3.2 High colour-None banding versus High colour-Banded (HN\_vs\_HB)

For the comparison of high colour-none banding and high colour-banding fish, there were 26 DEGs in the gut transcriptome, while no gene was DEG in the liver. Of the 23 genes up-regulated in the high colour-none banding fish, 4 fatty acid metabolism-relating genes and 2 oxidative stress-relating genes were determined (Table 2.5). Serum albumin (alb1, alb2), the most abundant protein in the plasma are considered as the long-chain fatty acid transporters when they bind together to form complexes then circulate in the plasma system<sup>136</sup>. Some radioactive-based studies proposed that astaxanthin associated with the serum lipoproteins, the main transporters of esterified fatty acids and serum albumin<sup>21</sup>. Therefore, we propose that alb1 and alb2 up-regulated in the gut increase the astaxanthin absorption and transport from the gut into the blood system, then depositing in the muscle or liver. Apolipoprotein C-II is identified as the co-factor for lipoprotein lipase (LPL) that binds to chylomicrons, very low density lipoprotein (VLDL) and high density lipoprotein (HDL)<sup>137</sup>. When binding to chylomicrons and VLDL, apoc2 activates triglyceride hydrolysis to release free fatty acids into the adipose tissues<sup>137,138</sup> (Fig. 2.25 and Fig. 2.26). Due to their hydrophobic property, carotenoids or astaxanthin are described to be closely associated with fatty acids and transported with them through the intestine and blood circulation<sup>139</sup>. Hence, there may be a higher uptake of astaxanthin from triglyceride hydrolysis by up-regulating apoc2-like in the high colour-none banding fish.

**Table 2.5** The selective DEGs in the comparisons of HN\_vs\_HB<sup>4</sup>

Tissue	Gene symbol	Gene	Log2 Fold change	Function
<b><i>Fatty acid metabolism</i></b>				
	alb1	Serum albumin 1	1.56	Long-chain fatty acid transporters
	alb2	Serum albumin 2	1.53	Long-chain fatty acid transporters
Gut	apoc2-like	Apolipoprotein C-II-like	1.77	Co-factor for lipoprotein lipase, stimulate triglyceride hydrolysis
	apoc1-like	Apolipoprotein C-I-like	1.46	Inhibitor of cholesteryl ester transfer protein (CETP)
<b><i>Oxidative stress, starvation, thermal acclimation and immune responses</i></b>				
Gut	hpx-like	Hemopexin-like	1.66	A heme-binding serum glycoprotein
	hp-like	Haptoglobin-like	1.76	Inhibiting its oxidative activity

<sup>4</sup> Note: Log2 Fold change  $\geq 1$ : upregulated in the high color-no banding fish; Log2 Fold change  $\leq -1$ : upregulated in the high color-banding fish.

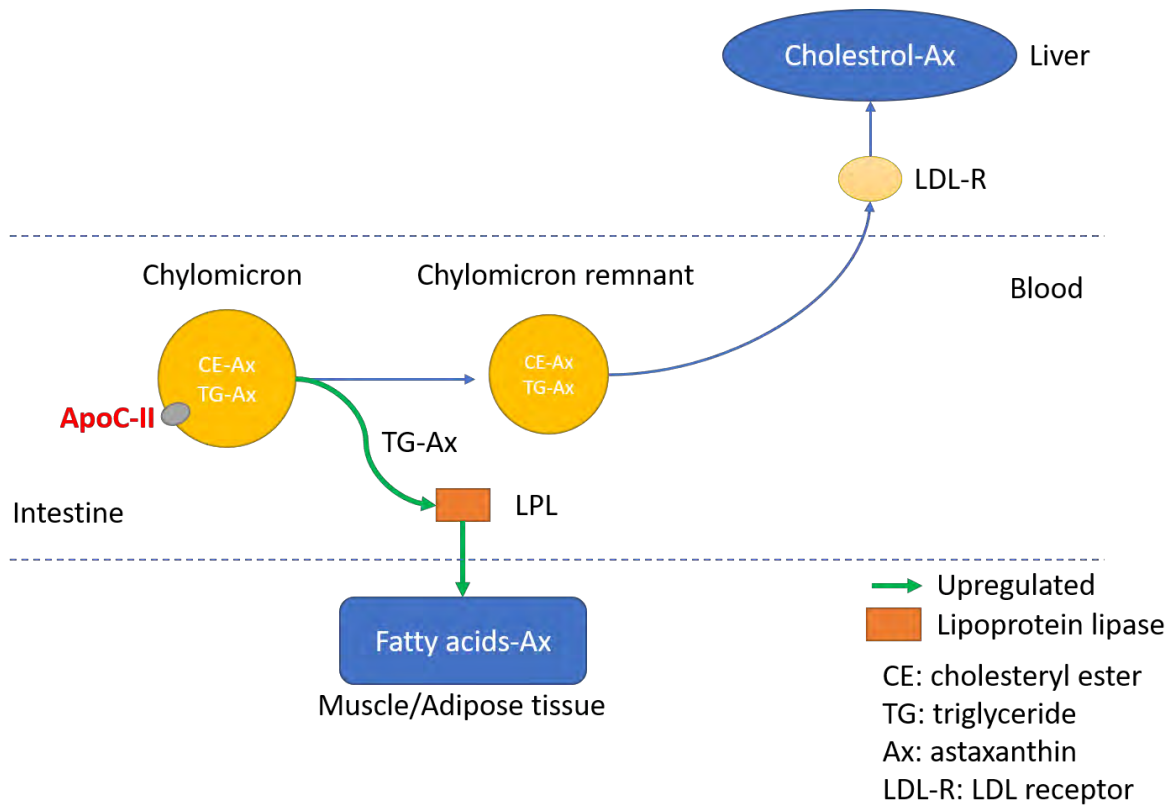


Fig. 2.25 The exogenous lipoprotein pathway modified from <sup>138</sup>

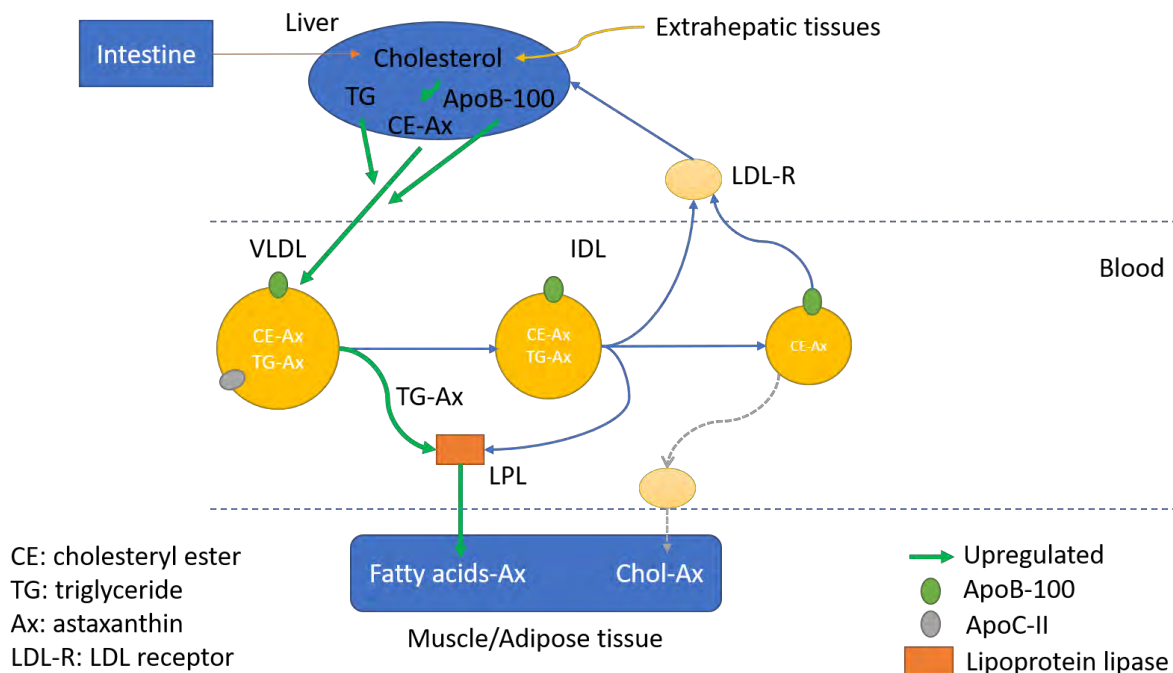


Fig. 2.26 The endogenous lipoprotein pathway modified from <sup>138</sup>

On the other hand, apolipoprotein C-I (apoc1) inhibits cholesteryl ester transferase protein (CETP) activity that leads to increased accumulation of cholesterol in HDL and decrease in low density lipoprotein (LDL) cholesterol level<sup>138,140</sup>. Thus, the up-regulation of apoc1 suggests that cholesterol as well as astaxanthin were stored in HDL to serve an unclear certain mechanism in reproduction later<sup>14</sup> and some other functions when fish maintain high flesh colour and no banding.

Hemopexin (hpx-like) and haptoglobin (hp-like) are known as plasma proteins, but they are also known as antioxidants, involved in prevention of heme-mediated oxidative stress and modulation of the acute phase response<sup>141,142</sup>. The up-regulation of these genes in the high colour-none banding fish perhaps correlates with better adaptation to oxidative stress than the high colour-banded fish.

### **2.3.3.3 High colour-Banded versus Low colour-Banded (HB\_vs\_LB)**

In the 7 and 17 DEG in the liver and gut, respectively, there were 16 genes that overexpressed in the low colour-banded fish, while 8 genes up-regulated in the high colour-banded fish. From previous studies in human and animals, several genes detected were previously proven to be related to the fatty acid metabolism, structure protein and responses of oxidative stress and starvation (Table 2.6). The high expression of glutamate-cysteine ligase regulatory subunit-like (glcm-like), type-4 ice-structuring protein-like (afp4-like) and phosphoserine aminotransferase 1 (psat1) suggests that the low colour-banded fish tolerate some stress of oxidation and heat<sup>143-145</sup> while the down-regulation of cathepsin L1-like (ctsl-like) suggests that the fish have been starved for more than 30 days<sup>146</sup>. The muscle structure is plausibly damaged when band 4.1-like protein 3 (epb41l3) is down-regulated<sup>147</sup>. Besides, the biosynthesis of fatty acids by modulating acyl-CoA-binding protein-like (dbi-like)<sup>148</sup> is upregulated in the low colour-banded fish. Therefore, the stresses from heat, oxidation and starvation for a long time perhaps caused the fish to lose a large amount of energy from muscle proteins and fatty acids. We hypothesize that it is the reason for flesh colour deterioration. The fatty acid biosynthesis seemed to be compensating for the lost energy that was used for responding to the stresses.

On the other hand, the high colour-banded fish had a degradation of fatty acids by up-regulating carnitine O-palmitoyltransferase 1, liver isoform-like (cpt1a-like)<sup>149</sup>. In this pathway, cpt1a-like was CPT1 and CPT2 that catalyzed for the conversion of Hexadecanoyl-CoA and L-Palmytoyl-carnitine in the process of degrading fatty acids (Fig. 2.27). But these fish also had a mechanism of cubilin (cubn) to reuptake ligands, such as lipoproteins and serum albumins<sup>150</sup> that are associated with carotenoids. This mechanism aids to cover a variety of essential elements transported by plasma lipoproteins and serum albumins<sup>151</sup> such as fatty acids and carotenoids. Comparing to the low colour-banded fish, the high colour-banded fish have an increased regulation of muscle contraction by up-regulating non-muscle caldesmon-like (cald1-like)<sup>131</sup>. Thus, we propose that a specific mechanism relating to cubn is activated to retain as much of catabolized fatty acids and carotenoids as the high colour-banded fish try to maintain their normal activities and flesh colour.

**Table 2.6** The selective DEGs in the comparisons of HB\_vs\_LB<sup>5</sup>

Tissue	Gene symbol	Gene	Log2 Fold change	Function
<b><i>Fatty acid metabolism</i></b>				
Liver	cpt1a-like	Carnitine palmitoyltransferase liver isoform-like	O-1, 1.44	Fatty acid degradation
	dbi-like	Acyl-CoA-binding protein-like	-1.51	Modulation of fatty acid biosynthesis
Gut	cubn	Cubilin (intrinsic factor-cobalamin receptor)	1.15	Involving in the endocytic uptake of many ligands
<b><i>Structure protein</i></b>				
Gut	cald1-like	Non-muscle caldesmon-like	1.21	Regulation of cell contraction and intracellular motional processes
	epb41l3	Band 4.1-like protein 3	-1.02	In intercellular junctions by binding actin
<b><i>Oxidative stress, starvation, thermal acclimation and immune responses</i></b>				
Liver	glcm-like	Glutamate-cysteine ligase regulatory subunit-like	-1.65	Response to oxidative stress
	afp4-like	Type-4 ice-structuring protein-like	-6.21	Up-regulated when Atlantic salmon was starved
	psat1	Phosphoserine aminotransferase 1	-1.32	Response to heat shock
Gut	ctsl-like	Cathepsin L1-like	1.22	Response to starvation

<sup>5</sup> Note: Log2 Fold change  $\geq 1$ : upregulated in the high color-banding fish; Log2 Fold change  $\leq -1$ : upregulated in the low color-banding fish.

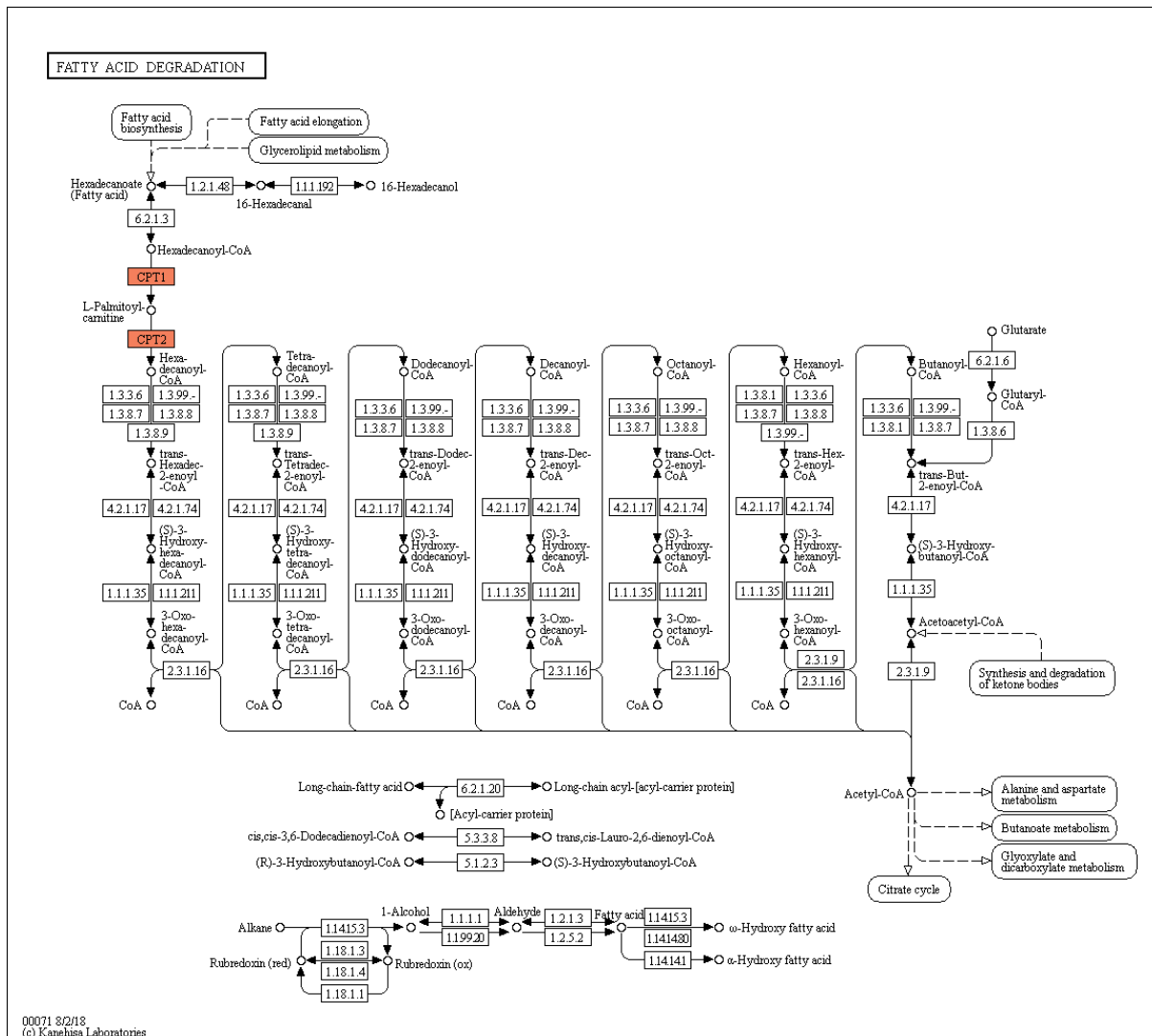


**Fig. 2.27** The pathway of fatty acid degradation with upregulated O-palmitoyltransferase 1, liver isoform-like (orange colour)

### 2.3.3.4 High colour-None banding versus Low colour-None banding (HN\_vs\_LN)

This comparison has the highest number of overexpressed genes among four pairs of comparisons. 101 and 60 genes were up-regulated in the high colour-none banding and low colour-none banding fish, respectively.

In the high colour-none banding fish, most up-regulated genes were related to fatty acid transportation, bile acid carriers and mechanism of preventing from oxidative stress and starvation (Table 2.7). Expression of serum albumin (alb1, alb2), apolipoprotein C-II and apolipoprotein B-100 suggested that there was an increased absorption of fatty acids and carotenoids into target tissues (Fig. 2.25 and 2.26), while apolipoprotein C-I and apolipoprotein A-I were up-regulated to accumulate much more fatty acids, especially cholesterol and carotenoids into HDL (Fig. 2.26 and 2.28)<sup>136,138,152</sup>. HDL is known to have a major role in carrying fatty acids and carotenoids to the ovary for reproduction in Atlantic salmon<sup>153,154</sup>. Solute carrier family 10 (sodium/bile acid cotransporter), member 2 (slc10a2) and gastrotropin (fabp6) were up-regulated in high colour-none banding condition. We suspect these protein transporters aid in the maintenance of the enterohepatic circulation of bile acids<sup>155,156</sup>. Thus, there was an accumulation of essential nutrients for reproducing in the high colour-none banding fish. By up-regulation of haptoglobin-like (hp-like), ependymin-like (epd1), hemopexin (hpx-like) and

cathepsin L1-like (ctsl1-like) genes, we hypothesize that these fish had some mechanisms to acclimate the change of thermal condition and protect them from oxidative stress<sup>141,142,146,157</sup>.

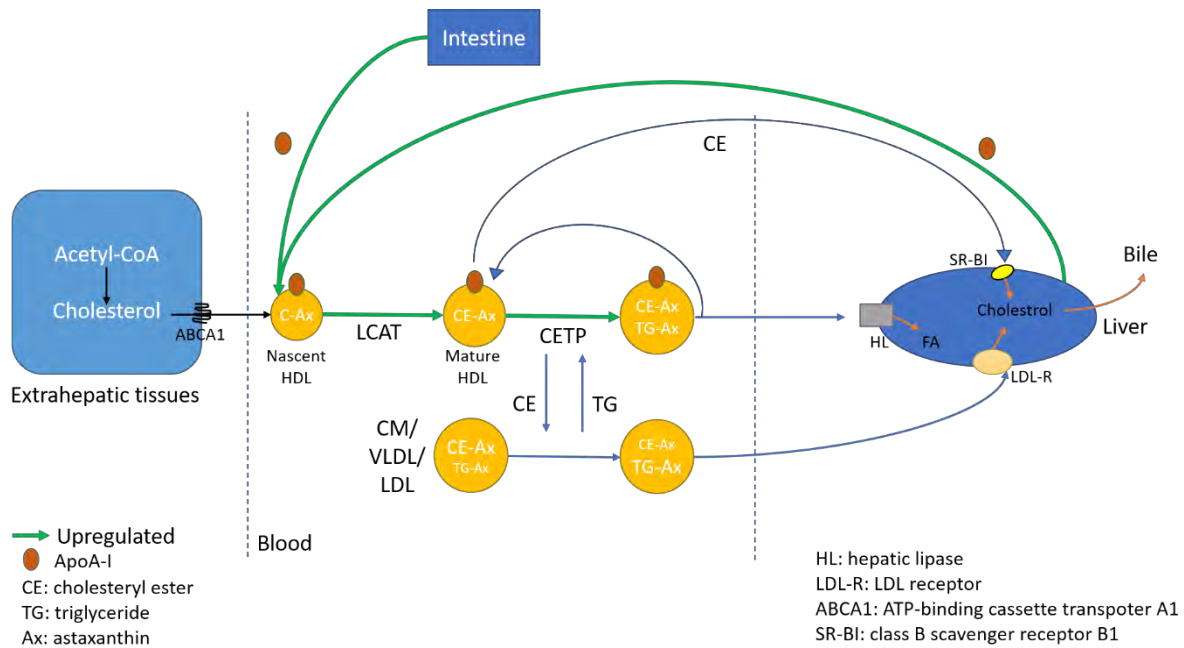


**Fig. 2.28** The pathway of HDL metabolism modified from<sup>138</sup>

In contrast, the low colour-none banding fish had some activities of responding to oxidative stress and acclimating to water temperature (Table 2.7). There were more highly expressed genes (*serp1*, *txndc17*, *cbr1*, *mdh1*, *cbs*, *g6pd*, *acat2*, *acly*, *pgd*) that are previously known to be related to responding to oxidative and thermal stress<sup>135,158–161</sup> as well as genes involved in the biosynthesis of antibiotics that annotated into KEGG pathways. Furthermore, nuclear receptor subfamily 0 group B member 2 (*nr0b2*) and short-chain specific acyl-CoA dehydrogenase, mitochondrial-like (*acads*) is recorded to be upregulated in the low colour-none banding condition. These genes are involved in bile acid and lipid homeostasis and the oxidation of short-chain fatty acids<sup>162–164</sup>. Hence, we propose that the low colour-none banding fish need more energy to synthesize antibiotics and react accordingly to stressful conditions from environment.

**Table 2.7** The selective DEGs in the comparisons of HN\_vs\_LN<sup>6</sup>

Tissue	Gene symbol	Gene	Log2 Fold change	Function
<b>Lipid metabolism</b>				
Liver	slc10a2	Solute carrier family 10 (sodium/bile acid cotransporter), member 2	1.72	Bile acid transporter
	nr0b2	Nuclear receptor subfamily 0 group B member 2	-1.62	Involving in bile acid homeostasis and lipid homeostasis
	fabp10a	Fatty acid-binding protein 10-A, liver basic (LOC106582922) (LOC106605182)	-1.11 -1.29	Involved in the transport of intracellular lipids
	alb2-like	Serum albumin 2-like	1.28	Long-chain fatty acid transporters
	fabp6	Gastrotropin	1.37	The major intracellular bile acid carrier
	acads	Short-chain specific acyl-CoA dehydrogenase, mitochondrial-like	-1.36	Catalyse the initial reaction of short-chain fatty acid $\beta$ -oxidation
Gut	alb2	Serum albumin 2	1.58	Long-chain fatty acid transporters
	alb1	Serum albumin 1	1.54	Long-chain fatty acid transporters
	apoc2	Apolipoprotein C-II-like	1.59	Co-factor for lipoprotein lipase, stimulate triglyceride hydrolysis
	apob	Apolipoprotein B-100	1.54	Structural protein, Ligand for LDL receptor
	apoa1	Apolipoprotein A-I	1.35	Structural protein for HDL, Activates lecithin:cholesterol acyltransferase (LCAT)
	apoc1-like	Apolipoprotein C-I-like	1.31	Inhibitor of cholesteryl ester transfer protein (CETP)
	fabp10a	Fatty acid-binding protein 10-A, liver basic-like	1.63	Involved in the transport of intracellular lipids.

<sup>6</sup> Note: Log2 Fold change  $\geq 1$ : upregulated in the high color-no banding fish; Log2 Fold change  $\leq -1$ : upregulated in the low color-no banding fish.

Tissue	Gene symbol	Gene	Log2 Fold change	Function
<b><i>Oxidative stress, starvation, thermal acclimation and immune responses</i></b>				
Liver	serp1	Stress-associated endoplasmic reticulum protein 1	-1.04	Responding to hypoxia and/or reoxygenation or other forms of stress
	txndc17	Thioredoxin domain-containing protein 17	-1.11	Protecting the ovary and/or oocyte from oxidative stress
	cbr1	Carbonyl reductase [NADPH] 1	-1.43	Protects pancreatic $\beta$ -cells against oxidative stress
	mdh1	Malate dehydrogenase, cytoplasmic	-1.04	Thermal stability enzyme
	cbs	Cystathionine beta-synthase	-1.38	
	g6pd	Glucose-6-phosphate 1-dehydrogenase	-1.67	Responding to oxidative stress
	acat2	Acetyl-CoA acetyltransferase 2	-1.66	
	acly	ATP-citrate synthase	-1.56	Responding to growth factor stimulation and during differentiation
	pgd	Phosphogluconate dehydrogenase	-1.44	
	epd1-like	Ependymin-like	1.43	Involving in the cold acclimation of fish
Gut	hp-like	Haptoglobin-like (LOC106587252) (LOC106581595)	2.02 1.64	Inhibits its oxidative activity
	hpx-like	Hemopexin-like	1.69	A heme-binding serum glycoprotein
	epd1-like	Ependymin-like	1.68	Involving in the cold acclimation of fish
	Ctsl-like	Cathepsin L1-like	1.12	Responding to starvation

### 2.3.4 Final remarks: transcriptome analysis

From the result of liver and gut transcriptomes, several groups of genes correlate in expression pattern to the reduced and banded flesh colour. Transcriptome analysis revealed multiple gene groups that participate in the maintenance of muscle structure, potentially affecting the banding. In contrast, the density of flesh colour was impacted by genes relating to fatty acid metabolism. Fish with reduced colour tended to upregulate genes associated with response to oxidative stress, thermal stress and starvation. Therefore, in further analysis, we intend to conduct a muscle transcriptome to analyze genes located in fish muscle that are involved in the structural protein organization and fatty acid metabolism. An immunohistochemistry of muscle samples will illustrate the difference of structural F-

actin fibers between two banded regions. Finally, we propose that a chemical analysis of astaxanthin and astaxanthin metabolites in different tissues can identify the pathway of astaxanthin, astaxanthin metabolism, and astaxanthin catabolism that influence the pale colour and banding in the Atlantic salmon flesh.

## **2.3.5 Materials and methods: library benchmark study and SNPs exploration**

### **2.3.5.1 Library preparation and sequencing**

In the comparisons of the liver and hindgut transcriptomes between various groups of flesh colour, the number of DEGs found in hindgut was higher than in the liver; hence the hindgut was deemed to be a more sensitive target that has a considerable effect on the salmon flesh colour. Hence, to compare the effectiveness of QuantSeq and TrueSeq libraries, 10 hindgut samples were selected from two groups: five of extremely high colour-none banding (HN) and five of extremely low colour-banded (LB) for sequencing using Illumina library preparation (these were the same samples used in the first, QuantSeq transcriptome study). Extracted RNA were sent to Novogene (Hong Kong) for library preparation using Illumina TrueSeq DNA PCR-Free Library Preparation kit, followed by sequencing on one Illumina HiSeq2500 lane (150 bp, pair-end reads). This sequencing step generated 10 data files with >6 GB each.

The TrueSeq data was analysed using the same bioinformatic pipelines that were used for the QuantSeq data. The quality of raw reads was examined using FastQC v.0.11.6<sup>124</sup>. After trimming by Trimmomatic<sup>165</sup>, the qualified pair-end reads were mapped onto the *S. salar* genome (Atlantic Salmon Genome - ICSASG\_v2, [https://www.ncbi.nlm.nih.gov/assembly/GCF\\_000233375.1/#/def](https://www.ncbi.nlm.nih.gov/assembly/GCF_000233375.1/#/def)) using HISAT2 v.2.1.0 with the default parameters<sup>125</sup>. Read counting was determined using HTSeq v.0.9.1<sup>126</sup>. For each comparison, genes with less than 10 reads across all samples were discarded.

### **2.3.5.2 Transcript coverage**

After mapping to the Atlantic salmon genome, all 20 BAM files from both TrueSeq and QuantSeq data were loaded onto RSeQC v2.6.4<sup>166</sup> to calculate transcript coverage. LOC106612115 gene coverage was visualized by using two BAM files from TrueSeq and QuantSeq of the same sample using Integrative Genomics Viewer<sup>167</sup>.

### **2.3.5.3 Differential expression analysis**

Differentially-expressed gene (DEG) analysis was conducted by DESeq2 in R (version 3.5.3)<sup>127</sup>. A gene was considered as DEG between two conditions when the following applied:  $|\log_2(\text{fold change})| > 1$ , p-adjusted value < 0.05. The number of DEGs from the two datasets (TrueSeq and QuantSeq datasets) was plotted on Venn diagram using InveractiVenn<sup>168</sup>.

### **2.3.5.4 RT-qPCR validation**

Five genes that were differentially expressed in both libraries and Five genes that were differentially expressed in one of the libraries, each with high log fold change, were chosen to run qPCR assay (a total of fifteen genes). Sixteen pairs of primers (for these fifteen genes and one house keeping gene) were designed using the 'Assay Design Center' available at the Roche website (<https://qpcr.probefinder.com/organism.jsp>), and listed in Table 2.8. Real-time quantitative polymerase chain reaction (RT-qPCR) was performed as previously described<sup>169</sup> with slight modifications to validate DEGs found in either or both sequencing datasets. cDNA templates were synthesized using Bioline Tetro Synthesis kit (Cat. No. BIO-65043) using the same RNA samples used for sequencing. Primers were mixed with the cDNA and FastStart Universal Probe Master (Rox; Roche

Diagnosics GmbH) and Universal ProbeLibrary Probe (Roche). The housekeeping genes (HKG) 18s rRNA served to normalize the quantification. qPCR cycles included 10 min incubation at 94 °C, followed by 40 cycles of 94 °C for 10 secs and 60 °C for 30 secs, with green fluorescence measurement on each cycle at 60 °C. Reactions were performed in Rotor-Gene Q (Qiagen). Relative quantification was calculated by equilibrating to the level of HKG per sample and the sample with the lowest value ( $2^{-\Delta\Delta CT}$ ). Statistical analysis of the resulting relative quantities was performed using Wilcoxon test with  $P < 0.05$  considered as statistically significant.

**Table 2.8** Sixteen genes selected for validating with RT-qPCR

Gene ID	Group	Forward primer	Reverse primer
(mfi2) antigen p97 (melanoma associated)	QuantSeq library	cagcagggaaaagctacgg	tcactgtcccctgtgtagctc
(epdm-l) ependymin-like	QuantSeq library	aaccacacaatgcaagccta	agctccaacagccagatac
(lyama) lysosomal alpha-mannosidase	QuantSeq library	aacagctacctgcagacgtg	tttcttgagatgggaccac
(fabp1) fatty acid binding protein 1, liver	QuantSeq library	gggcaccaaggtcatagta	tcttctccagtaaaagctctg
(ferrn-M) ferritin, middle subunit-like	QuantSeq library	cgtgatgagtgaggcaat	cagggcctggtcacatt
(s2p4a-l) SH2 domain-containing protein 4A-like	TrueSeq library	gcaacagcacagacgaccta	atgttgctgtggtgggttct
(noxo1-l) NADPH oxidase organizer 1-like	TrueSeq library	atgggctggaggacatga	gctcaciaaagggtgtgtca
(fclt3-l) fucosyltransferase-3-like	TrueSeq library	atgagggcattcacaacaca	tcctccacacctgatgtcc
(tetn) tetranectin	TrueSeq library	gtcagtggtgtgctgtttgt	tctgttgaatgtggattgc
(ovcm2-l) ovochymase-2-like	TrueSeq library	cgttcctcagcaaccaag	gggatcggtggtccagtaa
(ldtn-l) ladderlectin-like	Both libraries	ctttgtgtcgcctctctg	gacattgtgagatattggctgc
(cd209-l) CD209 antigen-like	Both libraries	tggtcacaattaaataatgtttgg	gaatgtttatttagtcatgctgggtg
(es1p-l) ES1 protein homolog, mitochondrial-like	Both libraries	agttgactccagttactacaacag	gcagtctgggtcgtcttctc
(umy1b-l) unconventional myosin-1b-like	Both libraries	aggaatgcatgagattgt	accagctccagaaccgact
(glfsy) GDP-L-fucose synthase	Both libraries	ctgattggctgtcaagcaac	gaaggtttgactccccatga
(18S) 18S ribosomal RNA	House keeping gene	aggactccggttctattttgtg	cggccgtccctcttaac

### 2.3.5.5 Single nucleotide-polymorphisms (SNPs) analysis

From the Illumina TrueSeq data, two sets of variants were detected with FreeBayes<sup>170</sup>, a Bayesian genetic variant detector and BCFTools, a set of utilities that manipulate variant calls<sup>171</sup> designed to find small polymorphisms, specifically SNPs<sup>172</sup>. A set of tools written in Perl to merge all SNPs from each group was then used to compare and create a list of unique SNPs from each group. All SNPs were annotated and the effects of the SNP variants on genes and protein were determined with Ensembl Variant Effect Predictor (VEP)<sup>173</sup>. If any variant was considered a reliable SNP and led to a missense mutation, the protein sequence including this mutation was run on I-TASSER<sup>174-176</sup> to generate predicted protein three-dimensional models. Visualization of protein models was performed to see if

there are any changes in the protein structure with Swiss-PdbViewer 4.1.0 <sup>177</sup> (<http://www.expasy.org/spdbv/>).

## 2.3.6 Results and Discussion: library benchmark study and SNPs exploration

### 2.3.6.1 Library preparation and RNA-sequencing

Once the sequencing results from the two libraries were available, after trimming, we achieved an average of 1.9 million and 21.8 million reads for the QuantSeq and TrueSeq libraries, respectively, and the reads were mapped to the Atlantic salmon genome. There was not much difference in read mapping rates between the sequences from the two sources, with 85% and 88% of the reads from QuantSeq and TrueSeq aligning to the salmon genome, respectively.

### 2.3.6.2 Gene body coverage

The distribution of the mapped reads along transcripts is illustrated in Fig. 2.29a. The QuantSeq-Lexogen reads are mainly mapped to the 3' end of the transcripts while the TrueSeq-Illumina reads covered the transcripts entirely, with a slight decrease at the 5' and 3' ends.

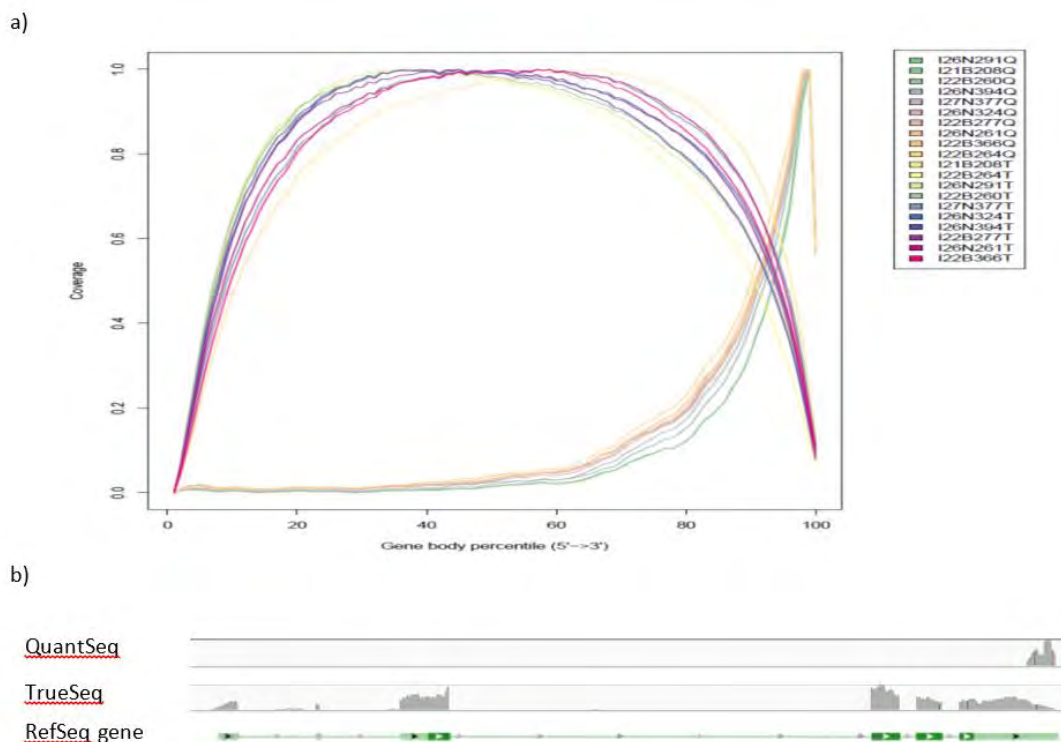


**Fig. 2.29** Gene body coverage (a) and SH2 domain-containing protein 4A-like (Sh24a) gene body coverage (b) from the QuantSeq and TrueSeq libraries<sup>7</sup>. Each line in Figure 1a represents the coverage of mapped reads from every library along with transcripts from the 5' to 3' ends in the whole Atlantic salmon genome. Figure 1b shows the distribution of mapped reads from QuantSeq and TrueSeq libraries on the exons of Sh24a gene from 5' to 3' end.

<sup>7</sup> Note: I21B208Q, I22B260Q, I22B264Q, I22B277Q, I22B366Q: low colour-banded fish samples from QuantSeq library; I26N261Q, I26N291Q, I26N324Q, I26N394Q, I27N377Q: high colour-no banding fish samples from QuantSeq library; I21B208T, I22B260T, I22B264T, I22B277T, I22B366T: low colour-banded fish samples from TrueSeq library; I26N261T, I26N291T, I26N324T, I26N394T, I27N377T: high colour-no banding fish samples from TrueSeq library.

To illustrate the gene body coverage at the single gene level, we used SH2 domain-containing protein 4A-like (Sh24a), where the gene body coverage showed a clear difference in mapping positions between the two libraries (Fig. 2.29b). The QuantSeq reads covered only the last exon at 3' end, while TrueSeq reads covered all exons of the gene with only a slight decline in the exon at the 5' end. Therefore, the QuantSeq method cannot detect gene isoforms correctly in multi-exonic genes that have long transcripts and alternative splicing to form multiple variants.

### **2.3.6.3 Distribution of reads on different transcript length**

TrueSeq quantification values were normalized to transcript length (to compensate for the increased proportion of mapped reads correlated with increased transcript length, since the TrueSeq reads cover the entire transcript), showing similarity in TrueSeq and QuantSeq sequencing data coverage (Fig. 2.30). These graphs illustrate that the depth of sequencing affects the identification of expressed genes based on the number of read counts. As can be expected, there are more expressed genes detected when the sequencing depth is much higher.

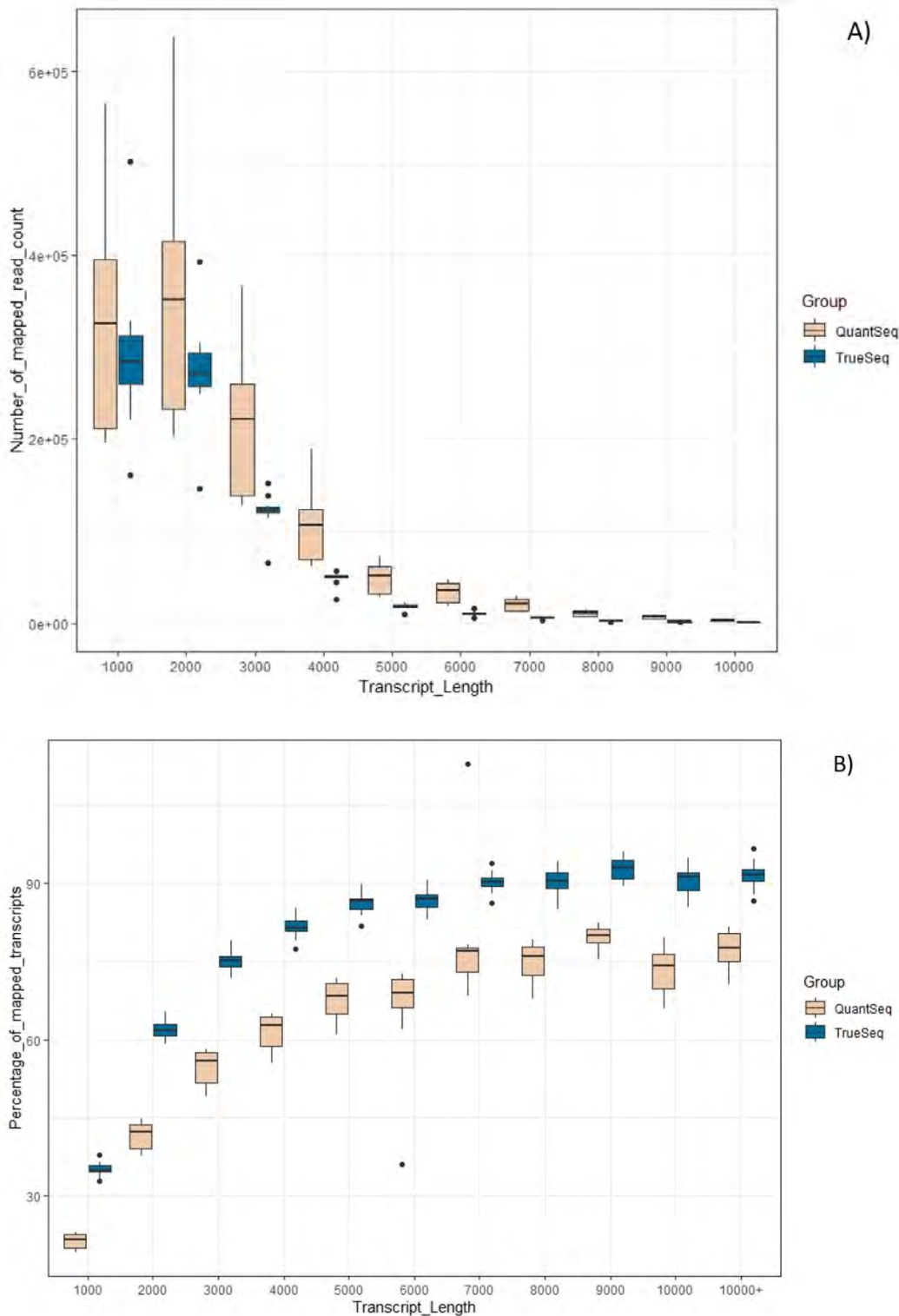


**Fig. 2.30** Read counts (A) and percentage of mapped reads (B) for transcripts of different lengths between QuantSeq and TrueSeq libraries.

#### 2.3.6.4 Differentially expressed genes

In the TrueSeq Illumina data, 191 DEGs were identified while only 50 DEGs were identified from the QuantSeq Lexogen data when the two subsample groups were compared. Out of these, only 11 DEGs overlapped between the two methods; all the 11 overlapping DEGs had high normalized counts (Fig. 2.31). These 11 genes relate to oxidative stress and immune response (Table 2.9). Interestingly, the high variation in expression of these 11 DEGs shows a similar pattern in the TrueSeq and QuantSeq

datasets (Fig. 2.31). The 11 overlapping DEGs have the highest expression of all DEGs in both datasets, providing a strong validation for both methodologies.

In conclusion, QuantSeq is a cost-efficient method to detect targeted genes with high expression levels. Due to the lower cost of library preparation, a higher number of samples could be analysed, which significantly reduces the number of false-positive DEGs detected. When dealing with lower expressed genes, the TrueSeq libraries are more accurate and provide more DEGs. Further validation using qPCR was performed on five DEGs in the QuantSeq data, 5 DEGs in the TrueSeq data and 5 overlapping DEGs.

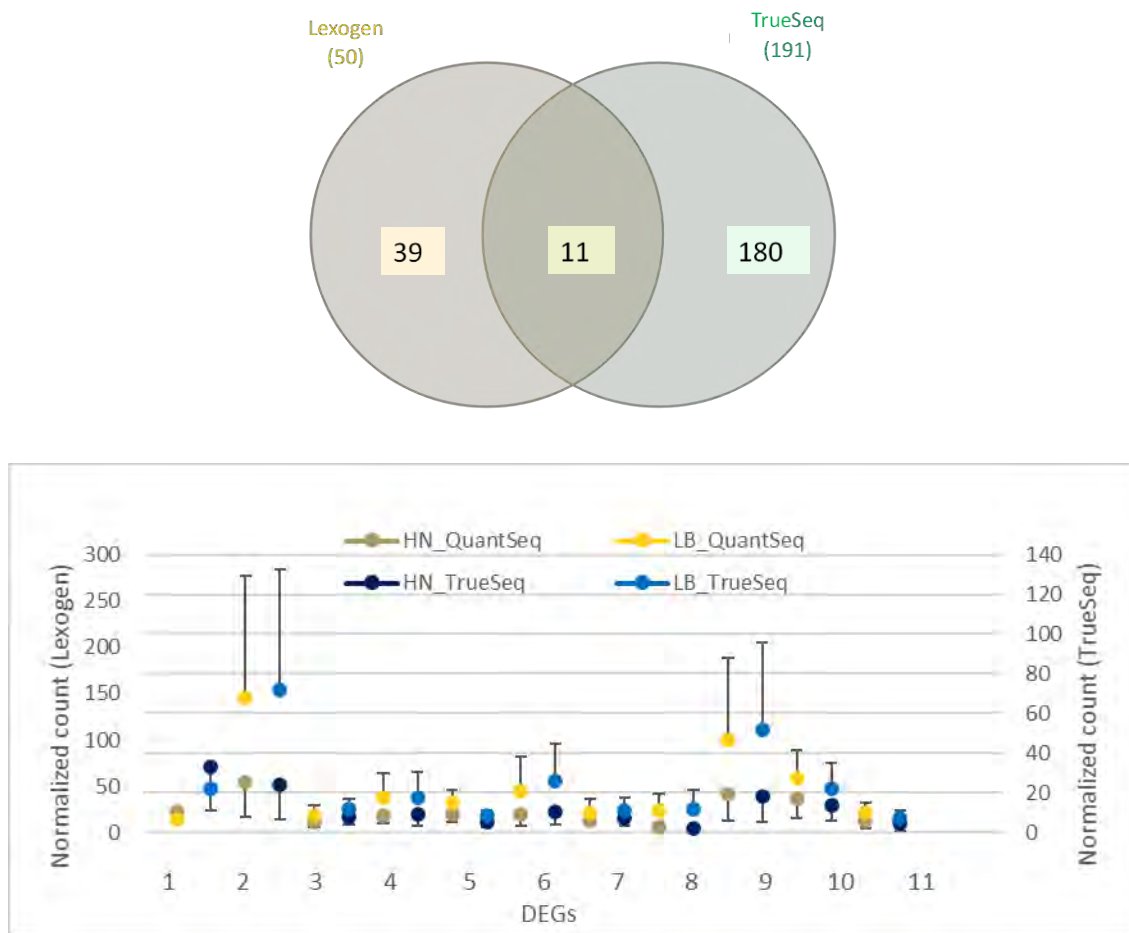


**Fig. 2.31** Venn diagram of DEGs from TrueSeq and QuantSeq libraries and the variation within biological replicates of the 11 DEGs in Lexogen and TrueSeq data<sup>8</sup>. HN - high colour none banding, LB - low colour, banding.

<sup>8</sup> Note: HN\_Lexogen: the normalised counting average of HN subset samples in each DEGs; LB\_Lexogen: the normalised counting average of LB subset samples in each DEGs; HN\_TrueSeq: the normalised counting average of HN subset samples in each DEGs; LB\_TrueSeq: the normalised counting average of HN subset samples in each DEGs; The number of DEGs is based on the order in the Table 2.9.

**Table 2.9** Eleven differential expressed genes that overlapped between the TrueSeq and QuantSeq libraries

No.	Function	Category
1	heme oxygenase-like	stress response (heavy metal and hypoxic stress)
2	ladderlectin-like	immune response
3	cytochrome b-245 light chain-like	immune response, stress response (ROS, hypoxia)
4	unconventional myosin-1b-like, transcript variant X8	structural protein, cell proliferation
5	arachidonate 5-lipoxygenase-activating protein, transcript variant X1	immune response
6	ES1 protein homolog, mitochondrial-like	metabolic process
7	sulfide:quinone oxidoreductase, mitochondrial-like	sulfur metabolism
8	dual oxidase 2-like	stress response
9	CD209 antigen-like	immune response
10	GDP-L-fucose synthase	metabolic process
11	carcinoembryonic antigen-related cell adhesion molecule 6-like	immune response

### 2.3.6.5 RT-qPCR validation

The expression trend of fifteen genes using RT-qPCR was similar between DEGs measured in both libraries and the qPCR validation (Fig. 2.32), however, only a handful of genes were significantly differentially expressed using qPCR. Out of 5 DEGs identified as DEGs in both libraries, there is only one gene, LOC106610399, which was also significantly differentially expressed in the RT-qPCR result ( $P < 0.05$ ). For 5 DEGs from the QuantSeq data, two genes, *fabp1* and LOC101448032, were significantly DEGs when using RT-qPCR, while there were three out of five DEGs expressed differentially in both TrueSeq data and RT-qPCR ( $P < 0.05$ ). This result confirms the conclusion above that the TrueSeq data performance on genes with low expression was much more precise than the QuantSeq data. In addition, although the first ten genes had high expression and the last five genes had low expression in both QuantSeq and TrueSeq data, the level of expression of the genes did not affect the RT-qPCR result. In RT-qPCR validation, it is evident that genes with high variation within biological replicates did not differentially express ( $P > 0.05$ ) even though they were picked as DEGs and expressed highly in the QuantSeq and TrueSeq data.

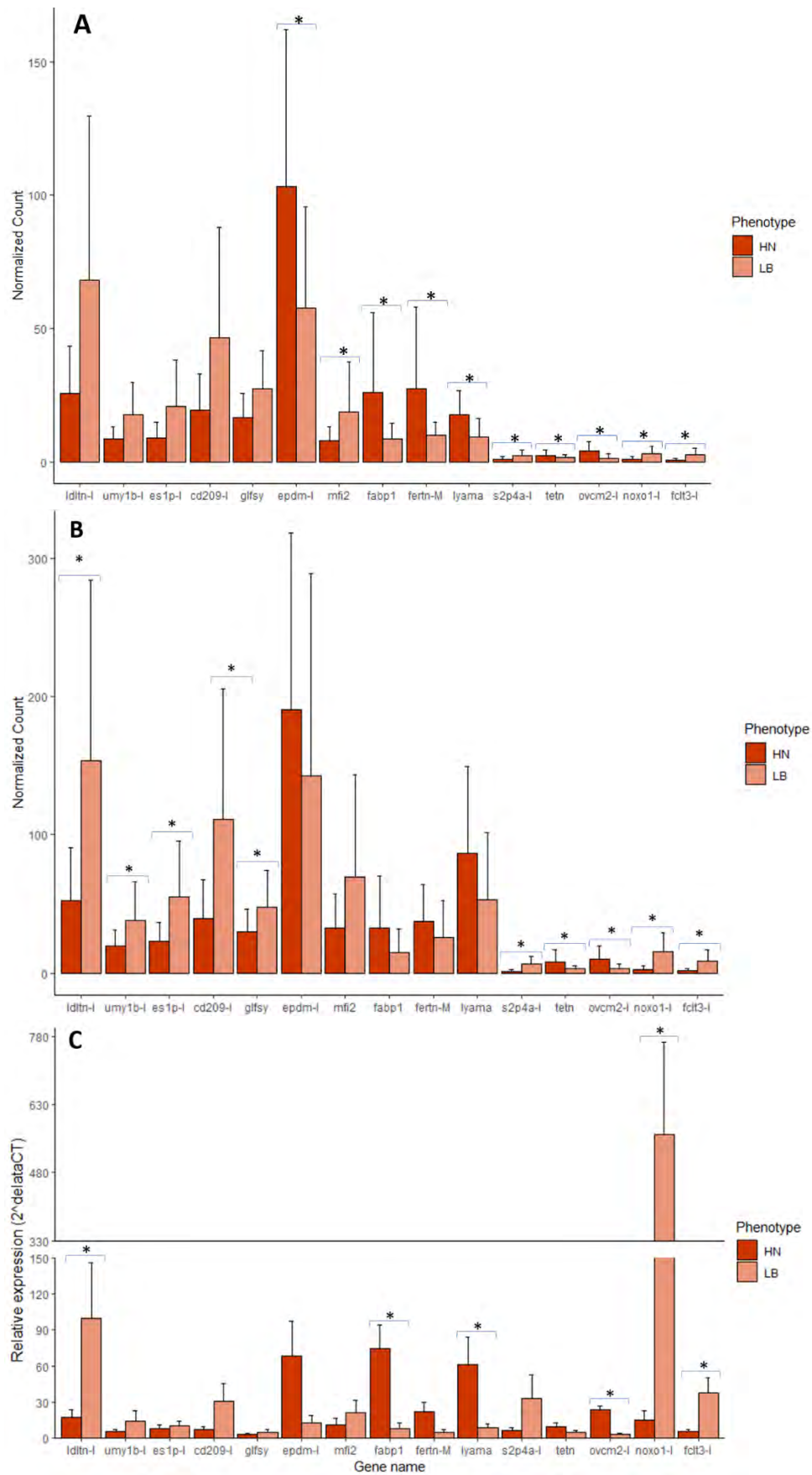


**Fig. 2.32** Comparison of variations within biological replicates of 15 DEGs in different libraries and RT-qPCR validation; a) In QuantSeq library; b) In TrueSeq library; c) In RT-qPCR.

### 2.3.6.6 SNP analysis

Using Illumina data with a high sequencing depth, we found several variants specific to samples of high colour-none banding or low colour-banded trait. In this analysis, we focused on variants which are located on DEGs or carotenoids-related genes and may cause a missense mutation, leading to a replacement of amino acids which could affect the protein structure. Most carotenoids-related genes did not have any variants that can be considered reliable SNPs because the read depth on these positions was low (less than 10 reads) or the alternative allele count was much lower than the reference allele count (Appendix 1). In Chinook salmon,<sup>178</sup> it was shown that a beta-carotene oxygenase 2-like (*bco2-l*), a flesh colour-associated gene including a SNP explained 66% of the variation in colour. In addition, two SNPs on two genes beta-carotene oxygenase 1 (*bco1*) and beta-carotene oxygenase 1 like (*bco1-l*) also showed a strong correlation to the flesh colouration in Atlantic salmon<sup>179</sup>.

Although our analysis also detected some variants on these genes, we cannot consider them reliable SNPs. However, we found Pro21Thr missense mutation, a valuable SNP located on ATP-binding cassette, sub-family G (white), member 8 (*abcg8*) that occurred in three of five individuals of high colour-none banding group (Appendix 1). The number of alternative allele observation count (AO) over number of observations for each allele (DPR) total read were 446/964, 397/857 and 259/541 for I26N261, I26N291 and I27N377 individuals, respectively. In humans and other mammals, *Abcg8* and *abcg5* (ATP-binding cassette, sub-family G (white), member 5) (also known as sterolins) expressed only in hepatocytes, gallbladder epithelium and enterocytes<sup>180</sup>. They participate in the physiological pathways involving dietary cholesterol and non-cholesterol sterols<sup>181</sup>. These sterolins are necessary to secreting cholesterol efficiently into bile and increase cholesterol levels in plasma and liver when the dietary cholesterol content changes<sup>182,183</sup>. It has been shown that a diet with 2% more cholesterol improved astaxanthin absorption and deposition as well as astaxanthin levels in the plasma of Atlantic salmon. At the same time, other supplements consisting of vitamin E, lutein, zeaxanthin and phytosterols did not lead to any increase<sup>184</sup>. On the other hand, a recent study found that dietary fatty acid composition did not influence astaxanthin concentration in white muscle tissue in Atlantic salmon<sup>37</sup>. Also, dietary pre-loadings with vitamin E ( $\alpha$ -tocopherol) could not prevent localised colour depletion in Atlantic salmon after exposure to thermal stress (probably excluding oxidative stress as cause of the depletion)<sup>185</sup>. Hence, in light of the aforementioned findings, only additional cholesterol in Atlantic salmon diets resulted in increased astaxanthin levels in the muscle, leading to a more intense flesh colouration. Finally, it was reported<sup>186</sup> that a missense mutation in *abcg2-1a*, resulting in the substitution of Asparagine with Serine in amino acid position 230 (Asn230Ser), is expected to be associated with flesh colour in Atlantic salmon because it is more prevalent in the pale than in the dark flesh phenotype. The complex *Abcg5/g8* was associated with carotenoid metabolism and predicted to function in limiting dietary carotenoid<sup>187</sup>.

In summary, it is possible that *abcg8* may play an important role together with *abcg5* in the control of secreting carotenoid-binding cholesterol and absorption of dietary carotenoids and mobilization of carotenoids in salmon.

When examining SNPs in DEGs, we identified reliable SNPs located in genes associated with immune response and oxidative stress. In the group of low colour-banded fish, a missense mutation on transmembrane protease serine 9-like (*tmprss9-l*) that causes the substitution of Histidine with Arginine in amino acid 22 (His22Arg) was present in all 5 analysed individuals. *Tmprss9* is commonly known as polyserase-I and was annotated by Gene Ontology including "proteolysis" and "integral component of plasma membrane". This gene could be a novel molecular biomarker of chronic inflammation in the salmon intestine<sup>188</sup>.

Moreover, in the genes dual oxidase 2-like (duox2-l) and dual oxidase maturation factor 1-like, we found up to 3 SNPs for each gene. Interestingly, three missense mutations, including Ser267Gly, Ala740Asp and Arg974Gln on duox2-l gene and three other missense mutations involving Leu55Phe, Ala213Thr and Glu239Gly on duoxa1-like were present in the same four of five low colour-banded fish. Dual oxidase 2 (duox2) is a member of the NADPH oxidase (NOX) family that generates reactive oxygen species (ROS). This enzyme catalyses the electron transfer from NADPH-FAD to  $O_2$ , generating superoxide ( $O_2^{\cdot-}$ ) or hydrogen peroxide ( $H_2O_2$ ) by reducing molecular oxygen<sup>189</sup>. Duox1 and duox2 function solely in the regulation of specific maturation factor known as duox activators, duoxA1 and duoxA2, respectively<sup>190</sup>. In a recent study, duox and duoxA proteins form stable heterodimers and co-translocate to the plasma membrane (Fig. 2.33a)<sup>191</sup>.

In human, Duox enzymes are available in the epithelial cell surface of mucosal and exocrine tissues, including the airways and gastrointestinal tract that defend against a wide range of pathogens<sup>192</sup>. Opposed to Nox1-5, duox enzymes have an extended N-terminal extracellular domain known as peroxidase homology (PoxH) domain, followed by an additional transmembrane segment and an intracellular loop containing two calcium-binding EF-hand motifs (Figure 2.33a,b). There is a switch in ROS generation from  $H_2O_2$  to  $O_2$ , which happens when duox2 is mismatched with duoxA1. Following that, the mismatched combination of duox2 + duoxA1 releases  $O_2^{\cdot-}$  together with  $H_2O_2$ , leading to the phenomenon of  $O_2$  leakage<sup>193,194</sup>.

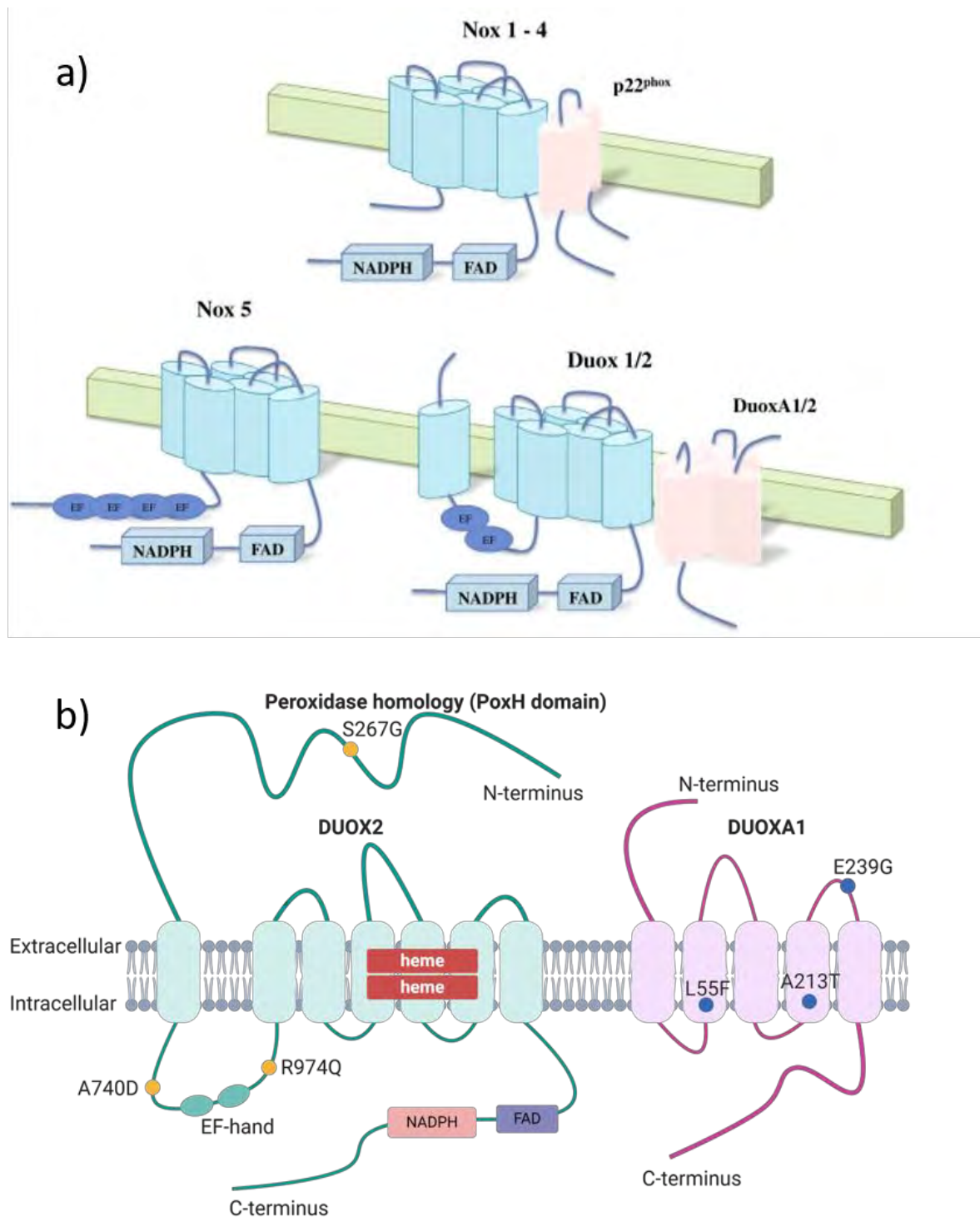


**Fig. 2.33** Structure of the NOX/Duox homologs (a) <sup>191</sup> and schematic illustration of SNPs on Dual oxidase 2 and Dual oxidase maturation factor (b)

In fish, although the biological functions of these genes may work differentially to humans, their mutation can lead to the mismatched complex which then affects their function of generating reactive oxygen species (ROS). In juvenile rainbow trout, dietary astaxanthin supposedly enhanced the antioxidant defence system, which plays a role in the inactivation of ROS <sup>195</sup>. Consequently, we

hypothesise that in fish containing such mutations, the deficiency of astaxanthin or carotenoids is due to strengthening their antioxidant capability.

### **2.3.7 Conclusions**

Lexogen QuantSeq is an economical method of library preparation that targets known genes with high expression and no splicing variants. For longer transcripts with many isoforms or unknown genes, it is recommended to apply the Illumina TrueSeq method where low expressed genes and gene isoforms can be discovered.

Using the TrueSeq sequencing platform, several valuable SNPs in genes relating to carotenoid-binding cholesterol and oxidative stress were found in both flesh colour phenotypes. We need to confirm if these SNPs have a strong relationship to flesh colour, in which case they can be used to further understand the mechanisms behind flesh colour in Atlantic salmon and be tested for suitability as markers for selective breeding programs.

*\*The following two paragraphs, although describing studies from samplings carried out during the trial reported in section 3 (specifically 3.2, post-summer assessment) were included in the current section as they represent an extension of the previous investigations and then still part of aim 2. The new studies aimed at deepening our knowledge of the correlation between gut microbiota and flesh colour as well as of molecular mechanisms and metabolism of flesh pigmentation processes\**

## 2.4 Assessing the pyloric caeca and distal gut microbiota correlation with flesh colour in Atlantic salmon (*Salmo salar* L., 1758)

(The entire section 2.4 has been published on the 16<sup>th</sup> of August 2020 on *Microorganisms* <https://doi.org/10.3390/microorganisms8081244> and the publication is included in this report with the same text structure)

### 2.4.1 Abstract

The Atlantic salmon (*Salmo salar* L., 1758) is a temperate fish species native to the northern Atlantic Ocean. The distinctive pink–red flesh colour (i.e., pigmentation) significantly affects the market price. Flesh paleness leads to customer dissatisfaction, a loss of competitiveness, a drop in product value and, consequently, severe economic losses. This work extends our knowledge on salmonid carotenoid dynamics to include the interaction between the gut microbiota and flesh colour. A significant association between the flesh colour and abundance of specific bacterial communities in the gut microbiota suggests that colour may be affected either by seeding resilient beneficial bacteria or by inhibiting the negative effect of pathogenic bacteria. We sampled 96 fish, which covered all phenotypes of flesh colour, including the average colour and the evenness of colour of different areas of the fillet, at both the distal intestine and the pyloric caeca of each individual, followed by 16S rRNA sequencing at the V3-V4 region. The microbiota profiles of these two gut regions were significantly different; however, there was a consistency in the microbiota, which correlated with the flesh colour. Moreover, the pyloric caeca microbiota also showed high correlation with the evenness of the flesh colour (beta diversity index, PERMANOVA,  $p = 0.002$ ). The results from the pyloric caeca indicate that *Carnobacterium*, a group belonging to the lactic acid bacteria, is strongly related to the flesh colour and the evenness of the colour between the flesh areas.

### 2.4.2 Introduction

The Atlantic salmon, *Salmo salar*, farmed in Tasmania, is one of the highest value aquaculture products in Australia and contributed AUD 756 million of the total AUD 1.3 billion of Australian aquaculture production in 2016–2017 (Australian Bureau of Agricultural and Resource Economics and Sciences, ABARES, 2018). The pink–red flesh colour in Atlantic salmon is considered as the most important criterion for a high-quality and high-value product <sup>11</sup>. Atlantic salmon reared in Tasmania are an introduced species and, despite a certain degree of genetic adaptation over a few decades, are still challenged by living in the upper limit of their temperature tolerance during summer. Therefore, when the water temperature exceeds 20 °C for a prolonged period of time during summer in Tasmania, the temperate Atlantic salmon suffer from thermal stress, aggravated by poor feeding as extreme as starvation, which eventually leads to a loss in flesh colour in part of the stock <sup>185</sup>. This loss in flesh colour, when persisting up to the harvest stage, can lead to a reduction in product value and moderate economic losses <sup>35,185</sup>.

In Atlantic salmon, there are two patterns of flesh colour loss: general flesh paleness and localized colour loss, which consists of differential colour tones between regions of the fillet <sup>35,185</sup> (**Error! Reference source not found.**). The colour difference is usually between the front dorsal, which is more prone to discolouration, and the central back region of the fillet, which retains colour better <sup>196</sup>. This phenomenon, commercially known as banding, is annually discernible between February and August in Tasmania, and it is usually recovered in most of the stock by harvest time. During this time, the fluctuation of water temperature is one of the reasons causing stress in fish <sup>41</sup> and induces feed reduction or cessation.

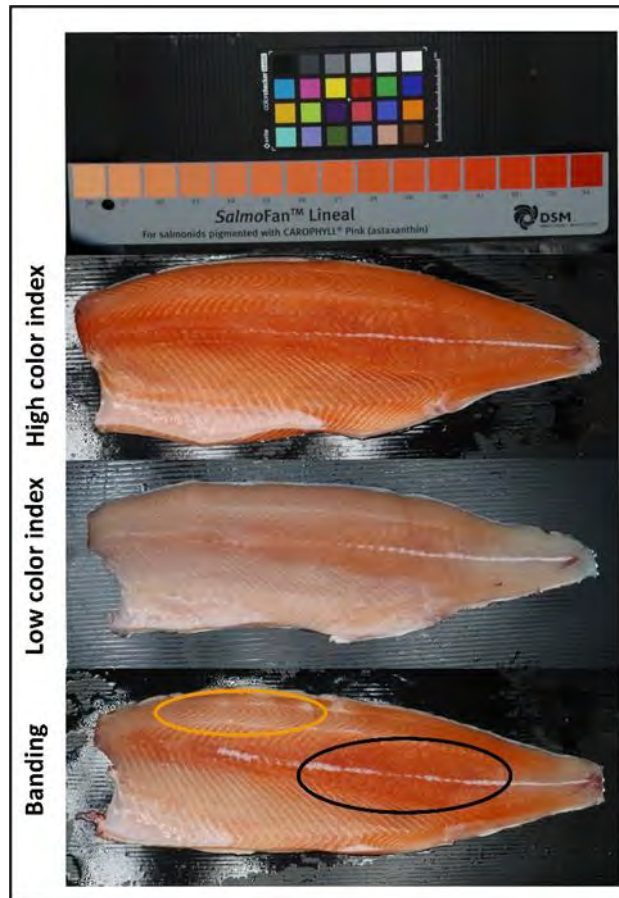


**Fig. 2.34** Examples of salmon fillets including high colour index with pink–red colour over whole fillet, low colour index with pale colour over whole fillet and banding with a colour difference between the dorsal (orange oval) and central back areas (black oval).

As a result, water temperature can also affect the fish gut microbiota in Atlantic salmon, as previously demonstrated<sup>59,83,89</sup> and confirmed in our recent study<sup>197</sup>, where we showed that changes in the distal gut microbiota profile correlates with flesh colour variation across different time points during the relevant period (February-August). Although it is clear that overall temperature fluctuation has an impact on colour loss during that period<sup>35</sup>, flesh colour variation correlation with the gut microbiota is independent of the change in water temperature<sup>197</sup>, since fish with reduced flesh colour have similar microbiota profiles in the distal gut regardless of the time point tested. However, only the distal gut region, which has been widely studied, was assessed<sup>197</sup>. Multiple studies report that the microbiota profile changes between different niches along the fish gut, resulting in significant variation in gut functionality<sup>86,198,199</sup>. For example, the pH, which is a fundamental property of the intestinal tract (enabling food digestion and absorption), changes along the gut due to the microbiota activity<sup>200</sup>.

The fish gut is a long digestive organ including foregut, midgut and hindgut, in which the foregut includes the oesophagus, stomach, pyloric caeca and the hindgut consists of the distal gut and anus<sup>201</sup>. Although there is no clear boundary to define these gut regions, they generally have different digestion roles including absorption (i.e. for proteins from the simple digestion in the stomach) and digestion (i.e. for the more complex proteins). As an example, the pyloric caeca is where most of the absorption occurs, facilitated by the large surface area, whereas digestion occurs primarily in the mid gut<sup>201</sup>. The different roles also correlate with different microbiota niches. The density, composition,

and function of the microbiota changes along the fish gut<sup>202,203</sup>, especially, there is the distinction and variance of the core microbiota and the transient microbiota which are related to the digesta<sup>204,205</sup>. A recent study has shown that the fish hindgut microbiota has a closer resemblance to the mammalian gut microbiota than to the surrounding environmental microbiota<sup>206</sup>, indicating that the core microbiota in the distal gut is not affected by the environment and implies a role in the interaction with the host. As evident from our previous study<sup>197</sup>, the composition of the distal gut microbiota correlates with the flesh colour. The other end of the gut, the pyloric caeca, has been studied mainly in the context of the dietary components, which affects the gut microbiota<sup>200,207</sup>. Although the change in microbiota composition along the gut has been confirmed<sup>86,198,199</sup>, there are no studies reporting the role of the pyloric caeca microbiota in the host phenotype. Interestingly, pyloric caeca is a more favourable niche of the probionts (i.e. probiotic bacteria) than any other part of the intestine in the Atlantic salmon and Atlantic cod<sup>208</sup>, which makes it an important gut region for further investigation. Given the significance of these two gut regions and the high likelihood of different microbiota presence between them, both were investigated to obtain a more comprehensive picture of any microbiota correlation with flesh colour variation which might give further insights into the occurrence of commercially unwanted phenotypes (i.e. general paleness or pronounced banding). To address this aim and reduce confounding factors, one sampling event was chosen, at a time-point when flesh colour recovery from thermal stress is observed to be differential across individuals from a single population kept under the same conditions and fed the same diet. In this study, the association of the microbiota profile in the pyloric caeca and the flesh colour index was examined, and the microbiota profile in the pyloric caeca, the distal gut and the flesh colour were correlated.

### **2.4.3 Materials and methods**

#### **2.4.3.1 Study design and sample collection**

The Atlantic salmon individuals analysed in the current study were sampled on April 2019 from an aquaculture lease in northern Tasmania (Australia) (same lease as in section 2.1 and<sup>197</sup>). The sampling timepoints were chosen based on commercial historical data showing that flesh colour deterioration starts to be manifested in March after the summer thermal stress and a period of poor feeding utilisation and starts recovering in most of the stock in the following months. The fish were previously stocked in 2018 and maintained in a cage containing approximately 35,000 individuals<sup>197</sup>. When the fish reached 23 months old, fish from two cages, which had similar sizes, were sampled. There was no specific treatment or nutritional trials associated with these fish. When sampled in April, the fish were on a commercial diet containing 40 ppm astaxanthin/40 ppm canthaxanthin. The sampling was conducted over two continuous days in April 2019, and it was carried out before feeding.

A total of 96 individuals were chosen to cover the variation in flesh colour and banding status (i.e. differential colour tone between the dorsal and the back area of the fillet), resulting in 96 samples each of pyloric caeca and distal gut. The flesh colour measurement was carried out visually on two areas of the fillet (front-dorsal and back-central) and based on the Roche SalmoFan Lineal Card (Hoffman-La Roche, Basel, Switzerland) (**Error! Reference source not found.**), ranging from 20-34, with an assumed minimum marketable grade of 25. When present, severity of banding was calculated as the colour score difference between the two areas of the fillet assessed and categorized as None (= 0), Moderate (= 1), and Severe ( $\geq 2$ ). The sample details can be found in the Supplementary Material (for Supplementary Material please refer to <https://doi.org/10.3390/microorganisms8081244>). Digestive tract samples were collected as described in<sup>197</sup>. Briefly, the fish abdomen was incised, and the pyloric caeca and distal part of the intestine (Figure 2.35) were aseptically exposed and severed. After opening the intestine longitudinally, a sample was collected (0.5 cm<sup>3</sup>) then washed three times

in sterile 0.9% saline solution to remove non-adherent (allochthonous) bacteria and digesta. The samples were immediately fixed in RNAlater and stored at -80°C until extraction. Two samples from the rearing water were also collected as the negative control for the background microbiota. Another two blank water samples were also included in the DNA extraction process as the negative control for this process. All procedures were carried out with the approval of the University of the Sunshine Coast Animal Ethics Committee (AN/E/16/12).

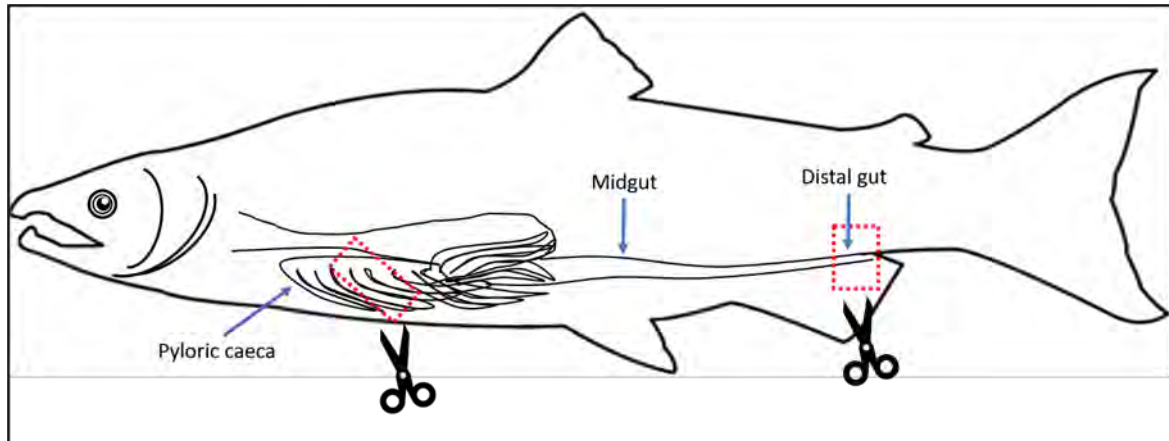


**Fig. 2.35** Schematic drawing of the salmon gastrointestinal tract with pyloric caeca: pyloric caeca, midgut and distal gut. Dashed red rectangles and scissors denote the two regions collected in this study.

#### 2.4.3.2 DNA extraction and MiSeq sequencing

A total of 196 samples were subjected to DNA extraction using the QIAamp BiOstic Bacteremia DNA Kit (Qiagen). DNA quality and quantity were checked with a NanoDrop™ 2000 Spectrophotometer and gel electrophoresis. The DNA was sent to the Ramaciotti Centre for Genomics (University of New South Wales, Sydney) for the PCR amplification of the hypervariable V3-V4 region between the 341 and 806 nucleotides of the 16S rRNA gene with the specific primers FW-5'-CCTAYGGGRBGCASCAG and RV-5'-GGACTACNNGGGTATCTAAT, and the purified amplicons served for library preparation followed by Illumina sequencing using MiSeq paired-end sequencing.

#### 2.4.3.3 Microbial community profiling

The microbial community profiling analysis was performed using Quantitative Insights into Microbial Ecology (QIIME 2) <sup>64</sup>. The quality filtering was performed using QIIME2 with the Phred score 19 <sup>64</sup>, followed by denoising by Deblur workflow <sup>65</sup>. Taxonomy was assigned by VSEARCH consensus taxonomy classifier trained on GreenGenes database 18\_5 with 97% Operational Taxonomic Units (OTUs) <sup>66</sup>, followed by generating the OTU table.

The OTU table was rarefied at 300 reads per samples, then the samples were grouped into categories. There were two datasets: Distal gut microbiota data and Pyloric caeca microbiota data. To analyse the data, the samples in each dataset were grouped by two categories: Flesh colour and Banding status. In the category Flesh colour, the data were grouped into four subgroups based on their colour assignment: Flesh21-22 (n=8), Flesh23-24 (n=20), Flesh25-26 (n=48) and Flesh27-29 (n=20). In the banding status category, the data was split into three subgroups included None-banding (n=10), Moderate-banding (n=62), and Severe-banding (n=24). The  $\alpha$ -diversity and  $\beta$ -diversity were computed using a nonparametric Kruskal-Wallis test and Unifrac distance, respectively <sup>69</sup>. PCoA were generated using Emperor in QIIME 2 <sup>209</sup>. The  $\beta$ -diversity's multivariate statistical analysis was carried out in QIIME 2 using the PERMANOVA test <sup>72</sup>.

The differential microbial taxa for each group was identified using Linear discriminant analysis Effect Size <sup>73,210</sup> provided by Dr. Huttenhower's lab with the LDA effect size of 3.5 and p-value < 0.05 (<https://huttenhower.sph.harvard.edu/galaxy/>). To identify niche taxa that possibly influence biologically relevant features in response to change in environmental conditions, the OTU was subjected to QIIME2 Gneiss <sup>74</sup>. The gradient clustering hierarchies were constructed for each category; Flesh colour and Banding status, followed by constructing the Simplicial Ordinary Least Squares Regression models to obtain the balance trees of microbiota taxa for each category <sup>74</sup>. Pearson's correlation was also applied to measure the strength of the correlation between microbiota taxa with a certain phenotype.

#### 2.4.3.4 Functional and metabolic pathway prediction

The function annotation of taxa composition was predicted by PICRUSt <sup>75</sup>. The predictive metagenome was categorized by function, followed by Redundancy analysis RDA (p < 0.05) and LEfSE analysis integrated in a multi-functional web-server Calypso (LDA 3.5 and p < 0.05) <sup>76</sup>.

### 2.4.4 Results

#### 2.4.4.1 The distinct difference between microbiota in the distal gut and the pyloric caeca

After quality control at a Phred score of 19, there was a total of 2,992,577 retained reads, which accounted for 95.3% of the total raw reads. The two datasets of microbiota, those from the distal gut and the pyloric caeca, were pooled together to assess the quality and diversity ( $\alpha$ -diversity (Shannon index) and  $\beta$ -diversity, respectively; Fig. 2.36). The Shannon index indicated that the microbiota in the pyloric caeca was richer and more diverse than that of the distal gut (Fig. 2.36A), with significantly differential microbiota composition between these two gut regions (Fig. 2.36B; PERMANOVA test  $p = 0.001$ ). Hence, there are two distinct microbiota populations inhabiting the distal gut and the pyloric caeca in *S. salar*.

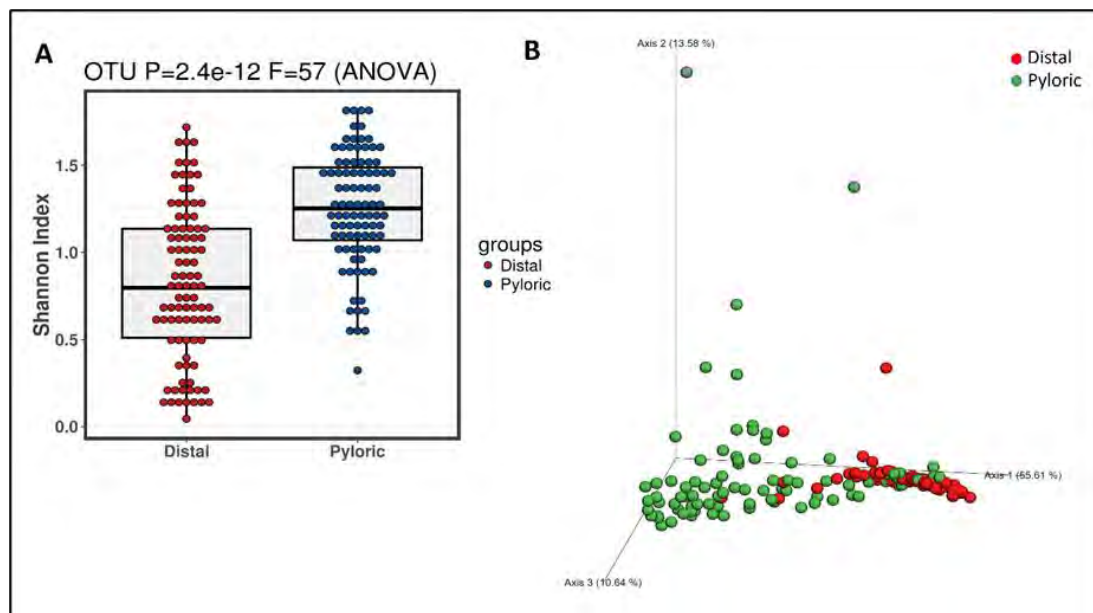


**Fig. 2.36** (A) The  $\alpha$ -diversity (Shannon index) and (B)  $\beta$ -diversity (principal coordinate analysis (PCoA)) by the weighted UniFrac distance between the microbiota in the distal gut and the microbiota in the pyloric caeca.

Further analysis of the microbiota population in both the distal gut and pyloric caeca indicated that the majority of taxa occupying the distal gut belonged to the class of *Gammaproteobacteria* (Fig. 2.37A, purple circles). However, in the pyloric caeca, almost all the bacteria classes had good presence (Fig. 2.37A, blue circles) with the exception of a significant part of the *Gammaproteobacteria* class. This observation is aligned with the  $\alpha$ -diversity (Shannon index) and  $\beta$ -diversity (PCoA) described above (Fig. 2.36). The results of the LEfSe analysis also align with these results by indicating that the representative taxa of the distal gut microbiota were *Vibrionaceae* (F), *Pseudoalteromonadaceae* (F) and *Photobacterium* (G), which belong to only one class, *Gammaproteobacteria*, whereas the representative taxa for the pyloric caeca microbiota were more phylogenetically diverse, with 20 taxa belonging to five classes: *Actinobacteria*, *Betaproteobacteria*, *Alphaproteobacteria*, *Gammaproteobacteria* and *Bacilli* (Fig. 2.37B).

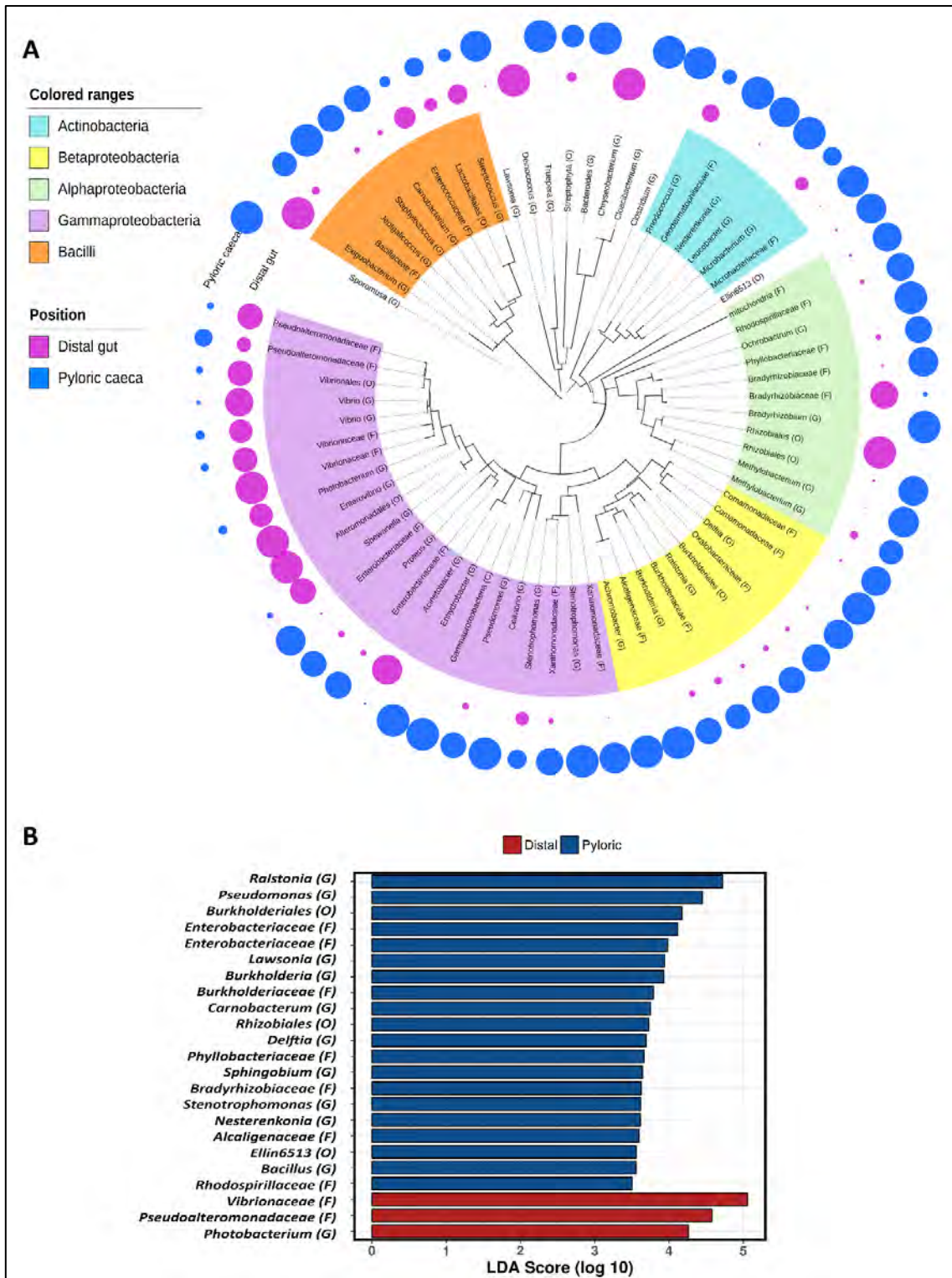


**Fig. 2.37** (A) A phylogenetic tree representing the microbiota of both distal gut and pyloric caeca. The bacteria classes of *Actinobacteria*, *Betaproteobacteria*, *Alphaproteobacteria*, *Gammaproteobacteria* and *Bacilli* are highlighted in sky-blue, yellow, light green, pink and orange, respectively. The outer rings of circles indicate the presence, as percentages, of the corresponding taxa in the distal gut (purple circles) and the pyloric caeca (blue circles). (B) The differential taxa representing the distal gut (red bars) and pyloric caeca (blue bars). Phylum, class, order, family, genus and species are shortened to P, C, O, F, G and S, respectively.

### 2.4.4.2 Distal gut microbiota correlates with salmon flesh colour

The microbiota in the distal gut dataset, once separated from the pyloric caeca dataset, was analysed in two categories: flesh colour and banding status. In each category, the phenotypes of the subgroups were distanced by the weighted UniFrac distance algorithm, and the statistical difference was analysed with the PERMANOVA test. However, only the microbiota in the flesh colour category was significantly different between phenotypes, with  $p = 0.031$ , whereas the banding category did not show any correlation with the distal gut microbiota ( $p = 0.143$ ). The distal gut microbiota was then further analysed by Simplicial Ordinary Least Squares Regression to identify the niches of the microbiota taxa for the flesh colour phenotypes. This regression model shows that the flesh colour phenotype alone accounted for up to 21.9% of the variance in the entire distal gut microbiota ( $R^2$  differences = 0.2194). Subsequently, the distal gut microbiota was subjected to Pearson's correlation analysis to show the related microbiota taxa that were strongly connected to the specific phenotype that formed different patterns (Fig. 2.38). In Fig. 2.38, the low colour index Flesh21-22 showed a high correlation with *Ralstonia* (G), *Rhodospirillaceae* (F), *Enterobacteriaceae* (F), *Phyllobacteriaceae* (F), *Microbacteriaceae* (F), *Vibrio* (G) and *Burkholderiales* (O). Flesh23-24 are abundant in *Propionibacterium acnes*, *Photobacterium* (G), *Burkholderia* (G), *Delftia* (G), *Microbacteriaceae* (F) and *Pseudomonas* (G) (Fig. 2.38). The phenotype of Flesh25-26's pattern is closest to Flesh23-24's and is highly correlated with *Propionibacterium acnes*, *Photobacterium* (G), *Chryseobacterium* (G), *Vibrio* (G) and *Carnobacterium* (G) (Fig. 2.38). Finally, the highest colour index is rich in a distinct group of microbiota, including *Sphingobium* (G), *Vibrionaceae* (F), *Stenotrophomonas* (G), *Bacillus* (G), *Lawsonia* (G), *Xanthomonadaceae* (F), *Methylobacterium* (G) and *Delftia* (G) (Fig. 2.38).

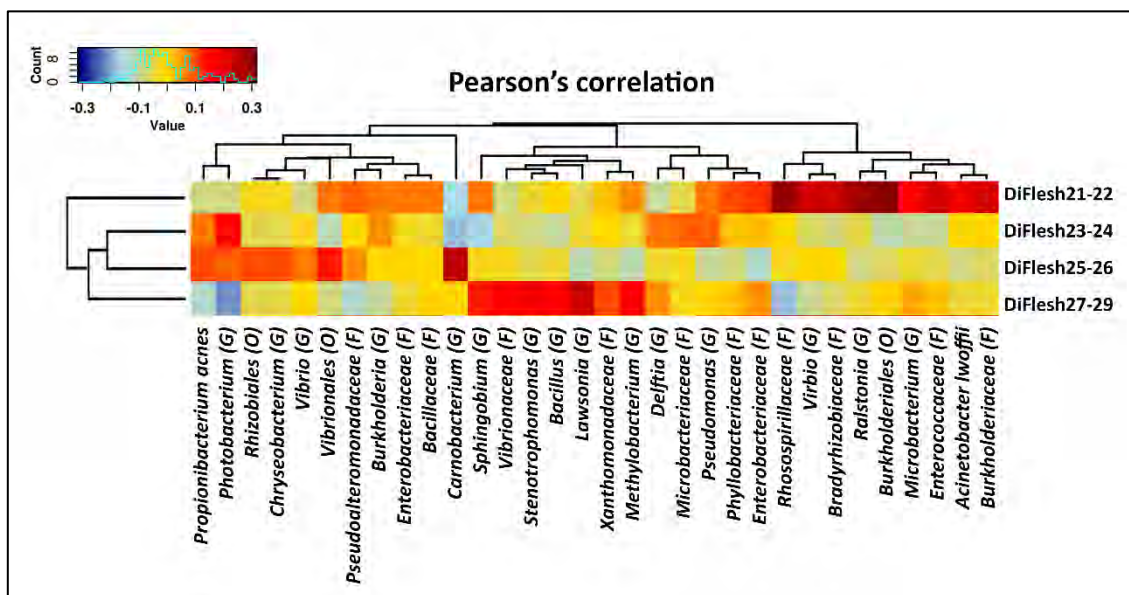
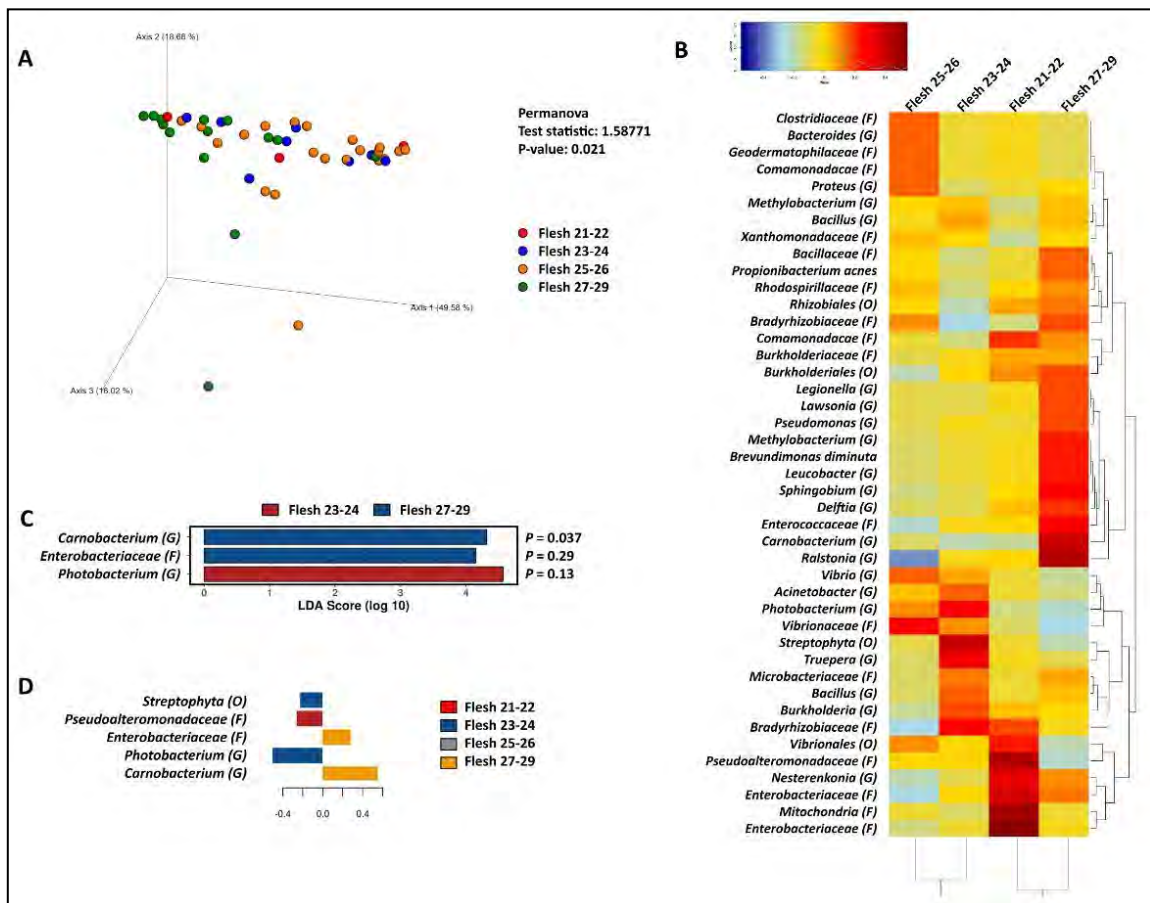


Fig. 2.38 Pearson's correlation between the distal gut microbiota and flesh colour phenotypes. The flesh colour phenotypes are presented as Flesh21-22 to Flesh27-29. The prefix "Di" represents the "distal gut" dataset. Phylum, class, order, family, genus and species are shortened to P, C, O, F, G and S, respectively.

### 2.4.4.3 The correlation of microbiota in the pyloric caeca with banding status

Due to the richness and phylogenetic diversity of the pyloric caeca data being higher than those that belonged to the distal gut, the pyloric caeca data were further rarefied with 853 reads per sample. The microbiota in the pyloric caeca dataset was analyzed based on two categories—flesh colour and banding status—with the weighted UniFrac distance algorithm, and statistical differences were tested with the PERMANOVA test. The microbiota in this gut region were significantly correlated with both

flesh colour (PERMANOVA,  $p = 0.021$ , Fig. 2.39A) and banding status (PERMANOVA,  $p = 0.02$ , Fig. 2.40A). Subsequently, the microbiota was subjected to a Pearson's correlation test to identify related microbiota taxa that strongly correlated with a certain phenotype of flesh colour (Fig. 2.39B) and banding status (Fig. 2.40B). According to the Pearson's correlation, Flesh27-29 was related to *Methylobacterium* (G), *Xanthomonadaceae* (F), *Bacillaceae* (F), *Propionibacterium acnes*, *Rhodospirillaceae* (F), *Bradyrhizobiaceae* (F), *Burkholderiales* (O), *Legionella* (F), *Lawsionia* (G), *Pseudomonas* (G), *Brevundimonas diminuta*, *Leucobacter* (G), *Sphingobium* (G), *Delftia* (G), *Ralstonia* (G), *Enterobacteriaceae* (F) and *Carnobacterium* (G) (Fig. 2.39B). Meanwhile, Flesh21-22 was related to *Vibrionales* (O), *Nesterenkonia* (G), *Enterobacteriaceae* (F), *Mitochondria* (F), *Enterococcaceae* (F) and *Pseudoalteromonadaceae* (F). However, performing a further statistical step in the LEfSE and sPLS analyses showed that the taxa contributing to Flesh27-29 were only *Carnobacterium* (G) (significantly differential, ANOVA  $p = 0.037$ ) and *Enterobacteriaceae* (F) (ANOVA  $p = 0.29$ ), and the taxa contributing to Flesh23-24 were only *Photobacterium* (F) (ANOVA  $p = 0.13$ ) (Fig. 2.39C,D). The other taxa appearing to be correlated according to Pearson's correlation neither contributed to nor were differentiated in the flesh colour phenotypes.



**Fig. 2.39** (A) Principal coordinate analysis (PCoA) of the pyloric caeca microbiota, which was distanced with the weighted UniFrac algorithm with the PERMANOVA test. The flesh colour phenotypes are presented as follows: Flesh21-22 in red, Flesh23-24 in blue, Flesh25-26 in orange and Flesh27-29 in green. (B) Pearson's correlation of the pyloric caeca microbiota and flesh colour phenotypes. The flesh colour phenotypes are presented as Flesh21-22 to Flesh27-29. (C) LEfSE analysis with ANOVA test for each differential taxon; Flesh23-24 in red and Flesh27-29 in blue. (D) Spare partial least squares regression analysis to reveal the composition of the taxa that contributed to the phenotypes: Flesh21-22 in red, Flesh23-24 in blue, Flesh25-26 in grey and Flesh27-29 in yellow. Phylum, class, order, family, genus and species are shortened to P, C, O, F, G and S, respectively.

In the correlation of the pyloric caeca and banding status, None-banding was correlated with *Comamonadaceae* (F), *Rhodospirillaceae* (F), *Nesterenkonia* (G), *Bradyrhizobiaceae* (F), *Ralstonia* (G), *Carnobacterium* (G), *Legionella* (G), *Leucobacter* (G), *Methylobacterium* (G), *Brevundimonas diminuta*, *Enterobacteriaceae* (F), *Pseudomonas* (G), *Delftia* (G), *Burkholderia* (G), *Bacillus* (G), *Sphingobium* (G), *Microbacteriaceae* (F) and *Propionibacterium acnes* (Fig. 2.40B). Meanwhile, Severe-banding was strongly correlated with *Vibrio* (G), *Streptophyta* (O), *Xanthomonadaceae* (F), *Acinetobacter* (G), *Bradyrhizobiaceae* (F), *Truepera* (G), *Geodermatophilaceae* (F), *Enterobacteriaceae* (F), *Pseudomonas* (G), *Enterobacteriaceae* (F), *Burkholderiales* (O) and *Propionibacterium acnes* (Fig. 2.40B). However, in the LEfSE and sPLS analyses, the taxa contributing to the phenotype of None-banding were only *Carnobacterium* (G) (significantly differential, ANOVA  $p = 0.0077$ ) (Fig. 2.40C, D). Only *Acinetobacter* (G), *Enterobacteriaceae* (F) and *Pseudomonas* (G) were significantly differentiated in the severe-banding group (LEfSE analysis, Fig. 2.40C); however, none of them contributed to the phenotype Severe-banding (sPLS analysis, Fig. 2.40D).

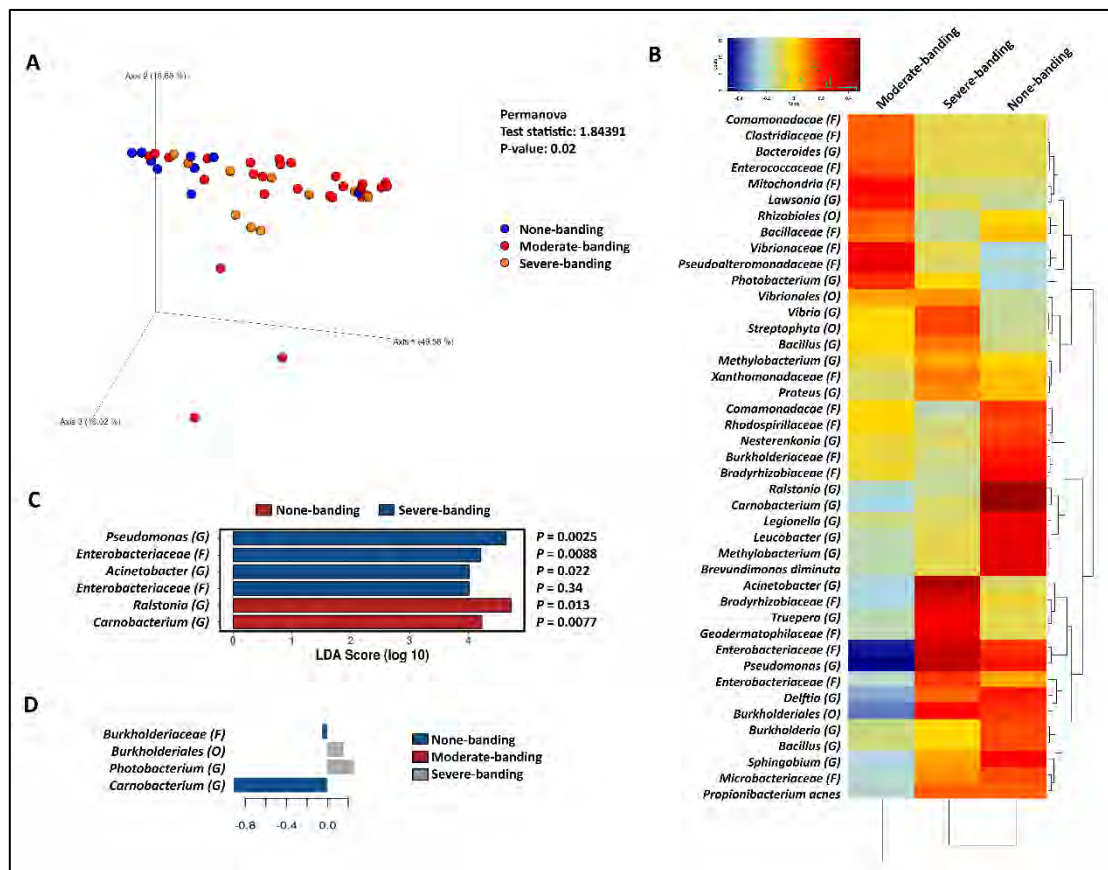


**Fig. 2.40** (A) Principal coordinate analysis (PCoA) of the pyloric caeca microbiota, which was distanced with the weighted UniFrac algorithm with the PERMANOVA test. The banding phenotypes are presented as follows: None-banding in blue, Moderate-banding in red, and Severe-banding in orange. (B) Pearson's correlation of the pyloric caeca microbiota and banding phenotypes: None-banding, Moderate-banding and Severe-banding. (C) LEfSE analysis with ANOVA test for each differential taxon; None-banding in red and Severe-banding in blue. (D) Spare partial least squares regression analysis to reveal the composition taxa that contributed to the phenotypes: None-banding in blue, Moderate-banding and Severe-banding in grey. Phylum, class, order, family, genus and species are shortened to P, C, O, F, G and S, respectively.

Since *Carnobacterium* (G) was the typical taxon in the good colour index Flesh27-29 and None-banding, *Carnobacterium* (G) was subjected to a regression model to identify the complex associations between the environmental variables (i.e., colour phenotypes) and the microbial taxon. The regression models show that, in the category of flesh colour, *Carnobacterium* (G) were significantly

correlated with the change in flesh colour (Pearson correlation  $R = 0.401$ ,  $p = 0.0057$ ; significantly differential for Flesh27-29 with ANOVA  $p = 0.037$ , Fig. 2.41A). Additionally, in the category of banding status, *Carnobacterium* (G) were significantly correlated with the change in banding status (Pearson correlation  $R = 0.353$ ,  $p = 0.016$ ; significantly differential for None-banding with ANOVA  $p = 0.0077$ , Fig. 2.41B).

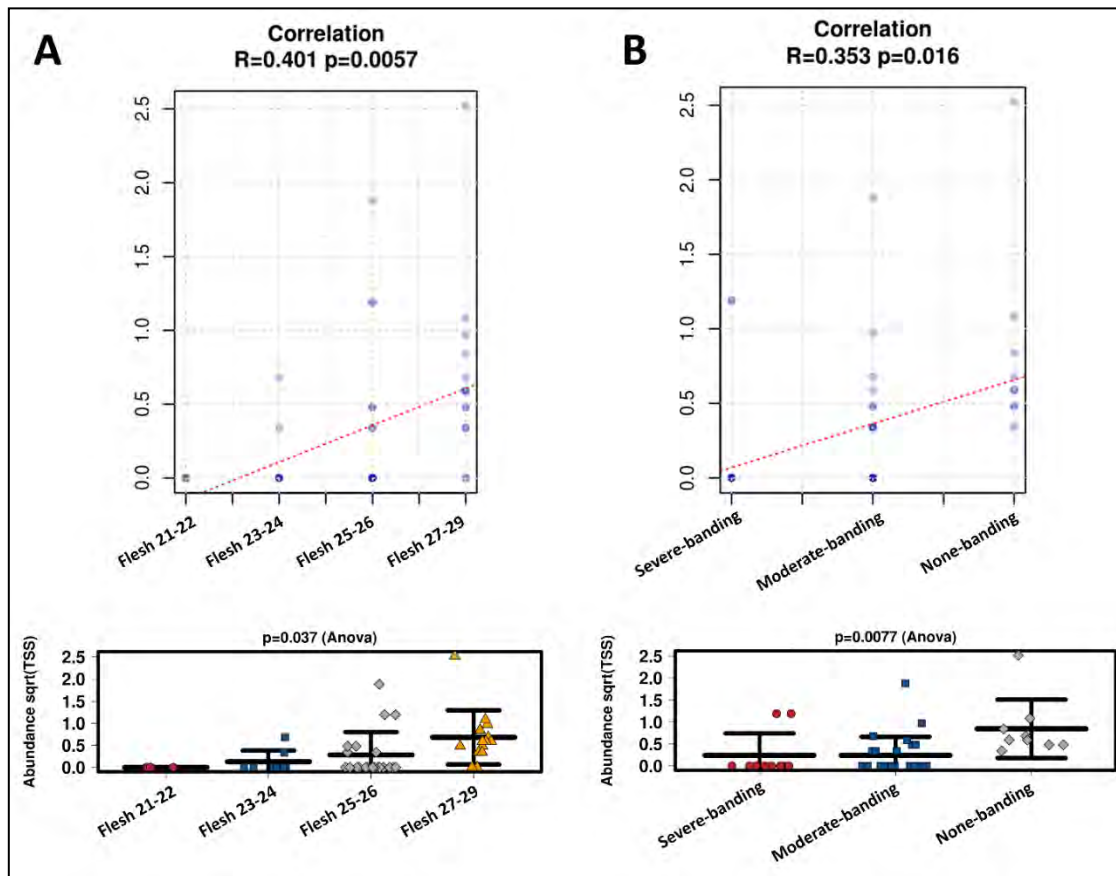


**Fig. 2.41** Regression model analysis to identify complex associations between phenotypes - (A) flesh-colour and (B) banding status - and *Carnobacterium* (G).

#### 2.4.4.4 Predictive function annotation of taxon composition related to banding in the pyloric caeca

The taxon composition of pyloric caeca was further analysed to predict the function categories that related to the differential taxa in the banding phenotypes. There were 6909 Kyoto Encyclopedia of Genes and Genomes KEGG groups, predicted and categorized into 328 KEGG metabolism pathways. The predictive functions were significantly distinctive for the banding category (RDA  $p = 0.044$ , Fig. 2.42A). The functions of taxa differentiated in the None-banding category focused on amino acids, fatty acids, energy (pyruvate), and carotenoid (terpenoid backbone) metabolism (Fig. 2.42B). However, the functions of the taxa in the Severe-banding category focused on sugar metabolism, bacterial chemotaxis, bacterial secretion systems, transcription and translation structure molecules, and peptidase (Fig. 2.42B).

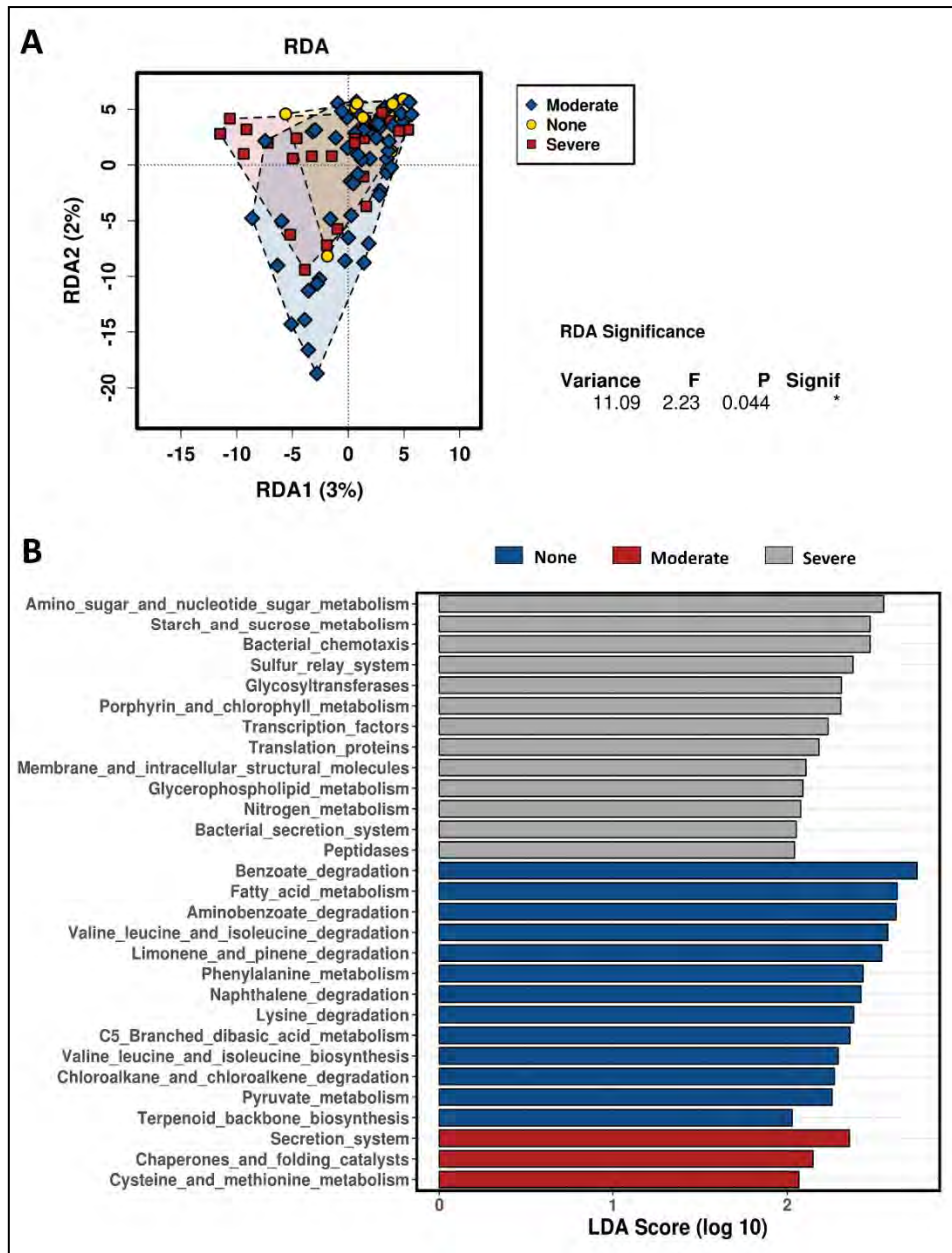


**Fig. 2.42** Functional annotation of the pyloric caeca taxon composition differentiated in the different banding phenotypes. (A) Redundancy RDA analysis with \*  $p < 0.05$ , and (B) LefSE analysis.

### 2.4.5 Discussion

In this study, the effect of microbiota in different niches of the salmon gut on flesh colour and banding status was investigated using samples from two different gut regions: the pyloric caeca and distal gut. The microbiota populations from the two regions were demonstrated to be distinct from each other, in agreement with other studies demonstrating that microbiota along the gut niches are different 86,198,199.

In a previous study, the correlation between the distal gut microbiota and flesh colour was demonstrated<sup>197</sup>. This effect was found to occur independently of the water temperature or the season's change. In this study, the influence of the distal gut microbiota on the change in flesh colour was confirmed. With the sampling in this study taking place at one time point only, the distal gut microbiota still showed variations that correlated with the change in flesh colour when using the

PERMANOVA test  $p = 0.031$  (Fig. 2.38). According to the simplicial ordinary least squares regression model algorithm, the distal gut microbiota composition could explain up to 21.9% of the change in salmon flesh colour. In microbiome studies, the regression model of the rooted balance tree is considered significant when the fitting coefficient  $R^2 > 0.1$ <sup>74,211</sup>. Therefore, this result strengthens the idea of a correlation between the distal gut microbiota and the flesh colour.

In our previous study<sup>197</sup>, a low colour index was correlated with *Pseudoalteromonadaceae* (F), *Vibrionaceae* (F) and *Enterobacteriaceae* (F) in the distal gut, which also dominated in the low colour group in both gut regions - the distal gut and pyloric caeca - in this study (Fig. 2.38 and 2.39). Despite the different seasons and environmental conditions between the two studies (the two sampling events took place 2 years apart), *Pseudoalteromonadaceae* (F), *Vibrionaceae* (F) and *Enterobacteriaceae* (F) still persisted in the low colour index group, indicating their core position as the symbionts in the altered-symbiosis microbiota composition. Altered symbiosis is defined as a status where the microbiota composition changes due to a change in host and environmental stresses; however, this change does not affect the host health<sup>108</sup>. *Pseudoalteromonadaceae* (F), *Vibrionaceae* (F) and *Enterobacteriaceae* (F) belong to *Gammaproteobacteria* (O), which are aerobic bacteria with diverse catabolism pathways that may affect the host physiology<sup>39,84</sup> and, in this specific case, possibly impact flesh colour.

In the high colour index group found in our previous sampling event in 2017<sup>197</sup>, the microbiota taxa that correlated with the flesh colour were *Xanthomonadaceae* (F), *Bacillaceae* (F), *Mycoplasmataceae* (F), *Phyllobacteriaceae* (F), *Commamonadaceae* (F). In the current study, *Xanthomonadaceae* (F) and *Bacillaceae* (F) only are in agreement with what previously found (Fig. 2.38 and 2.39). These findings imply the core symbiont role of *Xanthomonadaceae* (F) and *Bacillaceae* (F) in the high colour index group as being consistent despite the sampling occurring in a different year with different environmental conditions. It also confirms the consistency of the core microbiota within the gut regardless of the change of microbiota composition in surrounding water and in diet<sup>86-89</sup>. *Bacillaceae* (F) is considered as a beneficial bacteria group that is able to support the host's health by providing antibiotics, vitamins, and digestive enzymes<sup>96,212</sup>, as well as controlling opportunistic pathogens<sup>213</sup>. *Bacillaceae* (F) has been known as a probiotic solution at the early larval stage of common snook *Centropomus undecimalis*<sup>214</sup>, gilthead sea bream *Sparus aurata*<sup>215</sup> and grouper *Epinephelus coioides*<sup>216</sup>. Furthermore, *Bacillaceae* (F) possesses the carotenoid biosynthesis pathway and the pigment ranges from yellow to orange and red<sup>217,218</sup>. Therefore, it is possible that *Bacillaceae* (F) naturally contribute to high-quality flesh. On the other hand, *Xanthomonadaceae* (F) was the dominant taxa in the carotenoid metabolism pathway in our previous study<sup>197</sup>. *Xanthomonadaceae* was firstly found in plants and is able to produce the pigment xanthomonadins<sup>219,220</sup>. *Xanthomonadaceae* (F) is found as a dominant bacteria which suppresses pathogenic symbionts in plants<sup>221</sup> and establishes a symbiotic relationship with coral<sup>222-224</sup>, and the carotenogenic chlorophyte algae *Haematococcus lacustris*, which is able to produce keta-carotenoid astaxanthin<sup>225</sup>. Therefore, in salmon, *Xanthomonadaceae* (F) is possibly a symbiont contributing to the carotenoid biosynthesis pathway. Hence, regardless of the change in the microbiota composition in the high colour index group, when comparing the sampling events in 2017 and 2019, and regardless of the difference in gut position, there were two consistent taxa, *Xanthomonadaceae* (F) and *Bacillaceae* (F), that correlated with the strong pink-red flesh colour.

The pyloric caeca microbiota data were richer and more diverse than those of the distal gut (Fig. 2.36 and 2.37). This microbiota was also significantly different between phenotypes—both flesh colour and banding categories—according to the weighted UniFrac distance (PERMANOVA  $p = 0.021$  and  $p = 0.02$ ) (Fig. 2.39A and 2.40A). In the high flesh colour index group - besides *Xanthomonadaceae* (F) and

*Bacillaceae* (F), which were consistent with those in the distal gut microbiota, confirming their core role in most of the digestive tract—the pyloric caeca microbiota also included some new taxa that differentially occupy this gut region (Fig. 2.39 and 2.40), especially *Carnobacterium* (G), which is highly correlated with both Flesh27-29 and None-banding (Fig. 2.41). *Carnobacterium* (G) belongs to the order of *Lactobacillales*, which is a functional order producing lactic acid as an essential metabolic end-product of carbohydrate fermentation<sup>226</sup>. The effect of lactic acid bacteria (LAB) has been widely studied in Atlantic salmon, since they contribute to maintaining host health<sup>227</sup>, stimulate the host immune response and help to protect the host against diseases<sup>228</sup>. The importance of LAB in aquaculture has been extensively reviewed<sup>229,230</sup>. Feeding a LAB-supplemented diet can control the colonization of the beneficial bacteria, leading to better control of diseases and stresses, and enhancing growth in salmonids<sup>47,231–233</sup>. The group of *Carnobacterium* has also been known as beneficial bacteria dominantly colonising various regions of the salmon gut (foregut, midgut and hindgut) and being able to inhibit the growth of pathogens<sup>232</sup>. A previous study has demonstrated that feeding *Carnobacterium* (G) as a probiotic to Atlantic salmon and rainbow trout had no harmful effects and also helped to increase the survival rate during infection challenges<sup>234</sup> due to its ability to produce bacteriocins and antimicrobial compounds<sup>235,236</sup>. Besides the immune-system-supporting function, the role of *Carnobacterium* (G) in fish may have another potential impact: pigmentation. In 2012, Hagi et al. demonstrated that multi-stressors in LAB such as oxidative stress, high temperature stress or envelope stress can be tolerated by carotenoid production<sup>237</sup>. In Hagi's study, a novel gene for carotenoid production, crtM-crtN, from *Enterococcus gilvus* was cloned into *Lactococcus lactis*, a LAB, to support this hypothesis<sup>237</sup>. In *Carnobacterium* (G), the carotenoid gene cluster consists of 4,4'-diaponeurosporenoate glycosyltransferase *crtQ*, 15-cis-phytoene synthase *crtM*, phytoene desaturase *crtN*, 4,4'-diaponeurosporene oxidase *crtP* and glycosyl-4,4'-diaponeurosporenoate acyltransferase *crtO*<sup>238</sup>. Hence, it is possible that *Carnobacterium* (G) can evoke their carotenoid synthesis cascade as a response to tolerate their stresses. *Carnobacterium* (G) were found in the Flesh27-29 and None-banding fish. It is possible that *Carnobacterium* (G) originated carotenoid is one of the carotenoid sources for the host. Additionally, *Carnobacterium* (G), with their ability of immune support, might be in part responsible for the host's better health in response to the thermal stress and therefore leads to the more efficient feed assimilation. Hence, feeding *Carnobacterium* (G) to Atlantic salmon as a probiotic to improve health, the immune system and pigment deposition is a potential biotechnology application. However, it is still not clear whether the correlations observed in the microbiota are the cause or the effect of the phenotypes observed. Therefore, further investigation of *Carnobacterium* (G) and their carotenoid gene expression under multiple stresses is needed.

The pyloric caeca data also showed a correlation between Severe-banding and a group of microbiota that were significantly differentiated: *Acinetobacter* (G), *Enterobacteriaceae* (F) and *Pseudomonas* (G) (Fig. 2.40). *Acinetobacter* (G) is known as a typical opportunistic pathogen that causes *Acinetobacter* disease in Atlantic salmon, channel catfish, common carp, rainbow trout and striped bass<sup>85</sup>. *Pseudomonas* (G) is found as an acute septicemic bacterial disease in fish<sup>85,239,240</sup>. More importantly, *Acinetobacter* (G) and *Pseudomonas* (G) are known as multi-antibiotic-resistant pathogens in aquaculture<sup>241–244</sup>, and *Acinetobacter* (G) has been used as an indicator of antibiotic resistance in the aquatic environment<sup>245–247</sup>. The antibiotic resistance of *Acinetobacter* (G) is of concern since its antibiotic resistance gene can be transferred horizontally to the surrounding microbiota community<sup>248</sup>. All the fish sampled in this study appeared healthy; however, those that were dominated by *Acinetobacter* (G) and other opportunistic bacteria might be experiencing an altered-symbiosis status. In an altered-symbiosis stage, although the health appearance does not change, the host initiates an

immune response in an attempt to overcome this short-term stress and return to a normal host–microbiome relationship<sup>108</sup>. Carotenoids are known to have multiple roles, both non-specific and specific, in the immune system<sup>249</sup>. There is evidence that carotenoid-supplemented diets can enhance the immune response parameters in rainbow trout *Oncorhynchus mykiss*<sup>250</sup>, common carp *Cyprinus carpio*<sup>251</sup> and Atlantic salmon *Salmo salar*<sup>18</sup>. The carotenoid trade-off for pigmentation and immunity has been demonstrated in the polychromatic midas cichlid *Amphilophus citrinellus*<sup>252</sup>. In the polychromatic midas cichlid, the fish itself must decide to allocate the limited carotenoid source for either pigment deposition or the enhancement of the immune system in response to stress<sup>252</sup>. Therefore, we hypothesize there is a trade-off between pigmentation and the immune response in the usage of carotenoids in Atlantic salmon, which leads to the pale flesh and Severe-banding. However, it is unclear if the carotenoid source for this trade-off is derived from the diet or is withdrawn from the fish muscle. A further experiment to examine the carotenoid level retained in the muscle of the fish in this study has been conducted and will be reported in a separate publication. These hypotheses need to be further investigated with supporting evidence from gene expression studies. In the function analysis of the taxa, the composition was differentiated in the different banding phenotypes and the metabolism pathways were significantly distinctive ( $p = 0.04$ , Fig. 2.42A). In the no-banding group, the functions of the microbiota taxa focused on amino acids, fatty acids, energy (i.e., pyruvate) and carotenoid (i.e., terpenoid backbone) metabolism (Fig. 2.42B). In this group, the representing taxa were *Carnobacterium* (G) (Fig. 2.41), which belongs to LAB, strongly supporting the hypothesis above that the beneficial taxa in this symbiosis stage communicated with the host via the intermediates in their metabolism cascade such as amino acids, carotenoids and fatty acids. Additionally, fat and fatty acids play a major role in the regulation of the transporter expression in the intestine, which affects carotenoid absorption<sup>253</sup>. Thus, in this no-banding group, the differential taxa occupy the pyloric caeca in a symbiotic manner. Conversely, the functions of the microbiota taxa in Severe-banding focused on sugar metabolism, bacterial chemotaxis, bacterial secretion systems, transcription and translation structural molecules, and peptidase (Fig. 2.42B). Bacterial chemotaxis is a signal–feedback loop between the bacteria and the environment<sup>254</sup>. This loop exists to maintain the communication and ensure the survival of the bacteria themselves in either favoured or stressed environments<sup>254</sup>. Any action performed by the bacteria on the environment returns as a physical-chemical signal that will be processed, regulated and decided by the bacteria before any new action is performed<sup>254</sup>. The other metabolism pathways in the severe-banding group include sugar metabolism, bacterial secretion systems, transcription and translation structural molecules, and peptidase, all helping the bacteria to achieve the chemotaxis<sup>255</sup>. In terms of host infection, it has been demonstrated that bacterial chemotaxis has a key role in the pathogenicity<sup>255</sup>. This once again supports the hypothesis above, that there was an altered symbiosis occurring in the severe-banding group.

#### **2.4.6 Conclusions**

The correlation of the distal gut microbiota and salmon flesh colour was re-confirmed in this study. *Xanthomonadaceae* (F) and *Bacillaceae* (F) were the two consistent taxa in individuals displaying high colour at the two sampling events (2017 and 2019). Additionally, the distinction between the microbiota in the distal gut and in the pyloric caeca was confirmed. This study has demonstrated the significant correlation of *Carnobacterium* (G) and high colour and the absence of regional colour loss (i.e., banding). We also demonstrated the correlation of the salmon pyloric caeca microbiota and the banding phenomenon. We hypothesize that there is a trade-off between the colouration and the immune activity in Atlantic salmon. This study further supports the role of microbiota in flesh colour dynamics and opens a path for managing this important commercial characteristic through microbiome manipulations.

## **2.5 Additional investigations on molecular and metabolic aspects of flesh colour**

### **2.5.1 Transcriptomic analysis on muscle and pyloric caeca associated with reduced flesh colour**

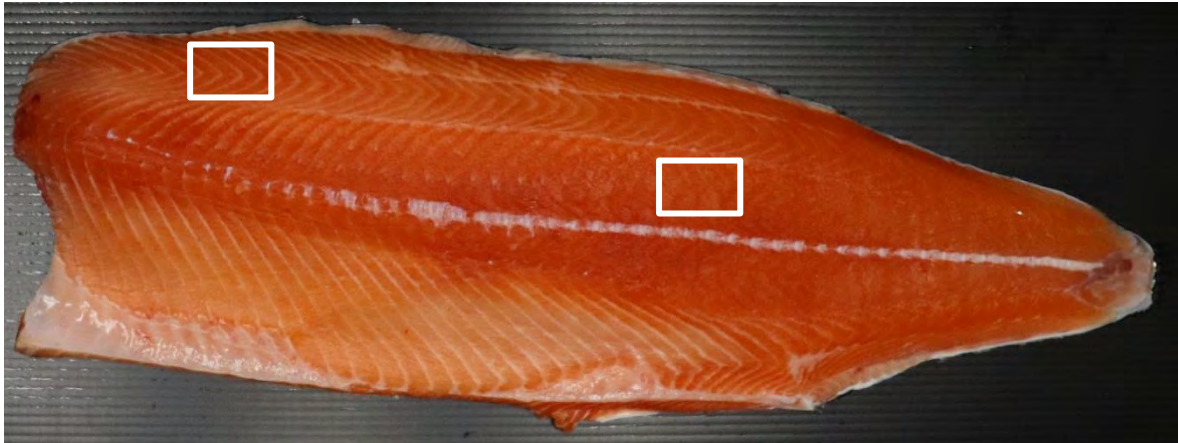
Fish obtain carotenoids through their diet, and absorb them through the digestive system<sup>14</sup>. The fish digestive system generally includes the foregut, midgut and hindgut, in which the foregut consists of the esophagus, stomach and pyloric caeca<sup>198</sup>. The pyloric caeca, a finger-like blind end tube structure is reported to extend the surface area for digestion and absorption<sup>256</sup>. It is also considered as the junction where channels from the liver and pancreas enter, and is proposed to be an important organ for chemical digestion, absorption, osmoregulation, food storage and lipid absorption<sup>257,258</sup>. Moreover, the pyloric caeca were found to have higher astaxanthin concentrations compared to hindgut in an *in vitro* experiment when exposing to micelle solubilised carotenoids in farmed Atlantic salmon and rainbow trout<sup>259</sup>. The peak chromatogram profile showing carotenoid uptake demonstrated a higher proportion of absorbed carotenoids in the salmon enterocytes suggesting that the pyloric caeca and hindgut play a vital role in carotenoid absorption of salmon<sup>260</sup>. Thus, we set to examine the pyloric caeca transcriptome to achieve a more thorough understanding of the influence of the digestive system on flesh colour. The muscle is the organ where stores of carotenoids amount up to 90% or more of the total body carotenoid content, regardless of species or kind of absorbed carotenoids<sup>261</sup>. Therefore, both the pyloric caeca and muscle tissues were chosen for further examination to see which genes are associated with the depletion of flesh colour after high summer temperatures to expand the investigations described in section 2.3.

#### **2.5.1.2 Materials and methods**

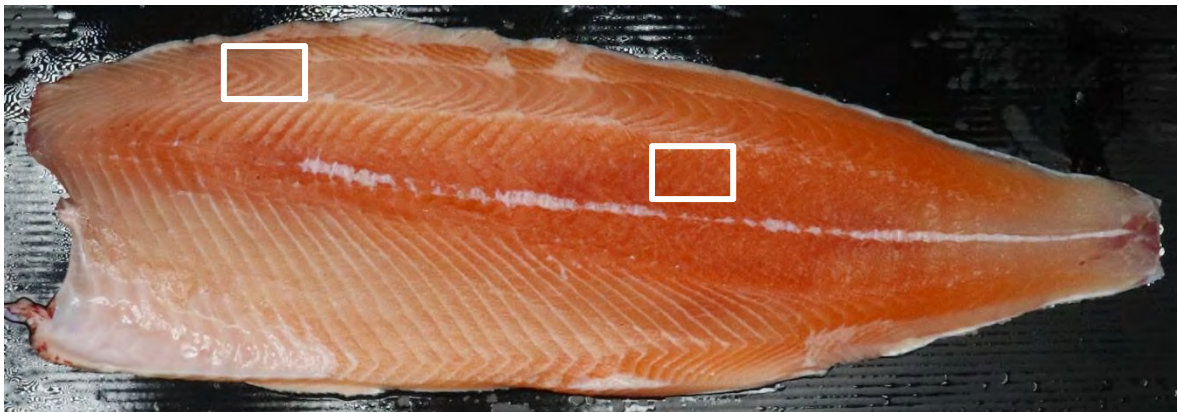
Fish with 140 g average weight were transferred to seawater at the same site of all aforementioned investigations (Rowella) and stocked into two cages 25(27) and 26(28) on 24<sup>th</sup>-25<sup>th</sup> of May 2018. During the seawater growout stage, fish were fed a commercial diet formula containing carotenoid supplementation. Carotenoid content was adjusted from 75 ppm through the winter to 80 ppm between spring and summer until harvest. During the summer of 2019, the water temperature increased and ranged from 18 to above 20°C. The sampling was then carried out after summer on the 2<sup>nd</sup> and 3<sup>rd</sup> of April. The average weight of the fish sampled was 2.2 kg. 1 gram of pyloric caeca (PC), muscle tissue from the front dorsal (FD) and the back central (BC) regions (Fig. 2.43 6, n = 100 per tissue) were collected from 100 fish kept under similar conditions in the two sea cages. Samples were snap-frozen with liquid nitrogen and kept in -80°C until analysis. Following identification of the flesh colour as previously described, fifteen fish were chosen and divided into three groups: high colour-no banding (HN), high colour-banded (HB), and pale colour (n = 5 per group, Table 2.10). Due to the flesh colour of HB and pale fish in the FD region being quite similar and the difference between two muscle regions (BC and FD) in pale fish being very small, only ten samples were selected from the front dorsal muscle region (HN and HB group) (Fig. 2.43).

##### **2.5.1.2.1 Transcriptomic analysis**

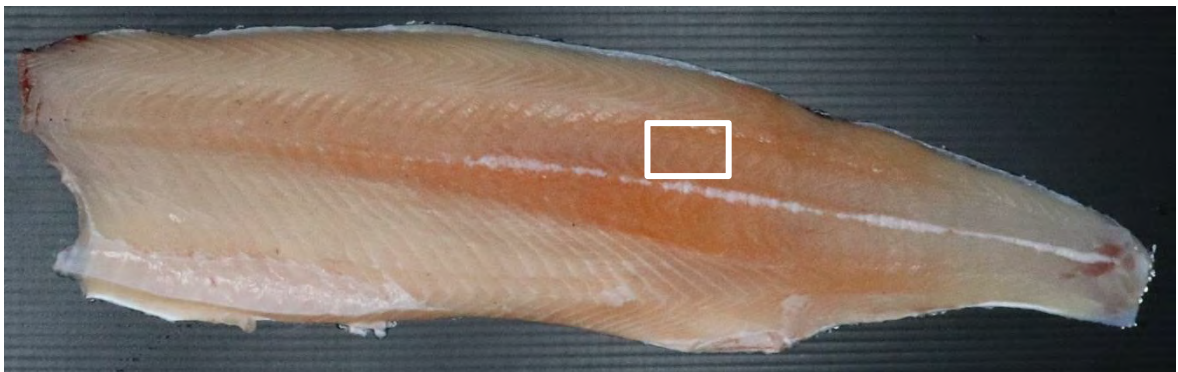
RNA was extracted from the pyloric caeca and two regions of muscle using TRIzol™ Reagent (Invitrogen™, Cat.No 15596026). The quantity and integrity of the extracted RNA was determined using NanoDrop 2000 spectrophotometer (ThermoFisher Scientific, USA) and gel electrophoresis. A total of forty qualified and quantified RNA samples were sent to Novogene for TrueSeq library preparation and sequencing with Illumina HiSeq2500.



**High colour – no banding (HN) fish**



**High colour – banded (HB) fish**



**Pale fish**

**Fig. 2.43** The grouping of experimental fish based on the flesh colour, and FD (front dorsal) and BC (back central) regions sampled are marked by white squares.

Principal component analysis (PCA) was plotted to visualize the distribution of gene expression data between different tissues and different colour groups within each tissue. Then, DEGs were analysed to compare the different phenotypes using DESeq2 in R (version 3.5.3)<sup>127</sup>. A gene was considered as DEG between two conditions when the following applied:  $|\log_2(\text{fold change})| \geq 2$ , p-adjusted value  $\leq 0.05$ . In the muscle samples, the FD and BC regions within each group (HN and HB) were compared. After that, a Venn diagram using InveractiVenn<sup>168</sup> was presented to establish whether there is any difference between HN and HB groups when comparing two muscle regions.

**Table 2.10** Forty samples selected for transcriptomic analysis<sup>9</sup>

No.	DNA ID	Gill Tag ID	Group	Selecting		
				Front Dorsal	Back Central	Pyloric caeca
1	80009790	0003	HB	P	P	P
2	80009694	0007	HN	P	P	P
3	80009782	0010	HB	P	P	P
4	80009888	0013	HB	P	P	P
5	80009877	0030	P		P	P
6	80009833	0045	P		P	P
7	80015430	0051	P		P	P
8	80009853	0055	HN	P	P	P
9	80009740	0059	HB	P	P	P
10	80009947	0061	P		P	P
11	80010000	0075	HN	P	P	P
12	80009682	0076	P		P	P
13	80009894	0085	HN	P	P	P
14	80009643	0087	HB	P	P	P
15	80009868	0100	HN	P	P	P

#### 2.5.1.2.2 RT-qPCR validation

The protocol was performed as described above (see 2.3.5.4). Briefly, primers were designed using the ‘Assay Design Center’ available at the Roche website (<https://qpcr.probefinder.com/organism.jsp>). After synthesis, cDNA templates were mixed with primers, FastStart Universal Probe Master (Rox; Roche Diagnostics GmbH) and Universal ProbeLibrary Probe (Roche). The housekeeping genes (HKG) 18S rRNA served to normalize the quantification. qPCR cycles included 10 min incubation at 94 °C, followed by 40 cycles of 94 °C for 10 secs and 60 °C for 30 secs, with green fluorescence measurement on each cycle at 60 °C. Relative quantification was calculated by equilibrating to the level of HKG per sample and the sample with the lowest value ( $2^{-\Delta\Delta CT}$ ). Statistical analysis of the resulting relative quantities was carried out to compare means of multiple groups, followed by Wilcoxon test (for two non-parametric groups) or Kruskal-Wallis (for multiple non-parametric groups) with  $P < 0.05$  considered as statistically significant.

#### 2.5.1.2.3 Muscle histology

From selected fish,  $n = 40$  FD and BC muscle samples ( $n = 20$  per group per each tissue) were fixed in Bouin’s solution (Cat/No. HT10132, Sigma-Alrich, USA) until processing. Fixed samples were sent to QIMR Berghofer Medical Research Institute (Queensland, Australia) for histological processing. Microscopic image analysis of sections with both longitudinal and transverse cuts was run on Masson’s trichrome stained sections. After that, microscopy images of these sections from each specimen were observed using Nikon Eclipse Ti microscope and Nikon NIS-Elements AR software to acquire the image results.

#### 2.5.1.3 Results and discussion

##### 2.5.1.3.1 General results

---

<sup>9</sup> HN: high colour – no banding; HB: high colour – banded; P: pale

The gene expression PCA plot shows the relationships among samples and the differences between tissues (Fig. 2.44). Fig. 2.44a shows the cluster of individual samples per tissue type. All PC samples clustered separately and distanced from the two other adjacent clusters of FD and BC muscle regions, validating the expected variance in gene expression between the different tissues. In the PC and BC muscle region, the samples of different colour type were clustered closely, with an overlap between them (Fig. 2.44b and c). The cluster of high colour – banded (HB) group covered the whole cluster of high colour – no banding (HN) and a part or whole cluster of pale group. Similar to the FD region, the clusters of HN and HB were partly overlapping (Fig. 2.44d).

The gene expression clustering of the HN and HB groups in the PC and BC muscle region is shown in Fig. 2.44b and c. There are hardly any DEGs observed in these comparisons (Fig. 2.45). The number of DEGs was highest between HN and pale fish with 142 DEGs in the PC and 271 DEGs in the BC muscle region. Accordingly, DEGs in the comparison of HB and pale group was 36 and 107 for PC and BC region, respectively. In the FD region, when comparing HN and HB fish, there were 82 DEGs, in which 61 genes were up-regulated and 21 genes were down-regulated, respectively.

The quantity and diversity of DEGs in the comparison of BC and FD regions within HN or HB groups were investigated through the transcriptomic analysis. Interestingly, in HN fish, the number of DEGs in the comparison of BC and FD was 300 genes, much higher than the 63 genes in the same comparison in the HB fish while the colour difference between these two regions in HN fish was less distinct than that observed in the HB fish (Fig. 2.46b). This result indicates that expression at the gene level was not only varied in the colour phenotypes but also differed between muscle regions (FD and BC). In contrast to the HB fish, gene expression between BC and FD region in HN fish varied when the fish could maintain the flesh colour level in suboptimal conditions. When comparing DEGs between HN and HB group, there are 57 overlapping genes and only 6 genes expressed in HB group (Fig. 2.46a).

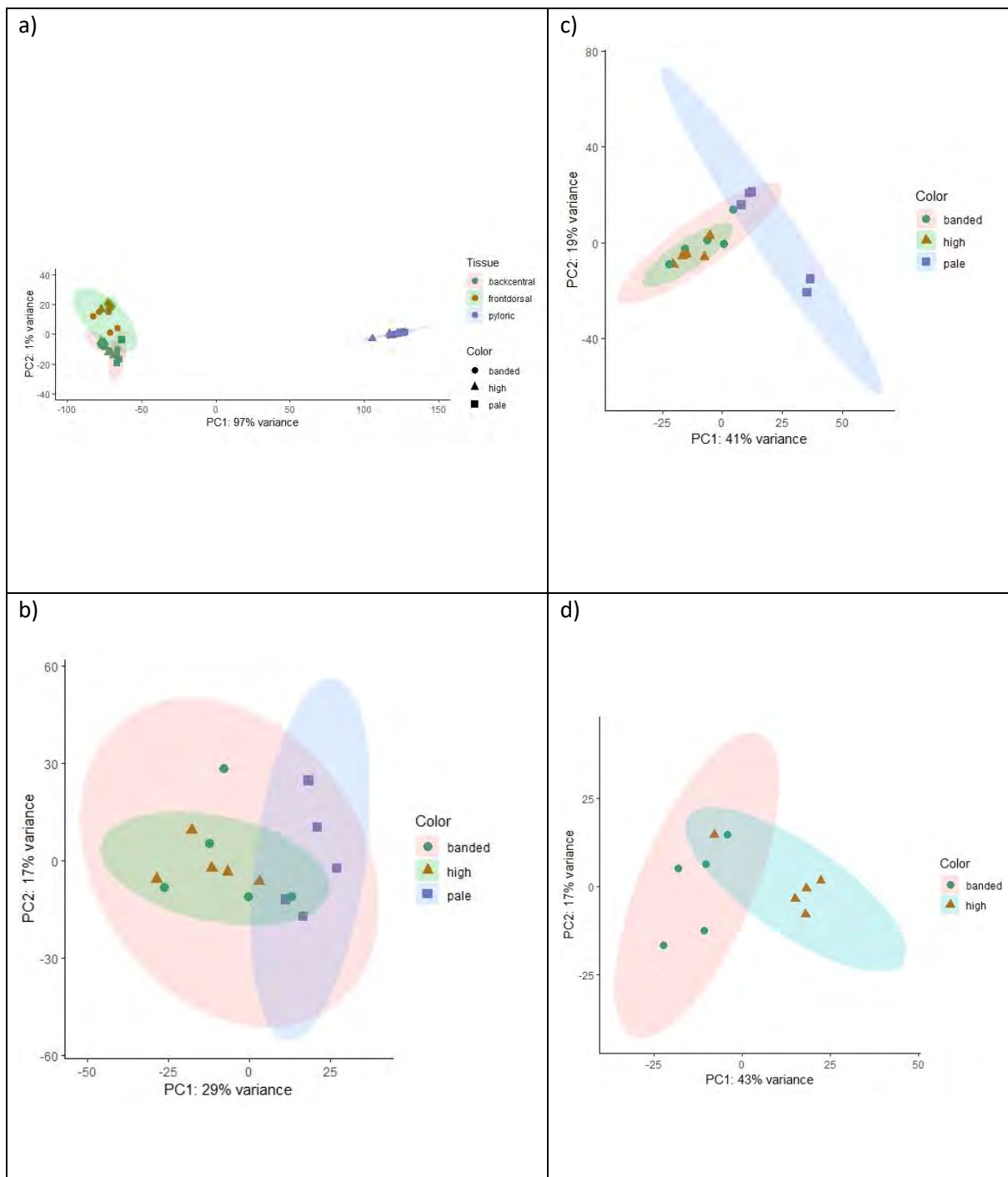


**Fig. 2.44** Principal component analysis (PCA) of sequencing data comparing different tissues and different groups within each tissue. a) The comparison of PC, FD and BC regions; b) The comparison of HN (high), HB (banded) and pale fish in the PC; c) The comparison of HN (high), HB (banded) and pale fish in the BC region; d) The comparison of HN (high) and HB (banded) fish in the FD region.

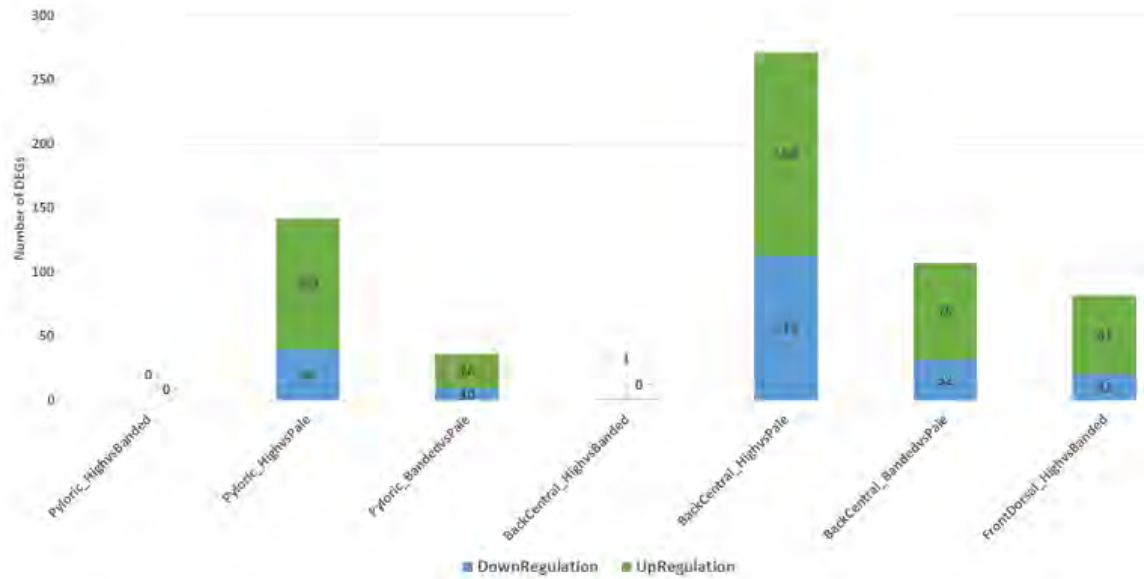


**Fig. 2.45** Differentially expressed genes in comparisons between different phenotypes for each tissue.

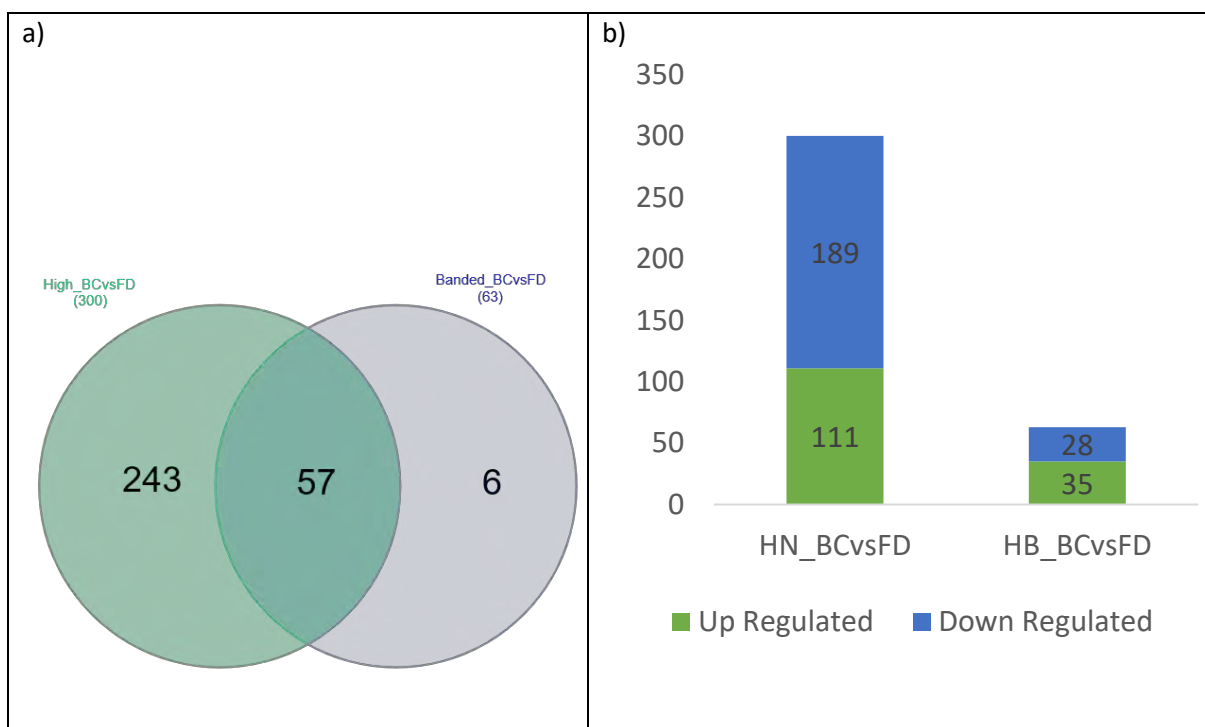


**Fig. 2.46** Visualization of genes differentially expressed (DEGs) between high colour - no banding (HN) and high colour - banded (HB) fish when comparing the back central (BC) and front dorsal (FD) regions. a) Venn diagram showing the overlapping DEGs between HN and HB groups b) The number of DEGs in HN and HB groups.

The results above indicated that there is a number of genes expressed differentially between HN, HB and pale fish and in different tissues ( $P < 0.05$ ). In PC and BC region, pale fish were significantly different from HN and HB fish. Although HN and HB varied in the flesh colour, there are hardly any DEGs in both those tissues while the difference was mainly found in the FD region, consistent with that being the region showing the most colour loss.

Regarding essential genes which associate with flesh colour loss and formation in Atlantic salmon, a transcriptomic analysis of muscle and pyloric caeca was carried out.

### 2.5.1.3.2 Comparison of different phenotypes (HN vs HB) in the front dorsal (FD) region

Regarding the flesh colour, there is a difference in the FD muscle region between high colour – no banding (HN) and high colour – banded fish (Fig. 2.43). This distinction was also reflected at the gene expression level. In HN fish, the majority of the upregulated genes encode for proteins involved in muscle contraction, collagens, calcium ion binding and metabolic processes, while genes relating to lipid and fatty acid metabolism were highly expressed in HB fish (Appendix 2.1). In connective tissue of fish muscle, collagen is the most abundant protein which contributes significantly to sustaining flesh integrity and muscle cohesiveness <sup>262,263</sup>.

Genes encoding muscle fibre proteins including troponin C, troponin T, troponin I, myosin heavy chain, myosin-binding protein C, slow type and fast type were upregulated in HN fish (Appendix 2.1). In rainbow trout, myocyte contractility is controlled by troponin C that fish express at low temperature <sup>264</sup>. The aforementioned study demonstrated that troponin C has an essential role in sustaining cardiac function when temperatures change, suggesting the presence of a similar mechanism in other salmonids. A recent study in crisp grass carp indicated that elevated reactive oxygen species, (ROS), caused an increase of flesh firmness, probably by disturbing calcium-binding, impairing actin-myosin interaction and interrupting collagen turnover, which mediates fragmentation of myofibrillar proteins <sup>265</sup>. Accordingly, in the present study, we hypothesize that muscle metabolism and structure in HN fish were maintained by upregulation of many genes involving calcium-binding, muscle contraction, collagens and glucose metabolism. In the present FRDC study, troponin C (TnC) also was upregulated in the front dorsal of HN fish compared to HB fish (Fig. 2.47). The role of troponin C in high thermal stress is still unclear, but it may be involved in compensating for the changes in calcium ion binding protein in the muscle, resulting in the muscular contractility.

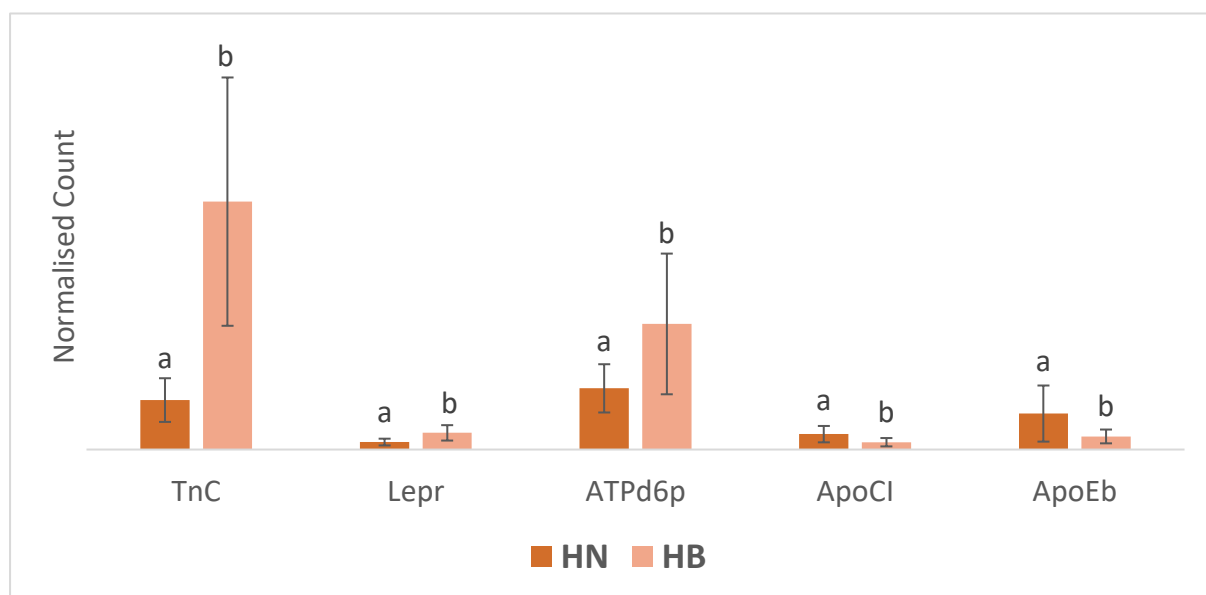


**Fig. 2.47** Important highly expressed genes in the front dorsal (FD) region. An average normalized count across transcripts is shown. Data is shown as Mean ± SE. (n =5). Means with different letters indicate significant differences (P < 0.05).

In addition, it has been proposed that lipid and glucose metabolism could be associated with the muscle fibre composition protein network through heat shock response, hence creating a protein-protein interaction network of muscle metabolism and structure <sup>266</sup>. An upregulated ATP-dependent 6-phosphofructokinase, muscle type-like (ATPd6p) gene in HN fish was found to be involved in glucose degradation of carbohydrate catabolism (Fig. 2.47). It was also found that ATPd6p, a glycolysis-related gene, was upregulated in yellow croaker when supplemented with hydroxyproline, leading to an increase in glucose-6-phosphate concentrations, pointing to a better utilization of carbohydrates <sup>263</sup>. These results indicate that in experimental fish exposed to oxidative and thermal stresses during summer, HN fish might enhance glucose catabolism, collagens of extracellular matrix components and calcium-binding associated with muscle contraction in order to maintain the body function under challenging conditions.

The factors mediating the physiological action of leptin, a pleiotropic hormone receptor, have been investigated in mammals for many years. Recent studies showed the role of leptin in digestion regulation and energy homeostasis in teleosts. Altogether, there is evidence that leptin regulates body weight, metabolism and food intake in fish, similarly to what happens in mammals. It was demonstrated <sup>267</sup> the involvement of the leptin system in the metabolic status of Atlantic salmon with both season and restricted feeding affecting leptin gene expression in the liver and leptin receptor in the brain. In the present study, leptin receptor-like (Lepr) sequences were downregulated in HB fish (or upregulated in HN; Fig. 2.47), possibly causing an imbalance in metabolism, food intake regulation and starvation.

We propose that in HB fish, lipid and fatty acid metabolism were upregulated through high expression of apolipoprotein C-I (ApoCI) and apolipoprotein Eb (ApoEb) (Fig. 2.47). ApoEb functions as an extracellular transporter for cholesterol and other lipids via binding to low-density lipoprotein (LDL) receptors on the target cell surface. ApoCI is the smallest exchangeable apolipoprotein and plays a key role in regulating plasma lipid metabolism and advancing cell growth <sup>268</sup>. ApoCI, which is the main structural component of high-density lipoprotein (HDL) and very-low-density lipoprotein (VLDL), inhibits the connection between ApoE and lipoprotein receptors <sup>269</sup>. Also, ApoCI acts as an inhibitor of hepatic lipase (HL) and an activator of lecithin:cholesterolacyl transferase (LCAT), enzymes involved in lipid metabolism. ApoEb serves in repair response to tissue injury, immunoregulation, and modulation of cell growth and differentiation <sup>270</sup>. Based on our present study, we hypothesize that the upregulation of ApoCI and ApoEb in HB fish enhances the synthesis of cholesterol esters in HDL catalysed by LCAT. These HDL particles could be delivered to the liver, where they are uptaken and catabolized (Fig. 2.48) <sup>138,271</sup>. Due to its hydrophobic characteristic, astaxanthin can bind to free cholesterol and then form cholesterol esters in HDL particles. This formation can result in reducing astaxanthin content in the front dorsal of HB fish, and in the depletion of flesh colour.

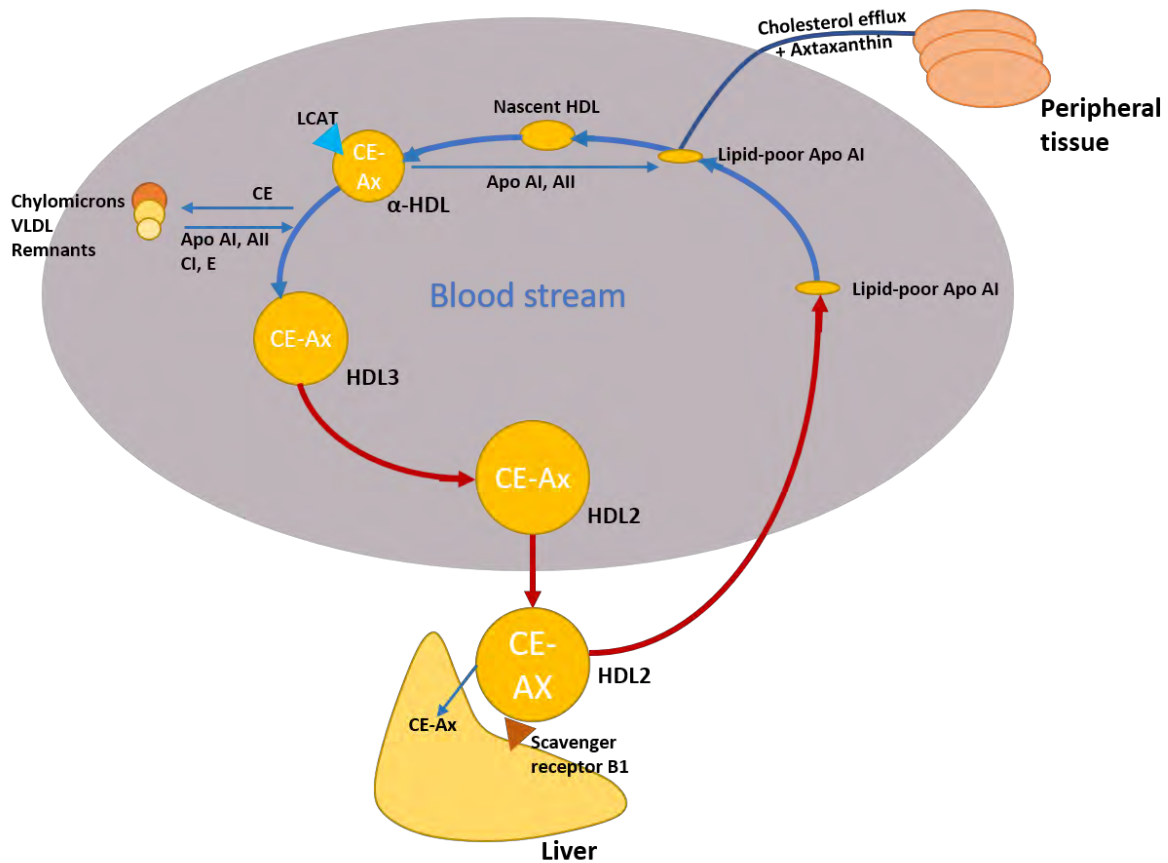


**Fig. 2.48** Reverse cholesterol transport from peripheral tissues to liver by high-density lipoprotein (HDL). HDL particles carry cholesterol from peripheral tissues to the liver and also embed cholesteryl esters (CEs) by interchanging them for triglycerides (TG) with TG-rich lipoproteins. Gathering of CEs transforms the particle to spherical HDL3. HDL3 transfers CE, ApoA, ApoC and ApoE to enlarge its particle size which matures into HDL2. HDL2 then disposes of CE by docking into the scavenger receptor type B class I (BI). In this way, HDL enables the maintenance of extracellular cholesterol pool. Modified from <sup>271</sup>. HDL, high-density lipoprotein; VLDL, very low-density lipoprotein; CE-Ax, cholesteryl ester-Astaxanthin; Apo AI, apolipoprotein AI; AII, apolipoprotein AII; CI, apolipoprotein CI; E, apolipoprotein E; LCAT, lecithin:cholesterolacyl transferase.

In conclusion, thermal stresses caused by high summer temperatures affects flesh colour and the FD region is where the effect manifests in the form of banding via pigments depletion. In light of what observed in HN fish, where there are signs of active support to muscle structural integrity and metabolism, which could have contributed to better retention of flesh colour, we hypothesise that discolouration occurs via impairment of the aforementioned processes. Furthermore, from the observations in HB fish, where metabolism and feed intake are likely impaired and lipid and fatty acid metabolism is upregulated, possibly causing mobilisation of carotenoids, we hypothesise that these processes are also involved in flesh colour loss.

### 2.5.1.3.3 Comparison of different phenotypes (HN vs HB vs pale) in the back central (BC) region

Similarly to the FD muscle region, in the BC there are many highly expressed genes which relate to the muscle fibre composition protein network, calcium ion binding, lipid metabolism and metabolic processes. Considering the DEGs involved in the muscle fibre composition protein network, there is a big difference in diversity and number of expressed genes.

Myosin light peptide 3-3, myostatin 1b, myosin light chain 3, actin alpha skeletal muscle-2 (acta2), myosin-binding protein H, thymosin beta, myomesin-2 and tropomyosin 1 (alpha) were upregulated in HN or HB fish compared with pale fish (Appendix 2.2). Acta2 genes were only upregulated in the BC

region of both HN and HB fish (Fig. 2.49). Since the actin protein is considered as a critical carotenoid-binding protein in salmon<sup>134</sup>, upregulation of *acta2* in the BC region might explain the better colour retention in that region in well-pigmented fish. Also, myostatin 1b (*Myo1b*) plays a role in the regulation of muscle growth and SNPs in *myo1b* gene were found to be associated with harvest traits in Atlantic salmon, including darker flesh colour and fat percentage<sup>272</sup>.

In contrast, obscurin, tropomyosin alpha-3 chain, tropomyosin beta chain, tropomyosin 3, four and a half LIM domains protein 1, myosin-binding protein C, nebulin and troponin T (tnT) were upregulated in pale fish (Appendix 2.2). Although little is known on the matter, troponin genes are closely related to the regulation of muscle contraction, in which tnT provides the binding of troponin to tropomyosin, a part of the thin filaments<sup>273</sup>. The aforementioned findings indicate that there is expression of a group of genes involved in the thin filaments and protein-connecting thin filaments in the group of pale fish. Darker colour is proposed to be linked with the filament size in Atlantic salmon flesh<sup>28</sup>. It was also found that nebulin and obscurin genes upregulated in small size rainbow trout, disregarding if they were fast- or slow-growing<sup>274</sup>. In the present study, pale fish were smaller than HN and HB fish (1.45 kg vs 2.58 and 2.35 kg mean weight of HN and HB fish, respectively). This result suggests that the smaller size pale fish tend to upregulate genes involved in the composition of thin filaments in the muscle fibre composition protein network. In addition, genes encoding collagens of extracellular matrix (ECM) were not highly expressed among groups in the BC region. This could indicate that the connective tissue was not significantly affected by thermal stresses in BC regions, which occurred in FD region. These results highlight how the components of muscle proteins in the two regions analysed varied dramatically between phenotypes. In summary, gene expression profiles relating to the muscle fibre composition protein network were distinctly different between the FD and BC muscle region. In which, actin alpha skeletal muscle and myostatin 1b could be considered as critical genes, possibly affecting flesh colour and muscle structure.

In the context of lipid metabolism, only lipase, hormone-sensitive (*Hsl*) and L-serine dehydratase/L-threonine deaminase-like (*Lsd/Ltd*) genes were upregulated in HN and HB fish compared with pale fish. Other genes involved in lipid metabolism were upregulated in pale fish (Appendix 2.2, Fig. 2.49). Hormone-sensitive lipase is an enzyme in lipolysis, which is considered as an indicator of fat content in tilapia<sup>275</sup>. It was found that L-serine dehydratase/L-threonine deaminase-like (*Lsd/Ltd*) could decrease the catabolism of fatty acids and amino acids<sup>276</sup>. In the pale group, lipoprotein lipase (*Lipase*) was upregulated. Lipase, a triacylglycerol lipase, has a role in the hydrolysis of chylomicrons to release free fatty acids<sup>14</sup>. Furthermore, fatty acid-binding protein intestinal-like (*Fabpi*) plays a role as a transporter of fatty acids through the cytoplasm to the liver and muscle<sup>277</sup>. The transport of carotenoids in salmon is proposed to be similar to the lipids transport<sup>14,184,260,278</sup>, and some dietary factors, such as lipid levels, cholesterol levels and fatty acids have links with increased carotenoid absorption<sup>279–282</sup>. In the present study, our results suggest increased delivery and release of fatty acids together with carotenoids in the BC muscle region of pale fish. Since it was demonstrated that the reduction in flesh pigmentation did not increase oxidative stress indices in Atlantic salmon after starvation at elevated temperature<sup>33,37</sup>, we propose that astaxanthin could be passively transported and consumed following lipid metabolism. Hence, higher consumption of fatty acids was likely to take place in pale fish to compensate for the shortage of fatty acids used as an energy source during the starvation period at high temperature during summer. Therefore, depletion of flesh colour might occur via concurrent catabolism of fatty acids and astaxanthin.

In addition, we found some interesting genes which would correlate with flesh quality and colour variation in the BC muscle region. The AMP deaminase enzyme catalyses deamination of adenosine monophosphate and contributes a vital function in energy metabolism. In the present study, *Ampd3*

was solely upregulated in pale fish (Fig. 2.49). Also, cathepsin L gene (Catl), a cysteine protease, was highly expressed in pale fish (Fig. 2.49). Catl is known to be the major proteolytic enzyme which affects muscular protein degradation <sup>273</sup>. It is likely that in fish under starvation due to thermal stress the proteolytic process was increased to compensate for the high consumption of energy. Also, since tropomyosin and actin muscle proteins are sensitive to Catl <sup>273</sup>, the upregulation of Catl in pale fish could result in actin degradation, which is the carotenoid-binding protein, resulting in carotenoid level reduction in the muscle.

In our study, stress response proteins were upregulated in HN and HB fish compared to pale fish, probably in reaction to the adverse effects of possible oxidative and thermal stress. Heat shock protein 70 (Hsp70) is reported to be a critical gene in the presence of thermal stress. High expression level of Hsp70 was shown to play a vital role in protecting cells from damage resulting from high-temperature stress <sup>283</sup>. In that study, the expression level of Hsp70 in pufferfish fed different dietary astaxanthin content under induced heat stress was examined. The results indicated that moderate supplementation of dietary astaxanthin could enhance Hsp70 gene expression and support cell protection. In our present study, the Hsp70 gene was upregulated in the BC muscle region of HN and HB fish (Fig. 2.49) where astaxanthin is better deposited and retained. In pale fish, where flesh colour is depleted, the Hsp70 gene was downregulated. This result is in agreement with previously published findings <sup>283–286</sup> and suggests that Hsp70 could be expressed to enhance the cell resistance to high thermal and oxidative stress when the accumulated astaxanthin level in the body tissue was high. Although its mechanism is still unclear, it can be hypothesized that there is a positive correlation between Hsp70 gene expression and body astaxanthin level.

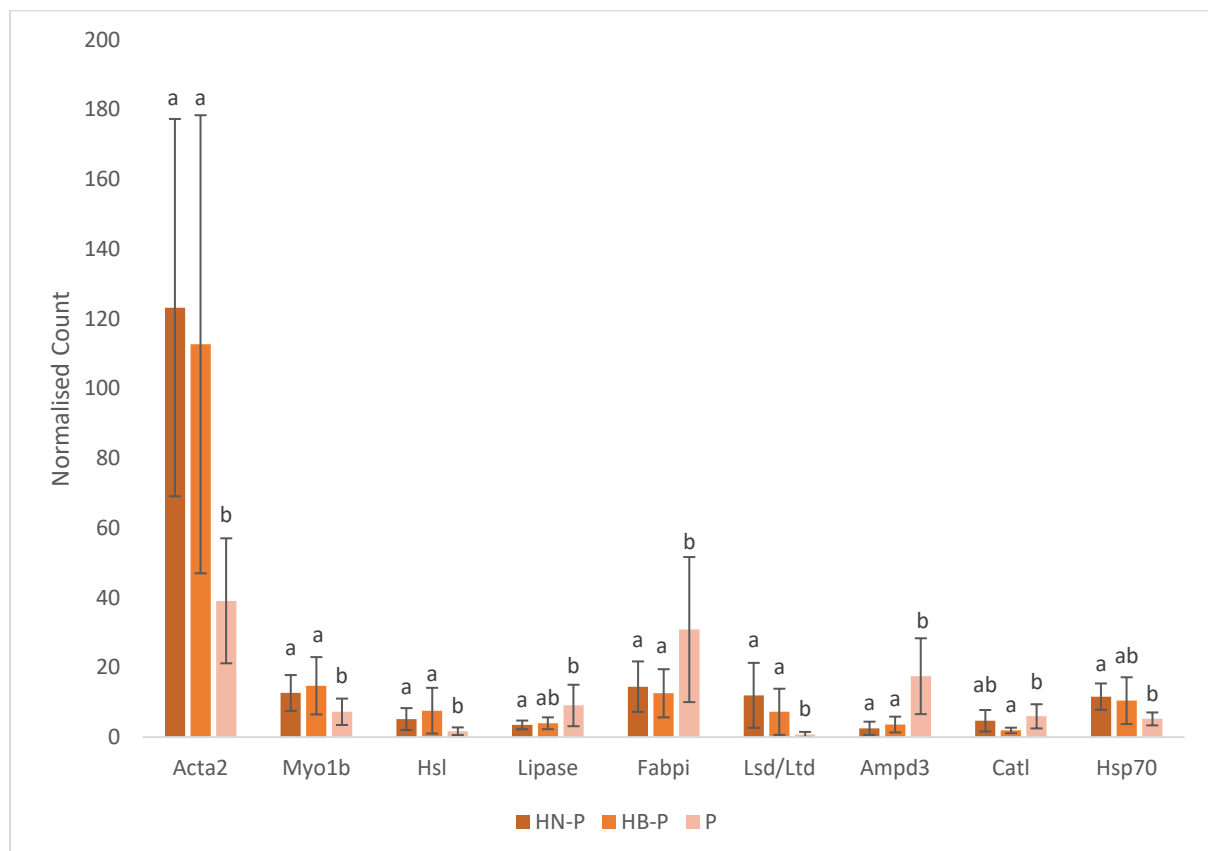


**Fig. 2.49** The expression of important highly expressed genes in the back central region: HN vs Pale and HB vs Pale. An average normalized count across transcripts is presented. Data is shown as Mean  $\pm$  SE, (n =5). Means with different letters indicate significant differences (P < 0.05).

#### **2.5.1.3.4 Qualitative microscopic image analysis of muscle from different regions and colour phenotypes**

Histological sections of muscle from the FD and BC regions were qualitatively analysed (Fig. 2.50 & 2.51). In salmon, carotenoids were demonstrated to bind muscle proteins<sup>13</sup>; therefore, the amount of carotenoids deposited and bound to muscle fibre proteins might decrease when the quantity of muscle myofibril proteins is reduced. Using histological observations, the morphological characteristics and flesh texture of the FD region between HN and HB fish were compared (Fig. 2.50). It is evident that there was a loss of myofiber-to-myocommata and myofibre-to-myofibre attachments in the HB fish (Fig. 2.50C), while these attachments were still stable in HN fish (Fig. 2.50A). The myocommata connective tissue is where collagens are distributed. Connective tissue or myofiber-myocommata attachment changes have been linked to the deterioration of fish flesh texture<sup>287,288</sup>. It was also found that myofibril detachment and modification in ECM protein (collagens) distribution linked with soft flesh texture of Atlantic salmon<sup>289</sup>. Therefore, although not measured in our study, in light of the aforementioned findings, flesh texture in FD region of HB fish might be softer compared to HN fish, and this will need to be examined further. Moreover, muscular atrophy was recorded in HB fish (Fig. 2.50D).

A positive relationship between flesh colour and fibre density was proposed, when higher fibre density and more medium-sized fibres occur simultaneously with a dark red flesh<sup>28</sup>. In a recent study<sup>37</sup>, it was proposed that localised carotenoids retention can be attributed to the variety of muscle fibre proteins in the fillet of Atlantic salmon. Therefore, myofibril degradation could be responsible for pigment depletion in FD region of HB fish in our study.

The histological sections show differences in BC muscle structure between HN, HB and pale fish (Fig. 2.51). In HN and HB fish, the connection between myocommata and myofibrils is tight, while it appears slightly looser in pale fish (Fig. 2.51A, C, E). The intermyofibrillar spaces in HN were relatively small, while the myofibrils size was comparatively large (Fig. 2.51B). In HB fish, the muscle structure seemed to be an intermediate between HN and pale fish. While the intermyofibrillar spaces and myofibrils size were similar to HN fish, the myofibrils looked atrophied and the intermyofibrillar spaces expanded (Fig. 2.51D). When comparing HN and HB fish with pale fish, the latter had significantly larger intermyofibrillar spaces, with most of myofibrils being atrophied (Fig. 2.51F). This could indicate muscle degradation (maybe caused by Cat1 as previously mentioned). Following several previous findings, the connection of myofibril-to-myofibril and myocommata-to-myofibril are associated with muscle quality<sup>287-289</sup>. This suggests that in the BC region of our study, the flesh texture could be partly degraded in HB fish and greatly degraded in pale fish. Therefore, we hypothesize that the firmness of BC muscle region in HN and HB fish could be higher than in pale fish. Since size and density of muscle fibre had a positive correlation with a redder flesh in Atlantic salmon<sup>28</sup>, it is suggested that deterioration of muscle fibre could explain the reduction of flesh colour in BC of the pale fish.

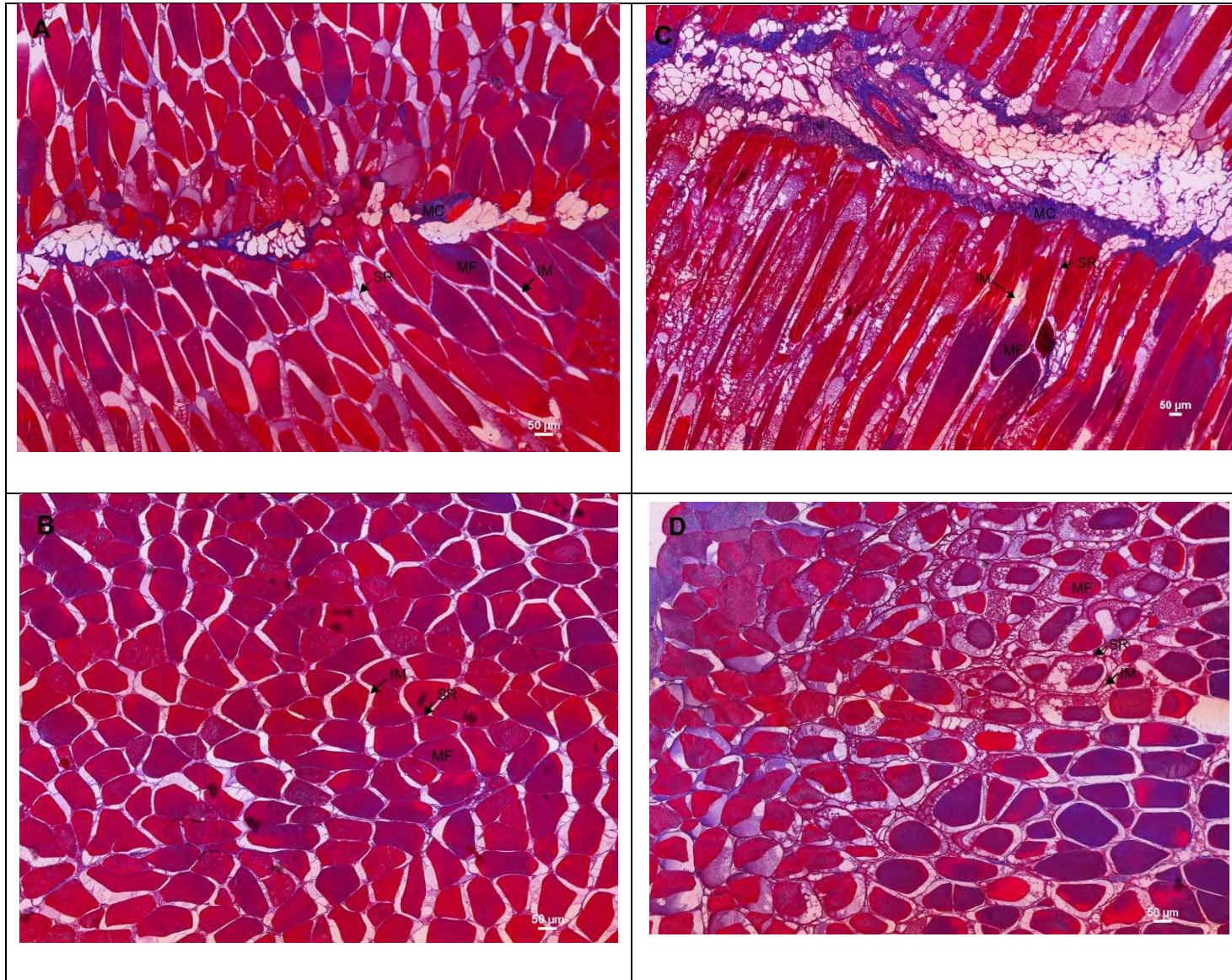


**Fig. 2.50** Microscopy images of muscle showing the structural variations among HN (A and B) and HB fish (C and D). Figures A and B present longitudinal sections, while Figures C and D show transverse sections. MF: myofibrils; MC: myocommata; SR: sarcoplasmic reticulum; IM: intermyofibrillar spaces.

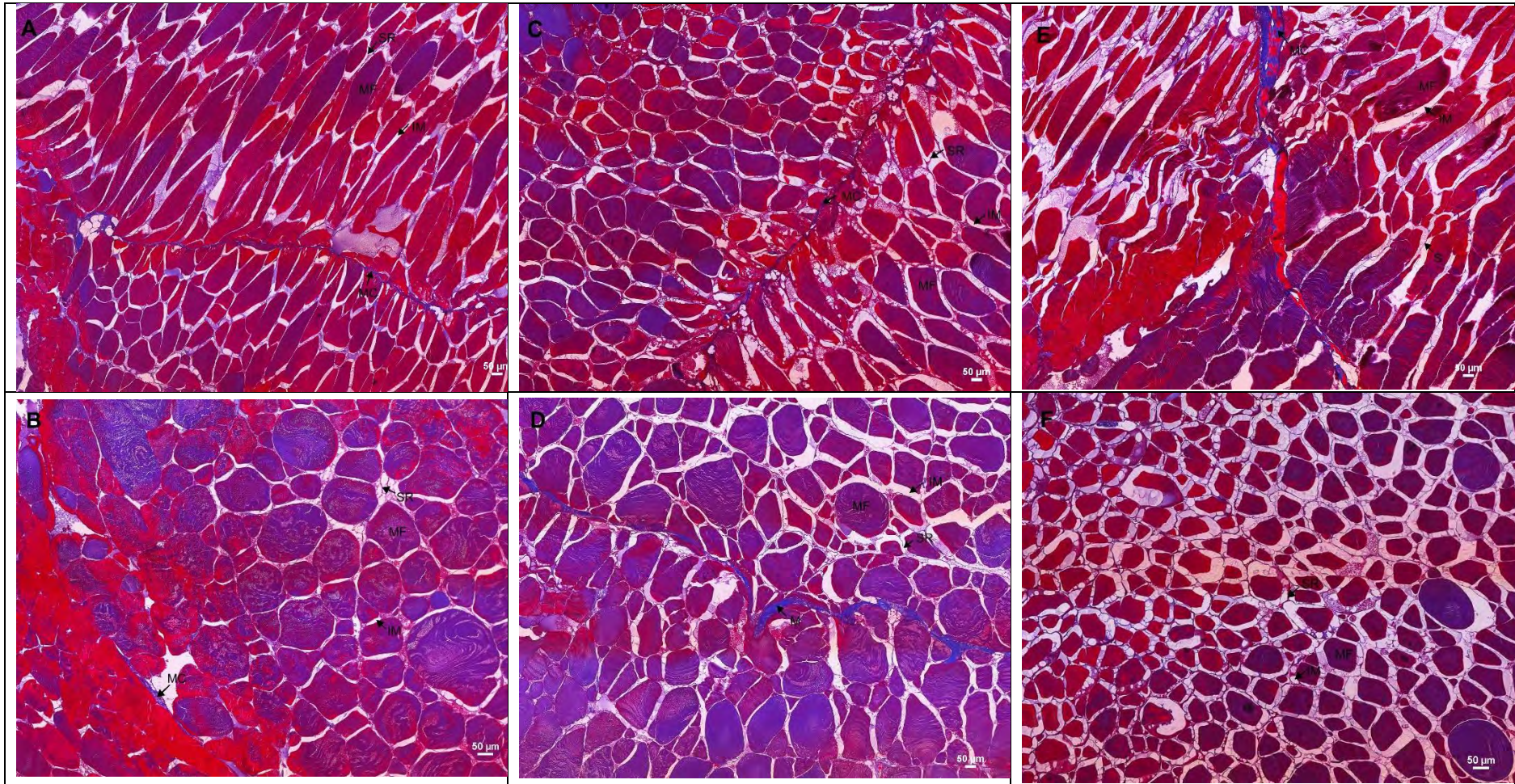


**Fig. 2.51** Histological sections of muscle showing structural variations among HN (A and B) HB fish (C and D) and pale fish (E and F). Figures A, C and E present longitudinal sections, while Figures B, D and F show transverse sections. MF: myofibrils; MC: myocommata; SR: sarcoplasmic reticulum; IM: intermyofibrillar spaces.

#### **2.5.1.3.5 Summary of muscle transcriptomic analysis**

In summary, there were several DEGs between the two muscle regions analysed when comparing HN or HB and pale fish. In the FD region, genes encoding muscle fibre composition protein network were significantly expressed with different levels of gene expression in each phenotype. In HB fish, the degradation of collagen in connective tissue could result in flesh softness while atrophy of muscle fibres might have led to the loss of flesh pigmentation. Because carotenoids bind to muscle proteins in the salmon flesh, we hypothesise that the atrophy of muscle proteins could cause an increase of mobilized carotenoid levels, which are in turn associated with the lipid and fatty acid transport and catabolized in the liver. Lipid and fatty acid metabolism was upregulated in the HB fish, probably to balance the impairment of energy metabolism and feed intake. Hence, their metabolism is possibly involved in the flesh colour depletion.

In the BC muscle region, the qualitative analysis of muscle histology shows that the structure of connective tissue was stable in both phenotypes. Following the transcriptomic analysis, we propose that the high expression of actin alpha skeletal muscle-2 (*Acta2*) and myostatin 1b (*myo1b*) genes in HN and HB fish could play a vital function in the muscle structure and may bind to carotenoids, leading to the distinct flesh colour in Atlantic salmon. Cathepsin L (*Cat1*) might explain reduced flesh pigmentation due to its deleterious effects on actin, a carotenoid-binding muscle protein. Besides, in pale fish genes responsible for the fatty acid metabolism, which leads to fatty acids being released, were upregulated and might be responsible for the shortage in fatty acid used as an energy source when fish were starving. Finally, in pale fish, genes involved in inflammatory responses were upregulated, while in HN and HB fish the up regulated expression of *Hsp70* gene could indicate a protection mechanism from environmental stresses which helps to retain colour.

#### **2.5.1.3.6 Comparison of different phenotypes (HN vs HB vs pale) in the pyloric caeca (PC)**

In the PC, most of the DEGs were upregulated in HN and HB fish compared with the pale fish. These DEGs are involved in the muscle fibre composition protein network, collagens in the extracellular matrix, lipid and fatty acid metabolism, transporters, enzymes, metabolic processes, heat shock proteins, oxidative stress, and inflammatory responses (Appendix 2.3). Among the genes associated with the muscle fibre composition protein network, only troponin C, skeletal muscle-like was upregulated in HB fish while the other genes were upregulated in HN fish. Both actin, aortic smooth muscle and actin, alpha skeletal muscle 2-like were significantly higher in HN fish; these genes are proposed to be involved in muscle contraction and binding to astaxanthin<sup>134</sup>. Alpha-actinin was proposed as an astaxanthin-binding protein in Atlantic salmon, although binding capacity was excluded for being responsible for colour variation<sup>13,134</sup>. Alpha-actinin-1-like (*aactn1l*) was upregulated in HN fish (Fig. 2.52), suggesting that it could play a role in flesh colour.

Regarding lipid and fatty acid metabolism, many genes encoding apolipoproteins (AI, AIV and CI, CII) were upregulated in both HN and HB fish compared with pale fish (Fig. 2.52). Lipoproteins are lipidated protein particles that transport hydrophobic substances in the hydrophilic environment of plasma<sup>271</sup>. The cores of lipoproteins contain hydrophobic molecules such as triglycerides and cholesteryl esters<sup>138,271,290</sup>. It has been proposed that the transport of carotenoids in salmon is similar to the lipid transport with astaxanthin associated together with triglycerides (TG) in lipoprotein spheres called chylomicrons<sup>14,184,260,278</sup>. In the digestive system, absorbed TG together with astaxanthin are transported by chylomicrons to the enterocytes then deposited in peripheral tissues (Fig. 2.53). Combining these previous findings with the upregulation of apolipoprotein genes related to lipid and fatty acid metabolisms found in our study, leads us to hypothesise that in HN and HB fish, the digestive system was maintaining a normal functioning with lipids being continuously metabolised and

deposited to peripheral tissues, possibly explaining better colour in both HN and HB relative to pale fish. To further support this, these apolipoprotein genes were downregulated in pale fish which likely more susceptible to starvation and weight loss, possibly impairing the normal functioning of digestive system as well as lipids and pigments mobilisation and deposition.

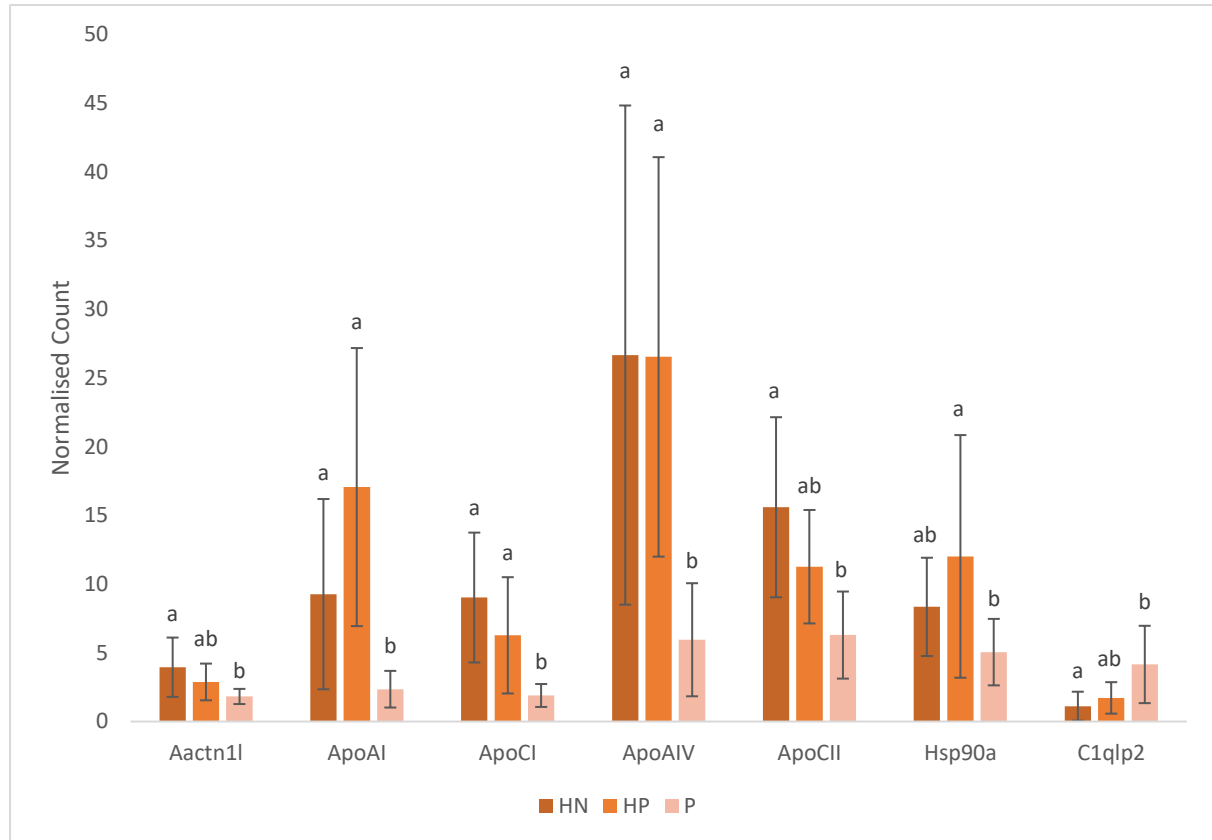


**Fig. 2.52** The expression of important highly expressed genes in the pyloric caeca (PC): HN vs Pale and HB vs Pale. An average normalized count across transcripts is presented. Data is shown as Mean  $\pm$  SE. (n =5). Means with different letters indicate significant differences (P < 0.05).

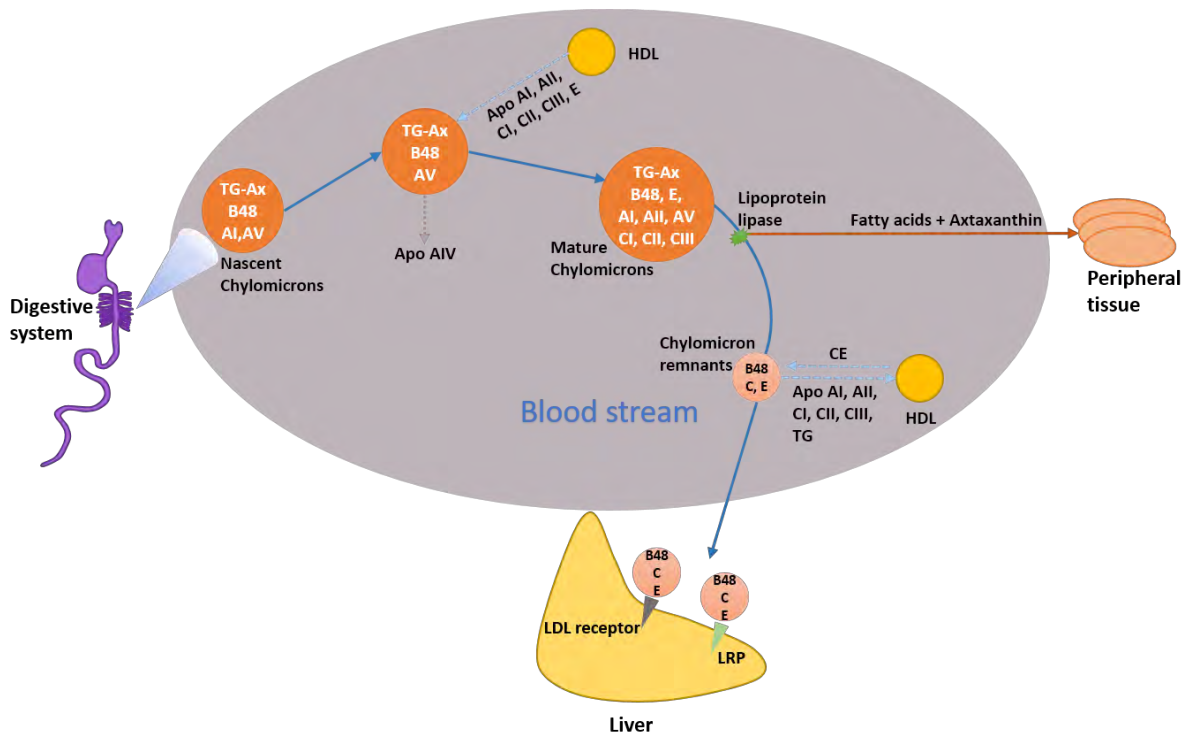


**Fig. 2.53** Apolipoprotein in the transport pathway of lipoprotein metabolism: the chylomicrons (modified from <sup>271</sup>). TG-Ax, triglycerides-Astaxanthin; B48, apolipoprotein B48; AI, apolipoprotein AI; AII, apolipoprotein AII; AIV, apolipoprotein AIV; AV, apolipoprotein AV; CI, apolipoprotein CI; CII, apolipoprotein CII; CIII, apolipoprotein CIII; E, apolipoprotein E; AII, CE, cholesteryl esters; LDL receptor, low-density lipoprotein receptor; LRP, LDL receptor-like protein.

Regarding stress responses in PC, gene expression analysis of the different phenotypes indicated that although exposed to the same environmental conditions, the stress response in HN, HB and pale fish varied. For instance, like Hsp70, HSP 90-alpha-like, a protein protecting the cell from oxidative and thermal stress<sup>291,292</sup> was significantly upregulated in HB fish. At the same time, complement C1q-like protein 2 (C1qlp2) gene relating to the immune system<sup>293,294</sup> was upregulated in pale fish (Fig. 2.52). Besides, most of the genes encoding for enzymes involved in energy and protein metabolism were strongly upregulated in HN and HB fish. The pyloric caeca, a finger-like blind end tube structure is reported to extend the surface area for digestion and absorption<sup>256</sup>. It is also considered as the junction where channels from the liver and pancreas enter, and is proposed to be an important organ for chemical digestion, absorption, osmoregulation, food storage and lipid absorption<sup>257,258</sup>. This could indicate that in pale fish the metabolism is activated and enhanced to respond to the energy requirement of the fish body by maintaining and protecting the cells from environmental stresses. In addition, cytochrome P450 1A was highly expressed in both HN and HB fish (Fig. 2.52). Cytochrome P450 1A (Cyp1a) is a member of the large cytochrome P450 superfamily which serves significant and essential roles in oxidative metabolism<sup>295</sup> and is also a critical catalyst to the activation and detoxification of different xenobiotics<sup>296</sup>. Previous studies found that some carotenoids, such as  $\beta$ -carotene, astaxanthin, canthaxanthin,  $\beta$  apo-8'-carotenal and lycopene could positively affect the activity of cytochrome P450 xenobiotic-metabolising enzymes<sup>297-301</sup>. Nevertheless, the effect of carotenoids on the pyloric caeca cytochrome P450 enzyme family has not been investigated before, and further investigation is required to understand the cytochrome P450 upregulation in our study. All in all, gene expression in the PC of HN and HB fish was higher than in pale fish. The DEGs were mostly involved in muscle fibre protein structure, lipid metabolism, metabolic processes and stress response. Alpha-actinin 1 and apolipoproteins expression could be strongly related to astaxanthin metabolism in fish from our study.

#### **2.5.1.3.7 Validation of DEGs using qPCR**

In order to validate the transcriptomics DEG results, several genes were chosen for analysis of their expression using qPCR: acta2, myo1b, lipase in BC, lepr, apoCl in FD and apoAI, aactn1l in PC. Overall, the trend of gene expression in both transcriptomes and qPCR was similar (Fig. 2.54). The significantly differential expression of acta2, myo1b, lipase, apoCl and apoAI was confirmed. Particularly, acta2, myo1b, apoAI were significantly downregulated in the pale group compared to the HN and HB groups ( $P < 0.05$ ). Interestingly, ApoAI was significantly upregulated in HB fish compared to HN fish ( $P < 0.05$ ), but there is no significant difference between HN and pale fish ( $P > 0.05$ ). In the meantime, the expression of ApoAI in pale fish was significantly downregulated compared to HN and HB fish ( $P < 0.05$ ) in the transcriptome analysis. ApoCl was upregulated in HB fish compared to HN fish in the qPCR assay ( $P < 0.05$ ).

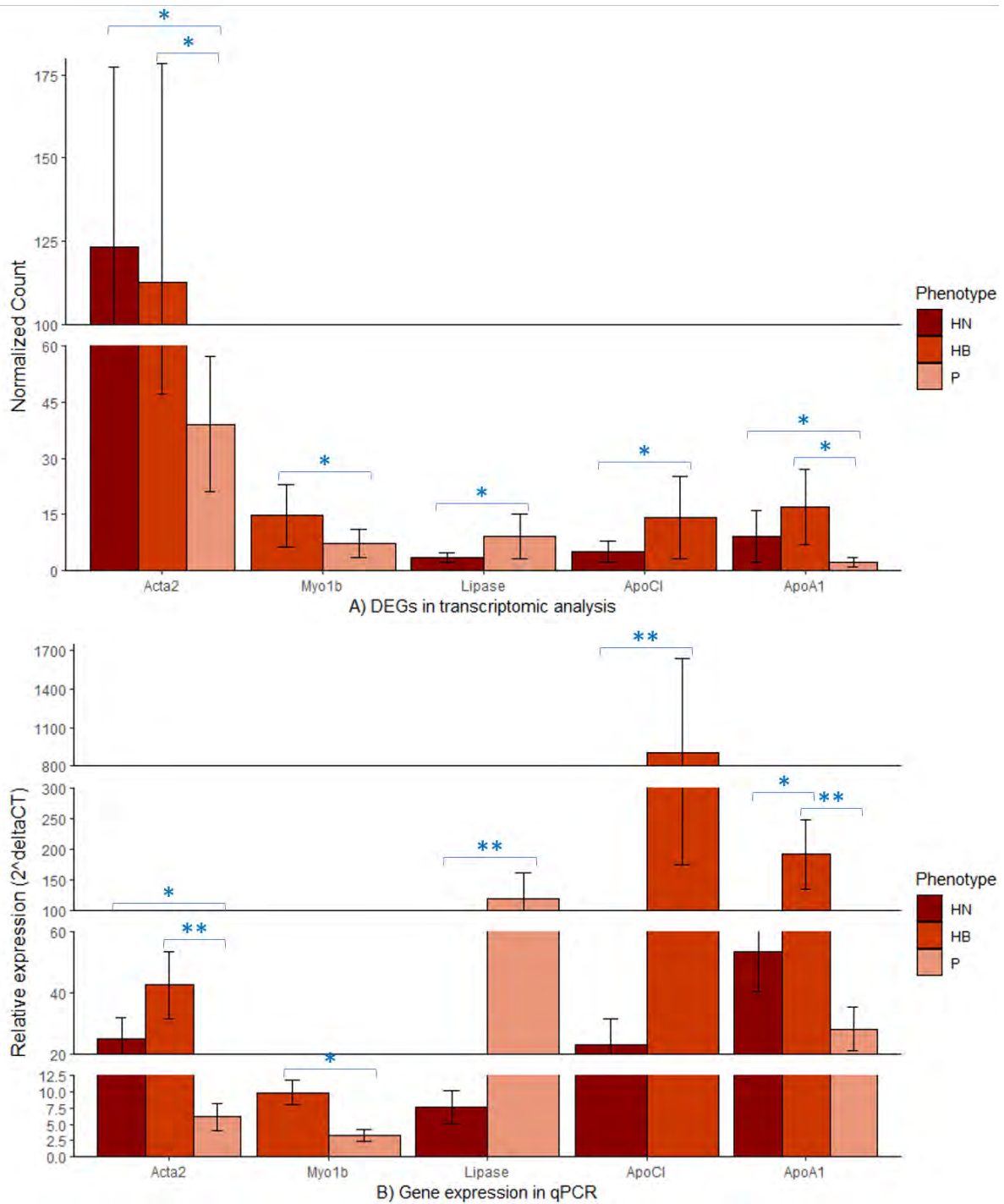


**Fig. 2.54** Some typical DEGs in multiple tissues were validated using qPCR. In back central (BC) region: Acta2, Myo1b and Lipase; in front dorsal (FD) region: Lepr, ApoC1; in pyloric caeca: ApoA1, Aactn1l. The averages significantly different from other ones are highlighted by “\*” ( $P < 0.05$ ) or “\*\*” ( $P < 0.01$ ) symbol.

#### 2.5.1.4 Conclusions

Thermal stress caused by high summer temperatures noticeably affected Atlantic salmon in our study. As a result, starvation is likely to have taken place for a prolonged period of time. Starvation negatively affects to different extent energy metabolism leading to localised colour depletion from the front dorsal (FD) muscle region (i.e. banding) or general discolouration in the whole fillet (paleness). It cannot be excluded that these two phenotypes are actually the same phenomenon manifested with

different severity depending on the individual response. Furthermore, fish subjected to starvation are likely to have increased protein and lipid catabolisms to use them as energy sources in order to compensate nutrient and energy deficiency.

The DEGs in muscle tissues were mainly related to the muscle fibre protein component network, the collagens in the extracellular matrix and carotenoids-binding proteins. At the same time, genes encoding for lipid metabolism functions (apolipoproteins) were significantly upregulated in HN and HB of both muscle tissues and the pyloric caeca. At the gene expression level, it seems likely that flesh pigment depletion is linked to muscle structural integrity and metabolism of protein and lipid. We hypothesise that the proteolytic process in muscle could cause carotenoid-binding proteins to become degraded, and as a consequence lead to the release of free carotenoids which are transported together with lipids as part of the lipid metabolic pathway. We suggest that actin alpha skeletal muscle-2 and myostatin 1b could play an essential function in binding carotenoids and so maintain colour in Atlantic salmon flesh, while Cathepsin L could be involved in carotenoid-binding protein degradation. Based on our results, we can assume that thermal stress is responsible not only for flesh discolouration, but also for loss of muscle texture and integrity.

In future studies, we recommend investigating further carotenoids-binding proteins in Atlantic salmon. Besides, since the function of apolipoproteins in the carotenoid metabolic pathway in Atlantic salmon remains elusive, it is necessary to study the role of apolipoproteins in the absorption, transportation, and metabolism of carotenoids.

### **2.5.2 Investigating the correlation between the metabolism of carotenoids and flesh colour in Atlantic salmon**

The metabolomic pathway of carotenoids is also a major component affecting the variation of flesh colouration in Atlantic salmon. The formation of flesh colour results from the absorption of carotenoids in the digestive system, their transportation, catabolism in liver and finally accumulation in the muscle. Hence, the investigation of carotenoid metabolism using metabolomic analysis in the Atlantic salmon is expected to provide information concerning the carotenoid pathway and explain the role of carotenoids in adapting to the thermal challenge the salmon faces in Tasmania.

Being fat-soluble, the key carotenoid astaxanthin is consumed, transported and delivered via the same pathway as fatty acids in salmon<sup>14</sup>. From the intestine, dietary astaxanthin is passively diffused through the intestinal lumen then transported into the bloodstream before it is deposited in the muscle<sup>139</sup>. Like other xanthophylls, astaxanthin is associated with triacylglycerols (TAGs) in a lipoprotein called chylomicron spheres. The chylomicrons-based astaxanthin are presumed to travel into the intestinal system through the primary blood vessels. While they are hydrolysed by lipoprotein lipases, chylomicrons become small enough to go through the endothelium of the liver where their specific apolipoproteins are recognized by specific receptors<sup>290</sup>.

The availability of astaxanthin metabolites in the biliary excretion of salmon it was previously demonstrated<sup>302</sup>. Although the accurate metabolism of astaxanthin in the salmonids liver has not been cleared, a previous study<sup>303</sup> has identified that the liver has an important role in carotenoid utilisation, especially the catabolism of astaxanthin. Thus, while the muscle is the astaxanthin storage site in salmonid, the liver has some important roles in the catabolism of astaxanthin to the astaxanthin metabolites that they are excreted into the intestinal part and reabsorbed<sup>302,303</sup>. Following that, the intestine is where astaxanthin from the food matrix is absorbed and products of metabolic astaxanthin or remnant astaxanthin are reabsorbed.

In nature, astaxanthin is present in stereoisomers, geometric isomers, free and esterified forms<sup>304</sup>. The majority of carotenoids found in nature are mainly all-trans isomers (E-isomers), while cis isomers

(Z-isomers) are thermodynamically less stable than the trans isomers<sup>304</sup>. Many studies indicated that there was a selective accumulation of E/Z isomers in salmonids tissue and plasma<sup>305,306</sup>. E-astaxanthin tended to retain in muscle and plasma, while Z-astaxanthin preferentially deposited in the liver<sup>305</sup>. Both E and Z-Ast were found in wild and cultured salmon, but only E-Canthaxanthin was detected in cultured salmon<sup>278</sup>. Besides, it was found that the high proportion of all-E-Ast in the Atlantic salmon muscle and plasma (73% and 61-64%, respectively) and proposed that all-E-Ast is likely the preferred Ast for muscle cells<sup>306</sup>.

Hence, the objectives of the present chemical study were to identify the utilization and distribution of dietary carotenoids in farmed Atlantic salmon. In order to examine the presence of carotenoid metabolites, pyloric caeca, gut, liver, muscle and plasma of 20 selected salmon samples, representing different colour phenotypes, were analysed. At first, carotenoids extracting procedures and the running of LC/MS were optimised. A semi-quantitative analysis was then employed, to detect all types of carotenoids and to identify which ones are present in Atlantic salmon. Subsequently, a quantitative analysis was conducted to determine the concentration of carotenoids in each tissue. The presence of different carotenoids in individuals presenting different flesh colour phenotypes is described.

### **2.5.2.1 Materials and methods**

#### **2.5.2.1.1 Standards and chemicals**

All-trans-Astaxanthin (E-Ast), trans-canthaxanthin (E-Can) and trans- $\beta$ -Apo-8'-carotenal (E-Apo) standards were purchased from Sigma-Aldrich Inc. (St. Louis, Missouri, United States). E-Apo was used as the internal standard. Methanol (MeOH), acetonitrile (ACN), water and formic acid (FA) of LC-MS grade, dichloromethane (DCM) of HPLC grade, Methanol of HPLC grade and butylated hydroxytoluene (BHT) were purchased from Merck Group (Darmstadt, Germany).

#### **2.5.2.1.2 Tissue and blood sample collection**

The sampling protocol was conducted following the method described in<sup>306</sup>. The sampling took place during the same event described in section 2.5.1.2. Briefly, blood samples were collected intracardially from 100 fish randomly chosen using labelled Li-heparinized vacuum sampling tubes immediately after delivering a non-recoverable blow to the head by using an electric stunner. Blood samples were stored on ice for less than 30 min before being centrifuged (1700 x g for 10 min) followed by plasma collection. After blood collection, fish were dissected to expose their viscera. The whole liver and intestine were collected and packed separately. The right fillet of each fish was filleted and the flesh score, as well as banding indexes evaluated before the muscle and skin, were detached for sampling. The measurement of flesh colour assessment is described in section 3.2.3.

Finally, plasma, two sections of muscle (BC and FD regions of interest), liver, pyloric caeca and hindgut from 20 individuals were chosen from the 100 individuals based on the colour type and the presence of banding. These 20 fish were then classified into four groups of colour type: high colour - no banding (HN), high colour - banded, low colour - banded and pale (n = 5 per group). All biological samples of the four groups were kept in -80°C freezer in darkness until analysis at the USC laboratory.

#### **2.5.2.1.3 Carotenoid extraction**

For carotenoid analysis, frozen samples were cut into small pieces, then 1 gram of each sample was homogenized completely. The plasma samples were thawed at room temperature.

The procedure of carotenoid extraction was conducted as described previously<sup>307,308</sup> with several modifications for the metabolomic analysis. The extracting solvent was a mixture of MeOH (containing 500 ppm BHT) and DCM with the ratio 1:3. One gram of the muscle, liver and intestine samples were

weighed accurately, then homogenized with the extracting solvent at a ratio of 1:4 for 30 seconds. After resting for 10 minutes, the homogenized solution was centrifuged for 10 minutes at 1700 x g. The plasma sample (1.0 mL) was mixed with the extracting solvent at a ratio of 1:4 and the process of extraction above was repeated. The supernatant was collected into a new tube then the procedure was repeated. After drying the solution using a GeneVac EZ-2 (SP Scientific, Warminster, United States), the extract was dissolved in MeOH-DCM (50:50, v/v). Then, the extract was filtered through a 0.22 µm membrane filter and 10 µL was used for HPLC analysis. trans-β-Apo-8'-carotenal was added to the filtered extract to get the final concentration at 100 µg/L before analysis.

#### 2.5.2.1.4 Preparing a standard solution

E-Ast and E-Can standards were dissolved in MeOH-DCM (50:50, v/v) at a concentration of 0.05 mg/mL. A serial dilution of the standards was prepared from  $12.5 \times 10^{-3}$  to 125 µg/L with 9 dilution steps (one order of magnitude apart). The internal standard E-Apo was also added to both the above standards and the analyzed extracts using the same final concentration of at 100 µg/L.

#### 2.5.2.1.5 Application of LC-MS using uHPLC/QTOF-MS (SCIEX X500R) for the analysis of carotenoid metabolites

Separation and semi-quantification of carotenoids were performed using a SCIEX ExionLC™ AC system coupled to Sciex 500R quadrupole time-of-flight mass spectrometer, provided with electrospray ionization source (ESI) conducted in the positive-ion mode. The chromatographic separation was extracted on an Agilent Zorbax RRHD Eclipse Plus C18 column (2.1x100 mm, 1.8 µm 1000 bar pressure limit) and Agilent Zorbax UHPLC Guard Eclipse Plus column, (2.1 mm, 1.8 µm column). The mobile phases were solvent A containing 0.1% formic acid MeOH:ACN:DCM (90:5:5, v/v/v) and solvent B water containing 0.1% formic acid. The column temperature was kept at 40°C and the flow rate was 0.5 mL/min. The gradient profile is described in Table 2.11. A volume of 5 µL was injected into the chromatogram system.

**Table 2.11** The LC gradient conditions used for the separation of carotenoids

Step	Time (min)	A (%)	B (%)
0	0.0	15	85
1	8.0	0	100
2	11.5	0	100
3	12.0	15	85
4	15.0	15	85

In order to acquire the mass spectrometer (MS) analyses of carotenoids profile, the MS parameters were set as follows: the MS scan time was 0.1 sec (100 – 1500 m/z), and each MS-MS scan was 50 – 1500 m/z. The source parameters were as follows: source temperature, 350°C; ion spray voltage, 4500 V; gas 1, 35 psi; gas 2, 45 psi; curtain gas (N<sub>2</sub>), 25; and collisionally activated dissociation (CAD) gas, 7. Sciex OS software version 1.2 was used for data analysis. E-Ast and E-Can were detected based on the retention time of the standards, the mass spectrometry (597.3938 m/z and 565.4045 m/z, respectively) with the mass error < 5 ppm and the mass resolution information from TOF-MS (time-of-flight mass spectrometry) and TOF-MS/MS (time-of-flight mass spectrometry/mass spectrometry) acquired data (Fig. 2.55). For other Ast isomers, Can isomers and carotenoids, the mass spectrometry, the TOF-MS and MS/MS data of each compound were processed and searched against mass libraries,

including the isotope and MS/MS matching in the formula finding algorithm with sufficient mass accuracy (within 5 ppm) in SCIEX OS v1.7 software (SCIEX, USA).

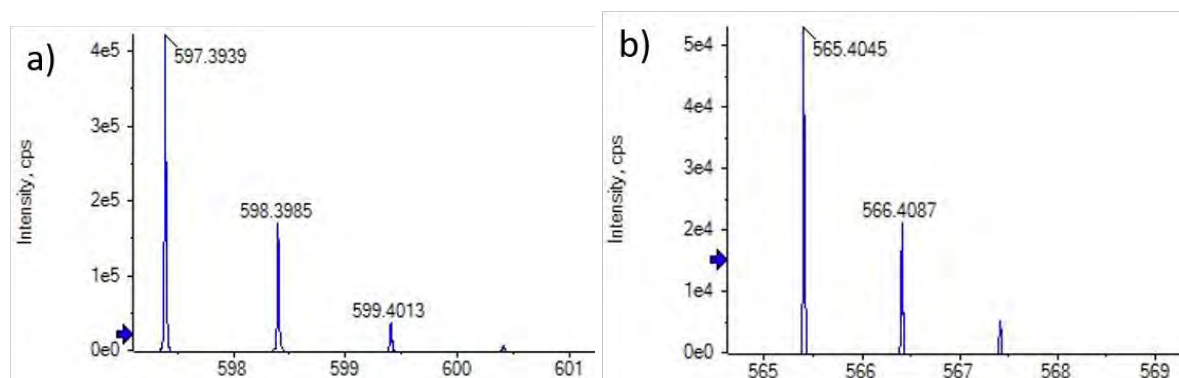


Fig. 2.55 The TOF-MS fragment ions of all-trans-Astaxanthin (a) and trans-Canthaxanthin (b) standards

### 2.5.2.1.6 LC-MS system with DAD-uHPLC/QQQ-MS (6470 Agilent Technologies) for the quantification of E-Ast/Can

UHPLC/MS/MS analysis was performed using DAD-uHPLC/QQQ-MS platform (diode array detection-Agilent uHPLC 1290/Agilent 6470 Triple Quadrupole LC/MS, Agilent Technologies USA) equipped with an Agilent RRHD Eclipse Plus C18 (1.8  $\mu$ m, 2.1 x 50 mm) column and Agilent UHPLC Guard Eclipse Plus C18 (1.8  $\mu$ m, 2.1 mm) guard column. The column temperature was kept at 40°C. A volume of 5  $\mu$ L was injected into the chromatographic system. The flow rate was set at 0.5 mL/min. Mobile phase were (A) water (containing 0.1% formic acid); (B) 0.1% formic acid MeOH:ACN:DCM (90:5:5, v/v/v). Initially, the gradient was set at 20% A and 80% B and kept in 0.5 min, which was linearly changed to 0% A and 100% B in 6.0 min then maintained in 5.5 min, followed by a further increase to 20% A in the next 0.5 min. Finally, the initial conditions were recovered and maintained for 2.5 min for column conditioning and the total run time was 15 min per sample.

For MS/MS analysis, the mass spectrometry was conducted in the positive mode and multiple reaction monitoring (MRM) mode is applied for E-Ast and E-Can, the target compounds. Detailed MS parameters were as follows: capillary voltage 5000 V, drying gas flow: 5.0 L/min, drying gas temperature: 200°C, nebulizer: 30 psi, nozzle voltage: 500 V, sheath gas flow: 12 L/min, sheath gas temperature: 400°C. MS data of E-Ast (precursor ion: 597.4 m/z), E-Can (precursor ion: 565.4 m/z) and  $\beta$ -Apo-carotenal (precursor ion: 417.3) were acquired using their retention time and product ions. The retention time, quantifier, qualifier product ions of E-Ast, E-Can and E-Apo are 3.500 min, 173.1 (collision energy (CE) 25), 147.1 (CE 25), 5.750 min, 203.1 (CE 17), 133.0 (CE 30) and 5.658 min 119.1 (CE 29), 109.1 (CE 25), respectively. E-Ast, E-Can and E-Apo were analysed not only based on the precursor ion (m/z) and product ion (m/z) but also monitored with UV-vis spectra at 480 nm.

## 2.5.2.2 Results

### 2.5.2.2.1 Quantification of all trans-astaxanthin and trans-canthaxanthin in multiple tissues and comparison of different flesh colour phenotypes

From the serial dilution of the standards, the standard curves of E-Ast and E-Can were built using the LC-MS system with DAD-uHPLC/QQQ-MS (6470 Agilent Technologies) (Fig. 2.56). Also, the limit of detection (LOD) and limit of quantification (LOQ) were determined for every standard. LOD and LOQ values of E-Ast and E-Can were  $12.5 \times 10^{-3}$  and  $25 \times 10^{-3}$   $\mu$ g/L, respectively.

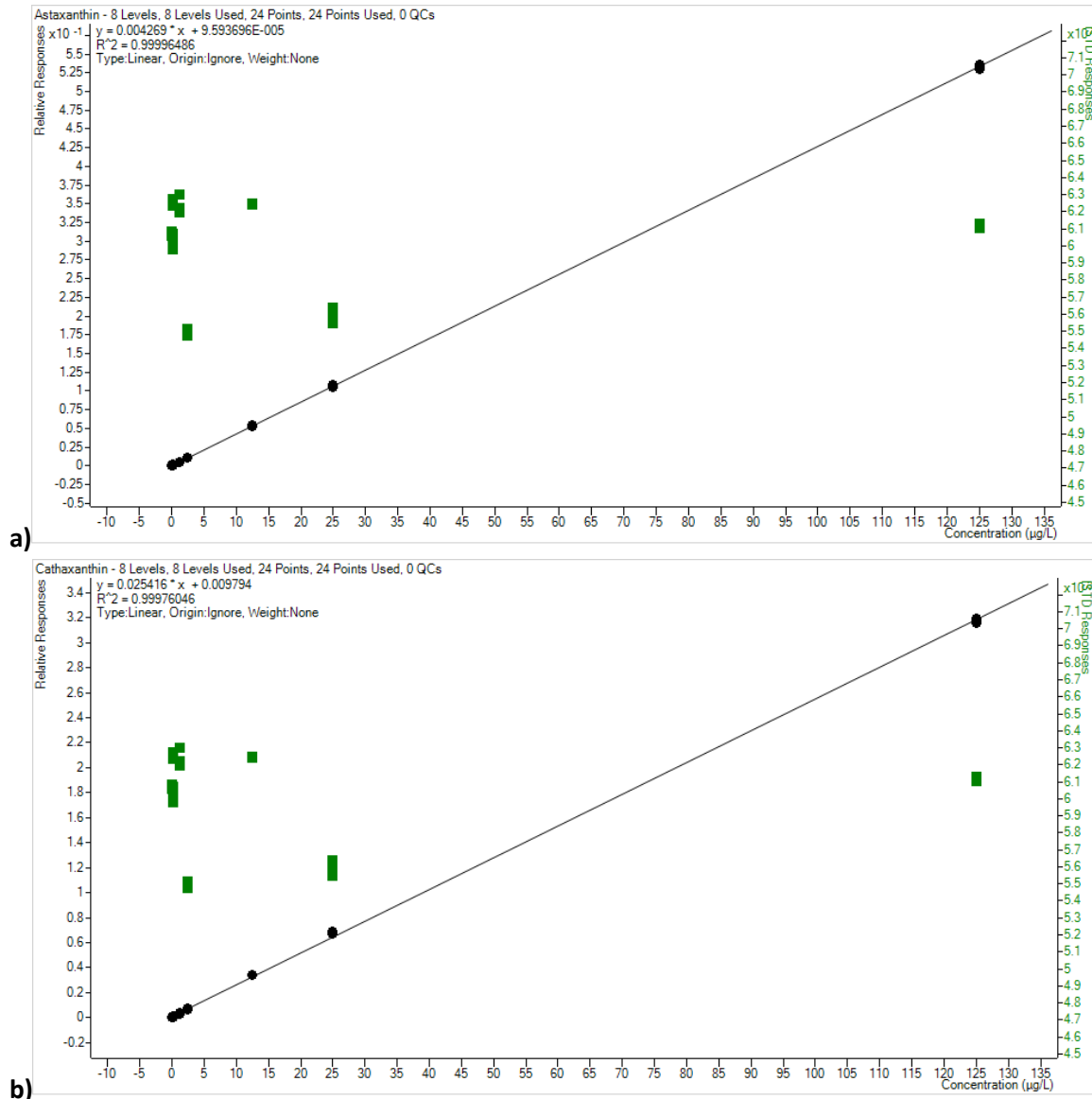


**Fig. 2.56** The standard curve for quantification using LC-MS/QQQ. a) astaxanthin; b) canthaxanthin. The black dots represent the standard values (E\_Ast or E-Can) while green dots stand for the internal standard (E-Apo).

In general, E-Ast and E-Can levels were the most abundant in BC region and HN group, in agreement with the highest flesh colour in the muscle region and in this group. Moreover, the overall highest carotenoid values were always highest in the HN group in all tissues tested (Table 2.12). The concentration of E-Ast was higher than E-Can in muscle, plasma, pyloric and hindgut. In contrast, the E-Can content was near double of E-Ast content in the liver. No significant difference ( $P > 0.05$ ) of E-Ast and E-Can were found in most analysed tissues between different low colour phenotypes (LB and pale fish). Only in the BC region, the E-Ast concentration in LB fish was significantly higher than in pale fish ( $P < 0.05$ ). In most of the tissues, the concentration of E-Ast and E-Can in HN fish was significantly higher ( $P < 0.05$ ) than that in HB, LB and pale fish, while the E-Ast in HN plasma and liver was not significantly different compared to HB fish ( $P > 0.05$ ).

In the plasma and liver, the HN group had significantly higher ( $P < 0.05$ ) concentration of E-Ast and E-Can compared to most of the other groups. The E-Ast and E-Can concentrations in LB and pale groups were not significantly different ( $P > 0.05$ ). E-Ast in the HB group was also higher than LB and pale group

( $P < 0.05$ ) while plasma E-Can in HB was significantly different to the other groups (HN, HB and pale group;  $P < 0.05$ ).

In FD muscle region and PC, the variation of E-Ast was the same as E-Can between the four flesh colour phenotypes. In FD region, the E-Ast and E-Can was highest in HN group ( $P < 0.05$ ) compared to other groups. There were also significant differences in E-Ast and E-Can between HB and paler groups (LB and pale;  $P < 0.05$ ), while these compounds were not different between LB and pale group. At the same time, only E-Ast and E-Can in HN fish was significantly different compared to the other groups ( $P < 0.05$ ).

In the BC region and hindgut, the E-Can in HN and HB fish was highest compared to other groups ( $P < 0.05$ ), while LB and pale fish were not significantly different ( $P > 0.05$ ). Regarding E-Ast concentration, there was no difference between HB and LB fish ( $P > 0.05$ ) but both had significantly higher concentration than pale fish ( $P < 0.05$ ). The result of the quantitative analysis is presented in Table 2.12.

**Table 2.12** Quantitative analysis of the concentration of all-trans-astaxanthin and trans-canthaxanthin in multiple tissues in comparisons of different flesh colour phenotypes using LC/QQQ-MS system.

Phenotype	Plasma (P)	BC muscle region	FD muscle region	Pyloric caeca (PC)	Hindgut (HG)	Liver (L)
<b>Astaxanthin (mg/L or mg/Kg)</b>						
HighNone	2.016 ± 0.117 <sup>a</sup>	3.492 ± 0.585 <sup>a</sup>	2.837 ± 0.374 <sup>a</sup>	2.620 ± 0.465 <sup>a</sup>	1.722 ± 0.159 <sup>a</sup>	0.752 ± 0.148 <sup>a</sup>
HighBanded	1.805 ± 0.247 <sup>a</sup>	2.234 ± 0.275 <sup>b</sup>	0.890 ± 0.108 <sup>b</sup>	0.385 ± 0.110 <sup>b</sup>	0.765 ± 0.104 <sup>b</sup>	0.580 ± 0.074 <sup>a</sup>
LowBanded	0.904 ± 0.346 <sup>b</sup>	1.623 ± 0.605 <sup>b</sup>	0.491 ± 0.121 <sup>c</sup>	0.290 ± 0.184 <sup>b</sup>	0.481 ± 0.142 <sup>c</sup>	0.278 ± 0.133 <sup>b</sup>
Pale	0.658 ± 0.205 <sup>b</sup>	0.989 ± 0.496 <sup>c</sup>	0.474 ± 0.131 <sup>c</sup>	0.252 ± 0.083 <sup>b</sup>	0.432 ± 0.006 <sup>c</sup>	0.310 ± 0.158 <sup>b</sup>
<b>Canthaxanthin (mg/L or mg/Kg)</b>						
HighNone	1.116 ± 0.078 <sup>a</sup>	1.351 ± 0.330 <sup>a</sup>	0.867 ± 0.176 <sup>a</sup>	0.679 ± 0.201 <sup>a</sup>	0.940 ± 0.312 <sup>a</sup>	1.748 ± 0.303 <sup>a</sup>
HighBanded	0.769 ± 0.198 <sup>b</sup>	0.909 ± 0.153 <sup>b</sup>	0.419 ± 0.104 <sup>b</sup>	0.097 ± 0.035 <sup>b</sup>	0.384 ± 0.099 <sup>b</sup>	1.138 ± 0.348 <sup>b</sup>
LowBanded	0.116 ± 0.048 <sup>c</sup>	0.536 ± 0.143 <sup>c</sup>	0.178 ± 0.017 <sup>c</sup>	0.021 ± 0.005 <sup>b</sup>	0.112 ± 0.015 <sup>c</sup>	0.401 ± 0.075 <sup>c</sup>
Pale	0.085 ± 0.026 <sup>c</sup>	0.400 ± 0.175 <sup>c</sup>	0.110 ± 0.033 <sup>c</sup>	0.032 ± 0.011 <sup>b</sup>	0.081 ± 0.006 <sup>c</sup>	0.566 ± 0.324 <sup>c</sup>

Data are presented as mean ± SD (n = 5). Data with different superscript letters in one column of each compound (Astaxanthin or Canthaxanthin) represent a significant difference between four flesh colour phenotype ( $P < 0.05$ ). HighNone, High colour-No banding fish; HighBanded, High colour-Banded fish; LowBanded, Low colour-banded fish; Pale, Pale fish. Significant differences determined by one-way ANOVA.

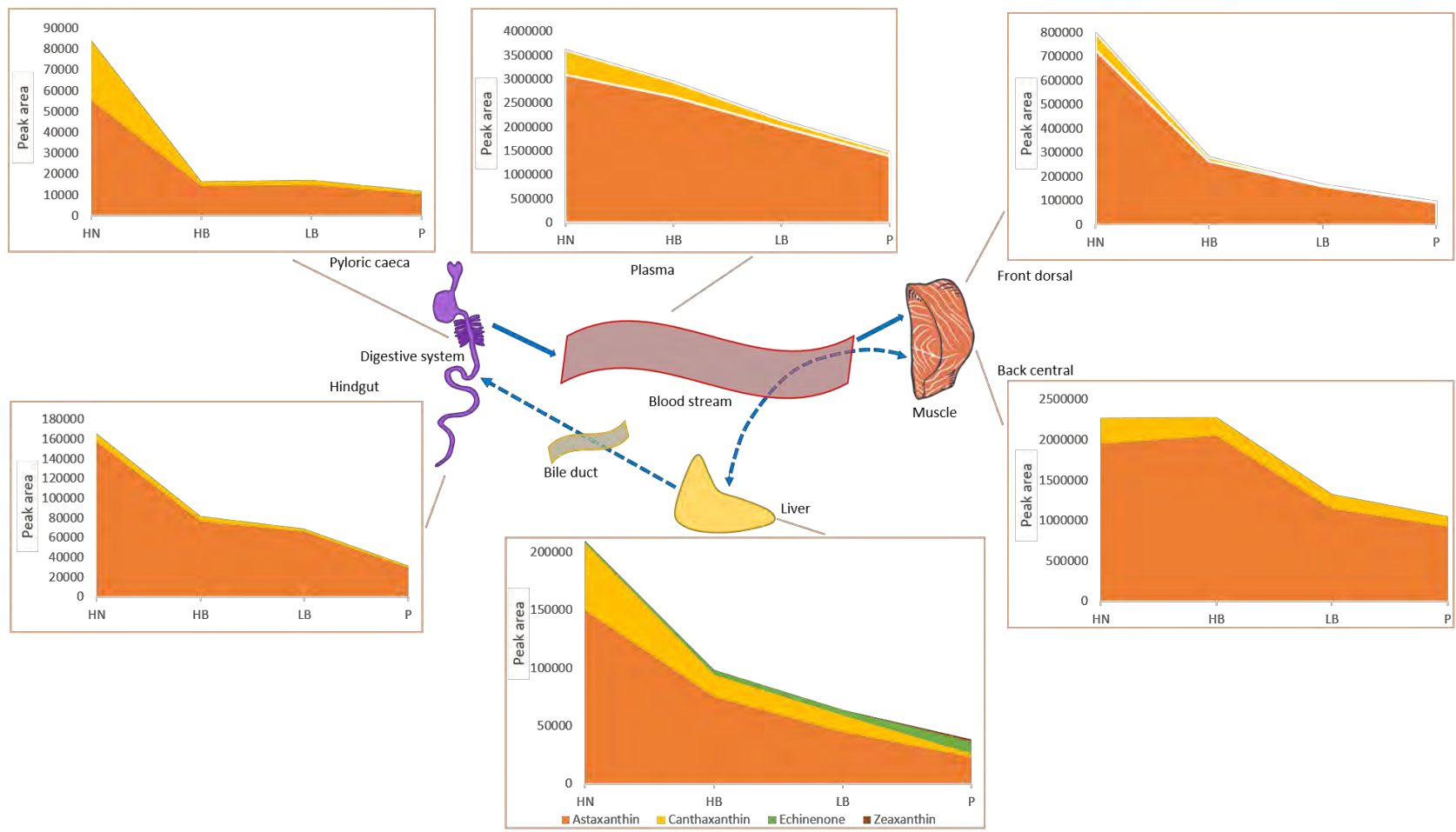


**Fig. 2.57** The predicted pathway and semi-quantitative analysis of astaxanthin, canthaxanthin and their metabolites in multiple organs of Atlantic salmon

#### **2.5.2.2.2 Determination of astaxanthin and canthaxanthin metabolites in multiple tissues in comparison of different flesh colour phenotypes**

The presence and relative concentration of astaxanthin (Ast) and canthaxanthin (Can) metabolites are reported in Fig. 2.57. Based on the retention time and TOF-MS result, Ast had several isomers detected at 3.69 and 4.94 min with the first two peaks overlapping. The isomers of Can were identified at 6.36, 6.48 and 6.95 min. Total Ast and Can were semi-quantified concurrently, and total Ast was higher than total Can in all tissues and plasma. Total Ast content was the highest in plasma (P), then decreasing following the order: back central (BC) > front dorsal (FD) > hindgut (HG) > liver (L) > pyloric caeca (PC). At the same time, total Can intensity declined following the the order: P > BC > FD > L > PC > HG. Total Ast content was much higher than Can, and total Can content was dramatically reduced in groups affected by flesh colour depletion.

In the liver, while total Ast concentration was higher than total Can concentration, E-Ast was lower than E-Can (Table 2.12). Echinenone (Ech) isomers, the canthaxanthin metabolites were only found in the liver with the retention time at 9.65 and 10.38 min. The Ech content significantly increased from HN to pale fish, in contrast with the reduction in total Can. Zeaxanthin (Zea) isomers, the astaxanthin metabolites were only detected in the liver of pale fish at the retention time of 9.78 and 10.28 min with very low concentration.

#### **2.5.2.3 Discussion**

##### **2.5.2.3.1 The usage of E-Ast/E-Can and total Ast/Can in farmed Atlantic salmon**

In Atlantic salmon aquaculture, both Ast and Can are supplied in the diet to give the unique natural flesh colour. In nature, Ast consists of many different *trans* and *cis* (E and Z) geometrical isomers, with all-trans being the dominant isomer<sup>309</sup>. Some studies indicated that the accumulation of E/Z isomer is selective in salmon tissue and plasma. All-E-Ast is retained selectively in muscle and plasma, while Z-Ast isomer was present in the liver<sup>305,310</sup>. A positive correlation between the dietary E-Ast and the redness of flesh colour in rainbow trout has been previously found<sup>308</sup>. In our present study, there was a difference in the proportion of E-Ast and total Ast between various tissues and plasma. There was approximately 50% of total Ast in plasma, followed by 31-40% and 3-11% in BC and FD, respectively. All-E-Ast mainly accumulated in BC, FD and plasma, with levels of 25-40%, 12-21% and 15-27% respectively. Therefore, we suggest that there are Z-Ast isomers in Atlantic salmon. Following that, deposition of E-Ast was prioritised in muscle, while *cis*-Ast isomers which were not deposited in muscle were transported in the blood stream. The distribution of E-Can in plasma, BC and FD and total-Can was similar to that of all-E-Ast and total-Ast (Fig. 2.58). However, the large proportion of E-Can in the liver indicated that a high amount of E-Can was catabolized there (in range of 26 to 44%), regardless of the flesh colour phenotype. Hence, we hypothesise that mainly E-Ast contributes to flesh colour formation in Atlantic salmon while E-Can might play another function in the body rather than solely participate to pigmentation of the flesh.

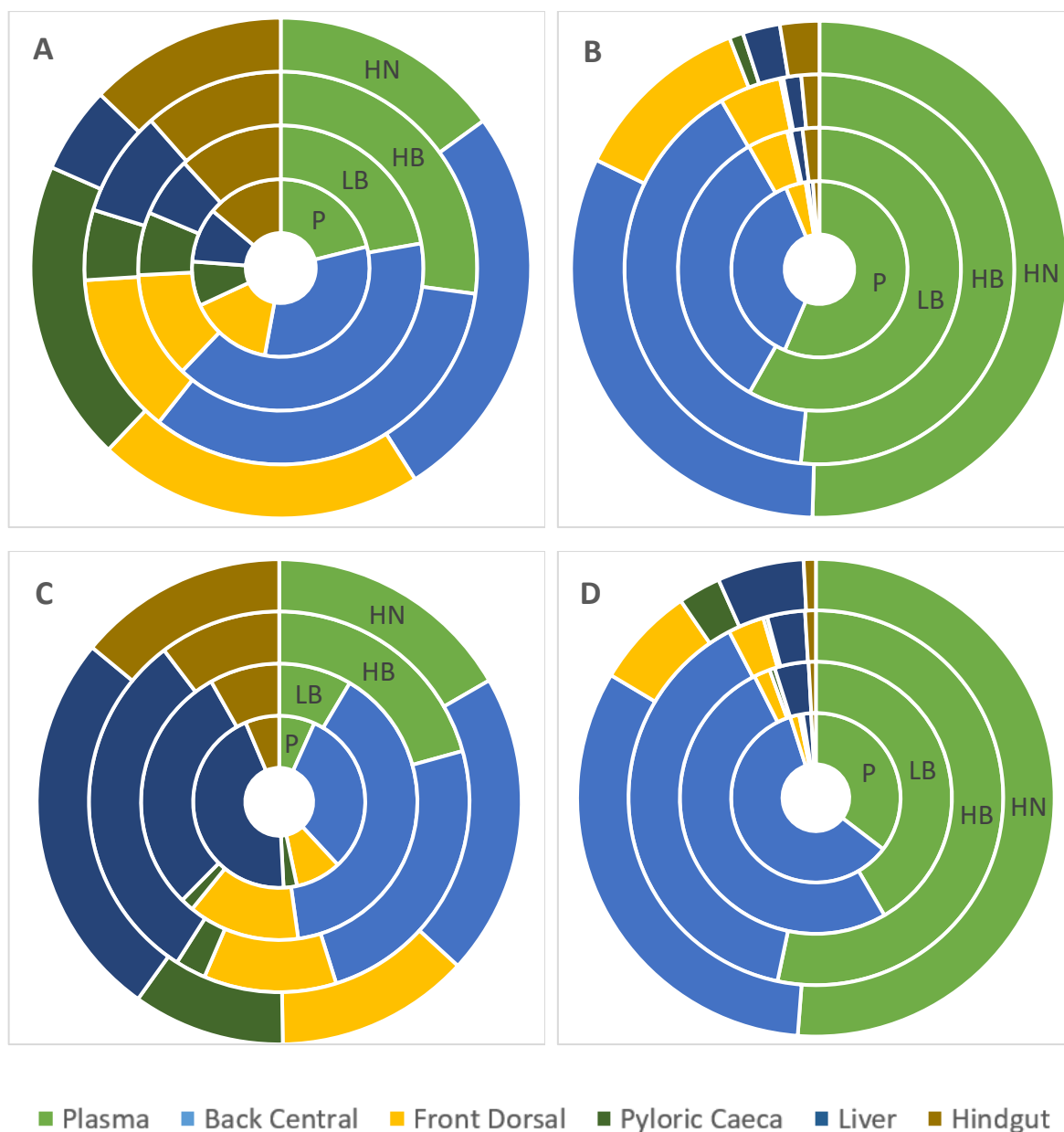


**Fig. 2.58** Comparisons between the proportion of E-Ast/E-Can and total Ast/Can in different flesh colour phenotypes and multiple tissues. A) The proportion of E-Ast; B) The proportion of total Ast; C) The proportion of E-Can; D) The proportion of total Can.

### 2.5.2.3.2 A hypothesized carotenoid metabolic pathway in Atlantic salmon

Following previous studies, the circulating pathway of carotenoids was illustrated as part of Fig. 2.57<sup>14,184</sup>. In our present study, the semi-quantitative analysis using the LC/MS-QTOF method indicated that Ast and Can were the most abundant carotenoids in farmed Atlantic salmon. However other carotenoids compounds were also identified and semi-quantified in different tissues: Echinenone (Ech) and Zeaxanthin (Zea) isomers were found in the liver. The liver is the main catabolic organ for carotenoids<sup>302,311</sup> and is considered to responsible for the loss of astaxanthin through catabolism<sup>303</sup>. As a catabolic hub, Ast and Can can be catabolized then converted to other carotenoid products. These presumed metabolic pathways are in agreement with the findings of Ech and Zea isomers in the

present study. Hence, we propose a pathway of carotenoid absorption, transport, deposition and metabolism in farmed Atlantic salmon. In general, uptake of Ast/Can from pyloric caeca is considered to associate with lipid transport and to circulate through the blood stream then deposited in peripheral tissues (muscle, skin, gonads)<sup>14</sup>. For the catabolism, Ast and Can could be transferred from the intestine or muscle to the liver, where they are transformed to Ast/Can metabolites. After that, both Ast/Can and Ast/Can metabolites can be secreted in the bile and then into the intestine where they might be reabsorbed.

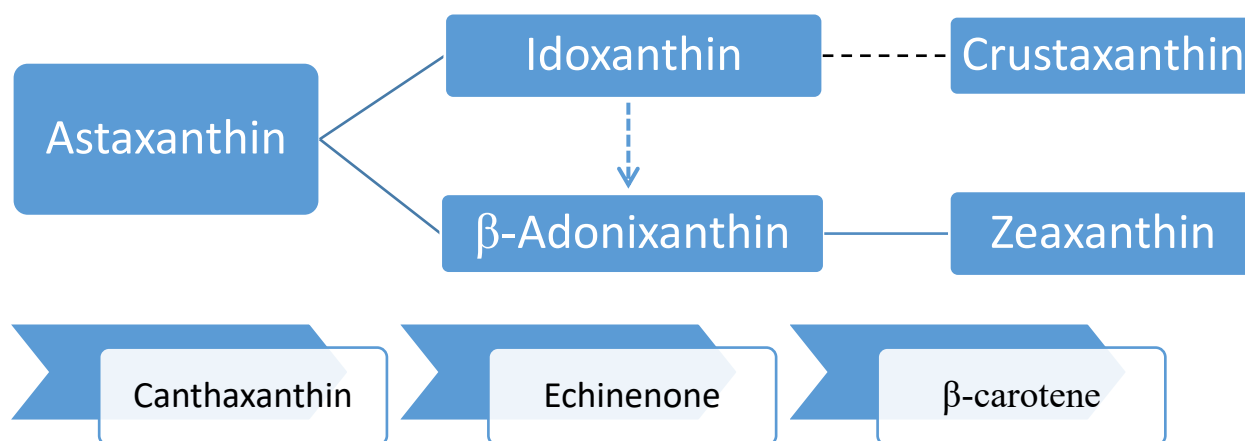


Fig. 2.59 The hypothesised metabolic conversion of Astaxanthin and Canthaxanthin from<sup>312</sup>

As some previous studies report, the metabolic pathway of Ast and Can is described in Fig. 2.59<sup>312-315</sup>. Zea was described as an Ast metabolite<sup>316</sup>. Although neither idoxanthin and  $\beta$ -adonixanthin could be found in our study, we hypothesize that there should be a transformation from Ast to Ast intermediate metabolites then Zea in the liver. In the same way as Ast metabolite, Ech isomers, Can metabolite was only detected in the liver. The Ech intensity was gradually increased from HN, HB, LB to pale fish. Because Zea and Ech were only found in the liver in small quantity, we propose that the Ast/Can catabolism occurs mainly in the liver. In other tissues and body fluids, this process might not exist or operates at a low level. Although the mechanism of Ast/Can catabolism still needs to be further investigated, there was a negative correlation of the Ast/Can conversion to Zea/Can and the flesh pigment depletion. In Atlantic salmon, beta-carotene oxygenase 1 (bco1) and beta-carotene oxygenase 1 like (bco1l) were 15,15' carotenoid oxygenases which related to pigment cleavage<sup>186</sup>. The upregulation of these genes was positively correlated with flesh colour depletion<sup>179</sup>. Hence, it is hypothesized that bco1 and bco1l could join in the catabolism of Ast and Can. Pale fish represent individuals starving due to thermal stress, so they had to use their energy storage to maintain several biological body activities. Only in pale fish, Zea was present at low levels in the liver, suggesting that the metabolism of Ast to Zea might be activated only in pale fish. A small amount of E-Ast converted to Zea was recorded in Atlantic salmon liver before<sup>316</sup>. Hence, we propose an E-Ast compensation in which E-Ast is transported from muscle to liver where it is catabolised and then converted into Zea. However, the function of this Ast metabolism remains unknown.

It has been found that the ratio of Ast/Idoxanthin (Ido) to be 2:1 in the Atlantic salmon flesh and the presence of Ido was also recorded in PC and ovary of 1.5 years-old salmon<sup>316</sup>. In our present study, neither Ido and  $\beta$ -adonixanthin were detected in the analysed tissues and plasma. Some recent studies

also could not detect Ido in Atlantic salmon <sup>37</sup>. It has been indicated that Ido apparently accumulates at a significantly high level of 30% of total carotenoids in the muscle of pre-adult Atlantic salmon <sup>317</sup>. Therefore, Ido concentration could be low in larger fish (2 years-old in our study). Regarding Zea isomers, our method could not accurately identify these isomers, since lutein, zeaxanthin and isozeaxanthin have the same molecule formula and molecular weight ( $C_{40}H_{56}O_2$ , 568.99 g/mol), which requires their standard to confirm based on the retention time. In the grow-out phase, a mixture of Ast and Can was supplied in the Atlantic salmon diet at 75-80 ppm to reach a beautiful, natural flesh colour; nevertheless, the present chemical analysis indicated that the Can might not contribute to the flesh colouration to the same extent as Ast, due to a higher proportion of Can found to be catabolized in the liver.

#### **2.5.2.4 Conclusions**

In this study, the analysis of carotenoid metabolites in Atlantic salmon shows that E-Ast has a key role in forming the unique colour in fish muscle. Thermal stress affects the distribution of carotenoids in muscle and other organs and plasma in fish body. The analysis suggests that perhaps Can is not incorporated in the flesh and hence perhaps is not required in the feed supplement at this life stage to the same extent as Ast, or that Can is preferentially catabolized in the current environmental conditions.

In further research, there are still several unclear matters that need to be clarified. From the confirmed semi-quantitative results, the existence of additional carotenoids was detected. The present Atlantic salmon diets may include the mixture of different Ast and Can isomers, while the result of chemical analysis indicated that it is likely only E-Ast correlate well with flesh colour. Hence, investigation of the efficiency of E-Ast, E-Can, total Ast and Can on the Atlantic salmon flesh colour is warranted. It will confirm the value of each carotenoid supplement to the salmon flesh colouration.

## Section 3

### **Aim 3: Establish if there is a correlation between genetic background and reduced flesh colour**

#### **3.1 Background and trial design**

This trial focused on an additional aspect concerning flesh colour loss which has not been investigated yet. Originally, the main aim of this trial was to assess whether there is a genetic component underlying flesh colour loss post-summer displayed by part of the stock. In fact, although it is well established that flesh colour is a heritable trait in Atlantic salmon, what remains elusive is if colour loss (i.e. general paleness or banding) and/or recovery from thermal stress, has a genetic component as well. The coexistence of good flesh colour or pale/banded fish post summer, after being grown in the same conditions and from the same population, suggests that genetics may play a key role in the issue.

During the final year of the project, the need for a one-year extension became evident in order to complete this trial. At the same time, Petuna's interest in the project had further grown and it was realised that there was an opportunity to utilise the above trial population for the establishment of a genetic improvement program. This led to the addition of three samplings and assessments in order to obtain a complete picture of the genetic effect on performance of Petuna stocks.

- A summer mortality DNA sampling and assessment
- A post-summer performance and colour assessment with DNA sampling
- A harvest performance and final colour assessment with DNA sampling

During the May 2017 spawning, the investigator at Petuna produced crosses (families, Fig. 3.1) from neomale (sex-reversed female) and female Atlantic salmon broodstock. The aim was to obtain an all-female population large enough (at least 150,000 fish at smolt stage) to be allocated to two dedicated sea water pens at the marine site Rowella where historically Atlantic salmon experienced a severe depletion of flesh colour which becomes evident after summer. DNA samples of the aforementioned broodstock had been collected pre-spawning from the adipose fin by using a Tissue Sampling Unit (TSU; a vial containing a fixative for preservation of DNA) and applicator (a gun with a punch cutter) (Allflex Pty Ltd, Australia) and sent for analysis by Xelect, Petuna's genetic service provider based in Scotland. After genotyping, each individual broodstock fish was assessed for pairing suitability based on the lowest coefficient of inbreeding combined with lowest level of relatedness (cut-off 0.05). The aim was to produce a population having as much genetic variation as possible and the lowest possible level of relatedness and inbreeding within the existing commercial circumstances.

During the freshwater phase, fish were reared in standard commercial conditions. The incubation stage was performed in dedicated tray-incubators (Marisource Inc., Tacoma, WA, U.S.A., Fig. 3.1), allowing the necessary analysis and evaluation of each individual cross before pooling at first feeding. The tray incubators had been purchased specifically for this trial. A total of 10 8-tray incubators were installed to individually allocate 160 progenies overall (each tray was divided in half to allocate two progenies separately at 5000 eggs/half tray) Fig. 3.1.



**Fig. 3.1** Panel showing the different steps of the spawning for the genetic component trial: A) fertilisation of eggs in a bowl with the label identifying the female used (fin-clip tube ID), B) Tray incubators with the cross female-neomale identification code (the neomale code is not reported for the following trays as position of trays will never change until pooling). Each tray was divided in half by using a segregator to allow allocation of two progenies, C) Dr Amoroso placing the fertilised eggs into a tray incubator.

The final population, after discarding some crosses due to normally occurring low fertility/low survival, was formed by the contribution of a total of 96 female and 16 neomale three years old broodstock. The critical dates are the following and represent the trial design:

- 17-18/5/2017 creation of 160 crosses (families) from unrelated broodstock and egg incubation at 8 °C
- 17/7/2017 eggs hatch
- 18/8/2017 first feeding of 96 pooled selected crosses (equal contribution of 3000 individuals/cross) at 12 °C
- 3/11/2017 population transferred to the grow out at 14-16 °C
- 2/2/2018 fish vaccinated and transferred into dedicated ponds
- 24-25/5/2018 fish transferred at 140 g to seawater (Rowella) and allocated into two pens at 75,000 fish each.
- 7/1/2019 – 25/3/2019 **summer mortality DNA sampling** from the two dedicated pens (25 and 26 then renamed 27 and 28 due to farm outline changes) (~1000 samples)
- 2-24/4/2019 **post-summer performance and colour assessment with DNA sampling** from the two dedicated pens (~2000 samples) + multiple tissue sampling by USC (subset of 100 samples from the 2000).
- 22/7/2019 – 2/8/2019 **harvest performance and final colour assessment with DNA sampling** from the two dedicated pens (~2000 samples).

The trial population was harvested in full and assessed at harvest during the end of July and the beginning of August 2019. During the marine phase, fish were treated as a standard commercial group, while avoiding any mixing with other stock types, and fed a commercial diet containing 75 ppm of carotenoids from transfer through winter, then 80 ppm from spring to summer through harvest. During the whole production cycle, in both freshwater and seawater, general performance and mortality did not differ from other stock types, implying that the trial population gives a reliable representation of what fish experience during standard production conditions.

### **3.2 Summer mortality DNA sampling and post-summer performance including colour assessment with DNA sampling**

These two assessments are presented in the same section as some of the analyses and calculations required samples from both.

#### **3.2.1 Aims**

The summer mortality sampling was added as part of the one-year project extension. After internal discussion within Petuna and all the project investigators, a task was added to understand if specific families cannot cope with high seawater temperatures and are subjected to higher mortality than other families. The literature on this topic is scarce and it is still unclear if there are specific traits linked to thermal tolerance in salmonids that can be effectively used for genetic selection. This task is then critical to understand, based on the results of both the post-summer and the harvest assessment, whether or not the best performing families and with best quality are actually being so throughout all the critical stages of the marine production cycle and are also less impacted by mortality.

The post-summer performance and colour assessment with DNA sampling is part of the original project objectives and targeted a critical timepoint in production to understand whether there is a genetic component underlying flesh colour loss post-summer displayed by part of the stock. This task acted as fulcrum for the other two tasks added to the project so that comprehensive information on Atlantic salmon thermal tolerance in Tasmania was generated. Being the only time of the year where different flesh colour phenotypes are displayed as a result of summer with high water temperatures and periods of voluntary starvation, this timepoint gave the investigators the opportunity to assess performance traits, with focus on colour, and link them to the genetics as well as collect samples from several tissues involved in the carotenoids metabolism. The latter (refer to section 2.4, 2.5) expanded our knowledge on the role played by different tissues and the microbiome in the occurrence of flesh colour loss or good colour in Atlantic salmon.

#### **3.2.2 Sampling design and methods of summer mortality DNA sampling**

The sampling was carried out twice a week over 12 weeks with the first sampling occurring on the 7<sup>th</sup> of January and the last on the 25<sup>th</sup> of March 2019. The sampling targeted the two cages containing the trial population (representing the original population split in half when transferred from freshwater to seawater). Xelect, Petuna's genetic service provider, indicated the number of samples to collect to be 1000 (approximately 500 per cage depending on mortalities availability) for this specific task in order to secure a good representation of all families present in the population. The maximum number of samples to be collected at any week was adjusted to match the usual mortality trend at the site which peaks immediately after periods of high temperatures (exceeding 20°C) and drops at decreasing temperatures, not to over- or under-sample during the events. Fig. 3.2 shows a clear correlation between mortality and temperature fluctuation. At the end of the sampling, a total of 963 samples

were collected (a slightly lower number than what was planned due to the number of mortalities available).

At each sampling event, the divers responsible for mortality collection were instructed to retrieve and store separately all the healthy-looking fish freshly deceased. This was done to avoid sampling fish which possibly died from other causes rather than thermal stress and to make sure DNA would still be of a suitable quality for genetic analyses and not excessively degraded. Immediately after collection, each fish was inspected by Dr Amoroso, and with the assistance of Petuna staff, a DNA sample (punch) was collected from the adipose fin by using the Tissue Sampling Unit (TSU). Samples were stored at -20°C temperature and at completion of the sampling sent to Xelect for DNA analysis.

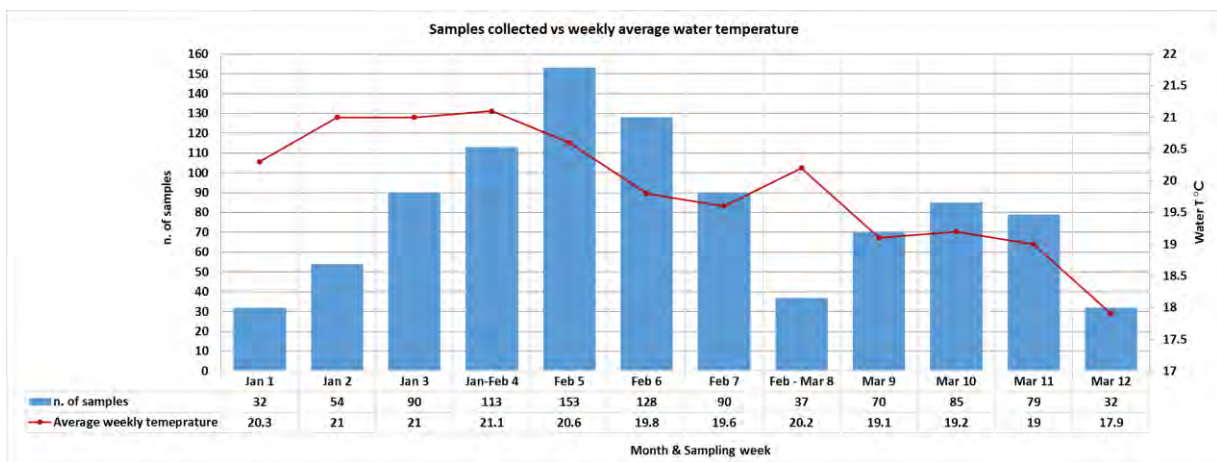


**Fig. 3.2** Number of samples collected (cages pooled) per week (weekly events pooled) plotted against the average weekly temperature at the site.

### 3.2.3 Sampling design and methods of post-summer assessment

The sampling was carried out from the 2<sup>nd</sup> to the 24<sup>th</sup> of April in Rowella and 2013 fish (approximately 1000 per cage) were sampled and assessed over nine days (approximately 225 fish assessed per day). At each sampling event, the required number of fish was collected by Petuna staff by using a box net. Fish were then dip netted, euthanized through a non-recoverable percussive blow to the head delivered by an automatic stunner, bled and immediately transferred to an ice slurry before assessing them. Weight (kg) and fork length (mm) were measured and externally detectable deformities (focusing on jaw and spine) were assessed and recorded. A DNA sample (punch) was collected from the adipose fin of each fish as described above. Fish were then manually gutted and filleted and the fillet from the right side of the body, trimmed, rinsed and blotted with a cloth to remove residual water which would interfere with the photographic process. A uniquely numbered waterproof tag was assigned to each fish so that all the information collected would match with the picture and the DNA sample. In order to assess and measure flesh colour, each fillet was positioned on a black plastic tray bearing the tag (Fig. 3.3) and inserted into a sealed black plastic lightbox (80x70x40 cm) with standardised light conditions. The lightbox was equipped with eight daylight 1050 lumen 10 W LEDs mounted on the lid and in order to have even diffusion of light and limit reflection from the bottom of the box, a polycarbonate diffused sheet was mounted to shield the light source. Pictures were taken with a Canon EOS 200D Digital SLR camera fitted in a hole in the centre of the light-box lid and with its lens just coming out from the diffused sheet. The camera lens was protected by the light emitted from the nearby source by inserting into a plastic pipe cut to slightly exceed the length of it. The camera was

set at f/22, 1/125 sec, ISO-3200, 6000x4000. The bottom of the lightbox contained a lineal SalmoFan™ and a X-Rite ColourChecker Classic Mini card for image analysis purposes (Fig. 3.3). All the images were sent to Xelect for image analysis and to develop a method for colour and banding measurement.

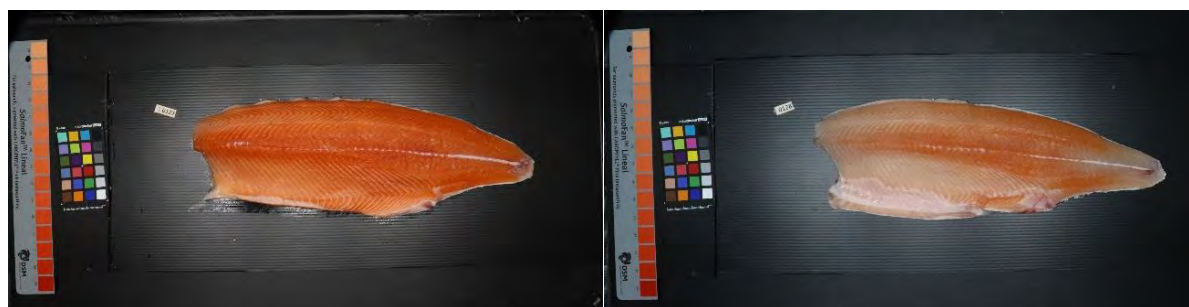


**Fig. 3.3** Images taken inside the lightbox with standardised light conditions during the post-summer assessment. A fillet with good colour (right) and one with reduced colour and banding (left).

### 3.2.4 Genetic methods

DNA was extracted from each sample using a standardised chelex and proteinase K digestion protocol and then diluted in nuclease-free water (1:50). A two-step PCR method was used to prepare DNA libraries suitable for amplicon sequencing on an Illumina Miseq instrument. All samples were then genotyped for a total of 116 SNPs located at 96 loci that are broadly distributed across the genome. Parentage assignment was conducted using Colony2 software (v.2.0.6.1)<sup>318</sup>. The assignment is based on a maximum likelihood approach by heuristically searching through possible relationships and comparing the statistical likelihood of a given relationship being valid in accordance with the SNP data and Mendelian inheritance. A list of the recorded crosses was provided by Petuna of which 96 dams were crossed with 16 males. Males were used multiple times.

### 3.2.5 Colour assessment methodology

A total of 8 different colour measurements were extracted according to the report on a previous assessment by CSIRO<sup>319</sup>. An example extract is shown in Fig. 3.4. A Python script using the *numpy* and *OpenCV* libraries was developed to analyse all 2013 images automatically.

The script extracted the SalmoFan™ and fillet from the background image. From each square,  $L a^*b^*$  and RGB measurements were extracted. SalmoFan™ flesh colour scores were also assessed by extracting mean RGB values from each region of the SalmoFan™ included in the image (100x100 pixels). The SalmoFan™ score was produced by calculating the Euclidean distance between the RGB of the extracted square and each SalmoFan™ region and selecting the SalmoFan™ region with the lowest distance. Manual colour scores were taken on a subsample of 52 individuals (eight regions per image) to validate the accuracy of the calculated SalmoFan™ scores.

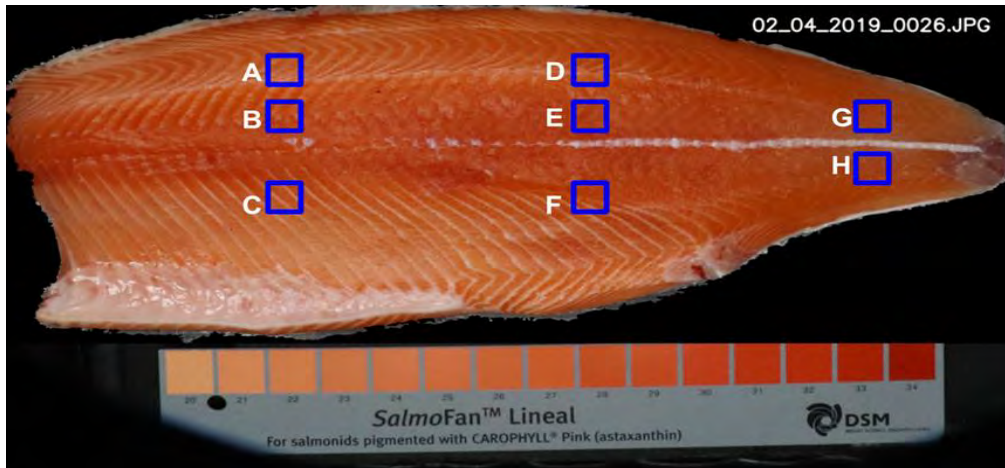


Fig. 3.4 Regions extracted from each fillet image.

### 3.2.6 Techniques to calculate flesh colour loss

For the current analysis, banding was calculated as the difference between the extracted  $a^*$  in region E and region A (E-A). E is the region which usually retain good colour and A is the one most affected by colour loss. High scores indicate larger differences in colour and thus more severe banding. While simple to calculate, the downside of this method is that fillets with complete colour loss tend to show little banding (small differences in colour between regions) despite a more severe phenotype. Part of the complication of quantifying the colour loss issue is the suspected ontogeny of localised colour loss. If we assume that the ontogeny of the banding pathology begins as banding in the dorsal and ventral region and then depigmentation gradually worsens until the entire fillet is rendered pale, then banding severity may not be reflective of the pathology severity. For instance, the most severely afflicted fish would be entirely pale and show little banding (Fig. 3.5).

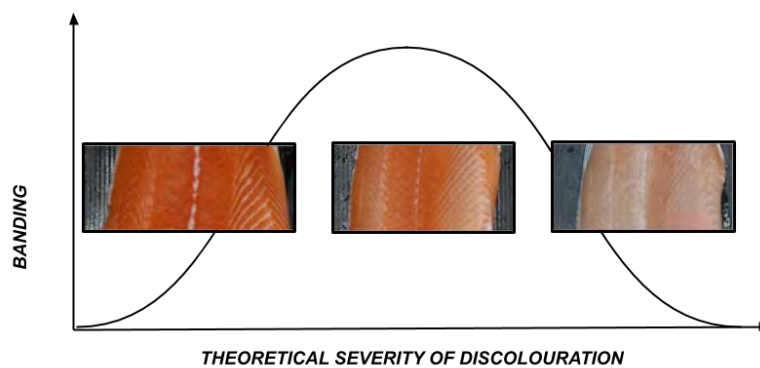


Fig. 3.5 Colour loss phenotype.

Xselect has then developed for Petuna a method to capture the severity of the pathology for trait measurement without losing resolution from use of banding indexes and average colour values alone. These are captured by three different trait measurements on two dorsoventral slices 40 pixels wide in the NQC (D-F) and trunk (A-C) regions (Fig. 3.6, example of D-F NQC slice):

- The **proportion** of a fillet slice that is above 25 on the SalmoFan™ (ROCHE in the graph) scale.
- The **colouration index** calculated as the sum of the median SalmoFan™ (ROCHE in the graph) values above and below 25 relative to the number of pixels ( $\text{medianHIGH} \times n_{\text{pixelsHIGH}} + (\text{medianLOW} \times n_{\text{pixelsLOW}})$ ).
- The **mean relative sum calculated** as the sum of the total SalmoFan™ (ROCHE in the graph) values for each slice relative to the number of pixels.

### 3.2.7 Statistical analysis

The influence of cage on overall intensity of colour ( $a^*$  value extracted from Region E, this was chosen as commercially relevant and used worldwide as quality assessment region) and banding patterns ( $a^* E - a^* A$ ) was assessed using Kruskal-Wallis tests. The relationship between body size and shape (weight and condition factor [k], respectively) and the above colour traits was assessed with ordinary least squares regression. Heritability was estimated for each trait with univariate animal models using cage as a fixed effect. Heritability can range from 0 = no genetic contribution to 1 = all differences on a trait reflect genetic variation. Genetic and phenotypic correlations for each pair of traits were estimated using bivariate animal model equations for each pair of traits, also including cage as a fixed effect. All the analyses were conducted in R <sup>320</sup> and figures were produced using the package ggplot2 <sup>321</sup>.

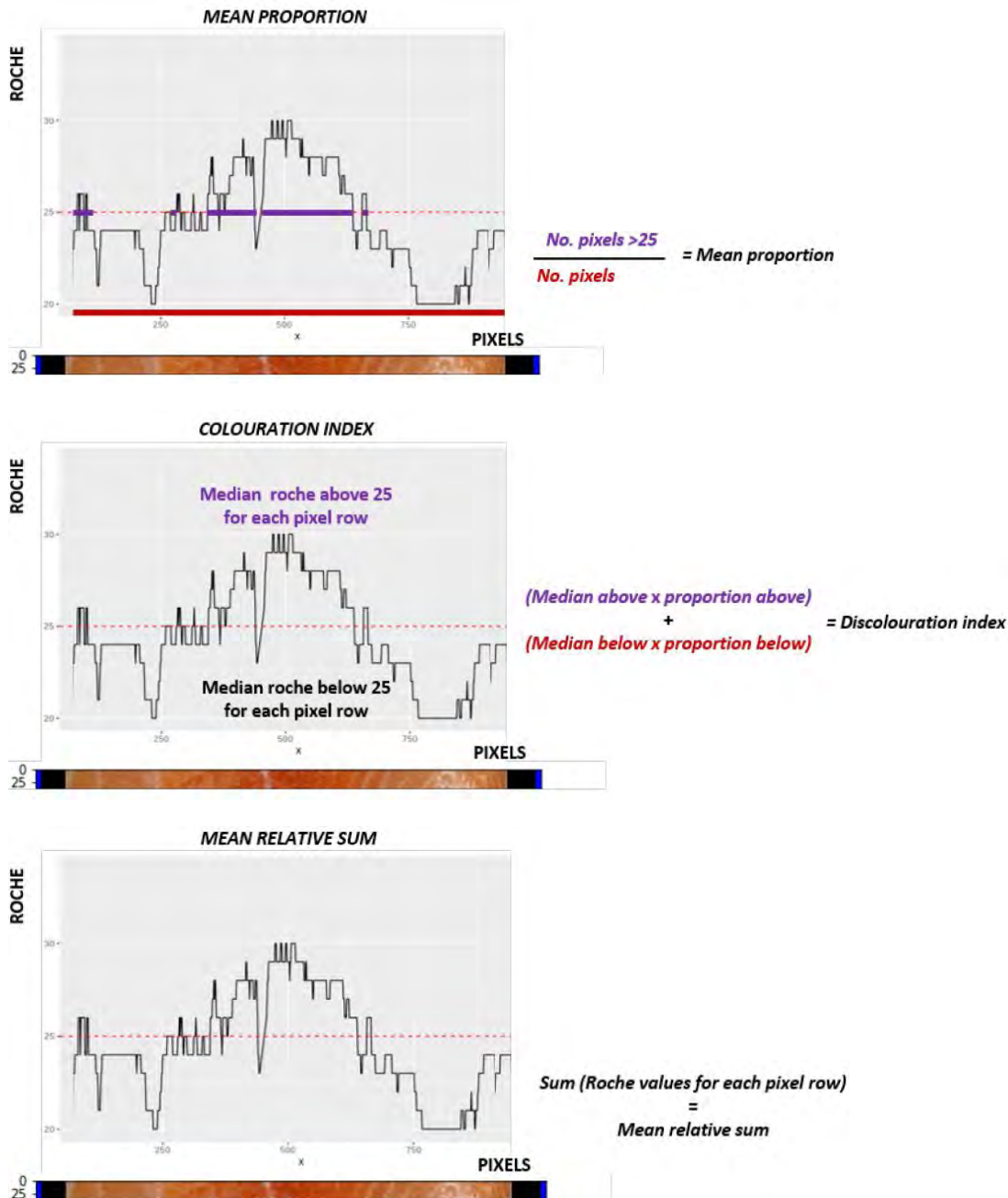


Fig. 3.6 Illustration of the three methods of capturing the level of flesh colour loss with image analysis on the NQC (D-F).

### 3.2.8 Results

#### 3.2.8.1 Assessment data

A wide range of weights and lengths were observed with little differences between cages (Fig. 3.7). Condition factors (k) were seen to be reasonably high, in consideration of the fact that the fish were subject to high temperatures and chronic feed cessation. Correlations between length and k indicate that some of these high measurements may be deformity outliers (Fig. 3.8). External deformities were recorded during the assessment however, a considerable number of deformities were noted on the images in the form of cartilage build up along the midline. External deformities included mostly spinal deformity and downward curvature of the lower jaw and both categories (at times concurring) affected less than 3% (combined prevalence <6%) of the population. Such low prevalence did not allow to

reliably run any analysis to understand the possible genetic effect on their occurrence. As expected, deformed individuals were smaller and paler than the average of the population due to being physically incapacitated to perform at the same level of normal individuals (data not shown).

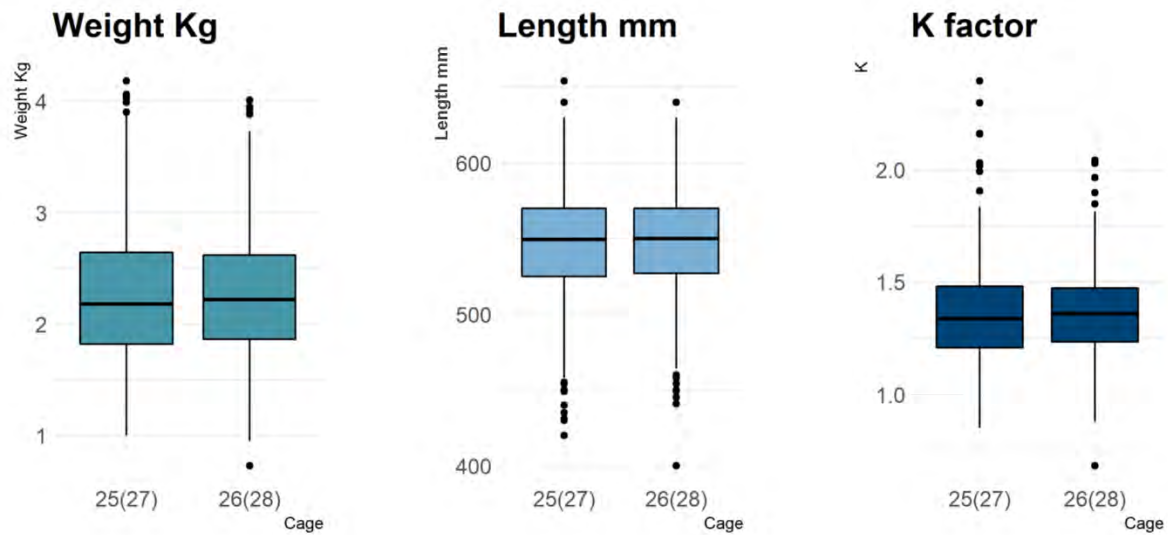


**Fig. 3.7** Relationship between size, traits and cage with original and re-assigned cage number in brackets.

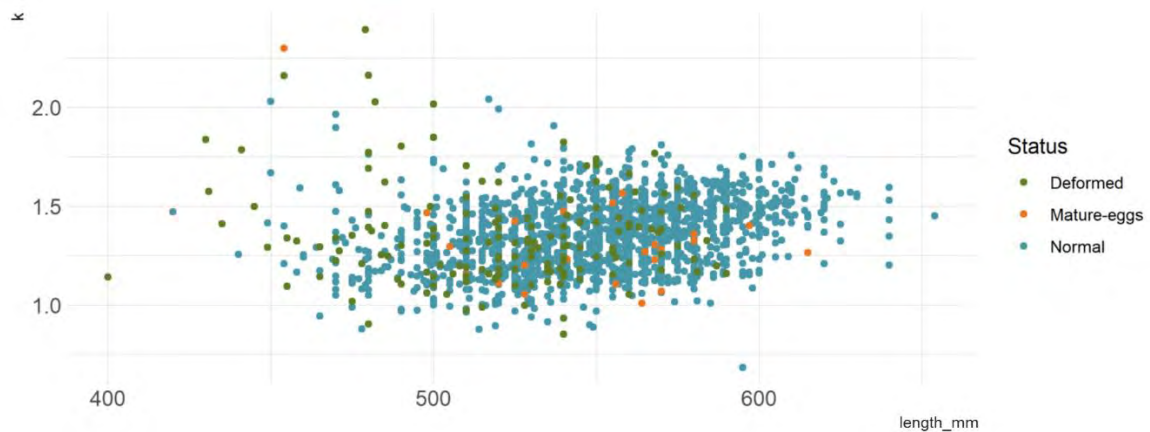


**Fig. 3.8** Relationship between length, condition factor, and deformity/maturity.

### 3.2.8.2 Parentage assignment

In total, 2821 individuals out of 3083 sampled (summer mortality + post-summer) were run in Colony2. The dropout rate is reasonably low considering the expected poorer sample quality of the mortality tissue samples. Of the 96 females and 16 males broodstock fish genotyped, 4 females and 3 males did

not genotype well. Hence, 92 of the 96 crosses were able to be fully assigned to 2717 individuals in total.

### 3.2.8.3 Mortality distribution

After DNA extraction, 906 out of the 963 samples collected were suitable for genotyping analysis. Estimated proportion of mortality was calculated as number of mortalities genotyped / (number of colour samples + mortality) genotyped per family.

The distribution of estimated proportion of mortality show that although all families assigned experienced some degree of mortality, there are specific families strongly associated with higher mortality in these environmental conditions (Fig. 3.9). This is supported by heritability estimates of 0.323 for this trait. Further investigation shows that family mortality trends are generally consistent across cages (Fig. 3.9). Consistency in family proportion of mortality was also observed between early and peak mortality periods (before and after the 25<sup>th</sup> of January, respectively) (Fig. 3.10), further highlighting how less thermal tolerant families are first affected by mortality when the temperature is not high enough to affect the majority of the population to the same extent. This was calculated as number of mortalities genotyped in a period (total mortality / number of April colour samples). Collectively these results demonstrate the suitability of using this trait for selective breeding of more robust offspring, more resistant to summer mortality and increasing seawater temperature in general.

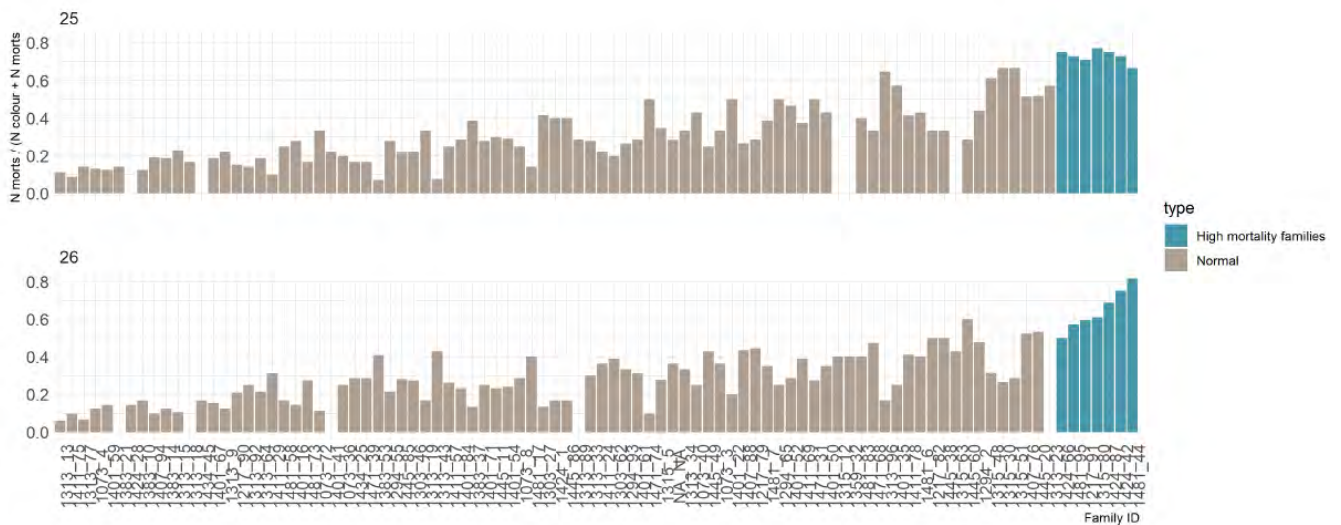


**Fig. 3.9** Proportion of mortality per family calculated as number of mortalities genotyped / (number of April colour samples + mortality) genotyped per family in each cage ranked from lowest to highest.

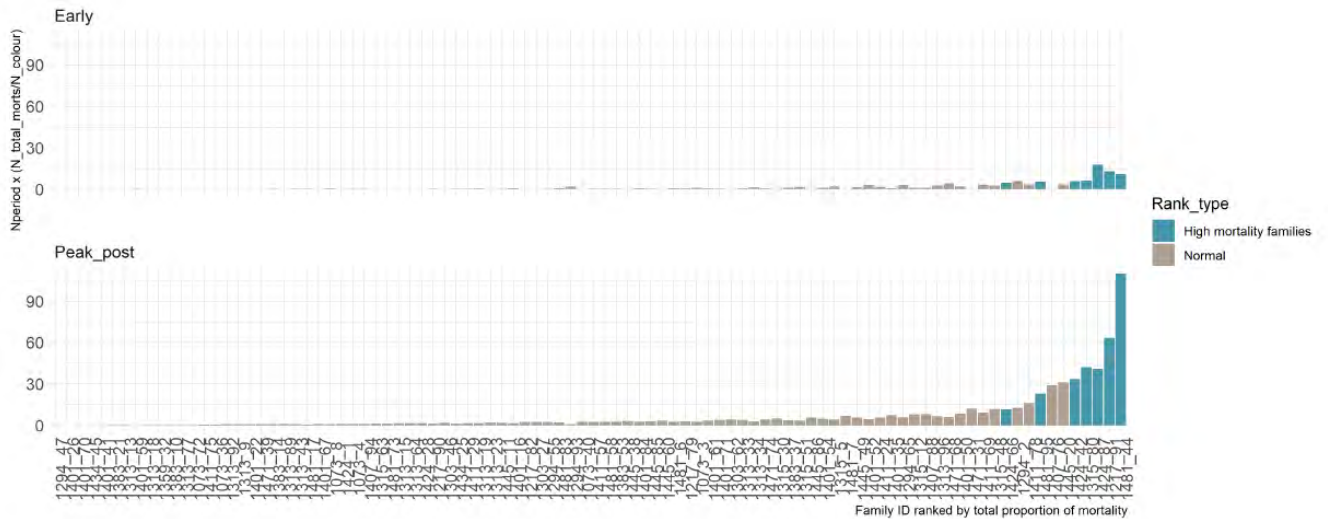


**Fig. 3.10** Proportion of mortality (cages pooled) per family in each period ranked from lowest to highest calculated as number of mortalities genotyped in a period (total mortality / number of April colour samples).

### 3.2.8.4 Flesh colour

There was a significant, but small effect of cage on region E (NQC) colour ( $a^*$ ) ( $P < 0.046$ ), with greater significant effects observed for the other colour traits mean proportion >25 SalmoFan™, colouration index and mean relative sum of SalmoFan™ values ( $P < 0.001$  for all). The distribution of the aforementioned traits with respect to cage is displayed in Fig. 3.11.

There was a significant relationship between size and shape (weight and condition factor  $k$ ) and all colour traits ( $a^*$  in region E, mean proportion >25, colouration index and mean relative sum;  $P$  values all  $< 0.001$ ; Fig. 3.12). Results show that similar correlation patterns are observed across all colour traits and slightly stronger correlations are observed with weight than condition factor.

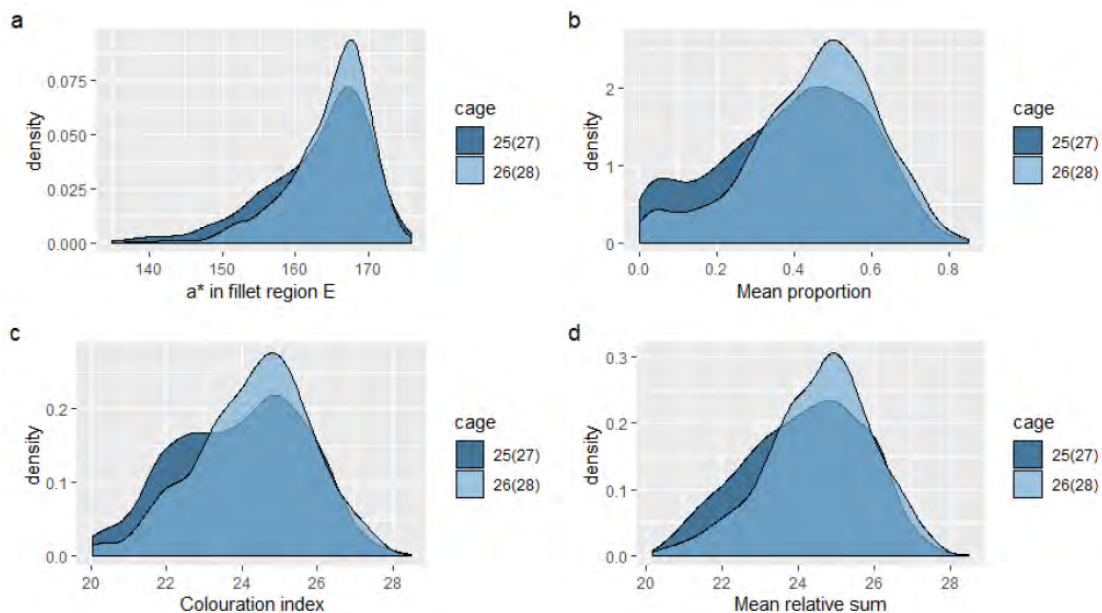


**Fig. 3.11** Relationship between colour  $a^*$  intensity (panel a), proportion >25 SalmoFan™ (panel b) colouration index (panel c), mean relative sum (panel d) and cage.

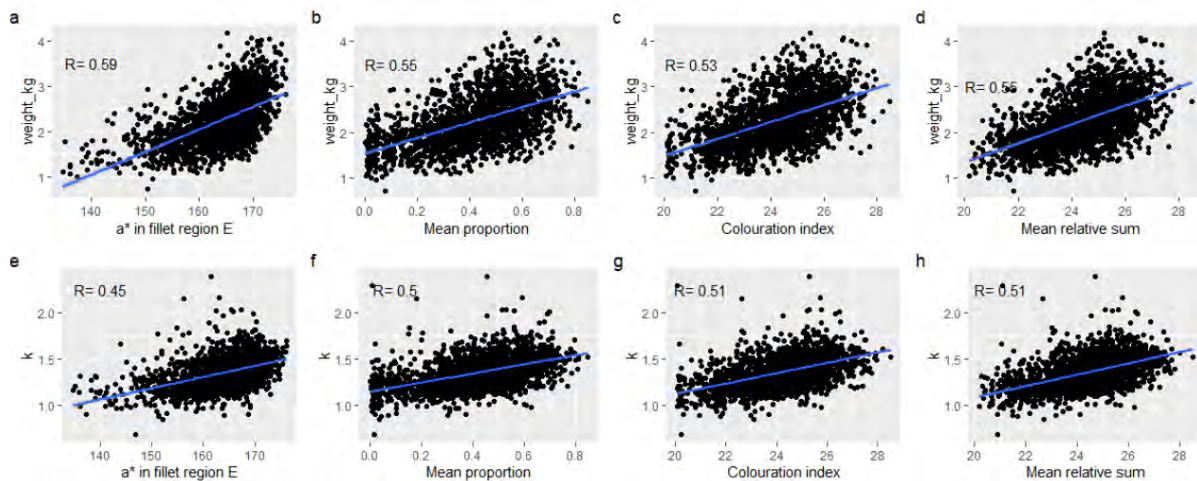


**Fig. 3.12** Relationship between weight and colour intensity (a), weight and proportion >25 SalmoFan™ (b), weight and colouration index (c), weight and mean relative sum of SalmoFan™ values (d), k and colour intensity (panel e), k and proportion SalmoFan™ values >25 (f), k and colouration index (g), k and mean relative sum of SalmoFan™ values (h).

### 3.2.8.5 Heritability and trait correlation

As colouration index and mean relative sum were so similar, the model for calculating heritabilities, genetic and phenotypic correlations struggled to converge and so the traits were repeated in two tables. Heritability estimates (highlighted, this number can range from 0 = no genetic contribution to 1 = all differences on a trait reflect genetic variation), genetic (above heritability) and phenotypic (below heritability) correlations are shown in Table 3.1 and 3.2. High heritability estimates were observed for weight and colour traits (regions A, E, G being the main focus). This demonstrates that there is a clear genetic effect on flesh colour as well as on colour loss in Petuna stocks. The aforementioned traits are therefore excellent candidates for selective breeding and the aim is to select for the least colour loss in the fillet in all regions. Both methods of colour measurements ( $a^*$  and estimated SalmoFan™) have high heritabilities and can therefore be feasibly used for selective breeding. Generally, higher heritability estimates were observed for  $a^*$  than for SalmoFan™ values with high correlations (>0.98) indicating  $a^*$  to be more favourable than SalmoFan™. This is expected as while  $a^*$  is a direct measurement, SalmoFan™ score is a value derived from  $a^*$ .

The E-A banding index showed good heritability (0.276). Once again, this demonstrates that there is a genetic effect not only on colour loss but also specifically on banding. However, as discussed previously, a crude banding index such as this may not be adequate in defining a general colour loss issue. The three different methods of quantifying overall colouration across the fillet slices proved to have higher heritabilities than the SalmoFan™ measurements in the E, A, G region and E-A (difference in heritability in this case is 0.276 vs 0.485 colouration index, 0.490 mean proportion >25 and 0.513 mean relative sum) and albeit still not as high as the  $a^*$  measurements. Nonetheless, this measurement represents the overall fillet colouration in contrast to pinpoint A, E, or other regions measurements and may therefore be the most appropriate for selective breeding purposes. Fig. 3.13 and 3.14 show the distribution of colour values found for each assigned parent, where the parents are reordered according to the highest and lowest colour on a SalmoFan™ scale.

All the different colour traits seem to positively correlate (both genetically and phenotypically) with each other, meaning that selection based on one region only would not lead to negative selection on another (Table 3.1 and 3.2). Most importantly, positive correlations were observed between weight

and all colour traits while a negative correlation was observed between weight and condition factor (being higher) and E-A (banding index) (Table 3.1 and 3.2). Fig. 3.15 shows how families of higher mean weights tend to have higher flesh colouration and *vice versa*. In addition, families with the highest proportion of mortality were also associated with smaller weights and lighter flesh colour (Fig. 3.15). This latter result tells us how poor performing fish post-summer are also more affected by summer mortality likely due to their lower thermal stress tolerance.

**Table 3.1** Heritability (highlighted), genetic and phenotypic correlations for size and colour traits excluding the mean relative sum values. Genetic correlations are above the heritabilities and phenotypic correlations below the heritabilities. Roche = SalmoFan™.

trait	Weight	K	E a*	A a*	G a*	E Roche	A Roche	G Roche	E-A	Prop>25	Col index
Weight	0.525	0.671	0.597	0.570	0.569	0.597	0.400	0.554	-0.386	0.486	0.427
K	0.683	0.344	0.494	0.554	0.608	0.502	0.507	0.571	-0.506	0.540	0.496
E a*	0.583	0.446	0.520	0.950	0.956	0.982	0.883	0.937	-0.657	0.923	0.912
A a*	0.612	0.520	0.809	0.564	0.895	0.922	0.973	0.869	-0.860	0.976	0.968
G a*	0.617	0.519	0.843	0.807	0.539	0.943	0.832	0.992	-0.591	0.894	0.891
E Roche	0.468	0.385	0.881	0.655	0.689	0.368	0.870	0.944	-0.612	0.927	0.920
A Roche	0.380	0.409	0.606	0.851	0.590	0.539	0.405	0.819	-0.898	0.985	0.981
G Roche	0.506	0.454	0.715	0.702	0.894	0.660	0.526	0.421	-0.551	0.872	0.871
E-A	-0.339	-0.347	-0.180	-0.724	-0.361	-0.061	-0.712	-0.335	0.276	-0.841	-0.826
Prop>25	0.535	0.503	0.844	0.859	0.796	0.780	0.761	0.715	-0.447	0.490	1.000
Col.index	0.522	0.513	0.805	0.843	0.769	0.753	0.751	0.689	-0.465	0.954	0.485

**Table 3.2** Heritability (highlighted), genetic and phenotypic correlations for size and colour traits excluding the colouration index. Genetic correlations are above the heritabilities and phenotypic correlations below the heritabilities. Roche = SalmoFan™.

trait	Weight	K	E a*	A a*	G a*	E Roche	A Roche	G Roche	E-A	Prop>25	Rel sum
Weight	0.525	0.671	0.597	0.570	0.569	0.597	0.400	0.554	-0.386	0.486	0.466
K	0.683	0.344	0.494	0.554	0.608	0.502	0.507	0.571	-0.506	0.540	0.533
E a*	0.583	0.446	0.520	0.950	0.956	0.982	0.883	0.937	-0.657	0.923	0.922
A a*	0.612	0.520	0.809	0.564	0.895	0.922	0.973	0.869	-0.860	0.976	0.972
G a*	0.617	0.519	0.843	0.807	0.539	0.943	0.832	0.992	-0.591	0.894	0.895
E Roche	0.468	0.385	0.881	0.655	0.689	0.368	0.870	0.944	-0.612	0.927	0.931
A Roche	0.380	0.409	0.606	0.851	0.590	0.539	0.405	0.819	-0.898	0.985	0.981
G Roche	0.506	0.454	0.715	0.702	0.894	0.660	0.526	0.421	-0.551	0.872	0.875
E-A	-0.339	-0.347	-0.180	-0.724	-0.361	-0.061	-0.712	-0.335	0.276	-0.841	-0.826
Prop>25	0.535	0.503	0.844	0.859	0.796	0.780	0.761	0.715	-0.447	0.490	0.997
Rel sum	0.534	0.513	0.839	0.863	0.797	0.788	0.770	0.722	-0.460	0.982	0.513

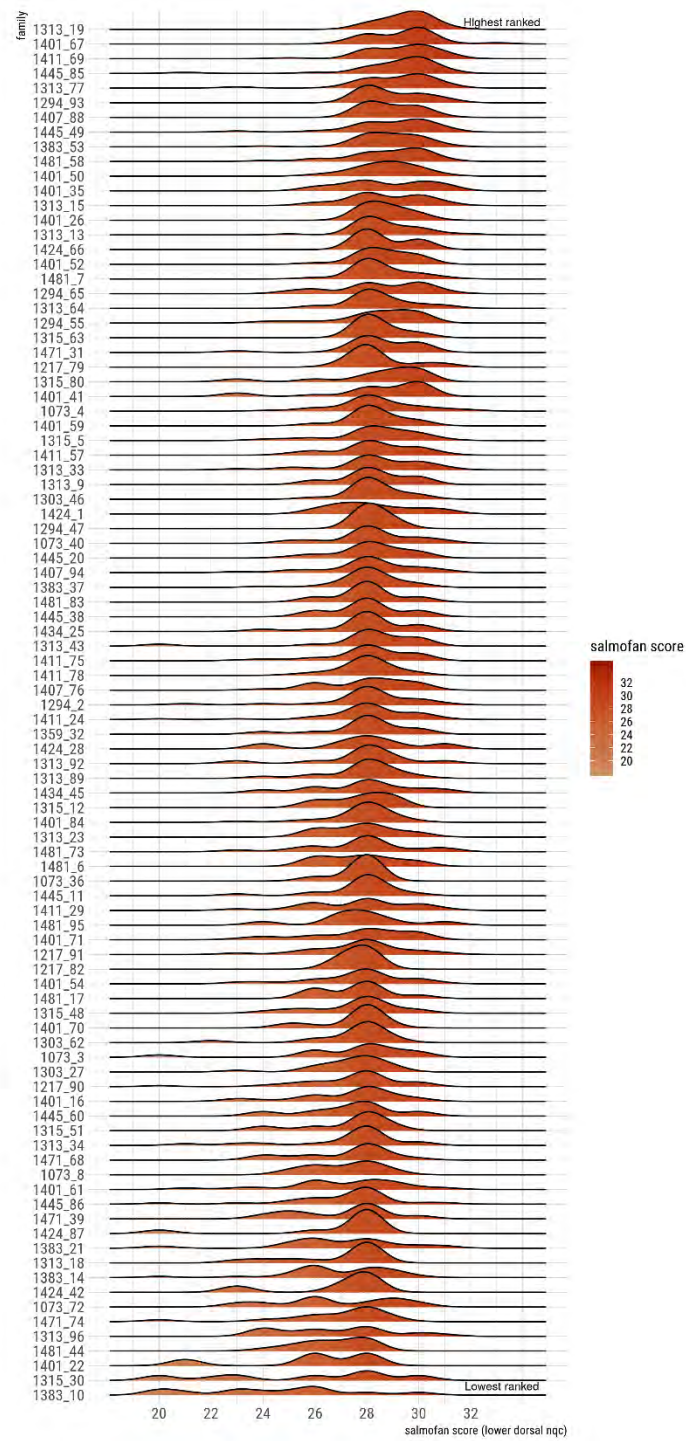
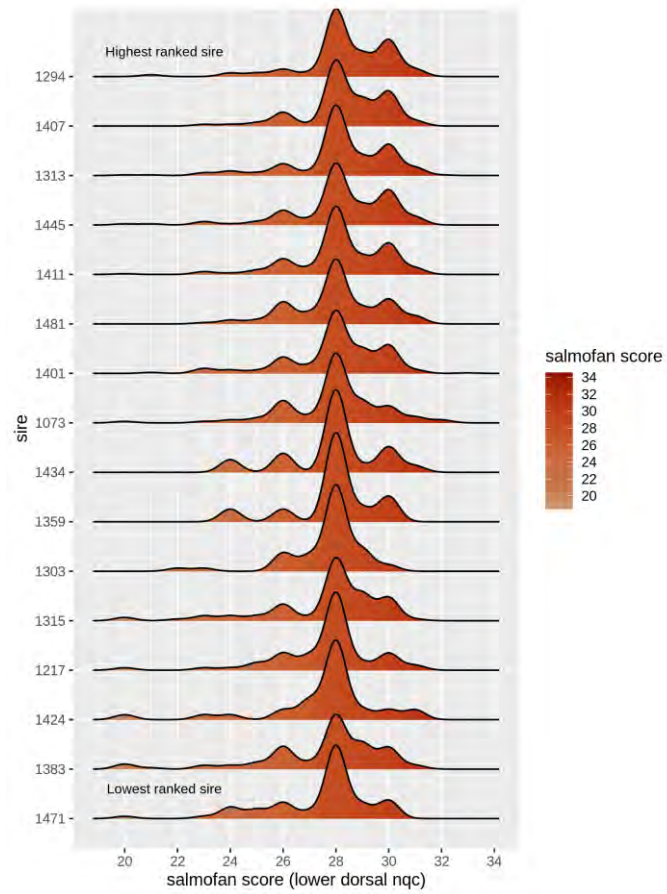
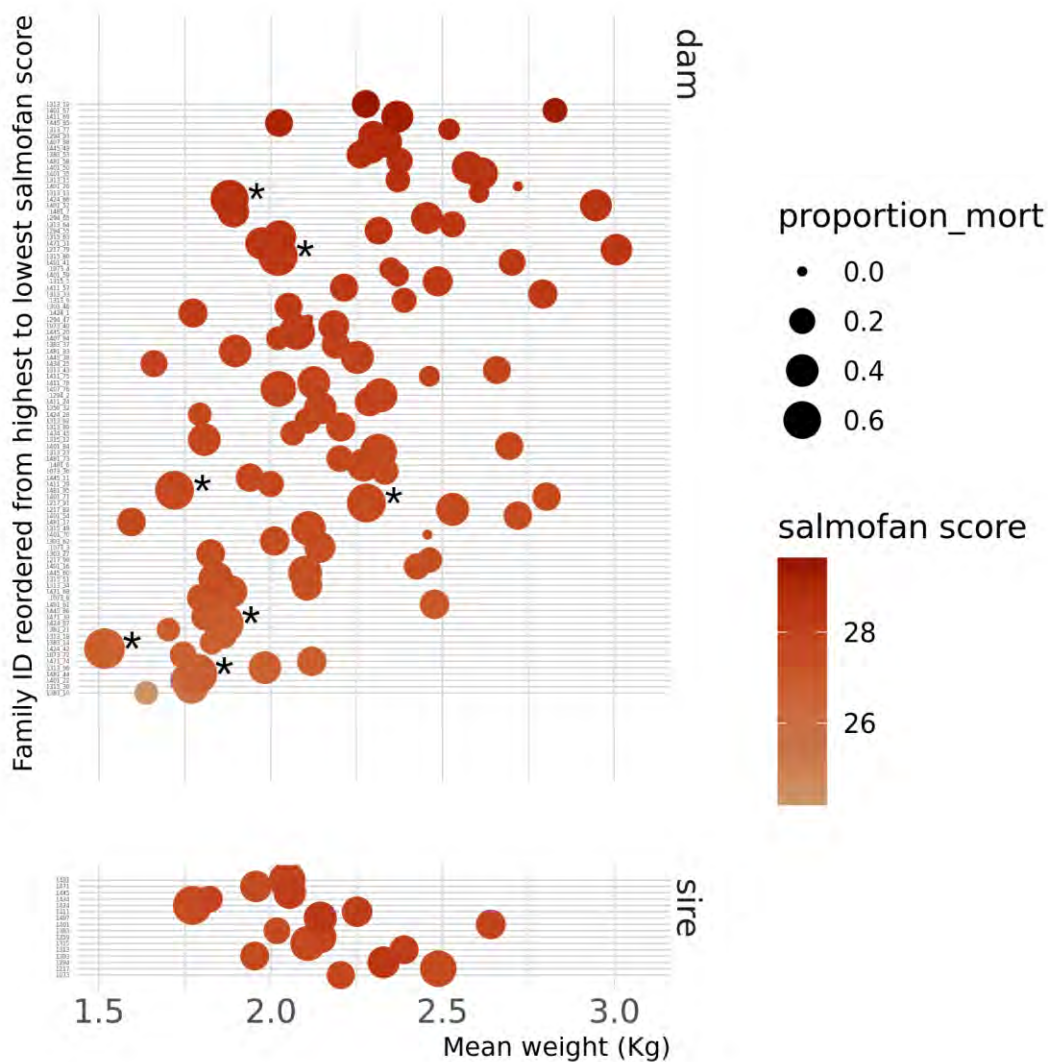


Fig. 3.13 Distribution of colour values in each family (assigned dam) reordered by the highest to the lowest colour (region E SalmoFan™).



**Fig. 3.14** Distribution of colour values in each family (assigned sire) reordered by the highest to the lowest colour (region E SalmoFan™).



**Fig. 3.15** Mean weight and colour (region E SalmoFan™), and proportion of mortality for each assigned parent, where the size of each circle is relative to the proportion of mortality associated with that family. High mortality families indicated in are denoted by an asterisk.

### 3.3 Harvest performance and colour assessment with DNA sampling

#### 3.3.1 Aims and commercial outcome

After the summer mortality and post-summer assessment, a final assessment to examine performance and colour and their genetic component was carried out when the trial population reached the harvest stage. This was done in order to obtain a complete picture of the genetic effect on performance of Petuna stocks and help to lay the foundation of a selective breeding program. Summer and post-summer period presented the most extreme phenotypes of high mortality, banded/pale flesh colour and reduced growth and it was critical to understand the genetic component of colour loss and thermal tolerance. In this assessment, the focus was on commercial traits of interest, which are higher final harvest weight and flesh colour. This final assessment also was fundamental to understand how strong

was the genetic correlation in those traits between post-summer and harvest, giving us further insight on how specific families perform during a full production cycle. Following the encouraging results of this trial, the Petuna selective breeding program was established and during the 2020 spawning we were able to produce the first production eggs with genetic gain based on the performance of the trial population by using their siblings, which were retained in freshwater.

### 3.3.2 Materials and methods

A total of 2100 individuals were harvested and assessed between the July 23<sup>rd</sup> and the 2<sup>nd</sup> of August 2019 from two cages, n. 21 and 27, both containing the top grade fish from the original trial population. In fact, after summer and following our previous assessment, the two original cages containing the trial population were both graded by size to create two new cages containing the top and the bottom grade of the whole population. This is a standard commercial practice aiming at reducing size variation in order to improve harvest and processing efficiency. Sampling only from the top grade was considered sufficient to achieve the information required. Nevertheless, sampling from the bottom grade would have helped to increase the accuracy of the genetic analysis. Unfortunately, it was impossible to sample from the latter due to operational constraints.

The harvest assessment was carried out in a very similar way to the post-summer assessment (although this time happening in Petuna's processing facilities in Devonport, Fig. 3.16) and the same analyses described in section 3.2 were repeated for these samples. Two additional traits were measured compared to the post-summer assessment: HOG (head on gutted) weight (kg) and gonads weight, expressed as gonadosomatic index (GSI) and calculated =  $(\text{gonad weight (g)}/\text{fish weight (g)}) \times 100$ . Nevertheless, these are not shown in the analysis as HOG weight was measured just for commercial purposes while GSI was not taken into account, as the fish showed a very low level of maturation.

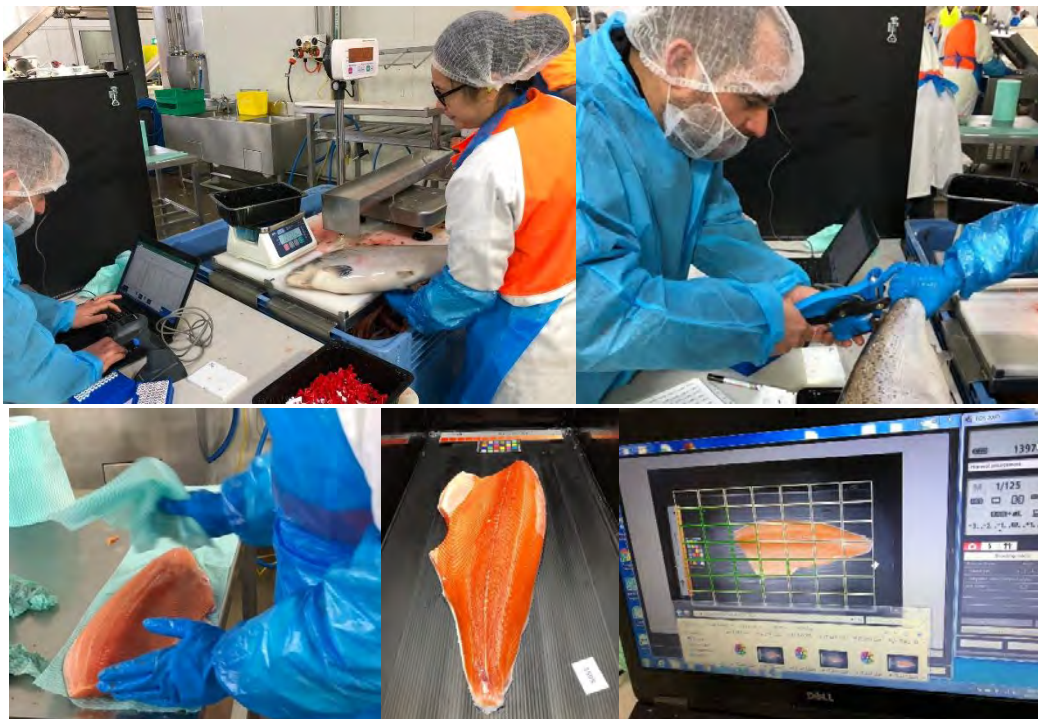


Fig. 3.16 Different tasks performed during the harvest assessment.

### 3.3.3 Results

Fish from both cages presented a good harvest size and a good condition factor at harvest (Fig. 3.17). In both cages approximately 88% of fish had a size > 3.5 kg and approximately 98% had a condition factor ( $k$ ) >1.4. A small effect of cage was observed on weight, length  $k$  and this was included as a fixed effect in the calculations (Fig. 3.17). As for the post-summer assessment, there was a clear association of deformed fish with higher condition factors (Fig. 3.18). Total prevalence of spinal deformities was very low at < 5% in both cages and it is thought to be mostly the result of external factors leading to compression or fusion of vertebral bodies which lead to a shorter shape and so higher condition factor.

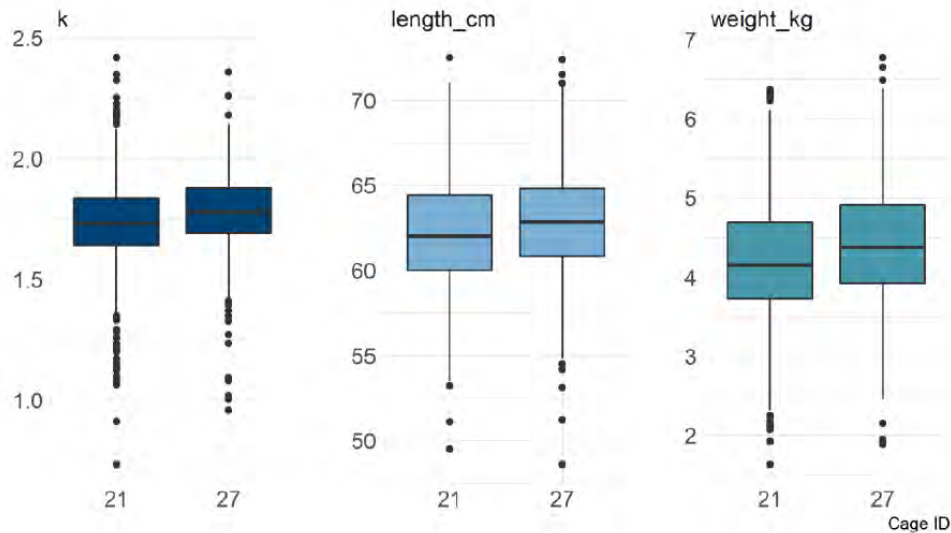


Fig. 3.17 Relationship between size traits and cage.

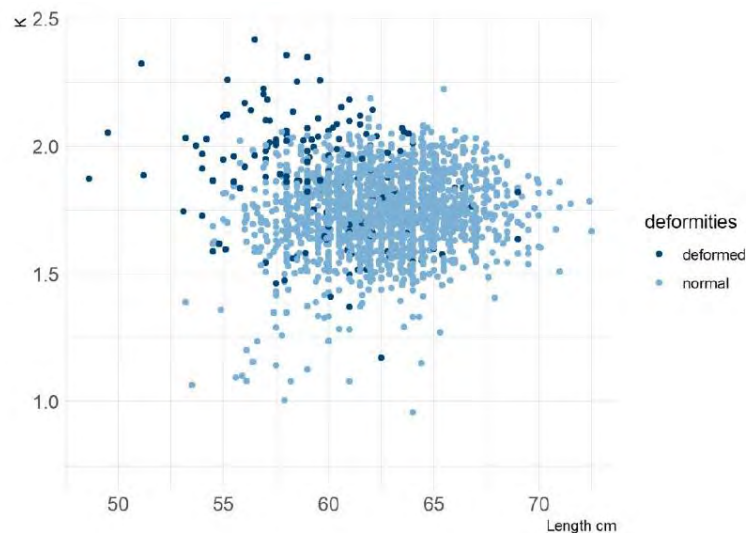


Fig. 3.18 Relationship between length, condition factor, and deformity.

Both harvest weight and colour are clearly heritable (0.45 and 0.38, respectively) and associated with family origin at final harvest (Table 3.3, Fig. 3.19 and 3.20) which is concurrent with the post-summer assessment. Harvest weight and colour heritability estimates are higher in the post-summer assessment compared to the final harvest (0.58 and 0.55 vs 0.45 and 0.38), which is expected given that the challenging conditions experienced in summer will influence a wider pedigree-associated expression of phenotypes associated with pigment retention and growth. The harvest assessment also only included the top grade of fish, which may have also reduced the ability to differentiate between high and low family performance and subsequently the heritability. Another critical finding was that both colour and harvest weight traits had a strong genetic correlation ( $> 0.6$ ) between the post-summer and final harvest assessment, supporting the suitability of the final harvest assessment to select for individuals with improved flesh colour and weight retention during the challenging summer environment. This is also supported by a good level of correlation of the family means for both traits at harvest and post-summer (Fig. 3.21 and 3.22).

Mortality had smaller negative genetic correlations with both colour and weight traits (Table 3.3 and Fig. 3.23) which is also supported by that found in the post-summer assessment, where generally the smallest and palest families are also associated with families of the highest mortality.

**Table 3.3** Trait heritability estimates (white text, blue background), genetic correlations (upper diagonal panel) and phenotypic correlation statistics (lower diagonal panel) considering all three assessments together. Phenotypic correlations calculation is possible for some traits only.

<i>TRAIT</i>	Harvest weight kg	Colour at harvest	Mortality (Summer)	Weight kg (post-summer)	Colour (post-summer)
<i>Harvest weight kg</i>	0.45	0.07	-0.07	0.67	0.05
<i>Colour at harvest</i>	0.39	0.38	-0.12	0.16	0.66
<i>Mortality (Summer)</i>			0.37	-0.16	-0.11
<i>Weight kg (post-summer)</i>				0.58	0.42
<i>Colour (post-summer)</i>				0.53	0.55

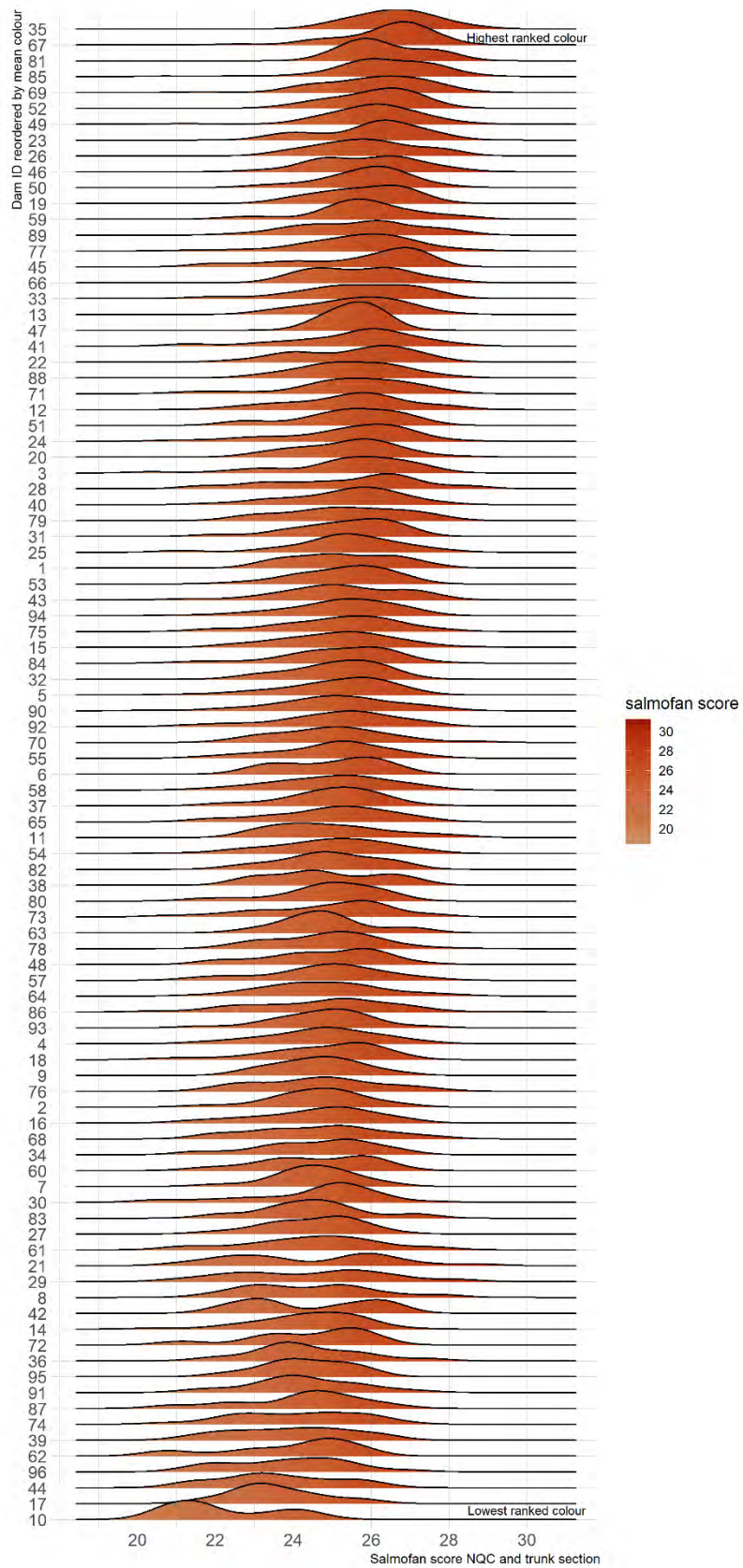


**Fig. 3.19** Distribution of individual colour values grouped by family (dam) reordered by mean family colour (mean relative sum of NQC and dorsal slice).

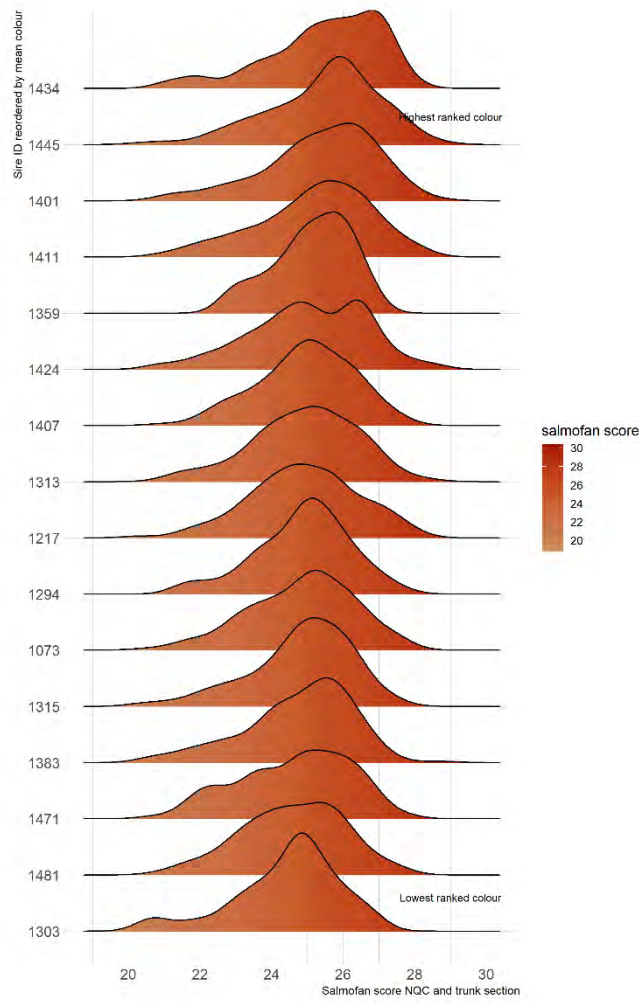


**Fig. 3.20** Distribution of individual colour values grouped by sire reordered by mean sire colour (mean relative sum of NQC and dorsal slice)

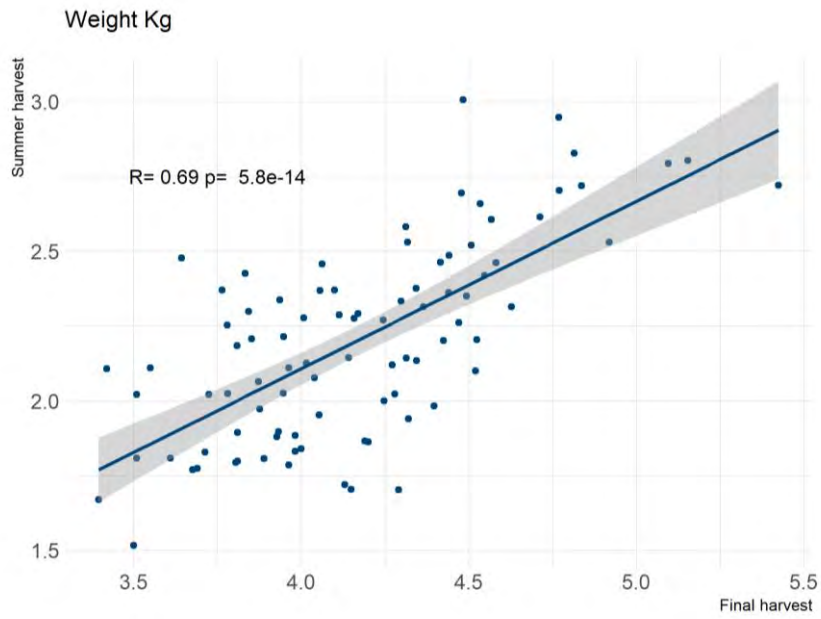


**Fig. 3.21** Relationship between family means of post-summer and harvest weight.

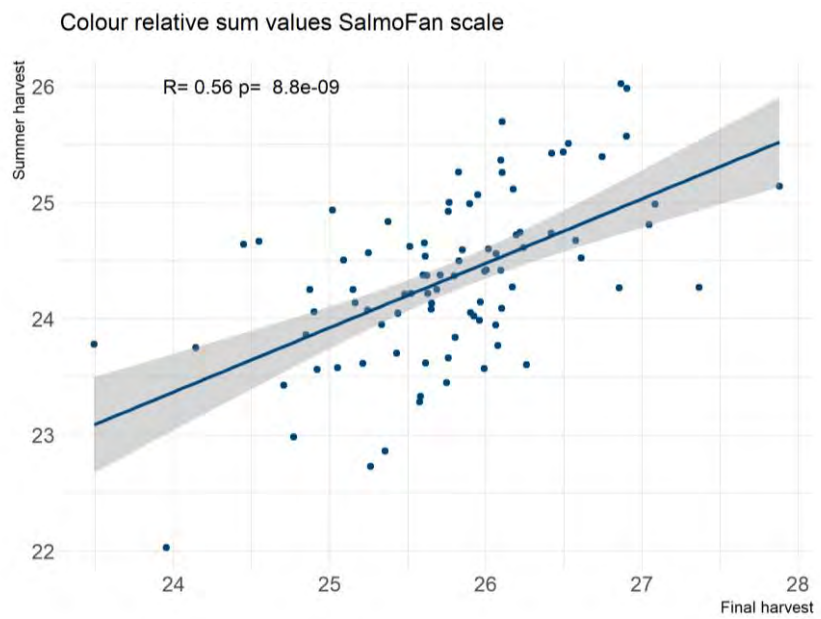


**Fig. 3.22** Relationship between family means of post-summer and harvest flesh colour.

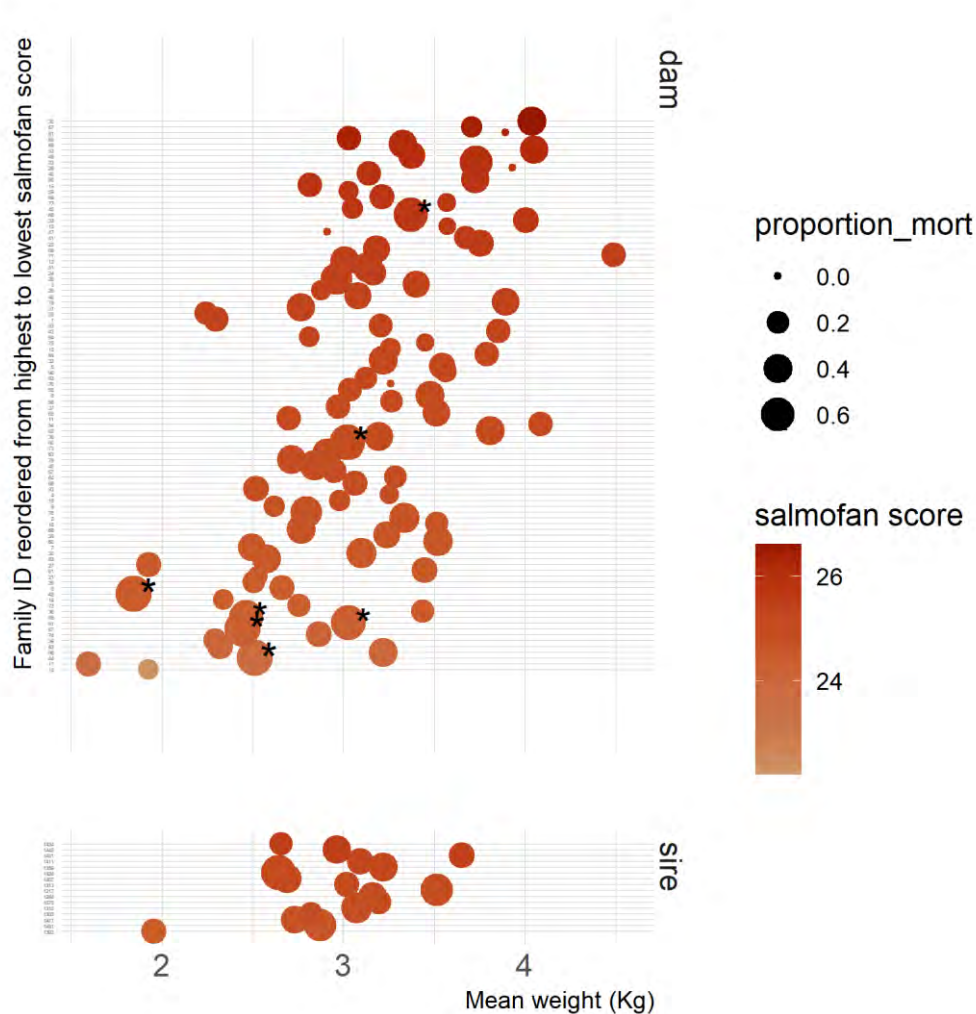


**Fig. 3.23** Relationship between family mean flesh colour, harvest weight and proportion of mortality. High mortality families indicated are denoted by an asterisk.

### 3.3.4 Conclusions

This trial represented the first thorough genetic investigation ever conducted on Petuna commercial stocks with more than 5000 fish genotyped and a major effort at all levels of the company. As detailed in the previous paragraphs, the investigation focused at first on assessing the possible genetic component underlying flesh colour loss post-summer displayed by part of the stock and also allowed parallel novel molecular investigations on flesh colour loss (section 2). The original aim of the trial was to confirm that flesh colour loss (i.e. general paleness or banding) and/or recovery from thermal stress, had a genetic component. A further aim was then added due to growing interest within Petuna, which was to obtain a complete picture of the genetic effect on performance of its stocks and eventually establish a selective breeding program.

Three assessments were carried out as part of the trial, investigating the genetics of summer mortality, post-summer performance and harvest performance. These three assessments taken together, were critical to understand whether or not the best performing families and with best quality were actually being so throughout all the critical stages of the marine production cycle and were also less impacted by mortality. The main results of the trial are:

- The **genetic component of summer mortality was confirmed** (presence of specific families strongly associated with higher mortality at high summer temperatures).
- The result mentioned above is also accompanied by the confirmation that **less thermal tolerant families are also affected by mortality when the temperature is not high yet** to affect the majority of the population, demonstrating the suitability of using this trait for selective breeding of more robust and tolerant to increasing seawater temperature offspring.
- Families with the highest proportion of mortality were also associated with smaller weights and lighter flesh colour (both post-summer and at harvest) confirming how **poor performing fish are generally more affected by summer mortality likely due to their lower thermal stress tolerance**.
- Medium heritability for banding and high heritability for both flesh colour and size were observed confirming **a clear genetic effect on localised and general flesh colour loss** and trait suitability for selective breeding.
- All traits assessed are correlated in a way that selection based on one would not lead to negative selection on another (critical finding for selective breeding purposes).
- **High heritability for both size and flesh colour confirmed at harvest.**
- Both size and flesh colour had a strong genetic correlation between the post-summer and harvest confirming that **individuals with better flesh colour and weight retention after the challenging summer conditions are also the best performing at harvest**.

All in all, this trial has produced critical and, in part novel, findings on the genetic component of flesh colour loss and performance of fish exposed to high summer water temperatures. The very clear and encouraging results have led to the establishment of the Petuna breeding program which has recently produced for the first time a generation of individuals with genetic gain. This represents the first step of producing fish that are more robust and thermal tolerant. This is particularly important in light of climate change and increasing seawater temperature, which will make it harder to produce Atlantic salmon, not just in Tasmania but all around the world. Although being one of the first places where the impact of climate change on Atlantic salmon aquaculture will be felt, Tasmania also represents an optimal experimental ground. In fact, here the industry can start experimenting and get ready, before other countries do, to cope with the new environmental challenges and eventually success in breeding “climate-proof” fish. The findings of this trial have demonstrated that this is achievable.

# Conclusions

This report has produced critical findings and addressed an important commercial issue with considerable economic impact on Atlantic salmon aquaculture: flesh colour loss following high summer water temperatures. This was done by establishing clear aims, all of them providing realistic expectations to be achieved. The tasks carried out during the project were diverse and had both a commercial as well as a deep scientific and analytical approach and produced new knowledge with likely spill-out to the rest of the industry.

It is appropriate to repeat in this section the aims of the project, which were three:

1. Identify the type of flesh colour variations and their prevalence at Petuna and assess the magnitude of their economic impact.
2. Identify molecular events associated with reduced flesh colour in several tissues.
3. Establish if there is a correlation between genetic background and reduced flesh colour.

With regard to **aim 1**, the investigators produced a literature review on the issue followed by an assessment of economic impact.

**Aim 2** involved two different sample collection events (2017 and 2019) and a considerable amount of analytical work which contributed to two different PhD projects at USC. So far two peer reviewed publications have been produced from that work and more are expected to be produced in the next few months. The tasks part of this aim helped to expand our knowledge on the mechanisms behind flesh colour variation and loss in Atlantic salmon following exposure to high summer seawater temperature. The tasks went from a general assessment of the occurrence and development of the trait to deeper investigations which contributed to the expansion of our knowledge of the mechanisms behind a complex phenomenon as flesh pigmentation in Atlantic salmon. The deeper investigations involved microbiome effect exploration as well as detection of the genes behind the molecular mechanisms and metabolic analyses of pigment distribution. By employing different techniques, we have shown how the phenomenon occurs, reoccurs, and develops during the production cycle. Most importantly, we have demonstrated a significant correlation between the microbiota and fillet colour, meaning that fish affected by colour loss or having good colour have different microbiota and that there are distinct groups of genes in the gut and liver expressing in either the fish affected by colour loss or the ones having good colour. We have also shown, for the first time, that *Carnobacterium* is abundant in fish not affected by flesh colour loss, shedding further light on the possible key role played by specific microbiota, and that different parts of the fish digestive system (i.e. pyloric caeca and hind gut) have distinct microbiota which can or cannot correlate with flesh colour loss. Furthermore, the gene expression analysis of critical tissues involved in the carotenoid metabolism, suggested that localised flesh colour loss is likely the result of a proteolytic process in muscle. Its degradation and loss of structural integrity leads to releasing carotenoids which are then transported with lipids. Finally, we provided new insights into the dynamics of two carotenoids commonly used in salmonids diets, Astaxanthin and Canthaxanthin.

**Aim 3** involved a long planning, set up phase and execution in order to create the first population ever at Petuna with known genetics and then to study it to understand the genetic effect of flesh colour loss and thermal tolerance in Atlantic salmon. As previously mentioned, this task attracted in a relatively short period of time a lot of attention within the company and eventually led to the establishment of a selective breeding program aiming at producing fish with improved flesh colour and thermal

tolerance and overall performance in a fast changing environment. From population creation to final assessment, this aim took two years to be completed and required a huge effort at all levels to make it succeed. After all the analytical work, we have demonstrated the presence of a clear genetic effect on flesh colour loss (as well as good colour) and performance in individuals assessed both post-summer (after thermal stress) and at harvest. A genetic effect was also found for thermal tolerance (reduced mortality) at high summer temperatures. Overall, we showed that it is possible to produce fish that are more robust and capable to withstand increasing seawater temperatures without trading off a critical quality trait as flesh colour and their performance being affected too much.

In conclusion, this project has shown how particular tasks can attract considerable commercial attention in a relative short period of time when they address directly a commercially relevant issue and offer, even before obtaining the results, methods or tools to tackle that issue. A clear example was a selective breeding program originating by one of the tasks of this project which investigated the genetic effect of flesh colour loss. Furthermore, all the microbiological, molecular and metabolic investigations have shown still how much we can understand about pigmentation in Atlantic salmon and how critical every piece of knowledge is added to the topic will be for all the stakeholders in the industry given the commercial importance of flesh colour as quality and welfare trait.

## Implications

*Assessment of the impact of the outcomes on end users such as management, industry, consumers, etc in Australia (where possible provide a statement of costs and benefits).*

This project has direct impact on the operation in Petuna, where practices have already changed in the context of the formation of a selective breeding program which will continue to benefit the company each generation. The specifics are clearly described in the conclusions section above.

## Recommendations

*For this PROJECT, provide recommendations on the activities or other steps that may be taken to further develop, disseminate or to exploit commercially the results.*

Petuna has adopted a change in practices following the project and will continue to develop their selective breeding program, fine tuning the desired traits. The scientific information secured by this project has been published or will be published in peer reviewed journals within the next 6 months. The close interaction and communication between the academic and industry partners ensure immediate uptake of the project outcomes.

### Further development

*Where this project DOES NOT fully solve or address all issues and more research and/or actions such as management changes are required provide recommendations for next steps.*

There is one area in particular which is worth further exploration.

1. The presence of distinct bacteria in fish with quality flesh colour compared with fish with pale of banded flesh is worth exploring and could end up being part of a probiotic treatment for improved salmon flesh.

# Extension and Adoption

*Outline how the project was (and will continue to be) extended and communicated to the end user, such as managers, other researchers, industry and where applicable the broader community.*

*If possible outline where project outputs were adopted – this may not always be possible at time of writing the final report.*

Scientific publications concerning gene expression and pigment distribution will be submitted within the next 6 months. Petuna management has been kept updated on a regular basis and project outputs adopted as described earlier.

## Project coverage

### 2019

- **www.salmonexpert.cl**  
Describen relación microbiota intestinal-pigmentación del filete en salmon Atlántico (Chilean aquaculture website mentioning our findings on salmon gut microbiota and pigmentation - in Spanish)  
<https://www.salmonexpert.cl/article/describen-relacin-microbiota-intestinal-pigmentacin-del-filete-en-salmn-atlntico/>
- **The Mercury**  
PETUNA'S CATCH OF THE DAY — BREEDING TO CLIMATE-PROOF (Local newspaper mentioning the contribution of this FRDC project to the development of Petuna's selective breeding program).  
[https://www.themercury.com.au/subscribe/news/1/?sourceCode=TMWEB\\_WRE170\\_a\\_GGL&dest=https%3A%2F%2Fwww.themercury.com.au%2Fnews%2Fopinion%2Ftalking-point-catch-of-the-day-how-breeding-can-climateproof-aquaculture%2Fnews-story%2F4ce47e9afb35aa848a15b67cf3891a92&metype=anonymous&mode=premium](https://www.themercury.com.au/subscribe/news/1/?sourceCode=TMWEB_WRE170_a_GGL&dest=https%3A%2F%2Fwww.themercury.com.au%2Fnews%2Fopinion%2Ftalking-point-catch-of-the-day-how-breeding-can-climateproof-aquaculture%2Fnews-story%2F4ce47e9afb35aa848a15b67cf3891a92&metype=anonymous&mode=premium)

### 2020

- **www.fishfarmingexpert.com**  
Breeding project Xelects 'climate proof' fish (International aquaculture website mentioning the contribution of this FRDC project to the development of Petuna's selective breeding program)  
[https://www.fishfarmingexpert.com/article/breeding-project-xelects-climate-proof-fish/?utm\\_campaign=newsletter\\_06\\_10\\_2020&utm\\_source=netflex&utm\\_medium=email](https://www.fishfarmingexpert.com/article/breeding-project-xelects-climate-proof-fish/?utm_campaign=newsletter_06_10_2020&utm_source=netflex&utm_medium=email)

## Glossary

All acronyms were described in the text.

## Project materials developed

At the time of submission, two manuscripts including parts of the investigations carried out during the current FRDC project were published on peer-reviewed journals:

- Nguyen, C.D.H.; Amoroso, G.; Ventura, T.; Elizur, A. Assessing the Pyloric Caeca and Distal Gut Microbiota Correlation with Flesh Color in Atlantic Salmon (*Salmo salar* L., 1758). *Microorganisms* 2020, 8, 1244. <https://doi.org/10.3390/microorganisms8081244>
- Nguyen, C.D.H., Amoroso, G., Ventura, T. *et al.* Atlantic Salmon (*Salmo salar* L., 1758) Gut Microbiota Profile Correlates with Flesh Pigmentation: Cause or Effect?. *Mar Biotechnol* (2020). <https://doi.org/10.1007/s10126-019-09939-1>

# Appendices

## Appendices to section 2.3 and 2.5

### Appendix 1. Table of SNP analysis in salmon presenting different color and banding phenotypes

Note: Several genes are highlighted in red to emphasize interesting SNPs.

#### 1. Low colour-banded fish

Gene name	Individual	Missense	DP:DPR	Note
Serum albumin (alb1)	I22B366	Att/Gtt Ile328Val	2: 0, 2	Carotenoid-related genes
SCARB1-like protein 2 (LOC100534606)	I22B366	aCg/aTg Thr425Met	2: 0, 2	Carotenoid-related genes
fucolectin-3-like (LOC106581127) (lectin family, behaving as true acute phase reactants) <a href="https://www.ncbi.nlm.nih.gov/pmc/articles/PMC3429948/">https://www.ncbi.nlm.nih.gov/pmc/articles/PMC3429948/</a>	I22B260 I22B264 I22B277	aGa/aTa Arg94Ile	69: 4, 65 19: 2, 17 4: 0, 4	DEG
cell division cycle-associated protein 3-like, transcript variant X2 (LOC106583386) (F-box-like protein, protein ubiquitination)	I22B264	Ggt/Agt Gly102Ser	45: 30, 15	DEG
transmembrane protease serine 9-like (LOC106600702)	I21B208 I22B260	cAc/cGc His22Arg	12: 8, 4 5: 2, 3	DEG

(proteolysis, integral component of plasma membrane, to be a novel molecular biomarker of chronic inflammation in the salmon intestine) <a href="https://link.springer.com/article/10.1007/s10126-016-9704-x">https://link.springer.com/article/10.1007/s10126-016-9704-x</a>	I22B264		30: 25, 5	
	I22B277		9: 7, 2	
	I22B366		44: 28, 15	
	I21B208	gTg/gCg Val6Ala	3: 1, 2	
	I22B264		14: 10, 4	
	I22B366		24: 12, 10	
short transient receptor potential channel 7-like, transcript variant X2 (LOC106604872)  central role in mediating apoptosis. <a href="https://www.fasebj.org/doi/10.1096/fj.08-119495">https://www.fasebj.org/doi/10.1096/fj.08-119495</a>	I22B277	tTc/tCc Phe386Ser	4: 0, 4	DEG
	I22B277	gCc/gTc Ala383Val	4: 0, 4	
probable ribonuclease ZC3H12D, transcript variant X2 (LOC106607746)  metal ion binding	I21B208	aCc/aTc Thr52Ile	18: 8, 10	DEG
	I22B366		13: 7, 6	
interferon-induced very large GTPase 1-like, transcript variant X2 (LOC106608810)  (immune response, ntributes to the cellular response to both type I and type II IFNs could lead to cell-autonomous resistance against various pathogens) <a href="https://www.ncbi.nlm.nih.gov/pmc/articles/PMC4519954/">https://www.ncbi.nlm.nih.gov/pmc/articles/PMC4519954/</a>	I21B208	cAg/ctg Gln1743Leu	7: 3, 4	DEG
uncharacterized protein KIAA1211 homolog, transcript variant X3 (LOC106560277)	I22B260	gCc/gTc Ala192Val	30: 9, 21	DEG
leucine-rich repeat-containing protein 49-like, transcript variant X4 (LOC106562345)	I22B260	aTGGCA/aCGGCC MetAla402-	4: 0, 4	DEG
	I22B366	403ThrAla	3: 0, 3	

	I22B366	AAGGgg/AAGAgg LysGly800- 801LysArg	35: 15, 18	
probable glutamate receptor (LOC106567361)	I22B260	gAa/gGa Glu314Gly	8: 2, 6	DEG
uncharacterized LOC106569063, transcript variant X2 (LOC106569063)	I22B260	gCt/gTt Ala65Val	75: 50, 25	DEG
RING finger protein 223-like (LOC106572190)	I22B264	Gcc/Acc Ala149Thr	46: 17, 29	DEG
	I22B277		11: 4, 7	
	I21B208	aCg/aTg Thr42Met	14: 7, 7	
aminopeptidase N-like (LOC106573760)	I22B264	Gac/Tac Asp912Tyr	44: 32, 12	DEG
Metalloproteinase inhibitor 3 (timp3)	I21B208	ttG/ttT Leu93Phe	20: 12, 8	DEG
zinc finger, DHHC-type containing 16 (zdhhc16)	I21B208	Atg/Ctg Met120Leu	5: 0, 5	DEG
	I22B260		12: 9, 3	
	I22B277	cGg/cAg Arg293Gln	12: 7, 5	
solute carrier family 40 (iron-regulated transporter), member 1, transcript variant X1 (slc40a1)	I21B208	cAg/cGg Gln403Arg	13: 9, 4	DEG
dual oxidase 2-like (LOC106584698)	I22B260	cGg/cAg Arg974Gln	157: 77, 80	DEG
	I22B264		79: 61, 18	
	I22B277		29: 24, 5	
	I22B366		104: 64, 40	

	I22B260	gCc/gAc Ala740Asp	101: 54, 47	
	I22B264		54: 35, 19	
	I22B277		16: 10, 6	
	I22B366		71: 50, 21	
	I22B260	Agt/Ggt Ser267Gly	129: 76, 53	
	I22B264		61: 23, 38	
	I22B277		16: 11, 5	
	I22B366		70: 31, 39	
<a href="#">dual oxidase maturation factor 1-like (LOC106584699)</a>	I21B208	Ctc/Ttc Leu55Phe	3: 0, 3	
	I22B260		125: 55, 70	
	I22B264		113: 78, 35	
	I22B277		35: 15, 20	
	I22B366		80: 51, 29	
	I22B260	Gct/Act Ala213Thr	44: 20, 24	
	I22B264		66: 19, 47	
	I22B277		18: 3, 15	
	I22B366		37: 15, 22	
	I22B260	gAa/gGa Glu239Gly	40: 17, 23	

	I22B264		57: 20, 37	
	I22B277		15: 4, 11	
	I22B366		46: 17, 29	
<b>NADPH oxidase activator 1 (nox1)</b>	I22B366	Ccc/Tcc Pro379Ser	29: 12, 17	DEG
<b>beta-carotene oxygenase 2 like (LOC101448038)</b>	I22B277	Cct/Tct Pro226Ser	30: 28, 2	Carotenoid-related genes
	I22B260	Tat/Cat Tyr213His	59: 55, 4	
	I22B277	cTg/cCg Leu60Pro	14: 12, 2	
	I22B277	cCa/cTa Pro52Leu	14: 12, 2	
	I21B208	aGc/aTc Ser2Ile	29: 27, 2	
<b>kinesin-like protein KIFC3, transcript variant X8 (LOC106587071)</b>	I22B277	gGa/gCa Gly443Ala	18: 8, 10	DEG
<b>beta-carotene 15,15'-monooxygenase 1 (bcmo1)</b>	I22B277	Ttt/Ctt Phe321Leu	16: 12, 4	Carotenoid-related genes
<b>multidrug resistance-associated protein 9-like (LOC106588137)</b>	I21B208	aCa/aTa Thr83Ile	14: 6, 8	DEG
	I22B260		10: 7, 3	
	I22B264		10: 8, 2	
<b>serine-aspartate repeat-containing protein F-like, transcript variant X2 (LOC106588966)</b>	I21B208	CAC/AGc His305Ser	16: 0, 16	DEG
	I22B264		10: 2, 8	
	I21B208	aAg/aTg Lys479Met	19: 0, 19	

	I22B264		13: 3, 10	
	I22B277		2: 0, 2	

DP: Read Depth

DPR: Number of observations for each allele (RO, AO)

RO: Reference allele observation count

AO: Alternate allele observation count

## 2. High colour-no banding fish

Gene name	Individual	Missense	DP:DPR	Note
SH3 domain-binding protein 5-like (LOC106581253)	I26N394	aaG/aaC Lys413Asn	31: 9, 22	DEG
	I27N377		18: 4, 14	
lysozyme g-like, transcript variant X1 (LOC106587409)	I26N261	Gtc/Atc Val97Ile	9: 2, 7	DEG
Fc receptor-like protein 5, transcript variant X2 (LOC106592009)	I27N377	Cct/Tct Pro485Ser	27: 7, 20	DEG
	I27N377	cAa/cGa Gln76Arg	26: 11, 15	
	I26N261	gAc/gGc Asp74Gly	7: 3, 4	
	I26N291		2: 0, 2	
	I27N377		26: 17, 9	
	I26N261	gaG/gaC Glu36Asp	6: 1, 5	

	I26N291		3: 0, 3	
	I27N377		30: 25, 5	
	I26N394	aGc/aTc Ser29Ile	4: 1, 3	
	I27N377		30: 5, 25	
	I27N377	gCc/gAc Ala16Asp	24: 20, 4	
cadherin-2-like (LOC106599706)	I27N377	gCg/gTg Ala646Val	15: 6, 9	DEG
myosin-10-like (LOC106601165)	I27N377	Atg/Gtg Met1194Val	14: 0, 14	DEG
synaptopodin-2-like, transcript variant X2 (LOC106602736)	I26N324	caACCC/caACAc GlnPro717-718GlnHis	37: 1, 34	DEG
Cbl proto-oncogene B, E3 ubiquitin protein ligase, transcript variant X1 (cblb)	I26N324	gCa/gTa Ala271Val	4: 0, 4	DEG
tenomodulin-like (LOC106604450)	I27N377	Cgc/Tgc Arg264Cys	7: 3, 4	DEG
glutathione S-transferase P (LOC100136484)	I26N291	Ggg/Tgg Gly13Trp	5: 0, 5	Carotenoid-related genes
interferon-induced very large GTPase 1-like, transcript variant X2 (LOC106608810)	I26N261	Acc/Gcc Thr154Ala	8: 0, 8	DEG
	I26N291		6: 4, 2	
	I26N261	Agg/Ggg Arg189Gly	8: 0, 8	
	I26N291		8: 2, 6	
UPF0577 protein KIAA1324-like (LOC106609435)	I26N261	Ata/Tta Ile809Leu	13: 0, 13	DEG
	I26N291		4: 0, 4	

ovochoymase-2-like, transcript variant X1 (LOC106610245)	I26N261	cAa/cGa Gln322Arg	21: 0, 21	DEG
ATP-binding cassette, sub-family G (WHITE), member 2 (Junior blood group) (abcg2)	I26N291	Gac/Aac Asp732Asn	40: 27, 12	Carotenoid-related genes
echinoderm microtubule-associated protein-like 1, transcript variant X5 (LOC106610626)	I26N324	cCt/cAt Pro640His	7: 0, 7	DEG
von Willebrand factor-like (LOC106561860)	I26N291 I27N377	Ttt/Ctt Phe428Leu	4: 0, 4 42: 0, 42	DEG
beta-1,3-galactosyl-O-glycosyl-glycoprotein beta-1,6-N-acetylglucosaminyltransferase 3-like (LOC106564978)	I26N394	CTa/CCa Leu21Pro	14: 0, 12	DEG
myotonin-protein kinase-like (LOC106567543)	I27N377	cAg/cTg Gln477Leu	6: 0, 6	DEG
aminopeptidase N-like (LOC106573760)	I26N261 I26N394 I27N377	atT/atG Ile948Met	4: 1, 3 9: 7, 2 13: 7, 6	DEG
probable polyketide synthase 1 (LOC106579692)	I26N324	ggCGAa/ggCAAa GlyGlu374-375GlyLys	22: 2, 18	DEG
solute carrier family 40 (iron-regulated transporter), member 1, transcript variant X1 (slc40a1)	I26N261	aaG/aaT Lys278Asn	9: 4, 5	DEG
5-aminolevulinate synthase, nonspecific, mitochondrial-like, transcript variant X2 (LOC106583798)	I26N291 I26N394	Ggg/Tgg Gly414Trp	34: 17, 17 52: 29, 23	DEG

beta-carotene oxygenase 2 like (LOC101448038)	I26N261	gCc/gTc Ala263Val	77: 73, 4	Carotenoid-related genes
microtubule-actin cross-linking factor 1-like, transcript variant X18 (LOC106588461)	I26N261	Caa/Aaa Gln3456Lys	5: 0, 5	DEG
	I27N377		4: 0, 4	
	I27N377	gGAAGA/gAAAGC GlyArg3656- 3657GluSer	8: 0, 8	
	I26N261	Gaa/Aaa Glu3851Lys	3: 0, 3	
	I27N377		12: 0, 12	
	I26N261	gaG/gaC Glu5559Asp	5: 0, 5	
ATP-binding cassette, sub-family G (WHITE), member 8 (abcg8)	I26N261	Ccc/Acc Pro21Thr	964: 518, 446	
	I26N291		857: 460, 397	
	I27N377		541: 282, 259	
extended synaptotagmin-like protein 2, transcript variant X2 (esyt2)	I26N291	Tcc/Gcc Ser681Ala	16: 8, 8	
	I26N394		18: 6, 12	
	I27N377		48: 22, 24	
non-SMC condensin II complex subunit G2 (ncapg2)	I26N291	Gtc/Ttc Val55Phe	8: 2, 6	DEG
	I26N394		10: 5, 5	
	I27N377		22: 13, 9	

probable polyketide synthase 1 (LOC106590295)	I26N394	Aag/Cag Lys796Gln	19: 11, 8	DEG
---	---------	-------------------	-----------	-----

**DP: Read Depth**

**DPR: Number of observations for each allele (RO, AO)**

**RO: Reference allele observation count**

**AO: Alternate allele observation count**

## Appendix 2. Differentially expressed genes in tested tissues

### Appendix 2.1. Up and downregulated DEGs in the front dorsal muscle tissue with HN compared to HB group.

Gene name	Production name	Log2 Fold Change HN-HB
<i>Muscle fiber composition protein network</i>		
mypc1	Myosin-binding protein C, slow-type	7.53
LOC106592374	myosin-binding protein C, fast-type-like	7.24
LOC106601538	myosin-binding protein C, fast-type-like, transcript variant X27	6.13
LOC106566456	troponin C, skeletal muscle-like	4.65
LOC106593408	myosin heavy chain, fast skeletal muscle-like	2.56
LOC106561014	troponin I, fast skeletal muscle-like	4.65
LOC106608163	thrombospondin-1-like	2.90
LOC106587936	troponin T, fast skeletal muscle isoforms-like	2.98
LOC106592039	troponin I, fast skeletal muscle-like, transcript variant X2	5.55
LOC106598177	myosin-binding protein C, slow-type-like	8.15
LOC106561017	troponin I, fast skeletal muscle-like	2.50
LOC106586085	myosin heavy chain, fast skeletal muscle-like	3.05
LOC106596578	myosin heavy chain, fast skeletal muscle-like	2.86
LOC106593168	myosin heavy chain, fast skeletal muscle-like	-2.79
LOC106598781	myosin-3-like	-6.29
LOC106564183	myosin heavy chain, fast skeletal muscle-like	-3.03
<i>Skeletal muscle collagens</i>		
LOC106600852	collagen alpha-1(I) chain-like	2.01
LOC100286406	collagen alpha-1(I) chain	2.13
LOC106596897	collagen alpha-1(XI) chain-like	2.09
LOC106569492	collagen alpha-1(XI) chain-like	2.40
LOC106610773	collagen alpha-1(XII) chain-like, transcript variant X2	2.27

LOC106570233	collagen alpha-1(XXII) chain-like	2.35
<i>Calcium ion binding</i>		
LOC106591443	parvalbumin alpha	4.63
LOC106602975	endosialin-like	2.12
LOC106586814	epidermal growth factor-like protein 6	2.13
LOC106590058	cadherin-20-like, transcript variant X3	2.60
LOC106608042	otoferlin-like	4.65
LOC106608069	otoferlin-like	3.04
LOC100380741	protein kinase C-binding protein NELL2	4.71
LOC106600583	calcium/calmodulin-dependent protein kinase II inhibitor 2-like	4.67
LOC106603872	stanniocalcin-2-like	-3.14
calcoco1	calcium binding and coiled-coil domain 1	-5.09
cacna2d4	calcium channel, voltage-dependent, alpha 2/delta subunit 4, transcript variant X3	-2.59
<i>Lipid and fatty acid metabolism</i>		
LOC106577511	apolipoprotein C-I-like	-2.15
LOC106577506	apolipoprotein Eb-like	-2.93
<i>Transporters</i>		
slc7a8	solute carrier family 7 (amino acid transporter light chain, L system), member 8, transcript variant X2	-2.75
LOC106577803	large neutral amino acids transporter small subunit 2-like	-4.29
<i>Enzymes, metabolic processes</i>		
LOC106566977	SRSF protein kinase 2-like	2.94
LOC106584036	leptin receptor-like, transcript variant X2	2.32
LOC106609470	casein kinase I isoform epsilon-like, transcript variant X2	2.76
LOC106563065	cGMP-dependent protein kinase 1-like, transcript variant X3	2.75
LOC106577304	inactive carboxypeptidase-like protein X2	2.09
LOC106585387	uncharacterized HIT-like protein Synpcc7942_1390	3.31

LOC106564838	inositol polyphosphate 5-phosphatase K-like	-2.04
--------------	---	-------

**Appendix 2.2. Up and downregulated DEGs in the back central muscle tissue with HN or HB compared to P group.**

Gene name	Production name	Log2 Fold Change	
		HN-P	HB-P
<i>Muscle fiber composition protein network</i>			
LOC100194643	myosin, light polypeptide 3-3		2.35
LOC106600781	myosin heavy chain, fast skeletal muscle-like		2.35
gdf-8	myostatin 1b		2.02
LOC106593179	myosin heavy chain, fast skeletal muscle-like		2.84
LOC106587486	actin, alpha skeletal muscle 2-like	3.19	2.99
LOC106575818	myosin light chain 3, skeletal muscle isoform-like	2.44	2.27
LOC106564730	actin, alpha skeletal muscle 2-like	2.7	2.57
LOC106589658	actin, alpha skeletal muscle 2-like	3.28	3.04
LOC106610721	actin, alpha skeletal muscle 2-like	2.51	2.51
LOC100194559	myosin binding protein H-like	2.31	2.13
LOC106596411	myosin heavy chain, fast skeletal muscle-like	2.54	2.41
LOC106593081	myosin heavy chain, fast skeletal muscle-like	2.76	3.86
LOC106566023	myosin-binding protein H-like, transcript variant X2	4.13	3.05
LOC106604357	thymosin beta	3.83	2.95
LOC106587535	myomesin-2-like, transcript variant X1	2.35	
LOC100194684	myomesin-2, transcript variant X4	2.09	
tpm1	tropomyosin 1 (alpha)	2	
LOC106574005	obscurin-like, transcript variant X1		-6.3
LOC106571564	tropomyosin beta chain, transcript variant X5	-5.7	-5.21
fhl1	Four and a half LIM domains protein 1	-3.19	-4.1
neb	nebulin	-5.7	-5

LOC106576332	myosin-binding protein C, slow-type-like	-3.97	-3.82
LOC106613530	obscurin-like, transcript variant X4	-3.54	-4.41
LOC106570192	tropomyosin alpha-3 chain, transcript variant X6	-3.48	-3.82
mybpc1	myosin binding protein C, slow type, transcript variant X17	-4.64	-4.25
LOC106587936	troponin T, fast skeletal muscle isoforms-like	-4.34	-4.66
tpm3	tropomyosin 3	-2.87	-2.87
LOC106574005	obscurin-like, transcript variant X1	-6.54	
<i>Calcium ion binding</i>			
pvalb2	parvalbumin 2		2.5
LOC106579972	calcium-binding mitochondrial carrier protein SCaMC-2-A-like	2.44	2.53
LOC106601823	parvalbumin beta 1	2.43	2.05
LOC106601787	parvalbumin beta 1	2.51	2.33
LOC100196652	calsequestrin-like	2.91	2.76
LOC106577762	perforin-1-like	3.22	2.63
LOC100137051	parvalbumin beta-like	2.81	2.46
LOC106601825	parvalbumin beta 1	3.67	3.22
LOC106606665	parvalbumin beta 1-like	3.76	3.04
LOC100195738	calcium/calmodulin-dependent protein kinase type II delta 1 chain	2.7	
LOC100194643	myosin, light polypeptide 3-3	2.46	
LOC106602935	calcium/calmodulin-dependent protein kinase type II subunit alpha, transcript variant X1	2.35	
LOC106584496	fibulin-1-like, transcript variant X2	2.05	
LOC106586628	calsequestrin-2-like	-5.92	
calcoco1	calcium binding and coiled-coil domain 1	-5.49	
LOC106572132	multiple epidermal growth factor-like domains protein 6, transcript variant X1	-3.17	
cacna2d4	calcium channel, voltage-dependent, alpha 2/delta subunit 4, transcript variant X3	-2.46	

LOC106606402	soluble calcium-activated nucleotidase 1-like	-2.1	
<i>Lipid and fatty acid metabolism</i>			
LOC106573544	lipoprotein lipase-like, transcript variant X3		-2.39
LOC106608508	fatty acid-binding protein, intestinal-like	-2.21	-2.58
lipe	lipase, hormone-sensitive, transcript variant X1	3.21	4.33
LOC106573544	lipoprotein lipase-like, transcript variant X3	-2.76	
LOC106585385	long-chain-fatty-acid--CoA ligase ACSBG2-like	-4.65	
LOC106580039	long-chain-fatty-acid--CoA ligase ACSBG2-like, transcript variant X3	-2.54	
<i>Transporters</i>			
LOC106566379	solute carrier family 25 member 33, transcript variant X3	2.54	2.59
slc1a5	solute carrier family 1 (neutral amino acid transporter), member 5	2.46	2.31
LOC106607984	solute carrier family 22 member 16-like, transcript variant X1	3.65	3.52
s2533	Solute carrier family 25 member 33	2.79	2.68
slc1a4	solute carrier family 1 (glutamate/neutral amino acid transporter), member 4	2.38	2.21
LOC106588049	asc-type amino acid transporter 1-like	4.4	4.2
LOC106588047	asc-type amino acid transporter 1-like	3.44	2.79
LOC106591035	asc-type amino acid transporter 1-like	3.41	
slc5a12	solute carrier family 5 (sodium/monocarboxylate cotransporter), member 12	6.12	
LOC106577148	monocarboxylate transporter 9-like, transcript variant X2	3.62	
LOC106605319	ammonium transporter Rh type B, transcript variant X1	2.67	
LOC106581541	high affinity cationic amino acid transporter 1-like	2.54	
LOC106601550	excitatory amino acid transporter 2-like, transcript variant X2	2.26	
LOC106580117	solute carrier family 2, facilitated glucose transporter member 11-like	2.03	
LOC100136540	solute carrier family 2, facilitated glucose transporter member 4	2.02	

slc15a1	solute carrier family 15 member 1	-4.35	
LOC106575053	solute carrier family 15 member 1-like	-4.35	
LOC106607031	solute carrier family 25 member 38-B-like, transcript variant X2	-3.3	
LOC106560560	solute carrier family 25 member 47-B-like, transcript variant X2	-2.95	
LOC106611409	solute carrier family 22 member 13-like, transcript variant X7	-2.84	
LOC106599714	solute carrier family 22 member 23-like, transcript variant X1	-2.2	
<i>Enzymes, metabolic processes</i>			
LOC106593297	ornithine aminotransferase, mitochondrial-like		2.56
LOC106603297	melatonin receptor type 1C-like, transcript variant X1		2.13
LOC106608345	L-threonine 3-dehydrogenase, mitochondrial-like, transcript variant X3	2.98	3.18
LOC106577392	ornithine aminotransferase, mitochondrial-like, transcript variant X1	2.77	2.5
LOC106570297	asparagine synthetase [glutamine-hydrolyzing]-like	2.44	2.5
LOC106583536	isotocin receptor-like		2.32
LOC106587738	glycine amidinotransferase, mitochondrial-like	2.54	2.21
abec2	Probable C->U-editing enzyme APOBEC-2	2.43	2.13
gadl1	glutamate decarboxylase-like 1	4.64	3.65
LOC106594092	acidic amino acid decarboxylase GADL1-like	4.37	3.93
LOC106595761	glycine amidinotransferase, mitochondrial-like	2.51	2.29
LOC106569611	nicotinamide riboside kinase 2-like, transcript variant X1	3.02	3.33
LOC106585298	L-serine dehydratase/L-threonine deaminase-like	7.98	6.55
LOC106613676	nicotinamide riboside kinase 2-like, transcript variant X1	2.6	2.77
LOC106579679	glucose-fructose oxidoreductase domain-containing protein 1-like, transcript variant X3		2.15
LOC106599743	myosin light chain kinase 2, skeletal/cardiac muscle-like, transcript variant X1		2.2
LOC106585270	bifunctional methylenetetrahydrofolate dehydrogenase/cyclohydrolase, mitochondrial-like	3.23	

LOC106577381	carbohydrate sulfotransferase 15-like	2.8	
LOC106593297	ornithine aminotransferase, mitochondrial-like	2.76	
prlr	prolactin receptor, transcript variant X2	2.75	
fadsd5	delta-5 fatty acyl desaturase, transcript variant X2	2.44	
LOC106582230	arylsulfatase D-like, transcript variant X2	2.43	
tpi1b	triosephosphate isomerase 1b	2.36	
LOC106572073	serine/threonine-protein kinase pim-1-like	2.14	
LOC106576221	carbohydrate sulfotransferase 11, transcript variant X1	2.02	
LOC100136484	glutathione S-transferase P	2.01	
LOC106561982	cathepsin L1-like		-3.28
LOC106611051	steroid hormone receptor ERR2-like, transcript variant X6		-3.91
ppip5k1	diphosphoinositol pentakisphosphate kinase 1, transcript variant X22		-2.67
adgrd1	adhesion G protein-coupled receptor D1, transcript variant X1	-3.08	-2.43
LOC106588431	glyceraldehyde-3-phosphate dehydrogenase-like	-5.92	-5.97
LOC106583986	microtubule-associated serine/threonine-protein kinase 2-like	-2.6	-2.02
LOC106587203	AMP deaminase 3-like, transcript variant X1	-5.59	-4.54
LOC106573163	AMP deaminase 3-like	-3.06	
ampd3	adenosine monophosphate deaminase 3	-2.56	
LOC106570220	CMP-N-acetylneuraminate-beta-galactosamide-alpha-2,3-sialyltransferase 1-like, transcript variant X1	-2.81	
LOC106575774	glycerol-3-phosphate dehydrogenase, mitochondrial-like, transcript variant X2	-2.33	
ppip5k1	diphosphoinositol pentakisphosphate kinase 1, transcript variant X22	-2.3	
LOC106607477	pyruvate dehydrogenase (acetyl-transferring) kinase isozyme 2, mitochondrial-like, transcript variant X2	-2.23	
LOC106561670	L-lactate dehydrogenase B-A chain-like, transcript variant X1	-2.08	
<i>Heat shock protein, Oxidative stress</i>			

LOC106588457	interleukin-11-like	2.69	2.05
LOC106599689	heat shock protein 30-like	3.92	
LOC100380717	heat shock 70 kDa protein 4, transcript variant X5	2.29	
LOC106567403	heat shock protein beta-1-like	2.07	
hsp11	Heat shock protein Hsp-16.1/Hsp-16.11	2.02	
hsp90ab1	heat shock protein 90kDa alpha (cytosolic), class B member 1	-2.39	

**Appendix 2.3. Up and downregulated DEGs in the pyloric caeca with HN or HB compared to P group.**

Gene name	Production name	Log2 Fold Change	
		HN-P	HB-P
<i>Muscle fiber composition protein network</i>			
LOC106566457	troponin C, skeletal muscle-like		2.07
LOC106573503	tropomyosin alpha-1 chain-like, transcript variant X13	2.04	
LOC106574241	desmin-like	2.3	
LOC106567840	unconventional myosin-Ic-like, transcript variant X9	2.21	
LOC106589147	myosin-11-like	3.43	
LOC106578961	actin, aortic smooth muscle	2.3	
LOC106575168	desmin-like	2.1	
LOC106587486	actin, alpha skeletal muscle 2-like	3.62	
LOC106564730	actin, alpha skeletal muscle 2-like	2.45	
LOC106591024	alpha-actinin-1-like	2.21	
LOC106606315	myosin heavy chain, embryonic smooth muscle isoform-like	3.3	
<i>Skeletal muscle collagens</i>			
LOC106567923	collagenase 3-like	2.61	
LOC106574770	collagen alpha-1(VIII) chain-like	3.1	
<i>Lipid and fatty acid metabolism</i>			
LOC106576157	patatin-like phospholipase domain-containing protein 2, transcript variant X1		3.01

LOC106569632	apolipoprotein A-I-like	3.98	5.73
LOC106577499	apolipoprotein A-I-like	2.21	2.58
LOC106605692	apolipoprotein A-IV-like	2.18	2.46
apoc1	Apolipoprotein C-I	4.54	3.48
LOC106605691	apolipoprotein A-IV-like	4.33	4.34
LOC106605686	apolipoprotein C-II-like	2.61	
elovl2	ELOVL fatty acid elongase 2	3.77	
LOC106613114	retinol-binding protein 2-like, transcript variant X3	2.03	
LOC106577505	apolipoprotein A-IV-like	2.99	
LOC106570214	1-phosphatidylinositol phosphodiesterase-like, transcript variant X2	-2.17	
<i>Transporters</i>			
LOC106560239	sodium-dependent phosphate transport protein 2B-like		5.51
LOC106611642	ATP-binding cassette sub-family A member 1-like, transcript variant X2	3.09	
LOC106604175	solute carrier family 25 member 48-like	3.93	
<i>Enzymes, metabolic processes</i>			
LOC106587091	gamma-butyrobetaine dioxygenase-like, transcript variant X4		2.04
LOC106608185	phospholipase B1, membrane-associated-like, transcript variant X2		7.81
LOC106590330	heme oxygenase-like		2.56
LOC106590030	heme oxygenase-like	2.67	3.43
LOC106583514	acidic mammalian chitinase-like	11.28	11.11
LOC106584746	brain aromatase, transcript variant X4	2.67	3.1
LOC106603538	diacylglycerol O-acyltransferase 2-like, transcript variant X3	3.64	2.48
cyp1a	cytochrome P450 1A	2.79	2.36
LOC106583514	acidic mammalian chitinase-like	11.28	
LOC106590030	heme oxygenase-like	3.39	

LOC106566646	renin-like	2.08	
LOC106565224	protein-glutamine gamma-glutamyltransferase 2-like	2.62	
LOC106566906	protein-glutamine gamma-glutamyltransferase 2-like	2.38	
LOC106567039	glycoprotein-N-acetylgalactosamine 3-beta-galactosyltransferase 1-B-like, transcript variant X2	2.8	
LOC106572886	protein-tyrosine kinase 6-like	4.25	
LOC106579695	leukocyte elastase inhibitor-like	2.25	
LOC106608514	1-phosphatidylinositol 4,5-bisphosphate phosphodiesterase epsilon-1-like, transcript variant X2	2.34	
LOC106570903	granzyme A-like	3.43	
LOC106565054	5'-nucleotidase-like, transcript variant X1	2.27	
ddn1	Duodenase-1	3.13	
LOC106567339	alpha-(1,3)-fucosyltransferase 7-like, transcript variant X1	2.54	
LOC106572314	calcium/calmodulin-dependent protein kinase type 1B-like, transcript variant X1	2.17	
LOC106583798	5-aminolevulinate synthase, nonspecific, mitochondrial-like, transcript variant X2	-2.1	-2.24
LOC106566237	5-aminolevulinate synthase, nonspecific, mitochondrial-like, transcript variant X2	-2.54	
LOC106569008	cholesterol 7-alpha-monooxygenase-like	-2.88	
LOC106608097	sulfotransferase 6B1-like	-2.65	
LOC106579692	probable polyketide synthase 1	-2.37	
<i>Heat shock protein, Oxidative stress and inflammatory response</i>			
LOC106608136	heat shock protein HSP 90-alpha-like		2.52
LOC106574825	OX-2 membrane glycoprotein-like	2.43	
LOC106584280	transcription factor AP-1-like, transcript variant X1		-2.01
LOC106607825	cyclic AMP-dependent transcription factor ATF-3-like	-2.19	-2.03
LOC106563105	complement C1q-like protein 2	-2.31	
LOC106588869	complement C1q-like protein 2	-3.82	

## References

1. Torrissen, O. J., W. Hardy, R., Shearer, K. D., Hardy, R. W. & Shearer, K. D. *Pigmentation of Salmonids: Carotenoid deposition and metabolism*. *Crit Rev Aquat Sci* vol. 1 (1989).
2. Skrede, G. & Storebakken, T. Instrumental colour analysis of farmed and wild Atlantic salmon when raw, baked and smoked. *Aquaculture* **53**, 279–286 (1986).
3. Storebakken, T. *et al.* Carotenoids in diets for salmonids. *Aquaculture* **65**, 279–292 (1987).
4. Torrissen, O. J. & Naevdal, G. Pigmentation of salmonids — Variation in flesh carotenoids of Atlantic salmon. *Aquaculture* **68**, 305–310 (1988).
5. Christiansen, R., Struksnæs, G., Estermann, R. & Torrissen, O. J. Assessment of flesh colour in Atlantic salmon, *Salmo salar* L. *Aquac. Res.* **26**, 311–321 (1995).
6. Torrissen, O. J. Strategies for salmonid pigmentation. *J. Appl. Ichthyol.* **11**, 276–281 (1995).
7. Torrissen, O. J. & Christiansen, R. Requirements for carotenoids in fish diets. *J. Appl. Ichthyol.* **11**, 225–230 (1995).
8. Rye, M. & Gjerde, B. Phenotypic and genetic parameters of body composition traits and flesh colour in Atlantic salmon, *Salmo salar* L. *Aquac. Res.* **27**, 121–133 (1996).
9. Sylvia, G., Morrissey, M. T., Graham, T. & Garcia, S. Changing Trends in Seafood Markets. *J. Food Prod. Mark.* **3**, 49–63 (1996).
10. Torrissen, O. J. Effective use of carotenoids for salmon flesh pigmentation. [https://brage.bibsys.no/xmlui/bitstream/handle/11250/109450/Torrissen\\_1996.pdf?sequence=1](https://brage.bibsys.no/xmlui/bitstream/handle/11250/109450/Torrissen_1996.pdf?sequence=1). (1996).
11. Sigurgisladdottir, S., ØTorrissen, O., Lie, Ø., Thomassen, M. & Hafsteinsson, H. Salmon quality: Methods to determine the quality parameters. *Rev. Fish. Sci.* **5**, 223–252 (1997).
12. Alfnes, F., Guttormsen, A. G., Steine, G. & Kolstad, K. Consumers' Willingness to Pay for the Color of Salmon: A Choice Experiment with Real Economic Incentives. *Am. J. Agric. Econ.* **88**, 1050–1061 (2006).
13. Matthews, S. J., Ross, N. W., Lall, S. P. & Gill, T. A. Astaxanthin binding protein in Atlantic salmon. *Comp Biochem Physiol B Biochem Mol Biol* **144**, 206–214 (2006).
14. Rajasingh, H., Øyehaug, L., Våge, D. I. & Omholt, S. W. Carotenoid dynamics in Atlantic salmon. *BMC Biol.* **4**, 10 (2006).
15. Bell, J. G. *et al.* Flesh Lipid and Carotenoid Composition of Scottish Farmed Atlantic Salmon (*Salmo salar*). *J. Agric. Food Chem.* **46**, 119–127 (1998).
16. Buttle, L., Crampton, V. & Williams, P. The effect of feed pigment type on flesh pigment deposition and colour in farmed Atlantic salmon, *Salmo salar* L. *Aquac. Res.* **32**, 103–111 (2001).
17. Baker, R. T. . T. M., Pfeiffer, A.-M. M., Schöner, F.-J. J. & Smith-Lemmon, L. Pigmenting efficacy of astaxanthin and canthaxanthin in fresh-water reared Atlantic salmon, *Salmo salar*. *Anim. Feed Sci. Technol.* **99**, 97–106 (2002).

18. Christiansen, R., GLETTE, J., LIE, Ø., TORRISSEN, O. J. & WAAGBØ, R. Antioxidant status and immunity in Atlantic salmon, *Salmo salar* L., fed semi-purified diets with and without astaxanthin supplementation. *J. Fish Dis.* **18**, 317–328 (1995).
19. Bjerkgeng, B. Carotenoid pigmentation of salmonid fishes - recent progress. In: Cruz -Suárez, L.E., Ricque-Marie, D., TapiaSalazar, M., Olvera-Novoa, M.A. y Civera-Cerecedo, R., (Eds.). *Avances en Nutrición Acuícola V. Memorias del V Simposium Internacional de Nutrició.* (2000).
20. Wathne, E., Bjerkgeng, B., Storebakken, T., Vassvik, V. & Odland, A. B. Pigmentation of Atlantic salmon (*Salmo salar*) fed astaxanthin in all meals or in alternating meals. *Aquaculture* **159**, 217–231 (1998).
21. Aas, G. H. H., Bjerkgeng, B., Storebakken, T. & Ruyter, B. Blood appearance, metabolic transformation and plasma transport proteins of <sup>14</sup>C-astaxanthin in Atlantic salmon (*Salmo salar* L.). *Fish Physiol. Biochem.* **21**, 325–334 (1999).
22. Xu, Y. & Ding, Z. Traced studies on metabolism of astaxanthin in Atlantic salmon (*Salmo salar*). *J Exp Zool A Comp Exp Biol* **301**, 317–323 (2004).
23. Christiansen, R., Lie, Ø. & Torrissen, O. J. Effect of astaxanthin and vitamin A on growth and survival during first feeding of Atlantic salmon, *Salmo salar* L. *Aquac. Res.* **25**, 903–914 (1994).
24. Torrissen, O. J. Pigmentation of salmonids: Interactions of astaxanthin and canthaxanthin on pigment deposition in rainbow trout. *Aquaculture* **79**, 363–374 (1989).
25. Vieira, V. L. A., Norris, A. & Johnston, I. A. Heritability of fibre number and size parameters and their genetic relationship to flesh quality traits in Atlantic salmon (*Salmo salar* L.). *Aquaculture* **272**, (2007).
26. Norris, A. T. & Cunningham, E. P. Estimates of phenotypic and genetic parameters for flesh colour traits in farmed Atlantic salmon based on multiple trait animal model. *Livest. Prod. Sci.* **89**, 209–222 (2004).
27. Johnston, I. A. *et al.* Patterns of muscle growth in early and late maturing populations of Atlantic salmon (*Salmo salar* L.). *Aquaculture* **189**, 307–333 (2000).
28. Johnston, I. A. *et al.* Muscle fibre density in relation to the colour and texture of smoked Atlantic salmon (*Salmo salar* L.). *Aquaculture* **189**, 335–349 (2000).
29. Skrede, G. *et al.* Developing a Color Card for Raw Flesh of Astaxanthin-fed Salmon. *J. Food Sci.* **55**, 361–363 (1990).
30. Misimi, E., Mathiassen, J. R. & Erikson, U. Computer vision-based sorting of Atlantic salmon (*Salmo salar*) fillets according to their color level. *J. Food Sci.* **72**, 1–6 (2007).
31. CIE. *Official Recommendations on Uniform Color Space, Color Difference Equations and Metric Color Terms. Suppl. No. 2 to CIE Publication No. 15. Colorimetry. Commission International de l'Eclairage. Paris.* (1976).
32. Folkestad, A. *et al.* Rapid and non-invasive measurements of fat and pigment concentrations in live and slaughtered Atlantic salmon (*Salmo salar* L.). *Aquaculture* **280**, 129–135 (2008).
33. Grünenwald, M. *et al.* Pigment-depletion in Atlantic salmon (*Salmo salar*) post-smolt starved

- at elevated temperature is not influenced by dietary carotenoid type and increasing  $\alpha$ -tocopherol level. *Food Chem.* **299**, 125140 (2019).
34. Einen & Skrede. Quality characteristics in raw and smoked fillets of Atlantic salmon, *Salmo salar*, fed high-energy diets. *Aquac. Nutr.* **4**, 99–108 (1998).
  35. Wade, N. M. *et al.* Effects of an unprecedented summer heatwave on the growth performance, flesh colour and plasma biochemistry of marine cage-farmed Atlantic salmon (*Salmo salar*). *J. Therm. Biol.* **80**, 64–74 (2019).
  36. Katikou, P., Hughes, S. I. & Robb, D. H. F. Lipid distribution within atlantic salmon (*Salmo salar*) fillets. *Aquaculture* **202**, 89–99 (2001).
  37. Grünenwald, M., Carter, C. G., Nichols, D. S., Adams, M. B. & Adams, L. R. Heterogeneous astaxanthin distribution in the fillet of Atlantic salmon post-smolt at elevated temperature is not affected by dietary fatty acid composition, metabolic conversion of astaxanthin to idoxanthin, or oxidative stress. *Aquaculture* **521**, 735096 (2020).
  38. Skjervold, P. O. *et al.* Properties of salmon flesh from different locations on pre- and post-rigor fillets. *Aquaculture* **201**, 91–106 (2001).
  39. Zarkasi, K. Z. *et al.* Atlantic Salmon (*Salmo salar* L.) Gastrointestinal Microbial Community Dynamics in Relation to Digesta Properties and Diet. *Microb. Ecol.* **71**, 589–603 (2016).
  40. Good, C. & Davidson, J. A Review of Factors Influencing Maturation of Atlantic Salmon, *Salmo salar*, with Focus on Water Recirculation Aquaculture System Environments. *J. World Aquac. Soc.* **47**, 605–632 (2016).
  41. Elliott, J. M. A. M. & Elliott, J. M. A. M. Temperature requirements of Atlantic salmon *Salmo salar*, brown trout *Salmo trutta* and Arctic charr *Salvelinus alpinus*: predicting the effects of climate change. *J. Fish Biol.* **77**, 1793–1817 (2010).
  42. Umeno, D., Tobias, A. V & Arnold, F. H. Diversifying carotenoid biosynthetic pathways by directed evolution. *Microbiol. Mol. Biol. Rev.* **69**, 51–78 (2005).
  43. Lozano, G. A. Carotenoids, Parasites, and Sexual Selection. *Oikos* **70**, 309–311 (1994).
  44. Hill, G. E. Is There an Immunological Cost to Carotenoid-Based Ornamental Coloration? *Am. Nat.* **154**, 589–595 (1999).
  45. Merrifield, D. L. *et al.* The current status and future focus of probiotic and prebiotic applications for salmonids. *Aquaculture* **302**, 1–18 (2010).
  46. Ray, A. K., Ghosh, K. & Ringø, E. Enzyme-producing bacteria isolated from fish gut: a review. *Aquac. Nutr.* **18**, 465–492 (2012).
  47. Gildberg, A., Johansen, A. & Børgwald, J. Growth and survival of Atlantic salmon (*Salmo salar*) fry given diets supplemented with fish protein hydrolysate and lactic acid bacteria during a challenge trial with *Aeromonas salmonicida*. *Aquaculture* **138**, 23–34 (1995).
  48. Ringø, E. *et al.* Histological changes in intestine of Atlantic salmon (*Salmo salar* L.) following in vitro exposure to pathogenic and probiotic bacterial strains. *Cell Tissue Res.* **328**, 109–116 (2007).

49. Gatesoupe, F.-J., Infante, J.-L. Z., Cahu, C. & Quazuguel, P. Early weaning of seabass larvae, *Dicentrarchus labrax*: the effect on microbiota, with particular attention to iron supply and exoenzymes. *Aquaculture* **158**, 117–127 (1997).
50. Sugita, H., Kawasaki, J. & Deguchi, Y. Production of amylase by the intestinal microflora in cultured freshwater fish. *Lett Appl Microbiol* **24**, 105–108 (1997).
51. Lindsay, G. J. H. & Harris, J. E. Carboxymethylcellulase activity in the digestive tracts of fish. *J. Fish Biol.* **16**, 219–233 (1980).
52. Gómez, G. D. & Balcázar, J. L. A review on the interactions between gut microbiota and innate immunity of fish. *FEMS Immunol. Med. Microbiol.* **52**, 145–154 (2008).
53. Rawls, J. F., Samuel, B. S. & Gordon, J. I. Gnotobiotic zebrafish reveal evolutionarily conserved responses to the gut microbiota. *Proc Natl Acad Sci U S A* **101**, 4596–4601 (2004).
54. Caramujo, M.-J., de Carvalho, C. C. C. R., Silva, S. J. & Carman, K. R. Dietary carotenoids regulate astaxanthin content of copepods and modulate their susceptibility to UV light and copper toxicity. *Mar. Drugs* **10**, 998–1018 (2012).
55. Saini, R. K. & Keum, Y.-S. Progress in Microbial Carotenoids Production. *Indian J. Microbiol.* **57**, 129–130 (2017).
56. Garcia-Asua, G., Cogdell, R. J. & Hunter, C. N. Functional assembly of the foreign carotenoid lycopene into the photosynthetic apparatus of *Rhodobacter sphaeroides*, achieved by replacement of the native 3-step phytoene desaturase with its 4-step counterpart from *Erwinia herbicola*. *Mol. Microbiol.* **44**, 233–244 (2002).
57. Garcia-Asua, G., Lang, H. P., Cogdell, R. J. & Hunter, C. N. Carotenoid diversity: a modular role for the phytoene desaturase step. *Trends Plant Sci.* **3**, 445–449 (1998).
58. Komori, M. *et al.* A Null Lesion in the Rhodopin 3,4-Desaturase of *Rhodospirillum rubrum* Unmasks a Cryptic Branch of the Carotenoid Biosynthetic Pathway. *Biochemistry* **37**, 8987–8994 (1998).
59. Neuman, C., Hatje, E., Bowman, J., Stevenson, H. & Katouli, M. *The effect of diet and environmental temperature on gut microflora of Atlantic Salmon.* (2012).
60. Reveco, F. E., Øverland, M., Romarheim, O. H. & Mydland, L. T. Intestinal bacterial community structure differs between healthy and inflamed intestines in Atlantic salmon (*Salmo salar* L.). *Aquaculture* **420–421**, 262–269 (2014).
61. Xia, J. H. *et al.* The intestinal microbiome of fish under starvation. *BMC Genomics* **15**, 266 (2014).
62. Gajardo, K. *et al.* A high-resolution map of the gut microbiota in Atlantic salmon (*Salmo salar*): A basis for comparative gut microbial research. *Sci. Rep.* **6**, 30893 (2016).
63. Bokulich, N. A. *et al.* Optimizing taxonomic classification of marker-gene amplicon sequences with QIIME 2's q2-feature-classifier plugin. *Microbiome* **6**, 90 (2018).
64. Caporaso, J. G. *et al.* QIIME allows analysis of high-throughput community sequencing data. *Nat. Methods* **7**, 335 (2010).

65. Amir, A. *et al.* *Deblur Rapidly Resolves Single-Nucleotide Community Sequence Patterns*. *mSystems* vol. 2 (American Society for Microbiology, 2017).
66. Rognes, T., Flouri, T., Nichols, B., Quince, C. & Mahé, F. VSEARCH: a versatile open source tool for metagenomics. *PeerJ* **4**, e2584 (2016).
67. Price, M. N., Dehal, P. S. & Arkin, A. P. FastTree 2 – Approximately Maximum-Likelihood Trees for Large Alignments. *PLoS One* **5**, e9490 (2010).
68. Ludwig, J. A. & Reynolds, J. F. *Statistical ecology: a primer on methods & computing*. (John Wiley & Sons, Inc., 1988).
69. Lozupone, C. & Knight, R. UniFrac: a New Phylogenetic Method for Comparing Microbial Communities. *Appl. Environ. Microbiol.* **71**, 8228–8235 (2005).
70. Vázquez-Baeza, Y. *et al.* Bringing the Dynamic Microbiome to Life with Animations. *Cell Host Microbe* **21**, 7–10 (2017).
71. Vázquez-Baeza, Y., Pirrung, M., Gonzalez, A. & Knight, R. EMPeror: a tool for visualizing high-throughput microbial community data. *Gigascience* **2**, 2016–2047 (2013).
72. Anderson, M. J. A new method for non-parametric multivariate analysis of variance. *Austral Ecol.* **26**, 32–46 (2001).
73. Segata, N. *et al.* Metagenomic biomarker discovery and explanation. *Genome Biol.* **12**, R60–R60 (2011).
74. Morton, J. T. *et al.* Balance Trees Reveal Microbial Niche Differentiation. *mSystems* **2**, (2017).
75. Langille, M. G. I. *et al.* Predictive functional profiling of microbial communities using 16S rRNA marker gene sequences. *Nat. Biotechnol.* **31**, 814 (2013).
76. Zakrzewski, M. *et al.* Calypso: a user-friendly web-server for mining and visualizing microbiome–environment interactions. *Bioinformatics* **33**, 782–783 (2016).
77. Borges, P. *et al.* Lipid digestion, absorption and uptake in *Solea senegalensis*. *Comp. Biochem. Physiol. Part A Mol. Integr. Physiol.* **166**, 26–35 (2013).
78. Remen, M., Sievers, M., Torgersen, T. & Oppedal, F. The oxygen threshold for maximal feed intake of Atlantic salmon post-smolts is highly temperature-dependent. *Aquaculture* **464**, 582–592 (2016).
79. Alabaster, J. S. & Gough, P. J. The dissolved oxygen and temperature requirements of Atlantic salmon, *Salmo salar* L., in the Thames Estuary. *J. Fish Biol.* **29**, 613–621 (1986).
80. Duston, J. Effect of salinity on survival and growth of Atlantic salmon (*Salmo salar*) parr and smolts. *Aquaculture* **121**, 115–124 (1994).
81. Stehfest, K. M., Carter, C. G., McAllister, J. D., Ross, J. D. & Semmens, J. M. Response of Atlantic salmon *Salmo salar* to temperature and dissolved oxygen extremes established using animal-borne environmental sensors. *Sci. Rep.* **7**, (2017).
82. Vikeså, V., Nankervis, L. & Hevrøy, E. M. Appetite, metabolism and growth regulation in Atlantic salmon (*Salmo salar* L.) exposed to hypoxia at elevated seawater temperature. *Aquac.*

- Res.* **48**, 4086–4101 (2017).
83. Zarkasi, K. Z. *et al.* Pyrosequencing-based characterization of gastrointestinal bacteria of Atlantic salmon (*Salmo salar* L.) within a commercial mariculture system. *J. Appl. Microbiol.* **117**, 18–27 (2014).
  84. Ivanov II, Littman, D. R., Ivanov, I. I. & Littman, D. R. Segmented filamentous bacteria take the stage. *Mucosal Immunol.* **3**, 209–12 (2010).
  85. Austin, B. & Austin, D. A. *Bacterial Fish Pathogens: Disease of Farmed and Wild Fish*. vol. XXVIII (1999).
  86. Navarrete, P., Espejo, R. T. & Romero, J. Molecular Analysis of Microbiota Along the Digestive Tract of Juvenile Atlantic Salmon (*Salmo salar* L.). *Microb Ecol* **57**, 550–561 (2009).
  87. Schmidt, V. T., Smith, K. F., Melvin, D. W. & Amaral-Zettler, L. A. Community assembly of a euryhaline fish microbiome during salinity acclimation. *Mol Ecol* **24**, 2537–2550 (2015).
  88. Bolnick, D. I. *et al.* Individuals' diet diversity influences gut microbial diversity in two freshwater fish (threespine stickleback and Eurasian perch). *Ecol Lett* **17**, 979–987 (2014).
  89. Neuman, C. *et al.* The effect of diet and environmental temperature on the faecal microbiota of farmed Tasmanian Atlantic Salmon (*Salmo salar* L.). *Aquac. Res.* **47**, 660–672 (2016).
  90. Dehler, C. E., Secombes, C. J. & Martin, S. A. M. M. Environmental and physiological factors shape the gut microbiota of Atlantic salmon parr (*Salmo salar* L.). *Aquaculture* **467**, 149–157 (2017).
  91. Roeselers, G. *et al.* Evidence for a core gut microbiota in the zebrafish. *ISME j* **5**, 1595–1608 (2011).
  92. Star, B., Haverkamp, T. H., Jentoft, S. & Jakobsen, K. S. Next generation sequencing shows high variation of the intestinal microbial species composition in Atlantic cod caught at a single location. *BMC Microbiol* **13**, 248 (2013).
  93. Liu, Y. *et al.* Deciphering microbial landscapes of fish eggs to mitigate emerging diseases. *ISME J.* **8**, 2002–2014 (2014).
  94. Uren Webster, T. M., Consuegra, S., Hitchings, M. & Garcia de Leaniz, C. Interpopulation Variation in the Atlantic Salmon Microbiome Reflects Environmental and Genetic Diversity. *Appl. Environ. Microbiol.* **84**, (2018).
  95. Cahoon, L. *et al.* *Swine waste as a source of natural products: A carotenoid antioxidant*. vol. 3 (2012).
  96. Merrifield, D. L., Dimitroglou, A., Bradley, G., Baker, R. T. M. & Davies, S. J. Soybean meal alters autochthonous microbial populations, microvilli morphology and compromises intestinal enterocyte integrity of rainbow trout, *Oncorhynchus mykiss* (Walbaum). *J. Fish Dis.* **32**, 755–766 (2009).
  97. Maquelin, K. *et al.* Raman spectroscopic typing reveals the presence of carotenoids in *Mycoplasma pneumoniae*. *Microbiology* **155**, 2068–2077 (2009).

98. Rud, I. *et al.* Deep-sequencing of the bacterial microbiota in commercial-scale recirculating and semi-closed aquaculture systems for Atlantic salmon post-smolt production. *Aquac. Eng.* **78**, 50–62 (2017).
99. Lokesh, J., Kiron, V., Sipkema, D., Fernandes, J. M. O. O. & Moum, T. Succession of embryonic and the intestinal bacterial communities of Atlantic salmon (*Salmo salar*) reveals stage-specific microbial signatures. *Microbiologyopen* **0**, e00672 (2018).
100. Llewellyn, M. S. *et al.* Parasitism perturbs the mucosal microbiome of Atlantic Salmon. *Sci Rep* **7**, 43465 (2017).
101. Wade, N., Goulter, K. C., Wilson, K. J., Hall, M. R. & Degnan, B. M. Esterified astaxanthin levels in lobster epithelia correlate with shell colour intensity: Potential role in crustacean shell colour formation. *Comp. Biochem. Physiol. Part B Biochem. Mol. Biol.* **141**, 307–313 (2005).
102. White, D. A., Page, G. I., Swaile, J., Moody, A. J. & Davies, S. J. Effect of esterification on the absorption of astaxanthin in rainbow trout, *Oncorhynchus mykiss* (Walbaum). *Aquac. Res.* **33**, 343–350 (2002).
103. Braceland, M. *et al.* The serum proteome of Atlantic salmon, *Salmo salar*, during pancreas disease (PD) following infection with salmonid alphavirus subtype 3 (SAV3). *J Proteomics* **94**, 423–436 (2013).
104. Zaripheh, S. & Erdman John W., J. Factors That Influence the Bioavailability of Xanthophylls. *J. Nutr.* **132**, 531S-534S (2002).
105. Deming, D. M. & Erdman, J. W. Mammalian carotenoid absorption and metabolism. *Pure Appl. Chem.* **71**, 2213–2223 (1999).
106. Danulat, E. Role of bacteria with regard to chitin degradation in the digestive tract of the cod *Gadus morhua*. *Mar. Biol.* **90**, 335–343 (1986).
107. Negi, S., Singh, H. & Mukhopadhyay, A. Gut bacterial peptides with autoimmunity potential as environmental trigger for late onset complex diseases: In-silico study. *PLoS One* **12**, e0180518 (2017).
108. Apprill, A. Marine Animal Microbiomes: Toward Understanding Host–Microbiome Interactions in a Changing Ocean . *Frontiers in Marine Science* vol. 4 222 (2017).
109. Davison, J. M. *et al.* Microbiota regulate intestinal epithelial gene expression by suppressing the transcription factor Hepatocyte nuclear factor 4 alpha. *Genome Res.* **27**, 1195–1206 (2017).
110. Sheng, Y. *et al.* The Presence or Absence of Intestinal Microbiota Affects Lipid Deposition and Related Genes Expression in Zebrafish (*Danio rerio*). *Front. Microbiol.* **9**, (2018).
111. Small, C. M., Milligan-Myhre, K., Bassham, S., Guillemin, K. & Cresko, W. A. Host Genotype and Microbiota Contribute Asymmetrically to Transcriptional Variation in the Threespine Stickleback Gut. *Genome Biol. Evol.* **9**, 504–520 (2017).
112. Heuston, S., Begley, M., Gahan, C. G. & Hill, C. Isoprenoid biosynthesis in bacterial pathogens. *Microbiology* **158**, 1389–1401 (2012).

113. McGarvey, D. J. & Croteau, R. Terpenoid metabolism. *Plant Cell* **7**, 1015–1026 (1995).
114. Boronat, A. & Rodriguez-Concepcion, M. Terpenoid biosynthesis in prokaryotes. *Adv Biochem Eng Biotechnol* **148**, 3–18 (2015).
115. Ichiyama, S., Shimokata, K. & Tsukamura, M. Relationship between mycobacterial species and their carotenoid pigments. *Microbiol Immunol* **32**, 473–479 (1988).
116. de Matos, G. F. *et al.* Bradyrhizobium sacchari sp nov., a legume nodulating bacterium isolated from sugarcane roots. *Arch. Microbiol.* **199**, 1251–1258 (2017).
117. Gao, J. L. *et al.* Rhizobium wenxiniae sp nov., an endophytic bacterium isolated from maize root. *Int J Syst Evol Microbiol* **67**, 2798–2803 (2017).
118. Hannibal, L. *et al.* Isolation and characterization of canthaxanthin biosynthesis genes from the photosynthetic bacterium Bradyrhizobium sp. strain ORS278. *J Bacteriol* **182**, 3850–3853 (2000).
119. Smith, P. F. & Rothblat, G. H. Comparison of lipid composition of pleuropneumonia-like and L-type organisms. *J Bacteriol* **83**, 500–506 (1962).
120. Smith, P. F. THE CAROTENOID PIGMENTS OF MYCOPLASMA. *J Gen Microbiol* **32**, 307–319 (1963).
121. Smith, C. V. H. and P. F., Henrikson, C. V. & Smith, P. F. Growth Response of Mycoplasma to Carotenoid Pigments and Carotenoid Intermediates. *J. gen. Microbiol.* **45**, **73–52**, 73–82 (1966).
122. Oral Mucosal Microbes. in *Atlas of Oral Microbiology* (eds. Zhou, X. & Li, Y.) 95–107 (Elsevier, 2015). doi:10.1016/B978-0-12-802234-4.00005-7.
123. Melancon, E. *et al.* Best practices for germ-free derivation and gnotobiotic zebrafish husbandry. *Methods Cell Biol.* **138**, 61–100 (2017).
124. Andrews, S. FastQC A Quality Control tool for High Throughput Sequence Data. <http://www.bioinformatics.babraham.ac.uk/projects/fastqc/> (2010) doi:citeulike-article-id:11583827.
125. Kim, D., Langmead, B. & Salzberg, S. L. HISAT: a fast spliced aligner with low memory requirements. *Nat. Methods* **12**, 357 (2015).
126. Anders, S., Pyl, P. T. & Huber, W. HTSeq--a Python framework to work with high-throughput sequencing data. *Bioinformatics* **31**, 166–169 (2015).
127. Love, M. I., Huber, W. & Anders, S. Moderated estimation of fold change and dispersion for RNA-seq data with DESeq2. *Genome Biol.* **15**, 550 (2014).
128. Götz, S. *et al.* High-throughput functional annotation and data mining with the Blast2GO suite. *Nucleic Acids Res.* **36**, 3420–3435 (2008).
129. Desmoulière, A., Geinoz, A., Gabbiani, F. & Gabbiani, G. Transforming growth factor-beta 1 induces alpha-smooth muscle actin expression in granulation tissue myofibroblasts and in quiescent and growing cultured fibroblasts. *J. Cell Biol.* **122**, 103 (1993).

130. Huber, P. A. J. Caldesmon. *Int. J. Biochem. Cell Biol.* **29**, 1047–1051 (1997).
131. Dąbrowska, R., Kulikova, N. & Gągola, M. *Nonmuscle caldesmon: Its distribution and involvement in various cellular processes.* vol. 224 (2004).
132. Paulin, D. & Li, Z. Desmin: a major intermediate filament protein essential for the structural integrity and function of muscle. *Exp. Cell Res.* **301**, 1–7 (2004).
133. Winder, S. J. & Ayscough, K. R. Actin-binding proteins. *J. Cell Sci.* **118**, 651 (2005).
134. Young, A. J. J., Pritchard, J., Lowe, G. M. M., Crampton, V. & Buttle, L. Reconstitution of muscle F-actin from Atlantic salmon (*Salmo salar* L.) with carotenoids-binding characteristics of astaxanthin and canthaxanthin. *Aquac. Nutr.* **23**, 1296–1303 (2017).
135. Yamaguchi, A. *et al.* Stress-Associated Endoplasmic Reticulum Protein 1 (Serp1)/Ribosome-Associated Membrane Protein 4 (Ramp4) Stabilizes Membrane Proteins during Stress and Facilitates Subsequent Glycosylation. *J. Cell Biol.* **147**, 1195 (1999).
136. Trigatti, B. L. & Gerber, G. E. A direct role for serum albumin in the cellular uptake of long-chain fatty acids. *Biochem. J.* **308**, 155–159 (1995).
137. Le, N. A., Gibson, J. C. & Ginsberg, H. N. Independent regulation of plasma apolipoprotein C-II and C-III concentrations in very low density and high density lipoproteins: implications for the regulation of the catabolism of these lipoproteins. *J. Lipid Res.* **29**, 669–677 (1988).
138. Feingold Kr Fau - Grunfeld, C. & Grunfeld, C. Introduction to Lipids and Lipoproteins BTI - Endotext.
139. Parker, R. S. *Absorption, metabolism, and transport of carotenoids.* *FASEB journal : official publication of the Federation of American Societies for Experimental Biology* vol. 10 (1996).
140. Dumont, L. *et al.* Molecular Mechanism of the Blockade of Plasma Cholesteryl Ester Transfer Protein by Its Physiological Inhibitor Apolipoprotein CI. *J. Biol. Chem.* **280**, 38108–38116 (2005).
141. Wassell, J. Haptoglobin: function and polymorphism. *Clin. Lab.* **46**, 547–552 (2000).
142. Tolosano, E. & Altruda, F. Hemopexin: Structure, Function, and Regulation. *DNA Cell Biol.* **21**, 297–306 (2002).
143. Nakamura, S. *et al.* Polymorphism in the 5'-flanking region of human glutamate-cysteine ligase modifier subunit gene is associated with myocardial infarction. *Circulation* **105**, 2968–2973 (2002).
144. Martin, S. A., Douglas, A., Houlihan, D. F. & Secombes, C. J. Starvation alters the liver transcriptome of the innate immune response in Atlantic salmon (*Salmo salar*). *BMC Genomics* **11**, 418 (2010).
145. Nota, B., Van Straalen, N. M., Ylstra, B. & Roelofs, D. Gene expression microarray analysis of heat stress in the soil invertebrate *Folsomia candida*. *Insect Mol. Biol.* **19**, 315–322 (2010).
146. Kim, Y.-O. *et al.* Molecular Cloning and mRNA Expression of the Liver-Specific Cathepsin L1 Gene of the Olive Flounder, *Paralichthys olivaceus*. *Biosci. Biotechnol. Biochem.* **75**, 1214–

- 1218 (2011).
147. Martins-de-Souza, D. *et al.* Prefrontal cortex shotgun proteome analysis reveals altered calcium homeostasis and immune system imbalance in schizophrenia. *Eur. Arch. Psychiatry Clin. Neurosci.* **259**, 151–163 (2009).
  148. Burton, M., Rose, T. M., Færgeman, N. J. & Knudsen, J. Evolution of the acyl-CoA binding protein (ACBP). *Biochem. J.* **392**, 299 (2005).
  149. Lanes, C. F. C., Bizuayehu, T. T., de Oliveira Fernandes, J. M., Kiron, V. & Babiak, I. Transcriptome of Atlantic Cod (*Gadus morhua* L.) Early Embryos from Farmed and Wild Broodstocks. *Mar. Biotechnol.* **15**, 677–694 (2013).
  150. Birn, H. *et al.* Cubilin is an albumin binding protein important for renal tubular albumin reabsorption. *J. Clin. Invest.* **105**, 1353–1361 (2000).
  151. Christensen, E. I., Verroust, P. J. & Nielsen, R. Receptor-mediated endocytosis in renal proximal tubule. *Pflügers Arch. - Eur. J. Physiol.* **458**, 1039–1048 (2009).
  152. Fasano, M. *et al.* The extraordinary ligand binding properties of human serum albumin. *IUBMB Life* **57**, 787–796 (2008).
  153. Ando, S., Takeyama, T. & Hatano, M. Isolation and Characterization of a Carotenoid-Carrying Lipoprotein in the Serum of Chum Salmon *Oncorhynchus-Keta* During Spawning Migration. *Agric. Biol. Chem.* **50**, 907–914 (1986).
  154. March, B. E., Hajen, W. E., Deacon, G., MacMillan, C. & Walsh, M. G. Intestinal absorption of astaxanthin, plasma astaxanthin concentration, body weight, and metabolic rate as determinants of flesh pigmentation in salmonid fish. *Aquaculture* **90**, 313–322 (1990).
  155. Vodenlich, A. D. *et al.* Identification of the 14 kDa bile acid transport protein of rat ileal cytosol as gastrotropin. *Biochem. Biophys. Res. Commun.* **177**, 1147–1154 (1991).
  156. Geyer, J., Wilke, T. & Petzinger, E. The solute carrier family SLC10: more than a family of bile acid transporters regarding function and phylogenetic relationships. *Naunyn. Schmiedebergs. Arch. Pharmacol.* **372**, 413–431 (2006).
  157. Tang, S.-J. *et al.* Cold-induced ependymin expression in zebrafish and carp brain: implications for cold acclimation. *FEBS Lett.* **459**, 95–99 (1999).
  158. Lin, J. J. & Somero, G. N. Temperature-Dependent Changes in Expression of Thermostable and Thermolabile Isozymes of Cytosolic Malate Dehydrogenase in the Eurythermal Goby Fish *Gillichthys mirabilis*. *Physiol. Zool.* **68**, 114–128 (1995).
  159. Wellen, K. E. *et al.* ATP-Citrate Lyase Links Cellular Metabolism to Histone Acetylation. *Science (80-. )*. **324**, 1076 (2009).
  160. Toyota, K., Williams, T. D., Sato, T., Tatarazako, N. & Iguchi, T. Comparative ovarian microarray analysis of juvenile hormone-responsive genes in water flea *Daphnia magna*: potential targets for toxicity. *J. Appl. Toxicol.* **37**, 374–381 (2016).
  161. Nicol, C. J., Zielenski, J., Tsui, L.-C. & Wells, P. G. An embryoprotective role for glucose-6-phosphate dehydrogenase in developmental oxidative stress and chemical teratogenesis.

- FASEB J.* **14**, 111–127 (2000).
162. Corydon, M. J. *et al.* Structural organization of the human short-chain acyl-CoA dehydrogenase gene. *Mamm. Genome* **8**, 922–926 (1997).
  163. Carter, B. A. & Shulman, R. J. Mechanisms of Disease: update on the molecular etiology and fundamentals of parenteral nutrition associated cholestasis. *Nat. Clin. Pract. Gastroenterol. & Hepatol.* **4**, 277 (2007).
  164. Gill, J. L., Bishop, S. C., McCorquodale, C., Williams, J. L. & Wiener, P. Identification of polymorphisms in the malic enzyme 1, NADP(+)-dependent, cytosolic and nuclear receptor subfamily 0, group B, member 2 genes and their associations with meat and carcass quality traits in commercial Angus cattle. *Anim. Genet.* **43**, 88–92 (2011).
  165. Bolger, A. M., Lohse, M. & Usadel, B. Trimmomatic: A flexible trimmer for Illumina Sequence Data. *Bioinformatics*. (2014).
  166. Wang, L., Wang, S. & Li, W. RSeQC: quality control of RNA-seq experiments. *Bioinformatics* **28**, 2184–2185 (2012).
  167. Robinson, J. T. *et al.* Integrative genomics viewer. *Nat. Biotechnol.* **29**, 24–26 (2011).
  168. Heberle, H., Meirelles, G. V., da Silva, F. R., Telles, G. P. & Minghim, R. InteractiVenn: a web-based tool for the analysis of sets through Venn diagrams. *BMC Bioinformatics* **16**, 169 (2015).
  169. Ventura, T., Fitzgibbon, Q., Battaglione, S., Sagi, A. & Elizur, A. Identification and characterization of androgenic gland specific insulin-like peptide-encoding transcripts in two spiny lobster species: *Sagmariasus verreauxi* and *Jasus edwardsii*. *Gen. Comp. Endocrinol.* **214**, 126–133 (2015).
  170. Garrison E, M. G. Haplotype-based variant detection from short-read sequencing. *arXiv preprint* vol. arXiv:1207 (2012).
  171. Li, H. *et al.* The Sequence Alignment/Map format and SAMtools. *Bioinformatics* **25**, 2078–2079 (2009).
  172. Danecek, P. & McCarthy, S. A. BCFTools/csqs: haplotype-aware variant consequences. *Bioinformatics* **33**, 2037–2039 (2017).
  173. McLaren, W. *et al.* The Ensembl Variant Effect Predictor. *Genome Biol.* **17**, 122 (2016).
  174. Zhang, Y. I-TASSER server for protein 3D structure prediction. *BMC Bioinformatics* **9**, 40 (2008).
  175. Roy, A., Kucukural, A. & Zhang, Y. I-TASSER: a unified platform for automated protein structure and function prediction. *Nat. Protoc.* **5**, 725–738 (2010).
  176. Yang, J. *et al.* The I-TASSER Suite: protein structure and function prediction. *Nat. Methods* **12**, 7–8 (2015).
  177. Guex, N., Peitsch, M. C. & Electrophoresis. SWISS-MODEL and the Swiss-PdbViewer: an environment for comparative protein modeling.
  178. Lehnert, S. J., Pitcher, T. E., Devlin, R. H. & Heath, D. D. Red and white Chinook salmon: genetic

- divergence and mate choice. *Mol. Ecol.* **25**, 1259–1274 (2016).
179. Helgeland, H. *et al.* Genomic and functional gene studies suggest a key role of *beta*-carotene oxygenase 1 like (*bco1l*) gene in salmon flesh color. *bioRxiv* 821652 (2019) doi:10.1101/821652.
  180. Patel, S. B., Graf, G. A. & Temel, R. E. ABCG5 and ABCG8: more than a defense against xenosterols. *J. Lipid Res.* **59**, 1103–1113 (2018).
  181. Hazard, S. E. & Patel, S. B. Sterolins ABCG5 and ABCG8: regulators of whole body dietary sterols. *Pflügers Arch. - Eur. J. Physiol.* **453**, 745–752 (2007).
  182. Yu, L. *et al.* Disruption of *Abcg5* and *Abcg8* in mice reveals their crucial role in biliary cholesterol secretion. *Proc. Natl. Acad. Sci.* **99**, 16237 (2002).
  183. Kortner, T. M., Gu, J., Krogdahl, A. & Bakke, A. M. Transcriptional regulation of cholesterol and bile acid metabolism after dietary soyabean meal treatment in Atlantic salmon (*Salmo salar* L.). *Br J Nutr* **109**, 593–604 (2013).
  184. Chimsung, N. *et al.* Effects of various dietary factors on astaxanthin absorption in Atlantic salmon (*Salmo salar*). *Aquac. Res.* **45**, 1611–1620 (2014).
  185. Grunenwald, M. *et al.* Pigment-depletion in Atlantic salmon (*Salmo salar*) post-smolt starved at elevated temperature is not influenced by dietary carotenoid type and increasing alpha-tocopherol level. *Food Chem* **299**, 125140 (2019).
  186. Zoric, N. *Characterization of genes and gene products influencing carotenoid metabolism in Atlantic* Karakterisering av gener og genprodukter involvert i karotenoidmetabolisme i *Philosophiae Doctor ( PhD ) Thesis Acknowledgments.* (2017).
  187. Herron, K. L. *et al.* The ABCG5 Polymorphism Contributes to Individual Responses to Dietary Cholesterol and Carotenoids in Eggs. *J. Nutr.* **136**, 1161–1165 (2006).
  188. Brown, T. D. *et al.* Functional Genomic Analysis of the Impact of Camelina (*Camelina sativa*) Meal on Atlantic Salmon (*Salmo salar*) Distal Intestine Gene Expression and Physiology. *Mar. Biotechnol.* **18**, 418–435 (2016).
  189. De Deken, X., Corvilain, B., Dumont, J. E. & Miot, F. Roles of DUOX-Mediated Hydrogen Peroxide in Metabolism, Host Defense, and Signaling. *Antioxid. Redox Signal.* **20**, 2776–2793 (2013).
  190. Hular, I. *et al.* A Single Copy of the Recently Identified Dual Oxidase Maturation Factor (DUOXA) 1 Gene Produces Only Mild Transient Hypothyroidism in a Patient with a Novel Biallelic DUOXA2 Mutation and Monoallelic DUOXA1 Deletion. *J. Clin. Endocrinol. Metab.* **96**, E841–E845 (2011).
  191. Drevet, S., Gavazzi, G., Grange, L., Dupuy, C. & Lardy, B. Reactive oxygen species and NADPH oxidase 4 involvement in osteoarthritis. *Exp. Gerontol.* **111**, 107–117 (2018).
  192. Ueyama, T. *et al.* The extracellular A-loop of dual oxidases affects the specificity of reactive oxygen species release. *J. Biol. Chem.* **290**, 6495–6506 (2015).

193. Morand, S. *et al.* Duox maturation factors form cell surface complexes with Duox affecting the specificity of reactive oxygen species generation. *FASEB J.* **23**, 1205–1218 (2008).
194. Zamproni, I. *et al.* Biallelic Inactivation of the Dual Oxidase Maturation Factor 2 (DUOXA2) Gene as a Novel Cause of Congenital Hypothyroidism. *J. Clin. Endocrinol. Metab.* **93**, 605–610 (2008).
195. Rahman, M. M., Khosravi, S., Chang, K. H. & Lee, S.-M. Effects of Dietary Inclusion of Astaxanthin on Growth, Muscle Pigmentation and Antioxidant Capacity of Juvenile Rainbow Trout (*Oncorhynchus mykiss*). *Prev. Nutr. food Sci.* **21**, 281–288 (2016).
196. Rajasingh, H., Våge, D. I., Pavey, S. a & Omholt, S. W. Why are salmonids pink? *Can. J. Fish. Aquat. Sci.* **64**, 1614–1627 (2007).
197. Nguyen, C. D. H., Amoroso, G., Ventura, T., Minich, J. J. & Elizur, A. Atlantic Salmon (*Salmo salar* L., 1758) Gut Microbiota Profile Correlates with Flesh Pigmentation: Cause or Effect? *Mar. Biotechnol.* (2020) doi:10.1007/s10126-019-09939-1.
198. Al-Hisnawi, A. *et al.* First report on the autochthonous gut microbiota of brown trout (*Salmo trutta* Linnaeus). *Aquac. Res.* **46**, 2962–2971 (2015).
199. Zhou, Z. *et al.* Molecular characterization of the autochthonous microbiota in the gastrointestinal tract of adult yellow grouper (*Epinephelus awoara*) cultured in cages. *Aquaculture* **286**, 184–189 (2009).
200. Ringø, E. *et al.* Effect of dietary components on the gut microbiota of aquatic animals. A never-ending story? *Aquac. Nutr.* **22**, 219–282 (2016).
201. Egerton, S., Culloty, S., Whooley, J., Stanton, C. & Ross, R. P. The Gut Microbiota of Marine Fish. *Front. Microbiol.* **9**, (2018).
202. Clements, K. D., Angert, E. R., Montgomery, W. L. & Choat, J. H. Intestinal microbiota in fishes: what's known and what's not. *Mol. Ecol.* **23**, 1891–1898 (2014).
203. Llewellyn, M. S., Boutin, S., Hoseinifar, S. H. & Derome, N. Teleost microbiomes: the state of the art in their characterization, manipulation and importance in aquaculture and fisheries. *Front. Microbiol.* **5**, (2014).
204. Nayak, S. K. Role of gastrointestinal microbiota in fish. *Aquac. Res.* **41**, 1553–1573 (2010).
205. Banerjee, G. & Ray, A. K. Bacterial symbiosis in the fish gut and its role in health and metabolism. *Symbiosis* **72**, 1–11 (2017).
206. Ktari, N. *et al.* Functionalities and antioxidant properties of protein hydrolysates from muscle of zebra blenny (*Salaria basilisca*) obtained with different crude protease extracts. *Food Res. Int.* **49**, 747–756 (2012).
207. Sun, H., Jami, E., Harpaz, S. & Mizrahi, I. Involvement of dietary salt in shaping bacterial communities in European sea bass (*Dicentrarchus labrax*). *Sci. Rep.* **3**, 1558 (2013).
208. Abid, A. *et al.* Dietary synbiotic application modulates Atlantic salmon (*Salmo salar*) intestinal microbial communities and intestinal immunity. *Fish Shellfish Immunol* **35**, 1948–1956 (2013).

209. Weiss, S. *et al.* Normalization and microbial differential abundance strategies depend upon data characteristics. *Microbiome* **5**, 27 (2017).
210. Eckburg, P. B. *et al.* Diversity of the human intestinal microbial flora. *Science* (80-. ). **308**, 1635–1638 (2005).
211. Rivera-Pinto, J. *et al.* Balances: a New Perspective for Microbiome Analysis. *mSystems* **3**, e00053-18 (2018).
212. Arena, A. *et al.* Antiviral and immunoregulatory effect of a novel exopolysaccharide from a marine thermotolerant *Bacillus licheniformis*. *Int. Immunopharmacol.* **6**, 8–13 (2006).
213. Xu, H.-M., Rong, Y.-J., Zhao, M.-X., Song, B. & Chi, Z.-M. Antibacterial activity of the lipopeptides produced by *Bacillus amyloliquefaciens* M1 against multidrug-resistant *Vibrio* spp. isolated from diseased marine animals. *Appl. Microbiol. Biotechnol.* **98**, 127–136 (2014).
214. Tarnecki, A. M., Wafapoor, M., Phillips, R. N. & Rhody, N. R. Benefits of a *Bacillus* probiotic to larval fish survival and transport stress resistance. *Sci. Rep.* **9**, 4892 (2019).
215. Suzer, C. *et al.* *Lactobacillus* spp. bacteria as probiotics in gilthead sea bream (*Sparus aurata*, L.) larvae: Effects on growth performance and digestive enzyme activities. *Aquaculture* **280**, 140–145 (2008).
216. Sun, Y.-Z., Yang, H.-L., Huang, K.-P., Ye, J.-D. & Zhang, C.-X. Application of autochthonous *Bacillus* bioencapsulated in copepod to grouper *Epinephelus coioides* larvae. *Aquaculture* **392–395**, 44–50 (2013).
217. Steiger, S., Perez-Fons, L., Fraser, P. D. & Sandmann, G. Biosynthesis of a novel C30 carotenoid in *Bacillus firmus* isolates. *J. Appl. Microbiol.* **113**, 888–895 (2012).
218. Köcher, S., Breitenbach, J., Müller, V. & Sandmann, G. Structure, function and biosynthesis of carotenoids in the moderately halophilic bacterium *Halobacillus halophilus*. *Arch Microbiol* **191**, 95–104 (2009).
219. Vauterin, L. *et al.* Towards an Improved Taxonomy of *Xanthomonas*. *Int. J. Syst. Evol. Microbiol.* **40**, 312–316 (1990).
220. Young, J. M., Wilkie, J. P., Park, D.-C. & Watson, D. R. W. New Zealand strains of plant pathogenic bacteria classified by multi-locus sequence analysis; proposal of *Xanthomonas dyei* sp. nov. *Plant Pathol.* **59**, 270–281 (2010).
221. Li, X. *et al.* Declined soil suppressiveness to *Fusarium oxysporum* by rhizosphere microflora of cotton in soil sickness. *Biol. Fertil. Soils* **51**, 935–946 (2015).
222. Polson, S. Comparative Analysis of Microbial Community Structure Associated with Acroporid Corals during a Disease Outbreak in the Florida Reef Tract. (2007). doi:10.13140/2.1.2852.4484.
223. Ceh, J., Raina, J.-B., Soo, R. M., van Keulen, M. & Bourne, D. G. Coral-Bacterial Communities before and after a Coral Mass Spawning Event on Ningaloo Reef. *PLoS One* **7**, e36920 (2012).
224. Godwin, S., Bent, E., Borneman, J. & Pereg, L. The Role of Coral-Associated Bacterial Communities in Australian Subtropical White Syndrome of *Turbinaria mesenterina*. *PLoS One*

- 7, e44243 (2012).
225. Kublanovskaya, A., Solovchenko, A., Fedorenko, T., Chekanov, K. & Lobakova, E. Natural Communities of Carotenogenic Chlorophyte *Haematococcus lacustris* and Bacteria from the White Sea Coastal Rock Ponds. *Microb Ecol* (2019) doi:10.1007/s00248-019-01437-0.
  226. Salvetti, E., Torriani, S. & Felis, G. E. The Genus *Lactobacillus*: A Taxonomic Update. *Probiotics Antimicrob Proteins* **4**, 217–226 (2012).
  227. Louis, P., Hold, G. L. & Flint, H. J. The gut microbiota, bacterial metabolites and colorectal cancer. *Nat. Rev. Microbiol.* **12**, 661–672 (2014).
  228. He, S. *et al.* Anti-Infective Effect of Adhesive Probiotic *Lactobacillus* in Fish is Correlated with Their Spatial Distribution in the Intestinal Tissue. *Sci Rep* **7**, 13195 (2017).
  229. Gatesoupe, F. J. Updating the importance of lactic acid bacteria in fish farming: natural occurrence and probiotic treatments. *J Mol Microbiol Biotechnol* **14**, 107–114 (2008).
  230. Ringø, E. & Gatesoupe, F.-J. Lactic acid bacteria in fish: a review. *Aquaculture* **160**, 177–203 (1998).
  231. Fečkaninová, A., Koščová, J., Mudroňová, D., Popelka, P. & Toropilová, J. The use of probiotic bacteria against *Aeromonas* infections in salmonid aquaculture. *Aquaculture* **469**, 1–8 (2017).
  232. Ringø, E. *et al.* Lactic acid bacteria associated with the digestive tract of Atlantic salmon (*Salmo salar* L.). *J. Appl. Microbiol.* **89**, 317–322 (2000).
  233. Gildberg, A., Mikkelsen, H., Sandaker, E. & Ringø, E. Probiotic effect of lactic acid bacteria in the feed on growth and survival of fry of Atlantic cod (*Gadus morhua*). *Hydrobiologia* **352**, 279–285 (1997).
  234. Robertson, P. A. W., O’Dowd, C., Burrells, C., Williams, P. & Austin, B. Use of *Carnobacterium* sp. as a probiotic for Atlantic salmon (*Salmo salar* L.) and rainbow trout (*Oncorhynchus mykiss*, Walbaum). *Aquaculture* **185**, 235–243 (2000).
  235. Leisner, J. J., Laursen, B. G., Prévost, H., Drider, D. & Dalgaard, P. *Carnobacterium*: positive and negative effects in the environment and in foods. *FEMS Microbiol. Rev.* **31**, 592–613 (2007).
  236. Pilchová, T., Pilet, M.-F., Cappelier, J.-M., Pazlarová, J. & Tresse, O. Protective Effect of *Carnobacterium* spp. against *Listeria monocytogenes* during Host Cell Invasion Using In vitro HT29 Model. *Front. Cell. Infect. Microbiol.* **6**, (2016).
  237. Hagi, T., Kobayashi, M., Kawamoto, S., Shima, J. & Nomura, M. Expression of novel carotenoid biosynthesis genes from *Enterococcus gilvus* improves the multistress tolerance of *Lactococcus lactis*. *J Appl Microbiol* **114**, 1763–1771 (2013).
  238. Voget, S., Klippel, B., Daniel, R. & Antranikian, G. Complete Genome Sequence of *Carnobacterium* sp. 17-4. *J. Bacteriol.* **193**, 3403–3404 (2011).
  239. Wiklund, T. & Bylund, T. *Pseudomonas anguilliseptica* as a pathogen of salmonid fish in Finland. *Dis. Aquat. Organ.* **8**, (1990).
  240. López, J. R., Lorenzo, L., Marcelino-Pozuelo, C., Marin-Arjona, M. C. & Navas, J. I.

- Pseudomonas baetica*: pathogenicity for marine fish and development of protocols for rapid diagnosis. *FEMS Microbiol. Lett.* **364**, (2016).
241. Watts, J. E. M., Schreier, H. J., Lanska, L. & Hale, M. S. The Rising Tide of Antimicrobial Resistance in Aquaculture: Sources, Sinks and Solutions. *Mar. Drugs* **15**, 158 (2017).
  242. Miranda, C. D. & Zemelman, R. Bacterial resistance to oxytetracycline in Chilean salmon farming. *Aquaculture* **212**, 31–47 (2002).
  243. Romero, J. L., Grande Burgos, M. J., Pérez-Pulido, R., Gálvez, A. & Lucas, R. Resistance to Antibiotics, Biocides, Preservatives and Metals in Bacteria Isolated from Seafoods: Co-Selection of Strains Resistant or Tolerant to Different Classes of Compounds. *Front. Microbiol.* **8**, (2017).
  244. Preena, P. G. *et al.* Diversity of antimicrobial-resistant pathogens from a freshwater ornamental fish farm. *Lett Appl Microbiol* (2019) doi:10.1111/lam.13231.
  245. Guardabassi, L., Petersen, A., Olsen, J. E. & Dalsgaard, A. Antibiotic Resistance in *Acinetobacter* spp. Isolated from Sewers Receiving Waste Effluent from a Hospital and a Pharmaceutical Plant. *Appl. Environ. Microbiol.* **64**, 3499 (1998).
  246. Guardabassi, L., Dalsgaard, A. & Olsen, J. E. Phenotypic characterization and antibiotic resistance of *Acinetobacter* spp. isolated from aquatic sources. *J Appl Microbiol* **87**, 659–667 (1999).
  247. Guardabassi, L., Dalsgaard, A., Raffatellu, M. & Olsen, J. E. Increase in the prevalence of oxolinic acid resistant *Acinetobacter* spp. observed in a stream receiving the effluent from a freshwater trout farm following the treatment with oxolinic acid-medicated feed. *Aquaculture* **188**, 205–218 (2000).
  248. Preena, P. G., Swaminathan, T. R., Kumar, V. J. R. & Singh, I. S. B. Antimicrobial resistance in aquaculture: a crisis for concern. *Biologia (Bratisl)*. (2020) doi:10.2478/s11756-020-00456-4.
  249. Chew, B. P. Role of Carotenoids in the Immune Response<sup>1</sup>. *J. Dairy Sci.* **76**, 2804–2811 (1993).
  250. Amar, E., Kiron, V., Satoh, S., Okamoto, N. & Watanabe, T. Effects of dietary  $\beta$ -carotene on the immune response of rainbow trout *Oncorhynchus mykiss*. *Fish. Sci.* **66**, 1068–1075 (2002).
  251. Anbazhagan, S. M. *et al.* Immune response and disease resistance of carotenoids supplementation diet in *Cyprinus carpio* against *Aeromonas hydrophila*. *Fish Shellfish Immunol* **40**, 9–13 (2014).
  252. Lin, S., Nieves-Puigdoller, K., Brown, A., McGraw, K. & Clotfelter, E. Testing the Carotenoid Trade-Off Hypothesis in the Polychromatic Midas Cichlid, *Amphilophus citrinellus*. *Physiol. Biochem. Zool.* **83**, 333–342 (2010).
  253. Reboul, E. Absorption of vitamin A and carotenoids by the enterocyte: focus on transport proteins. *Nutrients* **5**, 3563–3581 (2013).
  254. Auletta, G. Information and Metabolism in Bacterial Chemotaxis. *Entropy* **15**, 311–326 (2013).
  255. Matilla, M. A. & Krell, T. The effect of bacterial chemotaxis on host infection and pathogenicity. *FEMS Microbiol. Rev.* **42**, (2017).

256. Ray, A. K., Ringø, E., Kumar Ray, A. & Ringø, E. The Gastrointestinal Tract of Fish. in *Aquaculture Nutrition* 1–13 (John Wiley & Sons, Ltd, 2014). doi:10.1002/9781118897263.ch1.
257. Kasozi, N. *et al.* Histomorphological Description of the Digestive System of Pebbly Fish, *Alestes baremoze* (Joannis, 1835). *Sci. World J.* **2017**, 9 (2017).
258. Le, H. T. M. D. *et al.* Intestinal Function of the Stomachless Fish, Ballan Wrasse (*Labrus bergylta*). *Front. Mar. Sci.* **6**, 140 (2019).
259. White, D. A., Ørnsrud, R. & Davies, S. J. Determination of carotenoid and vitamin A concentrations in everted salmonid intestine following exposure to solutions of carotenoid in vitro. *Comp. Biochem. Physiol. Part A Mol. Integr. Physiol.* **136**, 683–692 (2003).
260. Page, G. I. & Davies, S. J. Tissue astaxanthin and canthaxanthin distribution in rainbow trout (*Oncorhynchus mykiss*) and Atlantic salmon (*Salmo salar*). *Comp. Biochem. Physiol. - A Mol. Integr. Physiol.* **143**, 125–132 (2006).
261. Foss, P., Storebakken, T., Austreng, E. & Liaenjen, S. Carotenoids in diets for salmonids: V. Pigmentation of rainbow trout and sea trout with astaxanthin and astaxanthin dipalmitate in comparison with canthaxanthin. *Aquaculture* **65**, 293–305 (1987).
262. Moreno, H. M. *et al.* Collagen characteristics of farmed Atlantic salmon with firm and soft fillet texture. *Food Chem.* **134**, 678–685 (2012).
263. Wei, Z. *et al.* Integrative analysis of transcriptomics and metabolomics profiling on flesh quality of large yellow croaker *Larimichthys crocea* fed a diet with hydroxyproline supplementation. *Br. J. Nutr.* **119**, 359–367 (2018).
264. Gillis, T. E. & Tibbits, G. F. Beating the cold: the functional evolution of troponin C in teleost fish. *Comp. Biochem. Physiol. Part A Mol. Integr. Physiol.* **132**, 763–772 (2002).
265. Yu, E. *et al.* Proteomic and metabolomic basis for improved textural quality in crisp grass carp (*Ctenopharyngodon idellus* C.et V) fed with a natural dietary pro-oxidant. *Food Chem.* **325**, 126906 (2020).
266. Yu, E.-M. *et al.* Proteomic signature of muscle fibre hyperplasia in response to faba bean intake in grass carp. *Sci. Rep.* **7**, 45950 (2017).
267. Trombley, S., Maugars, G., Kling, P., Björnsson, B. T. & Schmitz, M. Effects of long-term restricted feeding on plasma leptin, hepatic leptin expression and leptin receptor expression in juvenile Atlantic salmon (*Salmo salar* L.). *Gen. Comp. Endocrinol.* **175**, 92–99 (2012).
268. Shachter, N. S. Apolipoproteins C-I and C-III as important modulators of lipoprotein metabolism. *Curr. Opin. Lipidol.* **12**, (2001).
269. Paththinige, C. S., Sirisena, N. D. & Dissanayake, V. Genetic determinants of inherited susceptibility to hypercholesterolemia - a comprehensive literature review. *Lipids Health Dis.* **16**, 103 (2017).
270. Troesse, C. *et al.* Genome-Wide Transcription Analysis of Histidine-Related Cataract in Atlantic Salmon (*Salmo salar* L.). *Invest. Ophthalmol. Vis. Sci.* **50**, 5184 (2009).
271. Dominiczak, M. H. & Caslake, M. J. Apolipoproteins: metabolic role and clinical biochemistry

- applications. *Ann. Clin. Biochem.* **48**, 498–515 (2011).
272. Peñaloza, C., Hamilton, A., Guy, D. R., Bishop, S. C. & Houston, R. D. A SNP in the 5' flanking region of the myostatin-1b gene is associated with harvest traits in Atlantic salmon (*Salmo salar*). *BMC Genet.* **14**, 112 (2013).
273. Delbarre-Ladrat, C., Chéret, R., Taylor, R. & Verrez-Bagnis, V. Trends in Postmortem Aging in Fish: Understanding of Proteolysis and Disorganization of the Myofibrillar Structure. *Crit. Rev. Food Sci. Nutr.* **46**, 409–421 (2006).
274. Danzmann, R. G., Kocmarek, A. L., Norman, J. D., Rexroad, C. E. & Palti, Y. Transcriptome profiling in fast versus slow-growing rainbow trout across seasonal gradients. *BMC Genomics* **17**, 60 (2016).
275. Tian, J. *et al.* Dietary lipid levels impact lipoprotein lipase, hormone-sensitive lipase, and fatty acid synthetase gene expression in three tissues of adult GIFT strain of Nile tilapia, *Oreochromis niloticus*. *Fish Physiol. Biochem.* **41**, 1–18 (2015).
276. Qin, C. *et al.* Comparative analysis of the liver transcriptome of *Pelteobagrus vachellii* with an alternative feeding time. *Comp. Biochem. Physiol. Part D Genomics Proteomics* **22**, 131–138 (2017).
277. Venold, F. F. *et al.* Intestinal fatty acid binding protein (*fabp2*) in Atlantic salmon (*Salmo salar*): Localization and alteration of expression during development of diet induced enteritis. *Comp. Biochem. Physiol. A. Mol. Integr. Physiol.* **164**, 229–240 (2013).
278. Chitchumroonchokchai, C. & Failla, M. L. Bioaccessibility and intestinal cell uptake of astaxanthin from salmon and commercial supplements. *Food Res. Int.* **99**, 936–943 (2017).
279. Bjerkgeng, B. *et al.* Quality parameters of the flesh of Atlantic salmon (*Salmo salar*) as affected by dietary fat content and full-fat soybean meal as a partial substitute for fish meal in the diet. *Aquaculture* **157**, 297–309 (1997).
280. Nickell, D. C. & Bromage, N. R. The effect of dietary lipid level on variation of flesh pigmentation in rainbow trout (*Oncorhynchus mykiss*). *Aquaculture* **161**, 237–251 (1998).
281. Olsen, R. E., Kiessling, A., Milley, J. E., Ross, N. W. & Lall, S. P. Effect of lipid source and bile salts in diet of Atlantic salmon, *Salmo salar* L., on astaxanthin blood levels. *Aquaculture* **250**, 804–812 (2005).
282. Chimsung, N., Lall, S. P., Tantikitti, C., Verlhac-Trichet, V. & Milley, J. E. Effects of dietary cholesterol on astaxanthin transport in plasma of Atlantic salmon (*Salmo salar*). *Comp. Biochem. Physiol. Part B Biochem. Mol. Biol.* **165**, 73–81 (2013).
283. Cheng, C.-H., Guo, Z.-X., Ye, C.-X. & Wang, A.-L. Effect of dietary astaxanthin on the growth performance, non-specific immunity, and antioxidant capacity of pufferfish (*Takifugu obscurus*) under high temperature stress. *Fish Physiol. Biochem.* **44**, 209–218 (2018).
284. Pörtner, H. O. Climate variations and the physiological basis of temperature dependent biogeography: systemic to molecular hierarchy of thermal tolerance in animals. *Comp. Biochem. Physiol. Part A Mol. Integr. Physiol.* **132**, 739–761 (2002).
285. Zhou, C., Ge, X., Lin, H. & Niu, J. Effect of dietary carbohydrate on non-specific immune

- response, hepatic antioxidative abilities and disease resistance of juvenile golden pompano (*Trachinotus ovatus*). *Fish Shellfish Immunol.* **41**, 183–190 (2014).
286. Cheng, C.-H. *et al.* High temperature induces apoptosis and oxidative stress in pufferfish (*Takifugu obscurus*) blood cells. *J. Therm. Biol.* **53**, 172–179 (2015).
  287. Ando, M. Correspondence of collagen to the softening of fish meat during refrigeration. *Extracell. Matrix Fish Shellfish* (1999).
  288. Taylor, R. G., Fjaera, S. O. & Skjervold, P. O. Salmon Fillet Texture is Determined by Myofiber-Myofiber and Myofiber-Myocommata Attachment. *J. Food Sci.* **67**, 2067–2071 (2002).
  289. Torgersen, J. S. *et al.* Soft Texture of Atlantic Salmon Fillets Is Associated with Glycogen Accumulation. *PLoS One* **9**, e85551 (2014).
  290. Schneider, W. J. Lipoprotein receptors. *New Compr. Biochem.* **36**, 553–572 (2002).
  291. Oksala, N. K. J. *et al.* Natural thermal adaptation increases heat shock protein levels and decreases oxidative stress. *Redox Biol.* **3**, 25–28 (2014).
  292. Lin, X., Wu, X. & Liu, X. Temperature stress response of heat shock protein 90 (Hsp90) in the clam *Paphia undulata*. *Aquac. Fish.* **3**, 106–114 (2018).
  293. Maryoung, L. A. *et al.* Differential Gene Expression in Liver, Gill, and Olfactory Rosettes of Coho Salmon (*Oncorhynchus kisutch*) After Acclimation to Salinity. *Mar. Biotechnol. (NY)*. **17**, 703–717 (2015).
  294. Jalili, M. *et al.* Dietary fatty acid source has little effect on the development of the immune system in the pyloric caeca of Atlantic salmon fry. *Sci. Rep.* **9**, 27 (2019).
  295. Leiva, K. *et al.* Identification and functional characterization of the CYP51 gene from the yeast *Xanthophyllomyces dendrorhous* that is involved in ergosterol biosynthesis. *BMC Microbiol.* **15**, 89 (2015).
  296. Porter, T. D. & Coon, M. J. Cytochrome P-450. Multiplicity of isoforms, substrates, and catalytic and regulatory mechanisms. *J. Biol. Chem.* **266**, 13469–13472 (1991).
  297. Gradelet, S., Leclerc, J., Siess, M. H. & Astorg, P. O. beta-Apo-8'-carotenal, but not beta-carotene, is a strong inducer of liver cytochromes P4501A1 and 1A2 in rat. *Xenobiotica.* **26**, 909–919 (1996).
  298. Perocco, P., Paolini, M., Mazzullo, M., Biagi, G. L. & Cantelli-Forti, G.  $\beta$ -Carotene as enhancer of cell transforming activity of powerful carcinogens and cigarette-smoke condensate on BALB/c 3T3 cells in vitro. *Mutat. Res. Toxicol. Environ. Mutagen.* **440**, 83–90 (1999).
  299. Agarwal, S. & Rao, A. V. Tomato lycopene and its role in human health and chronic diseases. *C. Can. Med. Assoc. J. = J. l'Association medicale Can.* **163**, 739–744 (2000).
  300. Paolini, M. *et al.* Induction of cytochrome P450 enzymes and over-generation of oxygen radicals in beta-carotene supplemented rats. *Carcinogenesis* **22**, 1483–1495 (2001).
  301. Louisa, M., Suyatna, F. D., Setiawati, A. & Jusman, S. W. A. The effect of lycopene on the total cytochrome P450, CYP1A2 and CYP2E1. *Med. J. Indones.* **18**, (2009).

302. Torrissen, O. J. & Ingebrigtsen, K. Tissue distribution of <sup>14</sup>C-astaxanthin in the Atlantic salmon (*Salmo salar*). *Aquaculture* **108**, 381–385 (1992).
303. Page, G. . & Davies, S. . Hepatic carotenoid uptake in rainbow trout (*Oncorhynchus mykiss*) using an isolated organ perfusion model. *Aquaculture* **225**, 405–419 (2003).
304. Higuera-Ciapara, I., Félix-Valenzuela, L. & Goycoolea, F. M. Astaxanthin: A Review of its Chemistry and Applications. *Crit. Rev. Food Sci. Nutr.* **46**, 185–196 (2006).
305. Bjerkgeng, B. Carotenoid pigmentation of salmonid fishes recent progress. *Av. en Nutr. Acuicola V. Memorias del V Simp. Int. Nutr. Acuicola 19-22 Noviembre, 2000. Merida, Yucatan* (2000).
306. Ytrestøyl, T. & Bjerkgeng, B. Dose response in uptake and deposition of intraperitoneally administered astaxanthin in Atlantic salmon (*Salmo salar* L.) and Atlantic cod (*Gadus morhua* L.). *Aquaculture* **263**, 179–191 (2007).
307. Bjerkgeng, B., Hatlen, B. & Jobling, M. Astaxanthin and its metabolites idoxanthin and crustaxanthin in flesh, skin, and gonads of sexually immature and maturing Arctic charr (*Salvelinus alpinus* (L.)). *Comp. Biochem. Physiol. Part B Biochem. Mol. Biol.* **125**, 395–404 (2000).
308. Bjerkgeng, B. *et al.* Bioavailability of all-E-astaxanthin and Z-isomers of astaxanthin in rainbow trout (*Oncorhynchus mykiss*). *Aquaculture* **157**, 63–82 (1997).
309. Brotosudarmo, T. H. P., Limantara, L., Setiyono, E. & Heriyanto. Structures of Astaxanthin and Their Consequences for Therapeutic Application. *Int. J. Food Sci.* **2020**, 2156582 (2020).
310. Bjerkgeng, B. & Berge, G. M. Apparent digestibility coefficients and accumulation of astaxanthin E/Z isomers in Atlantic salmon (*Salmo salar* L.) and Atlantic halibut (*Hippoglossus hippoglossus* L.). *Comp. Biochem. Physiol. Part B Biochem. Mol. Biol.* **127**, 423–432 (2000).
311. Hardy, R. W., Torrissen, O. J. & Scott, T. M. Absorption and distribution of <sup>14</sup>C-labeled canthaxanthin in rainbow trout (*Oncorhynchus mykiss*). *Aquaculture* **87**, 331–340 (1990).
312. Schiedt, K., Leuenberger, F. J., Vecchi, M. & Glinz, E. Absorption, retention and metabolic transformations of carotenoids in rainbow trout, salmon and chicken. *Pure Appl. Chem.* **57**, 685–692 (1985).
313. Schiedt, K., Vecchi, M. & Glinz, E. Astaxanthin and its metabolites in wild rainbow trout (*Salmo gairdneri* R.). *Comp. Biochem. Physiol. Part B Comp. Biochem.* **83**, 9–12 (1986).
314. Abdulrahman S, A.-K. & Simpson, K. L. Metabolism of astaxanthin in the rainbow trout (*Salmo gairdneri*). *Comp. Biochem. Physiol. Part B Comp. Biochem.* **91**, 563–568 (1988).
315. Guillou, A., Choubert, G., Storebakken, T., de la Noüet, J. & Kaushik, S. Bioconversion pathway of astaxanthin into retinol2 in mature rainbow trout (*Salmo Gairdneri* Rich.). *Comp. Biochem. Physiol. Part B Comp. Biochem.* **94**, 481–485 (1989).
316. Schiedt, K., Mayer, H., Vecchi, M., Glinz, E. & Storebakken, T. *Metabolism of carotenoids in salmonids. Part 2. Distribution and absolute configuration of idoxanthin in various organs and tissues of one Atlantic salmon (Salmo salar, L.) fed with astaxanthin.* vol. 71 (1988).
317. Schiedt, K., Foss, P., Storebakken, T. & Liaaen-Jensen, S. Metabolism of carotenoids in

- salmonids—I. idoxanthin, a metabolite of astaxanthin in the flesh of atlantic salmon (*Salmon salar*, L.) under varying external conditions. *Comp. Biochem. Physiol. Part B Comp. Biochem.* **92**, 277–281 (1989).
318. Jones, O. R. & Wang, J. COLONY: a program for parentage and sibship inference from multilocus genotype data. *Mol. Ecol. Resour.* **10**, 551–555 (2010).
319. Taylor, R., Maynard, B., Clark, T., Wilkinson, R., Smullen, R., Bourne, S.C., Hines, B. Defining changes in Atlantic salmon during summer stress and recovery. CSIRO Agriculture and food 58pp. (2017).
320. R Core Team. R: A language and environment for statistical computing. R Foundation for Statistical Computing, Vienna, Austria. URL <https://www.R-project.org/>. (2017).
321. Wickham, H. *ggplot2: Elegant Graphics for Data Analysis*. Springer-Verlag New York. (2009).



# FRDC FINAL REPORT CHECKLIST

<b>Project Title:</b>	<b>Understanding flesh colour variation in Atlantic salmon: molecular mechanisms and genetic effect</b>		
<b>Principal Investigators:</b>	Dr Gianluca Amoroso - Aquaculture Scientist at Petuna Dr Chan D.H. Nguyen - PhD graduate, University of the Sunshine Coast Ms Thu T.M. Vo - PhD candidate, University of the Sunshine Coast Dr Tomer Ventura - University of the Sunshine Coast Prof Abigail Elizur - University of the Sunshine Coast		
<b>Project Number:</b>	2014-248		
<b>Description:</b>	This project looked at the impact of temperature on flesh colour and investigated the causes associated with poor quality flesh colour using molecular approaches, including the establishment of a selective breeding program that examined the genetic basis for colour and resilience to high temperatures.		
<b>Published Date:</b>	20/10/2020	<b>Year:</b>	2020
<b>ISBN:</b>	978-1-925476-12-5	<b>ISSN:</b>	XXXXXXXXXXXX (if applicable)
<b>Key Words:</b>	Atlantic Salmon, flesh colour, selective breeding, gene expression, microbiome, carotenoids		

Please use this checklist to self-assess your report before submitting to FRDC. Checklist should accompany the report.

	<b>Is it included (Y/N)</b>	<b>Comments</b>
<b>Foreword (optional)</b>	N	
<b>Acknowledgments</b>	Y	
<b>Abbreviations</b>	Y	Throughout the text, when first used
<b>Executive Summary</b>	Y	
- <b>What the report is about</b>		
- <b>Background – why project was undertaken</b>		
- <b>Aims/objectives – what you wanted to achieve at the beginning</b>		
- <b>Methodology – outline how you did the project</b>		
- <b>Results/key findings – this should outline what you found or key results</b>		
- <b>Implications for relevant stakeholders</b>		
- <b>Recommendations</b>		
<b>Introduction</b>	Y	
<b>Objectives</b>	Y	
<b>Methodology</b>	Y	For each of the 3 sections
<b>Results</b>	Y	

Discussion	Y	
Conclusion	Y	
Implications	Y	
Recommendations	Y	
Further development	Y	
Extension and Adoption	Y	
Project coverage	Y	
Glossary	Y	
Project materials developed	N	
Appendices	Y	
<b>EXTENSION</b>		
Extension plan developed?		
Extension undertaken?	Y	<b>The project outcomes have already been adopted by the industry</b>
If extension was undertaken, who was it undertaken with and was it successful? (Detail answer in comments section)	Petuna	<b>The company has already changed some of its practices based on the research described - the details are described in the final conclusions.</b>
If No, then is further extension necessary? With who? How? (detail answer in comments section)		